CHARACTERISTICS OF
STEADY AND UNSTEADY JETS

by

HENRY GREGORY GREEN

Thesis submitted for the degree of
Doctor of Philosophy
in the University of London
and for the
Diploma of Membership of the Imperial College

Imperial College of Science and Technology
Department of Mechanical Engineering

1986

ABSTRACT

Experimental results are presented for velocity and concentration characteristics of isothermal, turbulent round jets. The investigations have been carried out with steady and unsteady gas jets of: air, helium,Freon-12 and sulfurhexaflouride issuing into atmospheric and pressurized air surroundings. The Reynolds number range was 2000 - 70000.

For the steady jets, a combination of hot-wire anemometry, laser-induced Rayleigh scattering and sampling probes has been used to determine the velocity and concentration characteristics of jets of Freon and air into still air. The results show that the heavier density jet spreads more slowly than the ligher air jet. For a given Reynolds number, the concentration decays and spreads more rapidly than velocity and the difference is greater with the high density jet; the two jets have similar decay rates if their initial momentum is the same. Discrete frequencies in the near field were observed from the jet exit to around seven diameters downstream and appear to be associated with vortex pairing; the Strouhal number varies from 0.14 to 0.8 and scales with the inverse of jet momentum.

The unsteady jets have been investigated with a combination of laser-induced Rayleigh scattering, laser Doppler anemometry, shadowgraphy and Schlieren techniques and photodiode arrays to determine characteristics of the jet tip penetration, velocity and concentration fields. The influence of nozzle design is considered in detail for two diffusing and two contracting nozzles. Measurements are reported for jets of Freon-12 (CCl_2F_2) and sulfur hexafluoride (SF_6) issuing into still air and into the cylinder of a motored model engine at compression ratios of 0, 3.5 and 6.7. The results show increases in spread and decay for decreases in density ratio between the jet and its surround-

ings, which can result as a consequence of the jet density directly or by increases in the ambient air density due to the compression process. The photographic results indicate an initial rapid vortex growth at the jet front, followed by a steadying behaviour and concluded by the formation of a convecting vortex when the jet is turned off.

ACKNOWLEDGEMENTS

I would like to give many thanks to Professor J H Whitelaw for his encouragement, supervision and guidance throughout the work of this thesis.

Thanks are also given to the members of the Fluids Section who have participated with their many discussions, criticism and most of all interest in the work. Further thanks are due to members of Sandia National Laboratories, Livermore, Combustion Research Facility and to members of the Mechanical Engineering Department, U C Berkeley.

The financial support provided for this work by the Science and Engineering Research Council, United Kingdom and The Department of Energy, United States, is gratefully acknowledged

TABLE OF CONTENTS

		Page
ABSTRACT		i
Acknowledgements		iii
Table of Contents		iv
List of Tables		ix
List of Figures		xi
Nomenclature		xxiv
CHAPTER 1	INTRODUCTION	1
	1.1 TOPIC OF THESIS	1
	1.2 OUTLINE OF PREVIOUS WORK	1
	1.2.1 Averaged flow characteristics	4
	1.2.2 Organised flow	10
	1.2.3 Transient jets	20
	1.3 PRESENT CONTRIBUTION	24
	1.4 OUTLINE OF THESIS	25
CHAPTER 2	A LASER RAYLEIGH SCATTERING SYSTEM	26
	2.1 INTRODUCTION	26
	2.2 EXPERIMENTAL SYSTEM AND MEASUREMENT CONSIDERATIONS	30
	2.2.1 Measurements	30
	2.2.2 Optical and signal processing systems	31
	2.3 SIGNAL CHARACTERISTICS AND FILTERING	33

		Page
	2.3.1 Characteristics and detection criteria	33
	2.3.2 Filtering	35
	2.3.2.1 Amplitude filtering	35
	2.3.2.2 Initial rise filter	37
	2.3.2.3 Transient filter	39
	2.4 RESULTS AND DISCUSSION	42
	2.5 CONCLUSIONS	43
CHAPTER 3	THE NEAR FIELD OF STEADY JETS	63
	3.1 INTRODUCTION	63
	3.2 FLOW ARRANGEMENT AND MEASUREMENT TECHNIQUES	64
	3.3 RESULTS AND DISCUSSIONS	67
	3.3.1 Centreline characteristics	67
	3.3.2 Radial characteristics	69
	3.3.3 Higher moments and probability densities	71
	3.3.4 Energy spectra	74
	3.4 CONCLUSIONS	79
Appendix	MEASUREMENT UNCERTAINTIES	80
	3.1.A Uncertainty in velocity measurements	80
	3.2.A Uncertainty in concentration measurements	84
	3.3.A Uncertainty due to neglect of static pressure	86

		Page
CHAPTER 4	NON-COMPRESSING MODEL ENGINE	122
	4.1 INTRODUCTION	122
	4.2 EXPERIMENTAL SYSTEM	125
	4.2.1 Flow configuration	125
	4.2.2 Experimental techniques	127
	. Concentration measurements	127
	. Velocity measurements	127
	4.2.3 Measurement uncertainties	128
	4.3 RESULTS AND DISCUSSION	128
	4.3.1 Centreline distributions	130
	4.3.2 Radial distributions	133
	4.4 CONCLUSIONS	135
CHAPTER 5	COMPRESSING MODEL ENGINE	156
	5.1 INTRODUCTION	156
	5.2 EXPERIMENTAL SYSTEM	156
	5.2.1 Flow configuration	156
	5.2.2 Optical and signal processing systems	159
	5.2.3 Sources of error and uncertainties	159
	5.3 RESULTS FOR 3.5 CR ENGINE	163
	5.3.1 Centreline characteristics	165
	5.3.2 Radial characteristics	166
	5.3.3 Effect of nozzle type and piston geometries	167
	5.3.4 Effects of swirl	169

		Page
	5.3.5 Fuel jet spread and decay	170
	5.3.6 Effects of scaling and similarity characteristics	174
	5.4 RESULTS FOR 6.7 CR ENGINE	176
	5.4.1 Centreline distributions	176
	5.4.2 Radial distributions	178
	5.4.3 Temporal characteristics (autocorrelations)	181
	5.5 CONCLUSIONS	184
CHAPTER 6	CHARACTERISTICS OF TRANSIENT JETS	228
	6.1 INTRODUCTION	228
	6.2 EXPERIMENTAL SYSTEM	228
	6.2.1 Flow configuration	228
	6.2.2 Optical and signal processing systems	230
	6.3 RESULTS AND DISCUSSIONS	231
	6.3.1 Jet characteristics	231
	6.3.2 Comparison of technique results	233
	6.3.3 Tip penetration	233
	6.4 CONCLUSIONS	235
CHAPTER 7	CLOSURE	260
	7.1 FINDINGS AND CONCLUSIONS	260
	7.2 SUGGESTIONS FOR FURTHER WORK	262
Appendix A	A.1 Interpretation of LRS Signals	264

			Page
	A.2	Evaluation of Angular Scattering Cross-sections	270
	A.3	Experiments Using LRS	274
	A.4	Uncertainty, Sources of Noise and Data Analysis	278
		A.4.1 Uncertainty and noise	278
		A.4.2 Data analysis	280
Appendix B	B.1	Optical Considerations of LRS in Confined Flows	290
	B.2	Experimental System	291
	B.3	Light Transmission Through Flat Walls	292
	B.4	Light Transmission Through Cylindrical Walls	296
Appendix C	C.1	Microcomputer Software for Transient Flow Measurements	310
	C.2	Signal Processing	311
	C.3	Software Developments	312
		. Data sampling	312
		. Gating system control	315
		. Data analysis	315
		. Graphics	316
	C.4	Software Integration	317
REFERENCES			324

LIST OF TABLES

		Page
Table 2.1	Summary of optical probe developments and applications to the study of turbulent mixing	44
Table 2.2	Summary of percentage rejection of signal values using different filters	52
Table 3.1	Influence of density ratio on mean flow	89
Table 3.2	Summary of velocity spectra results for air, helium and Freon-12	90
Table 4.1	Geometric characteristics of model Diesel engine	137
Table 4.2	Injection characteristics	137
Table 4.3	Characteristics of laser Doppler anemometer	138
Table 4.4	Influence of nozzle and piston geometry and injection timing on jet spread	139
Table 5.1	Characteristics of the model engine (3.5 CR)	187
Table 5.2	Characteristics of the model engine (6.7 CR)	188
Table 5.3	Injection characteristics	188
Table 5.4	Influence of nozzle geometry, piston configuration and induction swirl on mean flow	189
Table 5.5	Influence of nozzle geometry, piston configuration and induction swirl on jet spread	190
Table 5.6	Influence of nozzle geometry, piston configuration and compression ratio on jet spread (absence of swirl)	191

		Page
Table 6.1	Summary of experimental conditions	237
Table 6.2	PDA optical parameters	238
Table 6.3	Values for a and n for the correlation of penetration distance and time (Freon-12 jets)	239
Table 6.4	Penetration parameter (α) experimental correlation	240
Table A.1	Summary of some useful refractive indices	272
Table A.2	Summary of claculations for σ_o	273
Table A.3	Estimates of uncertainties for typical LRS instrumentation conditions	279
Table B.1	Summary of optical properties of quartz, pyrex and perspex	294
Table B.2	Comparison of optical attenuation losses with LRS and a power meter	295
Table C.1	Input parameters for MONA.RUNX	318

LIST OF FIGURES

		Page
Figure 2.1	Line diagram of laser Rayleigh scattering optical arrangements and signal processing system	53
Figure 2.2	Scattered light intensity distribution (a) $x/d = 3$, $r/d = 0.65$ (b) $x/d = 3$, $r/d = 0.3$	54
Figure 2.3	Oscilloscope traces of laser Rayleigh scattering signals	55
Figure 2.4	Mean and rms concentration profiles along the jet radius at $x/d = 3$; comparison of unfiltered, amplitude filtered and sampling probe results	56
Figure 2.5	Schematic for initial rise filter, $\varepsilon_o = 0$	57
Figure 2.6	Schematic for initial rise filter, $\varepsilon_o > 0$	58
Figure 2.7	Difference filter (with different values of n) applied to LRS signals at (a) jet potential core, $x/d = 3$, $r/d = 0$ (b) $x/d = 5$, $r/d = 0.4$ (c) $x/d = 18$, $r/d = 0$ (d) $x/d = 3$, $r/d = 0.7$	59
Figure 2.8	LRS frequency spectra at a jet location $x/d = 3$, $r/d = 0.3$, with the parameter n set to (a) $n = 0$ (b) $n = 1$ (c) $n = 2$ (d) $n = 4$	60
Figure 2.9	Mean and rms concentration profiles along jet radius at $x/d = 3$, filtered results	61

		Page
Figure 2.10	Mean and rms concentration profiles along the jet radius at x/d = 5, filtered and unfiltered results compared	62
Figure 3.1	Spreading of jets; L_c and L_u designate the typical concentration and velocity potential core lengths, respectively	91
Figure 3.2	Centreline distributions of mean velocity and concentration	92
Figure 3.3	Centreline distributions of the rms of velocity and concentration signals	94
Figure 3.4	Radial profiles of mean velocity and helium trace concentration for air jet with Re = 16900	95
Figure 3.5	Radial profiles of mean velocity and concentration for Freon-12 jet with Re = 16900	96
Figure 3.6	Similarity in mean profiles of concentration (note that the same similarity characteristics results with the mean velocity profiles)	97
Figure 3.7	Axial characteristics of mass and mole fraction spread	98
Figure 3.8	Radial profiles of air jet (a) mean and (b) rms velocity signals at different Reynolds numbers (note that at Re = 5850, the air jet has the same exit momentum flux ρU_o^2 as the Freon-12 jet of Re = 16900)	99
Figure 3.9	Radial profiles of the rms of concentration signals for Freon-12 jet with Re = 16900	101

		Page
Figure 3.10	Probability densities for Freon-12 jet, Re = 16900 (a) centreline (b) x/d = 3 and (c) x/d = 9	102
Figure 3.11	Spectra of u-velocity fluctuations in air jet (a) centreline and (b) x/d = 3	103
Figure 3.12	Spectra of u-velocity fluctuations in Freon-12 jet (a) centreline and (b) x/d = 3	104
Figure 3.13	Spectra of u-velocity fluctuations in helium jet along the plane at x/d = 3	105
Figure 3.14	Typical LRS signals of concentration where periodic behaviour is exhibited by the flow (x/d = 3, r/d = .35): Freon-12 jet with Re = 16900	106
Figure 3.15	Centreline evolution of spectra of concentration fluctuations: Freon-12 jet with Re = 16900	107
Figure 3.16	Radial spectra of concentration fluctuations of Freon-12 jet (a) x/d = 1, Re = 16900 (b) x/d = 2, Re = 16900 (c) x/d = 3, Re = 16900 (d) x/d = 4, Re = 16900 (e) x/d = 5, Re = 16900 (f) x/d = 1, Re = 5860 (g) x/d = 2, Re = 5860 (h) x/d = 3, Re = 5860 (i) x/d = 4, Re = 5860 (j) x/d = 5, Re = 5860	108

		Page
Figure 3.A.1	Comparison of mean velocity determined with Pitot probe corrected and uncorrected for local density: Freon-12 jet, Re = 16900	118
Figure 3.A.2	Sensitivity of probe concentration measurements to variables of probe size, katharometer voltage and probe suction rate	119
Figure 3.A.3	Effects of probe size on measured (a) mean cocentration and (b) mean velocity (Pitot probe results shown uncorrected for local density): Freon-12 jet, Re = 16900	120
Figure 3.A.4	Mean concentration radial profiles measured at two locations to demonstrate effects of density weighting in regions of high turbulence with low and high levels of mean concentrations	121
Figure 4.1	Line diagram of model engine	140
Figuer 4.2	Nozzle geometries	141
Figure 4.3	Line diagram of LDA signal processing and optical arrangements	142
Figure 4.4	Time-averaged concentration of in-cycle fuel injection at two axial locations	143
Figure 4.5	Instantaneous Freon concentration at the nozzle exit for three consecutive jet firings; Nozzle A, Flat piston	144
Figure 4.6	In-cycle concentration as a function of distance from the nozzle along the centreline; Nozzle A, Flat piston	145

		Page
Figure 4.7	Centreline distributions of mean and rms concentration and velocity; Nozzle A, Flat piston	146
Figure 4.8	Centreline distributions of mean and rms concentration and velocity; Nozzle B, Flat piston	147
Figure 4.9	Centreline distributions of mean and rms concentration and velocity; Nozzle A, Re-entrant piston	148
Figure 4.10	(a) Radial distributions of mean and rms concentration and velocity at x/d = 2; Nozzle A, Flat piston (b) x/d = 4; Nozzle A, Flat piston	149
Figure 4.11	(a) Radial distributions of mean and rms concentration and velocity at x/d = 2; Nozzle B, Flat piston (b) x/d = 4; Nozzle B, Flat piston (c) x/d = 6; Nozzle B, Flat piston	151
Figure 4.12	Radial profiles of mean concentration (Nozzle A) as influenced by piston geometry and with fuel injection initiated at (a) 40 deg. BTDC and (b) 10 deg. ATDC	154
Figure 4.13	Rms concentration as influenced by piston geometry and fuel injection initiated at (a) 40 deg. BTDC and (b) 10 deg. ATDC	155

		Page
Figure 5.1	Nozzle geometries	192
Figure 5.2	In-cylinder calibration of LRS signals for variable compositions of Freon-12 percent in air: compression ratio 3.5	193
Figure 5.3	Time-averaged concentration of in-cycle fuel injection at exit plane of different nozzles (a) signals influenced by pressure (b) corrected for pressure influence	194
Figure 5.4	Time-averaged concentration of in-cycle fuel injection as a function of distance from the nozzle along the centreline: Nozzle A, Flat piston	194
Figure 5.5	Instantaneous Freon-12 concentration at x/d = 2.47 (x = 8mm); Nozzle A, Flat piston (a) signals influenced by pressure (b) corrected for pressure influence	195
Figure 5.6	Instantaneous Freon concentration (in the absence of compression) as a function of distance from the nozzle along the centreline: Nozzle A, Flat piston	196
Figure 5.7(a)	Centreline distributions of mean concentration as influenced by piston and nozzle geometry (absence of swirl)	197
Figure 5.7(b)	Centreline distributions of rms concentration as influenced by piston and nozzle geometry (absence of swirl)	198
Figure 5.8(a)	Radial distributions of mean concentration: Nozzle A, Flat piston (absence of swirl)	199

		Page
Figure 5.8(b)	Radial distributions of rms concentration: Nozzle A, Flat piston (absence of swirl)	200
Figure 5.9(a)	Radial distributions of mean concentration: Nozzle B, Flat piston (absence of swirl)	201
Figure 5.9(b)	Radial distributions of rms concentration: Nozzle B, Flat piston (absence of swirl)	202
Figure 5.10(a)	Radial distributions of mean concentration: Nozzle C, Flat piston (absence of swirl)	203
Figure 5.10(b)	Radial distributions of rms concentration: Nozzle C, Flat piston (absence of swirl)	204
Figure 5.11(a)	Centreline distributions of mean concentration as influenced by piston geometry and induction swirl: Nozzle A	205
Figure 5.11(b)	Centreline distributions of rms concentration as influenced by piston geometry and induction swirl: Nozzle A	206
Figure 5.12(a)	Centreline distributions of mean concentration as influenced by piston geometry and induction swirl: Nozzle C	207
Figure 5.12(b)	Centreline distributions of rms concentration as influenced by piston geometry and induction swirl: Nozzle C	208
Figure 5.13(a)	Radial distributions of mean concentration as influenced by piston geometry and induction swirl: Nozzle A	209
Figure 5.13(b)	Radial distributions of rms concentration as influenced by piston geometry and induction swirl: Nozzle A	210

		Page
Figure 5.14	Radial distributions of (a) mean and (b) rms concentration, as influenced by piston geometry and induction swirl: Nozzle C	211
Figure 5.15(a)	Growth rates of fuel jets as influenced by nozzle and piston geometry and induction swirl: Nozzles A and B	212
Figure 5.15(b)	Growth rates of fuel jets as influenced by nozzle and piston geometry and induction swirl: Nozzles C and D	213
Figure 5.16	Centreline distributions of mean concentration with Nozzles A and C against x/H as the axial co-ordinate	214
Figure 5.17	Self-similar profiles of the radial distributions of mean concentration with Nozzles A, B, C and D	215
Figure 5.18(a)	Centreline distributions of mean concentration as influenced by geometry and compression ratio (absence of swirl)	216
Figure 5.18(b)	Centreline distributions of rms concentration as influenced by geometry and compression ratio (absence of swirl)	217
Figure 5.19(a)	Radial distributions of mean concentration as influenced by piston geometry for compression ratio 3.5 with Nozzle A and SF_6 (absence of swirl)	218
Figure 5.19(b)	Radial distributions of rms concentration as influenced by piston geometry for compression ratio 3.5 with Nozzle A and SF_6 (absence of swirl)	219

		Page
Figure 5.19(c)	Radial distributions of mean concentration as influenced by piston geometry for compression ratio 3.5 with Nozzle A and Freon-12 (absence of swirl): see figure 5.8(a)	220
Figure 5.19(d)	Radial distributions of rms concentration as influenced by piston geometry for compression ratio 3.5 with Nozzle A and Freon-12 (absence of swirl): see figure 5.8(b)	221
Figure 5.20	Radial distributions of (a) mean and (b) rms concentration as influenced by piston geometry for compression ratio 6.7 with Nozzle A and SF_6 (absence of swirl)	222
Figure 5.21	Radial distributions of (a) mean and (b) rms concentration as influenced by piston geometry for compression ratio 6.7 with Nozzle C and SF_6 (absence of swirl)	223
Figure 5.22	Ensemble autocorrelation functions (based on 100 engine cycles) for SF_6 gas: Nozzle A (a) re-entrant piston, 3.5 CR (b) re-entrant piston, 6.7 CR (c) flat piston, 6.7 CR (d) re-entrant piston, 6.7 CR (ensembled along $\Delta\theta$, figure 5.4)	224
Figure 5.23	Single-cycle autocorrelation functions for SF_6 gas: Nozzle A (a) re-entrant piston, 3.5 CR (b) re-entrant piston, 6.7 CR (c) flat piston, 6.7 CR	226
Figure 6.1	Line diagram of flow system	241

		Page
Figure 6.2	Line diagram of instrumentation and optical arrangements for PDA. The inset shows the jet image as seen by the PDA and a typical signal output	242
Figure 6.3	Schlieren photographs of a transient jet of Freon-12 from Nozzle A with U_o = 37.7m/s. The time in between exposures is 0.2ms and with the last frame showing the steadying jet boundary obtained from long time exposure	243
Figure 6.4	Second firing of a similar jet as in figure 6.3. The last frame in this sequence is representative of the end time conditions as the jet approaches its "off" state	245
Figure 6.5	Freon-12 jet from Nozzle A, U_o = 37.7m/s	247
Figure 6.6(a)	Freon-12 jet from Nozzle B, U_o = 19.2m/s	248
Figure 6.6(b)	Freon-12 jet from Nozzle B (second firing), U_o = 19.2m/s	249
Figure 6.7(a)	Freon-12 jet from Nozzle B, U_o = 30.9m/s. The figure emphasizes the boundary and growth of the leading vortex at different time intervals of 0.2ms	250
Figure 6.7(b)	Similar jet as in (a), second firing	251
Figure 6.7(c)	Similar jet as in (a) and (b) (third firing) showing variation between axis of maximum penetration and that of the geometrical centreline	252
Figure 6.8	Freon-12 jet from Nozzle C, U_o = 60m/s. Typical leading vortex boundaries are shown and can be compared with results of figure 6.7	253

		Page
Figure 6.9	Instantaneous trace of jet fluid concentration at a measurement point (x/d = 1.5, r/d = 0) using LRS	254
Figure 6.10	Comparison of tip penetration data obtained with the PDA technique and those from the LRS and high speed film (Nozzle A, Freon-12)	255
Figure 6.11	Comparison of tip penetration data obtained with the PDA technique and those from the LRS and high speed film (Nozzle B, Freon-12)	256
Figure 6.12	Normalized penetration data for jets from Nozzle A, Freon-12	257
Figure 6.13	Normalized penetration data for jets from Nozzle B, Freon-12	258
Figure 6.14	Normalized penetration data for jets from Nozzle C with Freon-12, Nozzle A with SF_6 and Witze's (1980) air jets	259
Figure A.1	Rayleigh scattered light intensity as influenced by pressure for different Freon-12 concentration (%) in air (isothermal conditions)	285
Figure A.2(a)	Rayleigh scattered light intensities during an engine cycle (6.7 CR engine) obtained with intake of pure SF and pure air	286
Figure A.2(b)	Comparison of experiment and Rayleigh's theory for the scattered light intensity during an engine cycle interval (3.5 CR engine and with Freon-12 as intake gas). The theoretical result was obtained with equation A.19 and with the assumption that $\sigma(t)/\sigma = 1$; i.e. negligible temperature and pressure influence on refractive index	287

		Page
Figure A.2(c)	Comparison of experiment and Rayleigh's theory for the scattered light intensity during an engine cycle interval (6.7 CR engine and with SF_6 as intake gas). The theoretical results was determined as noted in figure A.2(b)	287
Figure A.2(d)	Similar results as in figure A.2(c) but obtained with air as the intake gas; the larger discrepancy indicated here between experiment and theory (assuming negligible influence of temperature on the refractive index variation) is due to the lower heat capacity of air	288
Figure A.2(e)	The same results as in figure A.2(c) and (d) but with account of temperature and pressure influence for both the number density and refractive index variations; the results shown were obtained with evaluating the corresponding polytropic exponents from the in-cycle measured pressure resulting with the use of the different gases (the values were 1.08 for SF_6 and 1.31 for air in the crank angle interval of interest, i.e. 330 to 360 degrees of crank angle)	289
Figure B.1	Centreline Freon-12 concentration (free jet)	304
Figure B.2	Radial Freon-12 concentration at x/d = 3 (free jet)	304
Figure B.3	Rayleigh signal as a function of incident laser light	305
Figure B.4	Experimental system for investigating the effect of flat and cylindrical walls on the Rayleigh signal from a Freon-12 jet	305

		Page
Figure B.5	Centreline Freon-12 concentration (confined jet): the bars denote maximum uncertainty	306
Figure B.6	Radial concentration at x/d = 5 (confined jet)	306
Figure B.7	Scattered light distribution in the presence or absence of cylindrical walls	307
Figure B.8	Radial distribution of scattered light (scattering from pure gases as indicated in cylinders of different optical materials)	307
Figure B.9	Axial distribution of scattered light (maximum variations indicated at different axial planes)	308
Figure B.10	Axial distribution of scattered light (confined transient Freon-12 jet)	308
Figure B.11	Detection of Rayleigh scattered light along the field of view of collecting lens (see figure 2.1) obtained by displacing the lens in increments of δ = .0375mm away from the focused beam centre	309
Figure C.1	(a) Line diagram of signal acquisition electronics (b) Flow chart of data channel select and sample	319
Figure C.2	Flow chart of measurement software	320
Figure C.3	Transition diagram of sampling routine "QUIK"	321
Figure C.4	Diagram of integrated software system "MONA"	322
Figure C.5	On-line measurement module configuration	323

NOMENCLATURE

A	constant (arbitrary)
A*	dimensionless area ratio $(d/dp)^2$
B	constant (arbitrary)
C	concentration
C_i	optical correction coefficient
C_f	signal intensity conversion factor
D	molecular diffusivity of a gas in air or total wall light transmission coefficient
E_o	voltage potential
G(f)	filter gain function
H(f)	frequency response function
H	clearance distance at TDC
$\bar{I}_g$	mean Rayleigh scattered light intensity for a gas (g)
I'_g	rms of Rayleigh scattered light intensity for a gas (g)
I_i	the i^{th} discrete Rayleigh scattered light intensity in a time series
I_o	Rayleigh scattered light intensity at a fixed reference condition (o) of pressure, temperature and concentration
I_s	Total Rayleigh scattered light intensity from an arbitrary gas mixture at arbitrary pressure and temperature
I(t)	instantaneous Rayleigh scattered light intensity (continuous signals)
J	Joules
$J_{\lambda,d\Omega}$	source function
K	instrumentation system empirical constant or kurtosis

K'	optical constant
L_c	concentration potential core length
L_u	velocity potential core length
M or MW	molecular weight of a gas (or species component)
M_o	exit momentum flux ($A\rho U_o^2$), $A = \pi r^2$
N	molecular number density (ρ/m)
N_L	Loschmidt's number
N_o	Avogadros's number
N_p or $\dot{N}_p$	photons/sec
P	absolute pressure
P(t)	time-varying absolute pressure
P_{atm}	absolute atmospheric pressure
P_{cr}	critical pressure ratio
P_p	total pressure measured by a Pitot probe
P_s	static pressure
P_u	absolute pressure at upstream conditions
P*	P_{atm}/P_u
ΔP	pressure drop
P(x)	probability of quantity x
R	universal gas constant or coefficient of reflected light
Re	Reynold's number, $dU\rho/\mu$
S	skewness
S_c	Schmidt number, ν/D
SNR	signal-to-noise ratio
St_d	Strouhal number based on exit diamter, fd/U_o

St_ρ	Strouhal number St_d scaled by the inverse of jet momentum, $fd/U_o(\rho_a/\rho_j)^{\frac{1}{2}}$
T	absolute temperature, ^oK
T(t)	time varying absolute temperature, ^oK
U, V, W	mean components of velocity along the longitudinal, radial and aximuthal directions in an axisymmetric flow, m/s
u',v',w'	rms components of fluctuating velocities along the longitudinal, radial and azimuthal directions in an axisymmetric flow, m/s
V or $\forall$	volume
X	mole fraction (percent by volume)
X_A	mole fraction of species A
X_i	the i^{th} discrete mole fraction in a time series
X(t)	the instantaneous mole fraction (continuous signals)
ΔX	the relative change in mole fraction
$\bar{X}$	mean mole fraction
X'	rms mole fraction
X'_d	rms mole fraction downstream
Y(t)	instantaneous mass fraction
$\bar{Y}$	mean mass fraction, $\frac{(\alpha+1)\bar{X}}{(\alpha\bar{X}+1)}$
Y'	rms mass fraction, $\frac{(\alpha+1)X'}{(\alpha\bar{X}+1)^2}$
a	coefficient or constant or particle radius
c	speed of light
d	nozzle diamter or particle diameter

f	frequency, Hz or KHz
Δf_{co}	frequency bandwidth (cut-off maxima)
f_o	fundamental frequency $f_o/2$ is the first sub-harmonic
g	acceleration due to gravity, 9.81 m/s^2
$\Delta^n g(x)$	n^{th} order forward difference of a time series
h	Planck's constant
k	a constant or a coefficient
k_1, k_2, k_3	spread constants for the centreline and radial mean flow properties
ℓ	optical length
m	polytropic exponent, or mass (total) or mass per molecule
m_o	mass of air oxygen atom
n	refractive index
$n(t)$	time varying refractive index
n_c	optical transmission coefficient for light collecting optics
n_L	optical transmission coefficient for light source optics
r	radial coordinate
r_e	effective nozzle radius, $r_o(\rho_j/\rho_a)^{\frac{1}{2}}$
r_{max}	radial distance of maximum rms intensity
r_o	nozzle radius
$r_{1/2}$	concentration half radius
$(r_{1/2})_u$	velocity half radius
$r_{1/2}/r_o$	spread parameter
Δr	the relative rate of change of signal amplitude

Δs	the average slope of signal amplitudes
sr	steradians
t	time
t_c	critical time
t_m	a measured time
t_r	a response time
t*	a dimensionless time coordinate, t/τ_j
t**	a dimensionless time coordinate, $k(\rho_j/\rho_a)^{\frac{1}{2}}/t^*$
Δt	a time interval, constant or random
v	voltage
$\vec{v}$	a vector field
x	axial coordinate
x_o or x'_o	mole fraction virtual origin
x_o"	mass fraction virtual origin
x_o^r	mole fraction virtual origin defined by $r_{1/2}/r_o$
x(t)	penetration distance as a function of time

Subscripts and overhead symbols:

CL	centreline
o	a reference condition
$\sim$	Favre-average
-	time-average

Greek symbols:

α	a constant or parameter $(\rho_j/\rho_a - 1)$ or $x(t)/\sqrt{t}\,\big\vert_{t_c}$
β	filter optimization parameter
δ	a small deviation in a quantity
ε	quantum efficiency
ε_o	filter frequency parameter
Ω	solid angle, sr
$\sigma(t)$	time varying Rayleigh scattering cross-section
σ	Rayleigh scattering cross-section
σ_i	Rayleigh scattering cross-section of i^{th} species
ρ_a or ρ_{amb}	density of ambient fluid
ρ_j or ρ_{jet}	density of jet fluid
ρ^*	depolarization ratio
μ	dynamic viscosity
μ_r	r^{th} factorial moment
λ	wavelength
ϕ	any instantaneous quantity
$\phi(f)$	phase function of a filter
θ	mass fraction or crank angle degrees
$\bar{\theta}$	mean mass fraction
$\Delta\theta$	crank angle interval
θ'	rms mass fraction
τ_j	jet time constant, r_e/U_o

τ_p	particle signal time
τ_R	Rayleigh signal time
$\langle\rho\phi\rangle/\langle\rho\rangle$	density weighted time-average
$\tilde{\phi}$	time-average of quantity ϕ
$\frac{\partial}{\partial\eta}$	gradient of a quantity along a coordinate η

CHAPTER 1 INTRODUCTION

1.1 TOPIC OF THESIS

The work presented in this thesis is concerned with the shear flow mixing which results from round turbulent gas jets issuing into a medium of equal or different density from that of the jet. The flows are axisymmetric and include steady and transient flow behaviour and are relevant to gas ejectors, fuel jets in combustors for marine and aircraft engines, fuel jets and sprays in internal combustion engines, and rocket engines. Improved understanding of the jet flows has been obtained by experiments with results which can also guide the development of computational methods and the formulation and calibration of turbulence models.

The purpose of the thesis is to present experimental results of velocity and concentration characteristics of round jets as described above and to report developments of experimental techniques particularly for measurements in transient and non-uniform density jets.

An outline of previous work is provided in the next section which includes a review of jet flows in terms of characteristics of averaged properties and their organised flow structures. The breadth of the review is for these characteristics as found along the initial and developed flow regions of steady and transient jets. The third section presents the approach and justification for the present work. An outline of the thesis is provided in the fourth section.

1.2 OUTLINE OF PREVIOUS WORK

Experimental investigations of jets have been many and reviews have been given by Hinze (1975), Rodi (1976, 1982), Chen and Rodi (1980), Ribeiro and Whitelaw (1980) and List (1982). Becker and Massaro (1968) report some interesting

historical notes on jet flows (dating to the mid 1800's) and much of the theory of the instability and sound generation mechanisms of jets was considered by Rayleigh (1894) in the first volume of his theory of sound. Physical understanding of the transport processes in jets has improved particularly over the last 37 years as a result of the combined developments of experimental techniques and of turbulence modelling. Jet flows, in general, are associated with three regions identified as the near field, the intermediate region and the self-preserving region which is often referred to as the fully developed jet, or self-similar region. Extensive analysis and the theory of turbulent jets has been reported by Abramovich (1963) and specific consideration of the mean profiles of turbulent jets (round, plane, radial, impinging, co-axial, annular, free and enclosed jets) by Rajarantnam (1976). More general results are summarized below and in the next sub-section. A second sub-section reviews organised flow behaviour and a third sub-section reviews transient jets. At the end of each sub-section a summary of the information presented is provided.

Ducted jets have been considered by Becker, Hottel and Williams (1963, 1967) and Otis (1976); plane jets by Bradbury (1965, 1967), Bashir and Uberoi (1975) and Pope (1984) who invluded an extensive review. Two phase (particle laden) jets have been investigated by Hetsroni and Sokolov (1971) and Subramanian and Ganesh (1984); the mixing in the interaction zone of inclined jets by Becker and Booth (1971) and jets in an opposing stream by Elghobashi et al (1981). The radial jet has been discussed and examined by Hekestad (1966) and Witze and Dwyer (1977) and jets with swirl by Morse (1980) and Gibson and Younis (1986). Free co-axial jets have been investigated by Maczynski (1961) and Durão (1971), confined co-axial jets by Habib and Whitelaw (1979) and

annular jets by Ko and Chan (1979). Round jets into a crossflow were investigated in the classic study by Crabb, Durao and Whitelaw (1981) and jet penetration in supersonic and transonic crossflow by Manela and Seginer (1986). Most of the references have emphasized the study of mass and momentum transport in near or fully developed jet flow regions. Emphasis on the near field mean flow characteristics have been given to coaxial jets by Forstall and Shapiro (1950), Durão and Whitelaw (1972), Ribeiro and Whitelaw (1976) and Ko and Au (1981); axi-symmetric jets by Isloam and Tucker (1980) and the plane two-dimensional jet and idealized mixing layer conditions by Scott and Rask (1977) and Carlomagno (1985). Detailed measurements of mean velocity, turbulence intensities and shear stresses, and particularly the exit boundary layer characteristics and their influence on the mean flow for round jets, have been reported by Davies, Barrat and Fisher (1962), Bradshaw, Ferris and Johnston (1964), Sami et al (1967), Boguslawski and Popiel (1979), Lau et al (1979), David and Davies (1979), Islam and Tucker (1980), Hussain and Husain (1980), Kibens (1980) and Zaman and Hussain (1984).

The axisymmetric, turbulent round jet is a special class of complex shear flow as discussed by Townsend (1976) and Bradshaw (1983) and with scales and characteristics as summarized by Hinze (1975), Lessen (1978) and Cantwell (1981).

The sub-section which follows presents discussions associated particularly with the averaged quantities of round, steady jets and includes consideration of the influences of jet density and initial conditions. Also concerned with steady jets is sub-section 1.2.2, but with emphasis on organised flow characteristics and similar observations for non-circular turbulent jets. The combined characteristics of averaged quantities and organised flow behaviour are discussed at the end of sub-section 1.2.2 and in connection with jet noise.

1.2.1 Averaged flow characteristics

The jet investigations have shown conclusively that the transport of vector and scalar fields in jets differ and that the turbulence characteristics of the vector and scalar are also different as suggested by the many investigations of spectra; see, for example, Batchelor (1959), Batchelor, Howells and Townsend (1959), Saffman (1960), Gibson (1963), Gibson and Schwarz (1963), Nye and Brodkey (1967), Hill (1978) and Gargett (1985) who considered the different dissipation scales of the scalar spectrum in contrast to those of the velocity spectrum. Liepmann, Laufer and Liepmann (1951) discussed the spectrum of isotropic turbulence and Antonia et al (1984) compared temperature spectra and examined the co-spectra of velocity and temperature; they showed a dependence of the temperature spectrum on the velocity spectrum. The important finding was that the temperature spectrum was influence by the u, v and w velocity fluctuations and especially near the centreline plane. Gibson and Schwarz (1963) examined the entire range of wave numbers of velocity, concentration and velocity fluctuations and considered the separate forms of the diffusivities and dissipation rates of the velocity and scalar fields; the measurements support the theories of Kolmogoroff and Batchelor. Similarly, Nye and Brodkey (1967) and Hill (1978) extended the work of Batchelor (1959), Batchelor et al (1959), and that of Gibson and Schwarz (1963) to confirm the characteristic differences in dissipation and diffusion.

Hinze and van der Zijen (1949) quantified the similarities and differences between the mean concentration, temperature and velocity fields of a free turbulent round jet and showed that the rate of spread for the scalar fields was greater than that of the velocity. Forstall and Shapiro

(1950) confirmed a similar relationship between vector and scalar fields for coaxial jets. Corrsin and Uberoi (1950) investigated velocity and temperature fields in a jet and showed the faster diffusion rate of heat over momentum and that the jet fluid density had an effect on spreading rate. Hottel (1953) discussed the structure of a round jet issuing into stagnant surroundings and presented an analogy between the transport of momentum and scalar transport. Sunavala, Hulse and Thring (1957) applied the results of Hottel (1953) to express the nozzle fluid concentration in terms of its reciprocal along the centreline and then used the concept of Thring and Newby (1953) of an equivalent nozzle diameter to evaluate an axial decay "constant" for the concentration field he analysis method of Sunavala, Hulse and Thring (1957) has been used extensively by many authors to quantify the mean characteristics of velocity, concentration and temperautre fields of round jets. Hinze (1975) has discussed the concept of Thring and Newby (1953) of an "equivalent diameter" to account for density differences and has shown that the same result can be obtained directly from an analysis of the conservation of exit momentum flux. A general velocity decay law (also accounting for the effects of density differences between the jet and ambient) has been proposed by Narain (1976) for three-dimensional jet flows, i.e. jets from circular, elliptical, triangular and rectangular orifices.

Ricou and Spalding (1961) considered the problem of entrainment in isothermal round jets with and without density differences between the jet and surroundings. They accounted for the effects of density in a similar manner to Sunavala, Hulse and Thring (1957) showing that the centreline decay of mass flux was hyperbolic and thus that the reciprocal behaviour of mass flux varied linearly with distance from the nozzle. Measurements of concentration fluctuations in a round turbulent jet were reported by Rosenweig, Hottel and

Williams (1961) and numerical predictions of concentration fluctuations by Spalding (1963). Rosenweig et al developed a novel experimental technique using smoke for a marker and detected the mean and rms concentration using light scatter principles. They compared the spectral density distributions for velocity, temperature and concentration and showed the velocity spectrum to be similar to that of the scalars but not exactly the same. They also showed that concentration fluctuations were relatively higher than those for temperature and velocity and provided evidence that analogies between concentration, velocity and temperature fields do not hold exactly. Subsequent work by Ambramovich et al (1969) and Sforza and Mons (1978) considered the mean radial spread and centreline decay of mass, momentum and temperature for jets of different densities and established the dependence of the spread of mass, momentum and temperature on density. The work of Ambramovich et al (1969) appears to be the only experimental work to consider the systematic variations in characteristics of spread of mass, momentum and temperature as affected by density ratio.

The numerical investigations of Weinstein and Todd (1963) of jets with large density ratios showed that the potential core length of a jet increased with increasing density ratio between the jet fluid and surroundings and that the potential core length was very sensitive to the initial velocity profile; they showed that changing from a flat (i.e. uniform) to a parabolic exit profile results in a marked increase in potential core length. They also predicted that the potential core length was shortened by increasing the velocity of a coaxial flow surrounding the jet and this has been confirmed by the experimental findings of Ambramovich et al (1969). Rankin and Sridhar (1978, 1981) considered the influence of initial velocity profile (uniform and parabolic) on the developing region

of laminar jets and Witze and Dwyer (1976) have considered the influence of laminar wall boundary layers on turbulent jet development and proposed a method to account for the mass and momentum defect due to the finite boundary layer thickness.

Wilson and Danckwerts (1964) reported on time-averaged velocity, temperature and temperature fluctuations in a heated turbulent jet and showed the faster spread of jets with lower density to result over those of heavier density. Becker, Hottel and williams (1967) refined the light scattering technique developed by Rosenweig et al (1961) and made measurements of the nozzle fluid concentration field of a round air into air jet; Shaughnessy and Morton (1977) also employed the principles of Rosenweig et al (1961), replacing the light source with a laser, to make measurements of particle concentration in a turbulent jet and attempted measurements of the micro- and integral-scales of the concentration fluctuations. Their work (and that of Becker, Hottel and Williams) was important in establishing that many of the atypical results reported up to that time were influenced by the measurement technique. The principal conclusions of the work by Becker, Hottel and Williams (1967) were that self-similar characteristics in mean and rms profiles of concentration were obtained by round jets and that centreline decay of mean concentration was hyperbolic in axial distance from the nozzle; similarly as established previously for the mean velocity decay. Torrest and Ranz (1970) developed a microconductivity probe to determine concentration fluctuations in round jets, multiple injection jets, a plane jet and a plane mixing zone and showed self-similarity characteristics were also established in the concentration fields determined for these flows; they reported particularly good agreement with the findings of Becker, Hottel and Williams (1967) for the concentration results of the round jet and, although not reported by

Torrest and Ranz, the self-preserving characteristics found for the plane jet by Bradbury (1965) in mean velocity and turbulence intensity were similarly present in the scalar fields reported by Torrest and Ranz of their plane jet.

Way and Libby (1971) were interested in turbulent flow with density differences due directly to jet fluid in contrast to temperature effects (and a Schmidt number of about 0.2) and used a jet of helium discharging into air to measure mean and fluctuating quantities of the helium concentration. They showed that a jet with density less than its surroundings results in increased mixing rate and higher relative intensity of velocity and concentration fluctuations in the near field and transition regions; the results show that the high frequency end of the velocity spectrum was not influenced by density and, as pointed out later by Libby (1977), the link between the relative density intensity and corresponding concentration intensity is based on mean concentration levels.

Birch, Brown, Dodson and Thomas (1978) examined the concentration field of a methane jet and critically assessed the dependence of results on experimental technique, as previously noted by Becker, Hottel and Williams (1967). Lockwood and Moneib (1982) compared scalar intensity levels obtained by different experimental techniques and showed in agreement with the conjecture of Becker et al (1967), that atypical values for both mean spread levels and intensity of fluctuations are a consequence of the measurement method. Chen and Rodi (1980) and Pitts (1986) have summarized a large number of experimental results of mean scalar and vector radial spread and centreline decay constants for equal and non-uniform density round jets and the data presented show clearly the dependence of jet spreading on density ratio between the jet and surroundings; as predicted, for example, by the earlier work of Corssin and Uberoi (1950), Thring and Newby (1953), Ricou and Spalding (1961),

Abramovich et al (1969) and Sforza and Mons (1978). More recent developments in experimental techniques have permitted the investigations of statistical characteristics of vector-scalar correlations and the study of temporal and mean flow behaviour in jets with non-uniform density; see, for example, Kinoshita et al (1978), Dyer (1979), Birch et al (1984), Pitts and Kashiwagi (1984), Schefer and Dibble (1985), Starner (1983, 1985, 1986) and Gulati and Driscoll (1986). Developments in theoretical methods have also allowed for detailed studies of velocity and scalar correlations with input from empirical results. In addition, new studies with theoretical models have been made of the properties and characteristics of turbulence intermittency and probability densities as reported by Kollmann (1984), Nguyen and Pope (1984), Givi, Sirinano and Pope (1984) and Pope (1984).

From the above review the following summary conclusions can be made for the averaged flow characteristics of steady jets:

The spreading and decay of mean and turbulent properties of jets are dependent on the density ratio between the jet fluid and ambient, ρ_j/ρ_a. As the ratio ρ_j/ρ_a increases the radial extent and centreline decay of mass momentum decrease and with opposite behaviour resulting when ρ_j/ρ_a decreases. The decay and spread of scalar fields is greater than that of a vector independent of the value of ρ_j/ρ_a.

The potential core length as well as the distance from the nozzle to the first vortex roll-up increase with increase in ρ_j/ρ_a and decrease with decrease in ρ_j/ρ_a. Jet mixing is more efficient when ρ_j/ρ_a is small. Jets with higher values of ρ_j/ρ_a show larger values for un-mixedness than those with lower values of ρ_j/ρ_a; that is, faster uniformity in mixing intensity results with lower density jets and to lower values.

There is good agreement in reported asymptotic values and constants for jets and with the similarity characteristics of the developed flow regions where most of the investigations have been carried out.

Initial flow regions to date have only been investigated in a limited number of studies and particularly lacking are measurements of both scalar and vector fields in the near field for jets with large density differences.

1.2.2 Organised flow

Jet flows have been shown to contain organised structures referred to by many authors as coherent structures. Reviews of organised motion and coherent structures in turbulent shear flows have been given by Coles (1981), Cantwell (1981), Hussain (1983), Gutmark and Ho (1983) and Aref (1983). As noted by Becker and Massaro (1968), the realization of existence, and observation, of organised structures in turbulent jets and flames dates from Leconte (1858). Visualization of the organised vortex flow patterns in the near field of round jets has been carried out by many authors including, for example, Davies et al (1962), Bradshaw et al (1964), Becker and Massaro (1968) and similarly in the plane jet by Hsia et al (1984) and in the mixing layer by Brown and Roshko (1974). Vortex formation in the near field of jet diffusion flames has also been visualized, for example, by Eickhoff and Winandy (1985) and Eickhoff (1982) has reviewed and discussed the nature of instability and organised structures in jet flames and there are interesting similarities to isothermal jets. Corke and Guezennee (1986) have considered the determination of "coherent content" in the near-wall region of a turbulent boundary layer and have proposed an objective manner by which to extract similar information from the

analysis of temporal data for other flows; coherence measurements in turbulent boundary layers have also been reported by Savas and Coles (1985). Mongal, Dimotakis and Broadwell (1984) investigated the reacting two-dimensional mixing layers and suggested that the processes of mixing and entrainment in the mixing layer are dominated by large-scale structures. In the remainder of this sub-section we outline developments in the understanding of organised flow behaviour, particularly in round jets; coherent and organised flow structures in coflowing jets have been documented by Perry and Lim (1978). Overall information is presented in the next two paragraphs followed by more detailed discussions.

The near field of uniform density round jets has been examined by Michalke and Fuch s (1975), Yule (1978), Maestrello and Fung (1979), Whiffen and Ahuja (1983), Long and Arndt (1984) and Durao and Pita (1984). Much of the emphasis by these authors has been on the nature and magnitude of naturally occurring oscillations and their amplification by external sources.

Large scale coherent flow structures have been reported in the intermittent region of self-preserving round jets by Kamori and Ueda (1985) and in the nearly self-preserving region by Tso, Kovasznay and Hussain (1981). Since the mixing layer investigations of Brown and Roshko (1974), continuing interest has remained with the organised structures in the turbulent mixing layer, where many similarities to round jet structures have been found; see, for example, Zaman and Hussain (1984), Dziomba and Fiedler (1985) Brown and Troutt (1985) and Hussain and Zaman (1985). Dziomba and Diedler (1985) documented the effect of initial conditions on the downstream development of the mixing layer and have shown similar effects result with the round jet; a disturbed initial boundary layer leads to increased spreading and entrainment and they documented the sensitivity of flow periodicity and development to (even

small) external disturbances by the flow rig.

Csanady (1963) demonstrated experimentally for a plane jet that augmentation of the near field vortical structures by external vortices resulted in broadening of the downstream (turbulent region) and hence that a jet is made to "slow" down in shorter axial distances than would result in the absence of external disturbances; Bradshaw, Ferris and Johnston (1964) drew similar conclusions concerning externally excited behaviour. However, neither Csanady nor Bradshaw et al related the effects of augmentation to improved mixing or influence on entrainment for the jet.

Davies, Fisher and Barrat (1963) experimentally determined turbulence characteristics in the initial (mixing) region of a round turbulent jet and expressed the statistical (averaged) nature of the turbulence in terms of kinematic similarities. They showed that differences existed between the local mean and convection velocities and pointed out some of the vortex features of the initial region. The work carried out by Bradshaw, Ferris and Johnston (1964) considered in detail the flow structure and turbulence features in the near field of a round jet. They explained further the convection and mean velocity differences observed by Davies, Fisher and Barrat (1963) to be due to the large eddy dominance of the near field mixing region. Clark and Kit (1980) have summarized the experimental shear layer, plane wall jet and plane orifice jet. The general indications are that the convection velocity U_c has a value of between 0.5 and 0.6 of the mean exit velocity U_o ($0.5 < U_c/U_o < 0.6$); Becker and Massaro have reported similar values and with the value of U_c/U_o for round jets remaining between 0.55 and 0.60. The ratio U_c/U_o is defined to be proportional to the wavelength λ of the vortex train or $U_c/U_o = f\lambda/U_o$ where f is the vortex passage frequency; Becker and Massaro referred to $f\lambda/U_o$ as a dimensionless wave velocity and Clark and Kit as the dimensionless vortex convection velocity.

Sullivan, Widnall and Ezekiel (1973) used a two-component laser Doppler velocimeter to measure axial and radial velocity distributions in vortex rings resulting from pulsing air through a sharp-edged orifice. They found that vorticity was concentrated in the vortex ring core for both thick core and thin core vortex rings and that the vortex rings were unstable to azimuthal perturbations; a less conclusive finding was that vorticity became more diffuse at lower Reynolds numbers. Maestrello and Fung (1979) measured the instantaneous near field pressure fluctuations of a round subsonic jet and found that a quasi-periodic structure first appears as a rolling-up of the mixing layer within one nozzle diameter and at a distance of three nozzle diameters they observed the initial periodic structure to be fully developed and with a value for the Strouhal number based on nozzle diameter d ($St_d = fd/U_o$) between 0.3 and 0.4 with the structure disappearing beyond the potential core.

Crow and Champagne (1971) performed a detailed study of the noise producing region of a round jet using Schlieren photography and hot-wire anemometry. They observed the evolution of orderly flow with increasing Reynolds number. For Reynolds number between 100 and 1000 the instability of the jet evolves from a sinusoid to a helix and finally to a train of axisymmetric waves; theoretical treatment of large scale eddies in the jet near field is given by Liu (1974); Petersen (1978) studied the influence of wave dispersion on vortex pairing and Plaschko (1979) the helical instabilities. At a Reynolds number of about 10000, the boundary layer of the jet is thin and Crow and Champagne (1971) observed two kinds of axisymmetric structures:

(i) surface ripples on the jet column which scale with the boundary layer thickness and become shorter as the Reynolds number approaches 10^5

and (ii) a train of large scale vortex puffs, the structure of which remains consistent and define an average Strouhal number St_d of about 0.3; the large scale puffs superimposed themselves on the surface ripples.

When external periodic surging of the jet was made, the surface ripples were suppressed. Moreover, with surging, the entrained volume flow increased 32% over the unforced case, and as noted above, this increased entrainment effect was not reported by Csanady (1963) or Bradshaw et al (1964). Crow and Champagne found that when they forced the jet at the exit with Strouhal number of $St_d = 0.6$, a violent subharmonic resulted at $St_d = 0.3$ which further resulted in a significant increase in jet spreading angle. One of the important findings by Crow and Champagne was that as the Strouhal number goes below 0.45, a forced wave becomes highly dispersive and attains an amplitude large enough to break-up the jet column; forcing serves to effectively shift the virtual origin of the jet upstream and thus lead to increased entrainment and spread nearer to the nozzle. Hasan and Hussain (1982) have also documented the increased entrainment of excited jets and have emphasized the importance of initial conditions.

Other important findings by Crow and Champagne were that the fundamental and subharmonic together dominate the first six jet diameters and then fall to zero and that the Strouhal number, defined at the end of the potential core, is associated with the remaining dominant vortex frequency and thus this defines the 'preferred mode' of the jet.

Michalke and Fuchs (1975) performed a theoretical and experimental investigation of the noise produced by the mean flow turbulence interaction of a circular subsonic jet (Reynolds number of about 4×10^5). They reported that the large structures formed in the near field contributed to the

far field jet noise and showed that axisymmetric wave-like pressure components existed in jets. The scale of the coherent structures λ was found by Michalke and Fuchs to be roughly proportional to the local width of the shear layer, this fact was first emphasized by Laufer, Kaplan and Chu (1974). Michalke and Fuchs also found the convection velocity of the vortex structures to be $U_c = 0.65U_o$ or from $St_d = fd/U_o$, the scaling of λ with d is given by $\lambda/d = (U_c/U_o)/St$ or $\lambda/d \sim St^{-1}$.

Yule (1978), Yule and Chigier (1979) and Chigier and Yule (1979) reported on coherent structures in round jets and in turbulent flames from round fuel nozzles. Yule (1978) found, for an air jet over a range of Reynolds numbers of 7.1×10^3 to 2.1×10^4, that the Strouhal number increased with increase in Reynolds number; in all cases Yule found the Strouhal number to be between 0.35 and 0.45 when defined at four diameters from the nozzle exit. The spectra reported by Yule showed consistently that, within the first six nozzle diameters, a fundametnal frequency gave way to a subharmonic which defined a Strouhal number $St_d \simeq 0.3$ by around six nozzle diameters.

Sreenivasan, Antonia and Britz (1979) observed in the far field of a heated round jet well-defined patterns in the turbulent signals at both moderate and high Reynolds numbers. They associated the organised signal patterns with well-defined flow patterns and the temperature fluctuations, as represented by the signal rms intensity, were analysed to be typical of a region of maximum production of turbulent energy. Sreenivasan et al concluded that, in spite of the limitations of single point measurements in obtaining information about three-dimensional structures, it was reasonably clear that large scale patterns or excursions in turbulent signals arise when large scale structures cross the measuring probe. They suggest that

the large turbulent structures carries a significant part of the Reynolds shear stress.

Chevray and Tutu (1978) used a heated round jet where the temperature was a dynamically passive scalar and reported that large scale turbulent motions were responible for the bulk momentum and heat transport; the same conclusion was proposed by Mungal, Dimotakis and Broadwell (1984). The investigations of Chevray and Tutu showed that small scales are more efficient in transporting heat than in transporting momentum.

As noted by Zaman and Hussain (1980) for a laminar boundary layer at a jet exit, pairing of vortex rings is stable and occurs regularly in space and time for Reynolds numbers below 50000 but the pairing process becomes intermittent with increasing Reynolds number or fluctuating intensity in the initial boundary layer. Further discussions are given by Hussain and Zaman (1981) and Hussain (1983) where it is suggested that two length scales exist in the near field of the round jet. The first is the shear layer thickness, θ, and the second the jet width. For an unexcited, laminar axisymmetric shear layer, a natural instability has been defined as $0.017 > St_\theta > 0.011$ where $St_\theta = f\theta/U_o$. The value of $St_\theta = 0.017$ is associated with what Hussain has termed a maximum amplification rate and the value 0.011 with maximum amplification. It has also been proposed by Hussain that the natural instability is a result of some kind of "feedback" from downstream coherent structures which are involved in triggering the instability.

Kalghatgi (1980) used a laser based technique to investigate the vortex structures in the near field of air and CO_2 jets. He suggested that the heavier the jet fluid was relative to ambient fluid, the nearer the convection velocity U_c of the structures was to the jet exit velocity U_o and that the asymptotic value of U_c was approached closer to the nozzle exit in contrast to investigations

where the density of jet and ambient fluid were the same. Olsen and Wasserbauer (1980) considered the effects of temperature on jet noise and found that increased temperature resulted in a small decrease in sound level and caused only a small shift in the spectra.

Sarohia and Massier (1980) investigated the effect of density on noise radiated from subsonic jets and showed that a direct role was played by density in the flow development and radiated noise. Using helium and nitrogen, they were able to interchange the role of density and found that the centre flow displaced the annular mean profile, was dependent on the centre flow momentum flux ρU_o^2 and that the entrainment of low density centre flow was much greater than the high density centre flow. They concluded that a denser gas leads to less noise and that the directional pattern of radiated noise is dependent on the density of the jet. From the work reported by Kalghatgi (1980), Olsen and Wasserbauer (1980), Sarohia and Massier (1980) and Hussain (1983) it is clear that the many investigations of jets, their organised structures and the influences of near field on the far field and vice versa, have not established means to reduce noise from jets or to control acoustic interactions. For instance, during the initial launches of NASA's space shuttle Columbia, acoustic feedback was monitored in the structural stability data of the shuttle prior to lift-off and the cause was traced to a standing acoustic wave resulting from the blast of the rocket engines (highly turbulent jets) against the launch pad. The practical solution was to reshape the launch pad in a slight wedge and flow large amounts of water beneath the rocket engines to result in incoherent wave patterns.

Literature dealing with control and understanding of jet flows and noise includes, for example, Bradshaw et al (1964), Schaffar (1979), Nelson et al (1981), Durbin (1983), Long and Arndt (1984), Seiner and Yu (1984), McGowan and Larson

(1984) and Whitaker and Morrison (1984). These authors have considered the turbulence characteristics, correlation between centreline velocity fluctuations and far field noise, the fluid dynamics of flow excited resonance, aerodynamic noise in moving media (and from a spreading jet), noise at low Reynolds numbers and high speed subsonic jets, and acoustic near field properties. More basic results and developments in control of jet mixing, noise reduction and turbulence suppression have been reported by Hill and Greene (1977) who discovered the "whistler nozzle", Hasan et al (1984) who have used the whistler nozzle in attempts to modify jet noise, Hussain and Hasan (1985) who have noted reduction in jet noise by suppression of turbulence and Zaman (1985) who has investigated far field noise similarly to Hussain and Hasan (1985) and Kibens (1980).

The above review of organised flow characteristics in steady jets can be summarized as follows:

Round jets have been shown to have a preferred mode which is associated with frequences corresponding to Strouhal numbers ($St_d = fd/U_o$) of 0.3 to 0.65. By preferred mode it is meant that, under the combined effects of linear and non-linear dynamics, a maximum amplitude of u'/U_o results in the near field of the jet; u' is the rms of the fluctuations in longitudinal velocity. The Strouhal number range referred to has been shown to apply to both excited and unexcited (i.e. natural) jets; provided in the case of excited jets that the excitation amplitude is small. There have been suggestions, however, that the natural preferred mode of the jet can occur at higher Strouhal numbers and Hasan and Hussain (1982) proposed that a condition for stable vortex pairing near the jet exit was associated with $St_d \sim 0.85$.

In many of the studies reviewed, excitation of the jet has been carried out in order to isolate and enhance the

preferred mode characteristics and thus simplify the study of the flow structure. The effects of excitation on mean flow are to increase the jet spread and the centreline velocity decay rate (represented by an upstream shift in virtual origin). The effects on entrainment rate require further study.

The overall results indicate the initial entrainment of irrotational surrounding fluid (Stewart, (1957)) into a jet results from the shearing action of the moving jet boundary and the consequence of this is a circumferential vortex pattern formed about a distance of one nozzle diameter from the exit plane. The vortex pattern remains fairly axisymmetric and stable in the azimuthal direction up to around three nozzle diameters where entanglement degenerates the symmetry and the chaotic form of turbulence results by a distance of about six nozzle diameters. Even when jets are excited to enhance the vortex formation, the symmetry of the vortex structures is only maintained up to about eight nozzle diameters away from the exit plane. The formation of near field vortex structures is independent of the exit shear-layer thickness. While it is likely that initiation of the vortex structures, and their association with shear layer growth, may stem from shear layer instabilities (very steep velocity gradients), an exact explanation of the mechanism is not yet available. Much remains unanswered with respect to the role of organised flow features in dominating the transport of heat, mass and momentum; only a limited number of experiments have noted the importance of organised structures in global transport and this has been in developed flow regions, Chevray and Tutu (1978), Sreenivasan et al (1979) and Mungal, Dimotakis and Broadwell (1984). Of more importance, however, is the lack of evidence to support the extension of findings in constant density jets to jets with substantial density differences. Way and Libby (1971) appear

as the only ones to report spectra for such a case (a pure helium jet discharging into air) but their measurements were made at low Reynolds number (3300) and at centreline locations towards the developed flow regions.

An appropriate remark concerning organised (coherent) flow structures appears to be that care should be taken with the interpretation of signals and statistics which show systematic features or regularity in form as they may or may not be physically significant. Thus the study of organised flow characteristics should follow with careful physical insight.

1.2.3 Transient jets

There have been fewer investigations of transient jets due in part to experimental difficulties. Transient (i.e. impulsively started) jets have received attention in connection with the fuel injection process in engines and gas ejectors. There have also been some fundamental studies but these have emphasized the modelling of start-up flow behaviour, Turner (1963). In the remainder of this subsection, review is made of the averaged flow and that of the time dependent characteristics of transient jets; generally, round jets are considered.

Hopkins and Robertson (1967) presented experimental and analytical results for the penetration of steady and unsteady liquid jets with equal and unequal densities to that of the ambient. The results showed that for the steady state penetration process (that is, the time after which the jet forgets its transient start-up), the jet velocity is much greater than the opposing stream velocity and, with unsteady penetration the velocity of penetration is less than one-half the jet velocity. Turner (1962) notes similar observations for the

starting plume. Hopkins and Robertson showed that the effects of different jet and ambient density could be accounted for by the square root of the density ratio and this is equivalent to scaling of the jet velocity with momentum, as in steady jets.

Phillips (1972) reported on the ignition of transient gas jets and showed high speed Schlieren photographs of the transient jet process for ignited methane jets. It is interesting to note the similarity of the near field vortex structures to those reported for steady jets and, by comparison to Phillips' results of non-ignited jets (where the density is greater than in the ignited jets), the increase in radial growth and slower penetration. Tanabe et al (1982) presented results for the impulsively started hydrogen jet and found that the penetration of the jet tip was defined by $x(t) = At^{\frac{1}{2}}$, where A was determined to be a function of the injection pressure. Their study appears to be one of the first to attempt measurements of instantaneous gas concentration and mean and rms of concentration in a transient jet. The conclusions of Tanabe et al were that the time-averaged concentration distributions in a transient jet were similar to those in a steady jet and that the initial growth and spread were greater.

Abramovich and Solan (1973) studied the initial development of transient laminar jets ($80 < Re < 500$) and their results show similar differences in velocity between the advancing front and steady jet as observed by Hopkins and Robertson (1967). Abramovich and Solan also proposed a universal scaling of the time and distance coordinates and this was discussed extensively by Kuo (1982), Kuo and Bracco (1982) and Kuo, Syed and Bracco (1986) who have additionally proposed a "universal curve" for the penetration characteristices of transient jets.

Studies involving transient gas jets from single and multiple nozzles have been reported by Ginzburg and

Ugryumov (1975). The effects of density on supersonic transient gas jets have been reported by Naboko et al (1977) and they showed that increasing the jet density results in an increase in penetration rate (using co-ordinates for time and distance which account for the density differences through the square root of density ratio) and that penetration distance scaled with time as $x = Bt^{\alpha}$. Naboko et al also presented plots of the density distributions in their non-stationary rarefied Ar and N_2 jets which show similar agreement to the characteristics of steady jets; as similarly noted by Tanabe et al (1982) with their hydrogen concentration measurements. Skibenko et al (1976) studied pulsed supersonic gas jets and showed radial distributions of mean density were also similar to those of steady jets (i.e. nearly Gaussian); their investigations were motivated by the need to develop a pulsed gas dynamic source of neutral particles for application in experiments of plasma physics; see also Musinski (1982) and Topham et al (1984).

Witze (1980) and Tanaka (1984) have considered the velocity and penetration characteristics of turbulent air-into-air jets. Witze has discussed the problems of measurements in transient jets and proposed that it was justified to treat transient jets as quasi-steady; that is, that after the initial transient of an impulsively started jet, the flow properties can be ensembled as in a steady jet. One of the most important findings of Witze (1980) was the definition of a jet time constant τ_j which he defined as the ratio of nozzle radius to exit jet velocity and showed that τ_j could uniquely characterize the behaviour and similarity of impulsively started incompressible jets. Bremhorst and Harch (1980) investigated the near field of transient air jets and established that similarity in radial mean and rms velocity existed for transient jets as in steady jets. From their studies, and those of Binder and Favre-Marinet (1973), Platzer, Simmons and Bremhorst (1978), Bremhorst and Harch

(1978), Favre-Marinet, Binder and Hac (1981) and Parikh and Moffat (1982), it is evident that faster entrainment and increased mixing rates result for transient jets over steady jets in the near field which thus leads to faster spread and mixing. Parikh and Moffat reported a similar vortex structure at the jet exit as found in steady jets when their jet was pulsed at a resonant frequency.

Transient jet behaviour is characteristic of the liquid fuel injection process as found in reciprocating engines and studies have been made to understand the jet tip penetration characteristics and with some analogies drawn to steady and transient gas jets, see, for example, Wakuri et al (1960), Dent (1971), Melton (1971), Hay and Jones (1972) and Yule et al (1985).

Similar investigations of noise from transient jets have been carried out as in steady jets and with examination of the spectral characteristics showing higher energy levels for the transient jets. One of the interesting findings is that the noise produced by a pulsed jet is composed of high frequency broad-band noise and low frequency tones at the pulse frequency and its harmonics. These findings, and similar problems of instability,as discussed for steady jets, have been reported by Anderson and Williams (1968), Middleton (1970), Hoggarth and Jones (1973), Bremhorst and Harch (1974), Hooker et al (1974) and Hooker (1981).

As is evident from the review of the transient jets, they have many characteristics similar to those of steady jets, particularly the characteristics of similarity in mean and rms profiles. One of the greater differences between steady and transient jets is the increased rate of spread and mixing which results for the transient jets. While the investigations which have been reported indicate many similarities inclusive of observed vortex formation at the exit plane, detailed measurements remain to be made to system-

atically consider the effects of jet density, initial conditions as result from nozzle geometry, and the interaction of ambient conditions on the consequent jet flow development, for instance: swirl, co-flowing streams, confinement etc.

1.3 PRESENT CONTRIBUTION

As was made clear in the last section, experimental work is needed to extend knowledge of turbulent mixing of uniform to non-uniform density shear flows; round jets offer a particularly attractive environment for such studies since they encompass features and scales typical of complex shear flows. The fundamental importance and nature of jet flows continues to be established but their application in practical environments requires understanding of the effects of the ambient environment on the jet; in-situ investigations are thus necessary. One important area is in internal combustion engines where there are complex interactions of many variables and further understanding is required of the mixing of a fuel jet with in-cylinder air prior to combustion. The number of experimental studies involving jet flows with substantial density differences has been few and no detailed studies of the velocity and concentration fields of the near field of variable density jets have been made for either steady or transient jets.

The contribution of this thesis is to the understanding of the steady jet flows which result from round nozzles discharging into still ambient air and the unsteady jet flows in the simulated pre-combustion air motion in reciprocating engines. The emphasis is on the near field flow and on the effects of uniform and non-uniform density jet fluid on the consequent mixing, spread-

ng, organised flow characteristics and scaling of the jet.

Measurement techniques have been developed to improve measurement accuracy and to allow measurements which would not otherwise have been possible. The techniques include laser Rayleigh scattering, laser velocimetry and photodiode arrays, which have [redacted] permitted non-intrusive measurements of concentration and velocity fields and of transient jet tip penetration characteristics.

1.4 OUTLINE OF THESIS

The work of the thesis is presented in the following six chapters. In Chapter 2 a laser Rayleigh scattering system is reported along with developments to signal analysis. Chapter 3 presents and discusses measurements of averaged quantities of velocity and concentration, and their spectrum, in the near field of round gas jets of uniform and non-uniform density. Chapter 4 and 5 report similar information for transient gas jets discharging into simulated conditions of the in-cylinder air in a reciprocating engine. The studies in Chapters 4 and 5 use a non-compressing and compressing model Diesel engine, respectively. Chapter 6 presents and discusses measurements of the tip penetration of transient gas jets with non-uniform density and discharging into still air and the scaling of the penetration characteristics is considered. Chapter 7 summarizes the more important conclusions.

CHAPTER 2 A LASER RAYLEIGH SCATTERING SYSTEM

2.1 INTRODUCTION

The basic principles of Rayleigh scattering are considered in detail by Fabelinskii (1968), Kerker (1969), van de Hulst (1981) and Barron (1982). These authors discuss the fundamental theory proposed by Lord Rayleigh (1871) as to the light scattering from small particles and subsequently proposed by Rayleigh (1899), from molecules. Tyndall (1869), with aerosols and smogs, attempted for some time to deal with the question which motivated development of Rayleigh's theory (1871) in order to answer: why is the sky blue? Rayleigh proposed a simple explanation based on a single dipole electrostatic model and showed that the scattered light intensity I_s from small particles was proportional to the incident light intensity I_o and inversely proportional to the fourth power of the incident light wavelength, λ; thus, the often quoted law of $I_s \alpha\ 1/\lambda^4$. Dimensional arguments show that the scattered light is also proportional to the square of the scatterer volume or that, if a characteristic length (say a diameter, d) is considered, the further relationship of proportionality to the sixth-power of scatterer size is established, or $I_s \alpha I_o d^6/\lambda^4$.

Rayleigh's theory is valid so long as the incident light wavelength is much greater than a characteristic size of the scatter particles (i.e. $\lambda >> d$). As reported, for example, by Kerker (1969), a requirement thoroughly investigated for the validity of Rayleigh's theory is the criterion between size and wavelength $d/2 \leqslant 0.05$. There is also an absolute minimum limit for Rayleigh scattering and this corresponds to density fluctuations in thermal equilibrium. Brillouin and Raman scattering losses tend to become negligible as the absolute minimum of Rayleigh scattering is approached and an account of these effects is given by Landau and Lifshitz (1960). As noted by Pitz et al (1976), Robben (1976) and Pitts and Kashiwagi (1984) and discussed by, for example, Fabelinskii (1968) and Barron (1982), radiation scattered by gas molecules

is spectrally broadened due to molecular translational motion and an evaluation of this broadening (assuming translation equilibrium) can be used to derive temperature information in turbulent flows but this will be bounded by the minimum limit for Rayleigh scattering.

For linearly polarized incident light, the scattered light at 90^{o} to the plane of polarization remains polarized and is 94% elastic (i.e. 94% unchanged in incident frequency) and not as sometimes suggested in the literature that Rayleigh scattering is the elastic scattering of light (i.e. no shift in frequency). While many experimental investigations to prove the validity of Rayleigh's theory were carried out, in particular during the 1960's with the advent of lasers*, its first application to a turbulent mixing problem appears to have been made by Graham, Grant and Jones (1974) who studied a turbulent, methane jet diffusion flame. The work of Robben (1976) assessed the feasability of using laser induced Rayleigh light scattering to study flows at turbulent frequencies up to 10^{4}. Pitts and Kashiwagi (1984) have reviewed the subsequent technological developments.

Table 2.1 gives a summary of basic and applied work involving Rayleigh scattering and other optical methods for measurement of scalar quantities; the emphasis is on the study of turbulent flows. The work of Becker (1976) provides the most rigorous assessment of the problems of light scatter experiments. Becker's work addresses the important problems of noise, optical interference and signal interpretation and, in particular, the statistical deconvolution of problems of electronic and optical noise. To date the work of Pitts and Kashiwagi (1984) has provided the most complete assessment

* George et al (1964) were the first to report measurements on the angular dependence of Rayleigh scattering using a laser. The results showed anomalous effects with respect to the theory. These were later confirmed by Watson and Clark (1965), however, to have been due to experimental difficulties; see also Rudder and Bach (1968)

of the application of laser Rayleigh scattering to the study of mixing in turbulent, isothermal flows.

As shown by the summary of Table 2.1, the development of optical probes has made possible the non-intrusive measurement of important scalar quantities such as instantaneous values of species concentration, temperature and density and their statistical characteristics in a variety of isothermal and combusting flows. In practice, however, all the techniques have limitations which can restrict their application and accuracy and these are associated with signal strength, purity and cleanliness of the flow field and considerations of temporal and spatial resolution.

As is well known, one of the major drawbacks of laser Rayleigh scattering (LRS) is the errors which can result in the interpretation of signals when particles greater than a given size occur in the measurement volume and the problem has been discussed by Graham (1979), Dibble et al (1981), Takagi et al (1982), Leipertz (1982) and Arcoumanis et al (1984). As a result of particle scatter interference, the application of LRS has been restricted to flows with clean coflowing streams or to confined flows where the intake gases can be filtered and, even under these conditions, the particle presence cannot be eliminated. The problem of particle-scatter interference can arise with particles larger than about 0.05λ in the observation volume, where λ is the incident beam wavelength. In free, coflowing and confiend flows, arbitrary numbers of particles exist that meet this criterion and their detection in the LRS signal will depend on their trajectory through the Gaussian beam intensity. In complex flows, such as free reacting and non-reacting jets and as found in combustor rigs and internal combustion engines, reduction in the number of particles is less easily accomplished and difficulties resulting in LRS measurements require the use of methods such as those described here.

It is interesting to note that the recent work by Haumann and Leipertz (1984) suggests that Mie (particle-scattering) contributions will be characterized by frequencies "substantially higher" than those corresponding to the molecular (Rayleigh) scatter. These authors have used a form of Rayleigh scattering photon correlation and their conjecture of the frequency characteristics is not generally applicable.

In the present Chapter, interest is in the signal processing problem associated with particle-scatter interference in the LRS signals and its removal by direct digital filtering techniques without the added efforts of correlation techniques. Two simple yet effective methods of digital filtering are presented and the results discussed with reference to measurements in a free turbulent jet. The design of any filter requires that a critical assessment be made of its purpose and function. Discussions as found, for instance, in the work of Piersol (1971), Otnes and Enochson (1978) and Chatfield (1984), should make clear the many difficulties which can arise. Most important is that the choice or design of any filtering operation should, with minimal bias, aim to achieve a practical solution to a specific problem; it is not possible to conjecture, therefore, that any one attribute of a problem or solution will be by itself complete. The specific problem here is differentiating between signals due to laser light scattered from molecules and that from particles.

In the following section, the experimental system and measurement objectives are described. The third section describes signal detection criteria and the digital filters developed along with their application and a fourth section presents and discusses typical results. Concluding remarks are made in the final section.

2.2 EXPERIMENTAL SYSTEM AND MEASUREMENT CONSIDERATIONS

2.2.1 Measurements

The measurements to be reported in Chapters 3, 4, 5 and 6 include ensembled averaged and instantaneous species concentrations as detected in binary gas mixtures using LRS. The LRS system used to achieve the measurements is discussed in detail below and instrumentation arrangements have been made to permit measurements in steady and unsteady gas jets discharging into quiescent atmospheric air and for unsteady gas jets discharging into conditions of the compressed air in the cylinder of a model Diesel engine. The three parameters which will influence measured LRS signals are: species concentration, the ambient pressure and the ambient temperature. The general relationship between these parameters and the detected scattered light intensities (see, for example, Graham et al (1974)) is given by

$$I_s = \frac{KP}{T} \Sigma \sigma_i X_i$$

where K is an experimental constant, P and T the absolute pressure and temperature, X_i the mole fraction of the i^{th} species and σ_i the respective Rayleigh scattering cross-sections. The equation for the scattered light intensity I_s is considered in detail in Appendix A with explicit form given for the different measurement conditions and the computation of the quantities of mean concentration, variance, skewness and kurtosis. In the present chapter, the scattered light intensities result from measurements made in an isothermal, binary mixture formed by a steady turbulent jet of Freon-12 vapour (Reynolds number of 16900) issuing into room air; the jet and flow configuration (and fluid mechanics) are described in detail in the next chapter. The interest in the present chapter is, as noted, with the removal of particle

scatter interference from the LRS signals. The problems of photon statistics as discussed by Pike (1969) and those of photomultiplier noise as discussed by Robben (1971, 1976) and Becker (1976) are dealt with here in the same manner as reported by Pitts and Kashiwagi (1984) and as presented in Appendix A.

The LRS results obtained in the Freon jet are compared with the mean Freon mole fraction distributions additionally obtained with a gas sampling probe under isokinetic conditions and used in the manner described by Crabb and Whitelaw (1979), and others, with an uncertainty in the exit plane of the jet of $\sim$1.5%. The mean mole fraction results $\bar{X}$ are compared for the unfiltered LRS signal, the filtered signal based on amplitude criteria (Arcoumanis et al (1984)) and the new methods reported in Section 2.3 below. The time-averaged rms values of the concentration fluctuations $\bar{X}'$ determined by the optical probe for both filtered and unfiltered signals are also compared. We note that an absolute comparison of mean values obtained with the LRS and those by the sampling probe is not strictly valid since, even under isokinetic conditions the probe results tend toward a density weighted average, i.e. $\langle\rho\phi\rangle/\langle\rho\rangle \neq \langle\phi\rangle$, where ϕ is an instantaneous scalar property; in contrast, the optical probe detects the volume time-average $\langle\phi\rangle$. An assessment of the differences between results of the pdf from the probe and optical method indicates differences up to 10% of unity, but proper selection of sampling probe size and a suction rate close to isokinetic can reduce the differences between $\langle\rho\phi\rangle/\langle\rho\rangle$ and $\langle\phi\rangle$ to around 2% of unity.*

2.2.2 Optical and signal processing systems

A diagram of the LRS system optical arrangement and signal instrumentation is shown in Figure 2.1. An argon-ion laser (Spectra-Physics 164-06) was operated at either 488.0

* Note that the 2% is not a generalization, but is applicable to the results here. There are cases where (for instance, in a premixed flame) $\langle\rho\phi\rangle=1.5\langle\rho\rangle\langle\phi\rangle$ as can result from use of different measurement techniques. Attempts must therefore be made to obtain a true time-average before comparing to LRS results.

or 514.5nm and over a range of power between 0.5 and 1.0W; for the results of this chapter the laser was operated at 514.5nm and 0.7W. The laser provides a vertically polarized beam with an exit diameter of around 1.5mm. The beam was first expanded to 4.5mm using a 3x beam expander (Spectra Physics) and passed through a half-wave retardation plate (Ealing, 33-3211), to rotate the plane of polarization to horizontal, and focused to a beam waist diameter of about 100μm over a length of 1mm with a 200mm focal length lens (L_1). The laser beam after propagating through the flow is dumped into a light trap. The scattered light was collected with a 300mm focal length lens (L_2) over a solid angle of 0.071 sr and at 90 degrees relative to the observation volume and plane of polarization. The collected light was passed through a rectangular slit arrangement (1mm x 0.1mm) at the entrance to the photomultiplier (EMI 9816B having an S20 cathode and operated at 1400VDC); the dimensions of the slit defined an observation volume of $0.005mm^3$ based on the half intensity diameter of the incident beam; the 0.1mm slit dimension was parallel with the beam. Prior to entering the photomultiplier (PM) the collected light was optically filtered by a 10nm interference filter (Melles Griot) centred at the incident wavelength with indicated maximum optical transmission by the supplier of 63%. The filtered light was focused with a 25.4mm diameter lens (L_3) through a 500μm pinhole. The power supply for the PM was a Brandenburg model 2475R. The anode current was converted to a voltage with a 1 MΩ high precision resistor and input to a variable band-pass filter (Krohn-Hite model 3200); the typical cut-off frequency range used was 2KHz to 5KHz. Output from the filter was input to be visualized into an oscilloscope. The signal was then amplified and digitized at a rate of 30KHz and sampled at a variable frequency (26KHz max) by a micro-computer. Sources of error and uncertainty are discussed in Appendix A and problems associated with optical interference in Appendix B.

2.3 SIGNAL CHARACTERISTICS AND FILTERING

2.3.1 Characteristics and detection criteria

Figure 2.2 shows typical light scatter intensity distributions, obtained in digital form, at two near field locactions in a turbulent jet; one is towards the shear layer (Figure 2.2(a)) and one in the inner region associated with large scale structures (Figure 2.2(b)). The random arrival of particles can readily be seen as indicated by the cases when the amplitude of signals clearly exceed full scale. Particle presence, however, can also be observed for cases with amplitude comparable to the molecular scatter (see also Arcoumanis et al (1984)). Detailed photographic studies of the photomultiplier output as visualized on an oscilloscope, have been used in the present work and combined with digital results such as those of Figure 2.2 to identify further relevant signal criteria. Typical traces of signal output visualized on an oscilloscope are shown on Figure 2.3.

For isothermal gas mixtures, only one criterion is absolute and sufficient to infer particle-scatter (or other sources) being present in the LRS signal and that is:

(i) a scatter intensity is due to sources other than scattering from gas molecules when its amplitude exceeds the maximum amplitude determined for the scattering from the gas in the mixture with the largest Rayleigh scattering cross-section.

This can be established by calibrating the scatter intensity from each single gas. In contrast, for those cases when Rayleigh scattering is used for temperature measurements, the maximum would be associated with total mixture scattering at the lowest temperature (usually ambient).

Two weaker criteria can be inferred by the results of Figure 2.2 and these are:

(ii) the initial rise in signal amplitude appears greater for particle-scatter than for the molecular scatter, and

(iii) the subsequent rate of fall in amplitude is also greater but the time of return of the signal to the molecular scatter level will be dependent on the finite recovery time for the photomultiplier as well as the particle transit time.

From (iii), frequency criteria cannot be employed as the only basis for detecting particle scatter since, as shown by Figure 2.2, the characteristic times for the Rayleigh scattering can be less than, equal to or greater than those characteristic of the particle signals and clearly the SNR will further affect these results. The most difficult problem arises when the particle scatter amplitude tends toward the same level as results from the molecular fluctuating intensities and it is with this problem that particular interest lies (Figure 2.2(b)).

Particle-scatter detection in the measured photomultiplier output is dependent on the particle trajectory through the focused beam. Since the beam intensity distribution for laser light is Gaussian, partial beam crossing by particles sufficiently far from the beam centreline will go undetected but, when particles are sufficiently close to the beam centreline, some or all of the above criteria may be satisfied to an extent which will depend on particle size. For further details the reader is referred to the papers of Chew, Kerker and Cooke (1977(a), (b)) where an attempt has been made to deal theoretically with this optical detection problem. We note further that aspects of particle dynamics and optical detection are relevant to the present work, as discussed by Saffman (1962), Kerker (1969), Snyder and Lumley (1971), George and Lumley (1973), Melling and Whitelaw (1975), Becker (1976), Shaughnessy and Morton (1977), Nir and Pismen (1978), van de Hulst (1981) and Durst (1982). These authors have considered the various problems of particle motion in gases

and the detection of size, distribution and concentration; in particular the problem of random particle entrainment and size relative to the flow dynamics and optical detection. It is important to note that size range cannot be discriminatd by the filters described below, but only characteristics of the signals with attributes as described by the criteria (i), (ii) and (iii) above.

2.3.2 Filtering

2.3.2.1 Amplitude filtering

In the work of Arcoumanis et al (1984) a filter based on amplitude was described. This filter, defined by

$$I = \alpha I(t) \qquad (2.1)$$

where $I(t)$ is the instantaneous detected scatter intensity and α a parameter equal to zero or unity, was used to minimize the contributions of particle-scattering in the LRS signal. In practice, the LRS signals obtained for a measurement location, were processed on-line in order to establish if the amplitude of any of the signals is greater than a pre-determined threshold. When a signal in a particular series being checked was found to exceed the threshold, it was rejected from the series (α=0) and the assumption made that a symmetric number of the detected intensities immediately before and after the one found to exceed the threshold were also associated with the particle signal. The selection of a threshold amplitude and number of signal values associated with particle-scatter were made a priori and follow from a best estimate basis arrived at by examining a sample of the digitized photomultiplier output. (Figure 2.2 illustrates typical designations of threshold and particle time scales, τ_p, used to apply the filter).

For example, a maximum amplitude for the molecular scatter intensities at a given measurement location was estimated by visually examining the digitized photomultiplier output and thus it is supposed that scatter intensities detected above the visually determined maximum are due to contributions from sources other than molecular scatter. The estimate of the symmetric number of detected intensities associated with particle signal was arrived at in the same way and kept constant once established for the particular measurement location. As noted by Arcoumanis et al (1984), detected intensities associated with what appeared to be particle-scatter may be below the selected threshold, and were not removed by the filter and an estimate of the mean uncertainty was reported to be around 10% of unity for measurements toward the edges of their fuel jet where particle entrainment was expected to be greatest. A further assessment of this filter is given below.

Mean and rms values of the mole fraction concentration in the free jet of Freon issuing into room air are shown in Figure 2.4 and were obtained with this filter. Values of mean concentration obtained from a sampling probe are also shown on the figure together with those defined by the unfiltered LRS signal and the amplitude filtered signal. The rms of the concentration fluctuations based on the amplitude filtered LRS signal may also be compared with that obtained from the unfiltered signal. The mean values are up to 20% of unity higher than the probe measurements when filtering was not used and about 10% higher when it was. The rms values indicate that the unfiltered signal has absolute values between 3% and 7% higher than the filtered signal, depending on the radial location of the jet. It can be expected that the rms of the amplitude filtered signal will be higher than it should be when particle-scatter contributions remain embedded in the LRS signal (for example Figure 2.2(b)).

2.3.2.2 Initial rise filter

The filter described in this section makes use of the rapid rise time observed for particle signals. This initial rise filter was developed on the basis of the average slope characteristics of the signal.

The average slope for a trace of digitized signal X_i representative at each flow location where a measurement is made is computed and then used to define a filter. For a constant sampling time interval Δt, the magnitude of the average slope for N signal values is defined by

$$\Delta s = 1/N \Sigma |X_{i+1} - X_i| , \quad i=1 \text{ to } N-1 \qquad (2.2)$$

In addition, a parameter ε is then defined by

$$\varepsilon = \varepsilon_o \Delta s , \quad \varepsilon_o > 0 \qquad (2.3)$$

where the choice for ε_o determines the frequency characteristics of the filter.Figure 2.5 demonstrates the use of the filter for the case of ε_o=0. As shown by the figure, when an interval defining two minima and a maximum is found, the two quantities ΔX_1 and ΔX_2,as defined on the figure, are calculated. The calculation is made for all min-max-min sections of the time series formed by the scatter intensities X(t). If the condition is such that $\delta.\Delta X_j > \Delta s$, for j=1,2, and where δ is chosen to define the tolerance of deviation for ΔX_j from the average slope Δs, the signal values defined by either interval $m\Delta t$ or $(n-m)\Delta t$ are rejected. Usually δ is set constant throughout the filtering of the signal and we have found that the value for δ tends to remain in the interval $0.8<\delta<1.2$ over a large variety of differing signal characteristics, i.e. signals associated with both large and small variance.

Use of the parameter ε is demonstrated by Figure 2.6. As the signal record is scanned with a forward marching algorithm,

a change in the sign of the relative quantity $\Delta r = X_{i+1} - X_i$ from negative to positive indicates a rise of the signal. When $\Delta r>0$, comparison of the magnitude of $|\Delta r|$ with ε is made. For $|\Delta r|<\varepsilon$, the algorithm searches for $\Delta r>0$ and continues its forward march until $\Delta r>\varepsilon$. The larger the chosen value of ε the greater $n\Delta t$ becomes. When the number $n\Delta t$ has been found, and since the maximum value of X(t) over this interval has been kept track off, the min-max-min slopes $\delta.\Delta X_j$ are evaluated and compared with acceptance criteria. If satisfactory, a subroutine determines if any signal values in the interval $n\Delta t$ do not satisfy the condition $\Delta\delta_i$ which is related to the relative changes between the i^{th}-1, i^{th} and i^{th}+1 signal amplitudes and to initial rise characteristics and rms noise. A relative measure of the noise is given by $(2\Delta f_{co}/N_p)^{\frac{1}{2}}$ (or 1/(SNR)) as defined in section 2.2.

The values of the relative changes around a centred scatter intensity X_i define a result for X_{i-1} and X_{i+1} to be within $\Delta\delta_i = (1\pm\beta)X_i$. The value of β is optimized and is sensitive to the bandpass frequency, Δf_{co}; the value for β is defined in a range $.03<\beta<.06$ for the flow conditions of the present investigation and those as reported by Arcoumanis et al (1984), for example, and with testing of the filter on results obtained using cut-off frequencies (Δf_{co}) over a range between 2KHz ($\beta\simeq.03$) and 5KHz ($\beta\simeq.06$). Particle scatter intensities with amplitude less than the maximum of the interval $n\Delta t$ are detected by the above algorithm since it is associated with initial rise sensitivity as determined by a measure of the average signal slope.

The initial rise filter is sensitive to the choice of ε_o and δ, and requires optimization of a parameter, β. For $\varepsilon_o=0$, the filter acts as a high frequency cut-off since all intervals defining a minimum, maximum and minimum are tested for the average slope criterion given by equation 2.2. In practice, signal values with amplitude greater than the maximum calibrated for the pure gas having the largest Rayleigh scattering cross-section are removed prior to executing the

filter, the average slope for an arbitrary percent of signal values is computed and the values for ε_o and β are set to about 0.25 and 0.06, respectively, with δ usually equal to unity. The filtering algorithm is efficiently implemented with a microprocessor for rapid post signal processing.

2.3.2.3 Transient filter

This final filter aims to take direct advantage of the transient characteristics of particle-scatter. As indicated from results such as those of Figures 2.2 and 2.3, the particle-scatter is observed to be an abrupt transient which can become arbitrarily present in the more (overall) slowly varying molecular light scatter distribution. This interpretation suggests as one natural choice the use of a forward difference filter for purposes of emphasizing the particle scatter effect; removing the particle scatter contribution from the signal once emphasized is a separate problem and many standard algorithms may be used (eg. Otnes and Enochson (1978)).

Difference filters are well known in time-series analysis and provide an effective method for transient removals. The details are considered, for instance, in Jenkins and Watts (1969) and Box and Jenkins (1971). The general form for the n^{th} forward difference of a series is given by

$$\begin{aligned}\Delta^n g(x) = {} & f(x+nt) - nf(x+(n-1)t) \\ & + \frac{n(n-1)}{2!} f(x+(n-2)t) \\ & - \frac{n(n-1)(n-2)}{3!} f(x+(n-3)t) \\ & + \ldots + (-1)^n f(x) \end{aligned} \qquad (2.4)$$

The filter gain and phase function for the forward difference of n^{th} order are given by

$$G(f) = 2^n |\sin\pi f|^n, \quad -1/2\Delta t \leqslant f < 1/2\Delta t \tag{2.5}$$

$$\emptyset(f) = \begin{cases} n\pi f + n\pi/2 , & -1/2\Delta t \leqslant f < 0 \\ \\ n\pi f - n\pi/2 , & 0 \leqslant f < 1/2\Delta t \end{cases} \tag{2.6}$$

which indicate the amplification and phase shift of the i^{th} signal; the gain is maximum at the frequency $1/2\Delta t$. The frequency response is $G(f)\exp(j\emptyset(f))$; here $j = \sqrt{-1}$.

Results at various flow locations in the jet are shown in Figure 2.7 for n = 1, 2, 3, 4 and indicate several interesting features. Scattered light intensities are amplified in the differenced LRS light intensity distributions. The filter is high pass and the order n for the filter is the sensitive parameter and it can be chosen to bring out the required information. In practice we have found the choice for n=1 or 2 to provide sufficient sensitivity. Increasing the value for n results in attenuation of the low frequency components of the signal and is demonstrated by the computed frequency spectra shown in Figure 2.8.

When criteria such as (ii) and (iii) discussed in section 2.3.1 are satisfied by particle-scatter, the expected (and desired) result of using the filtering operation of equation (2.4) is: greater amplification of particle-scatter over the molecular scatter (Figure 2.7), Constantinides (1985). In contrast, when particle scatter is not present (for instance, Figure 2.7(a)) or not clearly detected (see discussion in section 2.3.1), the computed difference between consecutive signal amplitudes will not be significantly different and thus the differencing operations (2.4) will tend to show similar trends in the results for any value of n. Because the detected intensity is dependent on the particle size and its trajectory

through the Gaussian beam intensity, particles may give rise to particle-scatter signals which are not identifiable by any filter; the most difficult case results when particles are very small and cross at large distances from the beam centre, although still present in the measurement control volume (see Chew, Kerker and Cooke (1977a,b)).

As noted, the choice for n=1 or 2 provides in most instances sufficient sensitivity for the further aspect of removing the emphasized particle signal from the original signal record. For n=1, the filter is simply the first difference

$$Y(t) = X(t+1) - X(t) \tag{2.7}$$

which removes the low frequency characteristics of signal record X(t) (for example, such as those of Figuer 2.2(b)). The frequency response is

$$H(f) = 2j\exp(-j\pi f)\sin\pi f, \quad -1/2\Delta t \leqslant f < 1/2\Delta t \tag{2.8}$$

For the case n=2, the second forward difference results and is given by

$$Y(t) = X(t+2) - 2X(t+1) + X(t) \tag{2.9}$$

The usefulness of this filter is in removal of oscillating components from X(t) (i.e. Figures 2.2(a) and 2.7(b)). As shown in Figure 2.7, the particle effects are highlighted by including their characteristics over a complete cycle (doublet features at n=1,3...) of the particle-scatter time.

We note that further to the present methods, a signal modelling approach may be taken using autoregressive and moving average techniques (see Box and Jenkins (1971) and Chatfield (1984)) to identify particle-scatter in the LRS signals. For example, the work described by Rahimi and Mote (1983) makes use of a generalised approach to model a dynamic

signal spectrum which is convenient to use provided the frequency spacing of the particle-scatter and Rayleigh scatter is sufficiently large; even though this assumption is not always valid, we have used the spectrum modelling described by these authors and found it able to provide a further way to emphasize the presence of the particle signals. It is also interesting to note the analogy between the present problem of signal detection and frequency-modulated carrier-wave radars (FMCW) where the presence of hidden targets has to be detected in the return signal; many of the detection aspects are similar as described, for example, by Carr et al (1981).

2.4 RESULTS AND DISCUSSION

Results obtained with the digital filters discussed in sections 2.3.2.2 and 2.3.2.3 are presented in Figures 2.9 and 2.10; a detailed discussion of the fluid mechanics of these jet results is made in the following chapter. In Figure 2.9 the radial profile of Figure 2.4 is shown, together with the mean concentration results obtained with a sampling probe. The standard deviation between the two results is about 1.5% and is, in part, due to density weighting effects which, in the case of the sampling probe, result in slightly lower values. The rms of the concentration fluctuations is also shown and comparison between the unfiltered data, that filtered by the amplitude only filter (2.1) and the present digitally filtered results indicates that the amplitude filter overestimates the rms of the concentration by about 3% to 7% of the absolute values although the relative trend in the rms distribution is similar. Figure 2.10 shows mean and rms distributions for the same jet at a further location downstream (x/d=5). Again, the rms is higher with the unfiltered approach and the larger discrepancies are expected due to the increased mixing of the jet fluid with the surroundings and the consequent entrainment of particles. Agreement in the

mean concentration betweem the digitally filtered LRS data and sampling probe results remains within a standard deviation of 1.5%

In Figures 2.9 and 2.10 the results shown for the digital filters are similarly obtained with either the use of the initial rise filter (section 2.3.2.2) or the transient filter (section 2.3.2.3). When the initial rise filter is used, a larger percentage of data may be rejected than when the transient filter is used and the extent of the difference depends on the number density of particulate matter entrained (which is random). The statistical accuracy of the data is maintained by the number of data required for calculating the quantities of interest; a summary of typical values of rejection percent of signals is provided in Table 2.2.

2.5 CONCLUSIONS

The digitally filtered LRS data appears to circumvent the particle-scatter interference problem to a degree which is much improved over no filtering or filtering based only on amplitude criteria; frequency as a single criterion is not generally valid. The choice of filter scheme and justification for its use is clearly dependent on the LRS application under consideration and the required accuracy. In particular, it is clear that accurate measurements (uncertainty within 2% of unity in the mean) can be made in free flows with LRS but will require that a signal filtering approach be taken. It is concluded that even when particles are present in the measurement control volume, differentiating their scatter intensity from molecular scatter intensities will in some instances not be possible at all; in particular, when particles range in sizes sufficiently small or result in partial beam crossing at distances from the beam centre which, even for larger size particles, can result in light scatter intensities that are similar to the molecular scatter amplitudes.

Table 2.1 Summary of optical probe developments and application to the study of turbulent mixing

Author(s) (year)	Flow/Application	Remarks
Rosenweig, Hottel and Williams (1961)	Smoky (oil/air) 12.52mm free jet discharging into ambient air (Re = 26200)	Reported development of smoke scattered light measurement technique to measure intensity, correlation and spectral density of concentration fluctuations
Williams, Hottel and Gurnitz (1966)	Quantitative study of the effects of upstream turbulence on premixed gaseous flames	Reported on development of a technique similar to that of Rosenweig et al (1961) for measurements of mean and and fluctuating temperatures
Becker, Hottel and Williams (1967 (a),(b))	Free air jet marked with oil smoke discharging into air (Re = 54,000)	Extended the principles of the technique by Rosenweig et al (1967) to provide a detailed study of the concentration field of the round free jet
Wilson and Damkevala (1970)	Measurements in the shear layer of a 2.54cm jet operated at 105 and 210 m/s	Reported mass-density fluctucations using a crossed-Schlieren technique

Author(s) (year)	Flow/Application	Remarks
Davis (1971)	Measurements made for an air into air jet over a Mach number range $0.3 < M < 0.9$; jet exit diameter was 24.5mm	Used a single-beam Schlieren system to obtain quantitative measures of the intensity and spectral distributions of density gradients
Graham, Grant and Jones (1974)	Demonstrated the potential of Rayleigh scattering by measurements in the unburned region of a lifted jet diffusion flame (methane-air)	Application of the theory of Rayleigh to measurements in turbulent flows
Pitz, Cattolica, Robben and Talbot (1976)	Hydrogen-air flame from a 3.2mm diameter nozzle operated over an equivalance ratio range of 0.6 to 1.0 and Reynolds numbers range between 1300 and 2000	Used Rayleigh scattered light with a Febry-Perot interferometer to measure temperature and density; and concluded that Rayleigh scattering was viable for such measurements
Becker (1976)	Overview of the application of light scatter principles in connection with studies in turbulent transport and the quantities of interest	
Smith (1978)	Laminar hydrogen-air flame from a straight vertical burner (6.35mm i.d.); hydrogen exit velocity of 600cm/s	Obtained instantaneous temperature measurements in the flame using laser Rayleigh scattering

Author(s) (year)	Flow/Application	Remarks
Birch, Brown, Dodson and Thomas (1978)	Free isothermal ∿95% methane jet issuing from a 12.65mm tube into ambient air, Re = 16000	Used a Raman spectrometer to obtain the mean and higher moments and probability distributions of methane concentration
Black and Chang (1978)	Investigation of Freon-12 mean concentration of a free jet (1.5mm i.d. nozzle, $Re = 1.2 \times 10^5$) and mean gas temperature within a steady stoichiometric hydrogen-air/ flame	Used a laser Raman technique combined with optical scanning to allow lines of the flow field to be measured
Dyer (1979)	Propane jet from 2.0mm dia. tube with exit velocity of 21.1m/s (Re = 9790) surrounded by co-axial air flow (0.7m/s) to provide dust free environment	Rayleigh scattering to measure the turbulent concentration fluctuations to determine mean and rms fields and autocorrelation
Leipertz and Fiebig (1979)	Small single and multiple jets (two-dimensional, with ∿2mm exit channels). Typical jets were of N_2 and CO_2 with exit plane velocities of ∿1.7m/s	Raman spectroscopy to measure the concentration fields of N_2 and CO_2 jets; showed that 50μm local resolution could be obtained

Author(s) (year)	Flow/Application	Remarks
Muller-Dethlefs and Weinberg (1979)	Measure of the effects of additives (and other small perturbations) on burning velocities on normal and inhibited flames	Rayleigh scattering to measure the temperature T to determine the point where burning velocity equals the flow velocity (i.e. where T reaches its adiabatic value)
Rambach, Dibble and Hollenbach (1979)	Vertical turbulent jet diffusion flame from 1.6mm i.d. pipe. Coflowing air stream used to provide particle free surrounding for the flame	Rayleigh scattering to obtain probability distributions of temperature and determined profiles of mean and rms temperature
Smith (1980)	Measurement of temperature and nitrogen density in a combusting engine	Pulsed, spontaneous laser Raman spectroscopy to obtain mean temperature dependence on equivalence ratio as a function of cycle time in the engine
Dibble, Hollenbach and Rambach (1980)	Fuel jet from a 1.6mm pipe with Re = 4400; fuel composition was 37% methane and 63% hydrogen	Rayleigh scattering to to obtain temperature measurements which gave mean and higher moments, probability distributions and power spectrum for a turbulent jet diffusion flame

Author(s) (year)	Flow/Application	Remarks
Warshaw, Lapp, Penney and Drake (1980)	Hydrogen-air diffusion flame in a co-flowing jet combustor; fuel was supplied through a 3mm tube with co-flowing air through a 100mm dia. pipe	Demonstated the simultaneous measurement of temperature and velocity using combined Raman scattering and laser velocimetry to obtain temperature and velocity and density and velocity correlations
Cheng, Bill and Robben (1981)	Hydrogen-air combustion in a heated turbulent boundary layer. Equivalence ratio range was 0 to 0.2 with wall temperatures from 1100 to 1300^{o}K and free stream velocities from 14 to 22m/s	Obtained measures of mean, rms fluctions, probability density and spectral density using laser velocimetry and Rayleigh scattering
Dibble and Hollenbach (1981)	Premixed and diffusion flames from 2.54cm pipe (exit velocity of 4m/s, Re = 8000) and 1.6mm pipe (exit velocity 92m/s, Re = 4400), respectively. Coflowing air stream used	Reported spatially and temporally resolved measurements of temperature in premixed and non-premixed turbulent flames using Rayleigh scattering
Drake, Lapp, Penney, Warshaw and Gerhold (1981)	Low-turbulence hydrogen-air flames and premixed laminar propane-air flames and hydrogen-propane-air turbulent diffusion flames	Assessed the application of pulsed Raman spectroscopy to to temperature and concentration fluctuation measurements in turbulent diffusion flames

Author(s) (year)	Flow/Application	Remarks
Bill, Namer, Talbot and Robben (1982)	Rod stabilized flame into a flow containing grid-induced turbulence. The investigations were made for ethylene (C_2H_4) - air equivalence ratios ranging from 0.5 to 0.75	Rayleigh scattering to measure mean and rms density fluctuations and to estimate the probability density functions
Leipertz (1982)	Plane jet of CO_2 from 2mm channel with exit velocity of 1.7m/s and with and without N_2 coflowing	Rayleigh scattering to measure CO_2 concentration and compared results to those obtained with Raman spectroscopy
Escoda and Long (1983)	Freon-12 jet with exit velocity of 4.6m/s discharging into low speed coflowing nitrogen	Demonstrated that Rayleigh scattering combined with an entire field of view optical imaging could be used to study instantaneous large scale turbulent mixing and molecular diffusion
Namer, Bill, Talbot and Robben (1984)	Ethylene flame ($\phi \sim 0.5$) interacting with a Karman vortex street. Vortex shedding from a rod of 2 or 3mm dia. and with Re in the range of 73 to 500	Rayleigh scattering to measure instantaneous gas density and obtain mean, rms probability densities and power spectra of density

Author(s) (year)	Flow/Application	Remarks
Gouldin and Dandekar (1984)	Unconfined V shaped flame stabilized in grid turbulence on a 1.25mm rod	Measurements with Rayleigh scattering of mean and rms density and probabilities and power spectra
Rajan, Smith and Rambach (1984)	V-shaped propane-air premixed flame resulting from a 5cm x 5cm burner stabilized on a 1.6mm dia. rod	Density mean, rms and probability distributions were obtained with Rayleigh scattering from single and two point spatial measurements
Dibble, Kollmann and Schefer (1984)	Axisymmetric fuel jet (5.3mm i.d. nozzle) with exit velocity of 154m/s (Re = 24000, based on 22% argon in hydrogen composition). Coflowing airstream (8.5m/s)	Combined laser velocimetry and Raman scattering to simultaneously measure velocity and scalars in a ducted non-premixed turbulent flame
Arcoumanis, Green and Whitelaw (1984)	Non-compressing, model Diesel engine motored at 200rpm with a simulated fuel jet (Freon-12 vapour) injected to study air-fuel mixing	Demonstrated Rayleigh scattering to quantify mean and rms mole fraction of simulated fuel jets in engines

Author(s) (year)	Flow/Application	Remarks
Pitts and Kashiwagi (1984)	Methane, isothermal jet discharging into filtered coflowing air stream (Re = 4200)	Rayleigh scattering to study the methane concentration field mean, rms, skewness and kurtosis
Haumann and Leipertz (1984)	Premixed turbulent methane-air flame issuing from two-dimensional channels	Form of Rayleigh scattering and photon correlation technique to study flame temperature (mean and rms values)
Schefer and Dibble (1985)	Similar configuration as reported for Dibble, Kollmann and Schefer (1984) above	Combined laser-velocimetry and Rayleigh scattering to study velocity and density distributions and joint probabilities of velocity and density
Long, Levin and Fourguette (1985)	Coflowing mixed and non-premixed turbulent flames (CH_4)	Optical imaging based on a combination of Rayleigh and Raman scattering allowed instantaneous concentration and temperature distributions to be obtained simultaneously
Pitts (1986)	Turbulent jets of seven different gas pair combinations all with slow coflowing streams. Reynolds number range of 4000 to 12000	Rayleigh scattering to study the effects of density and Reynolds number on mixing in turbulent jets

TABLE 2.2 Summary of percentage rejection of signal values using different filters

Filter type:		% of signal values rejected per filter type		
		Amplitude	Initial rise	Transient
x/d	r/d			
3.0	0.0	0.0	0	0
	0.30	6.7	10.5	10.0
	0.65	11.8	16.5	15.5
	0.70	15.3	22.0	20.2
5.0	0.40	8.7	13.9	12.2
18.0	0.0	11.9	17.8	16.5

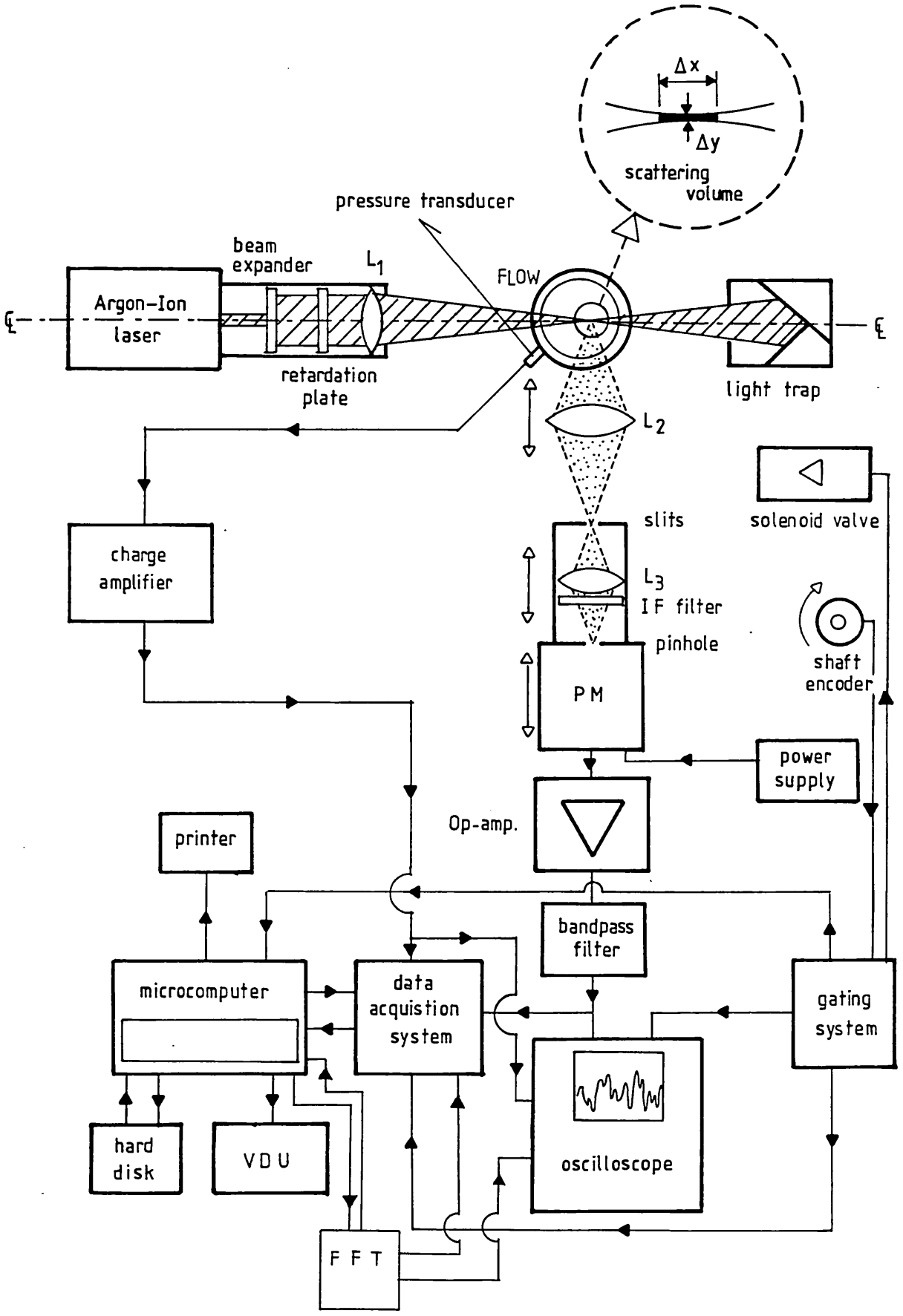


FIGURE 2.1 LINE DIAGRAM OF LASER RAYLEIGH SCATTERING OPTICAL ARRANGEMENTS AND SIGNAL PROCESSING SYSTEM

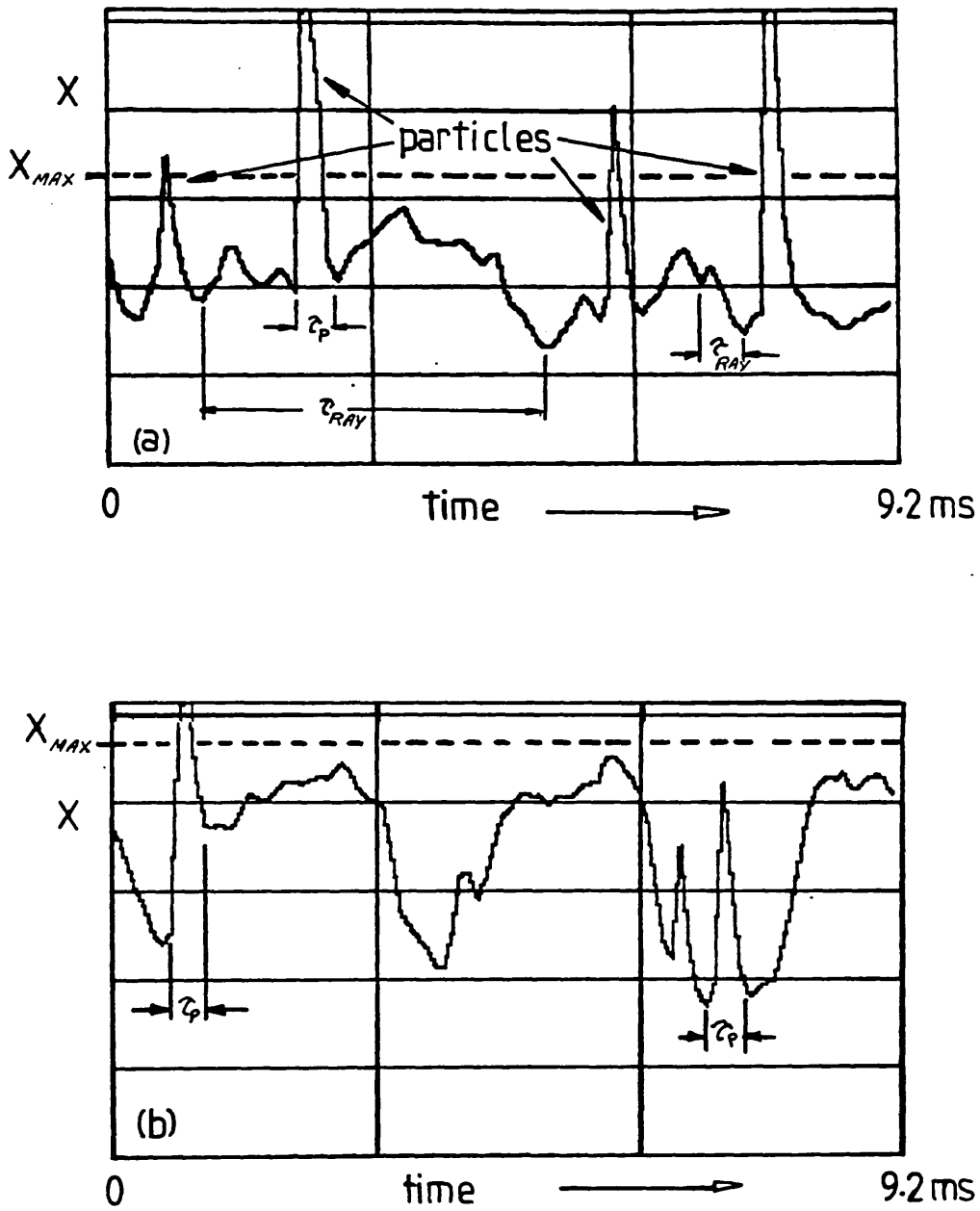
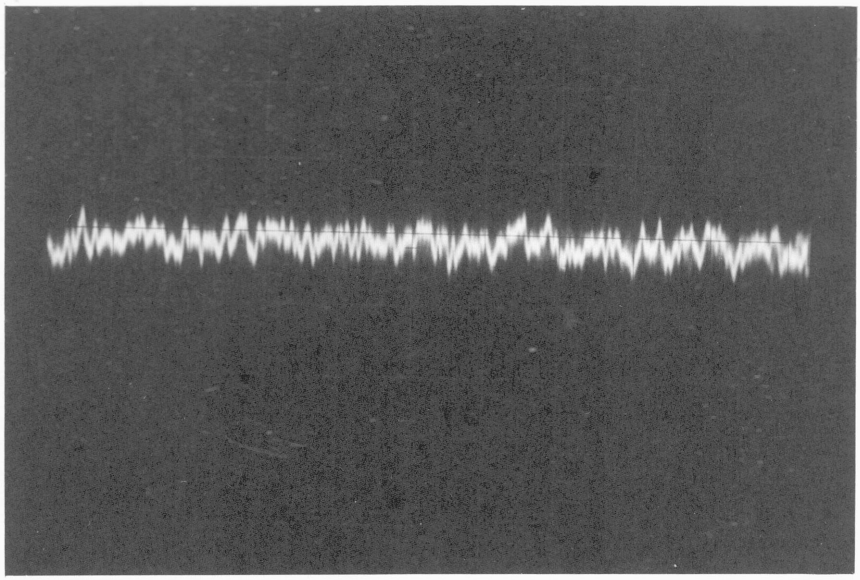
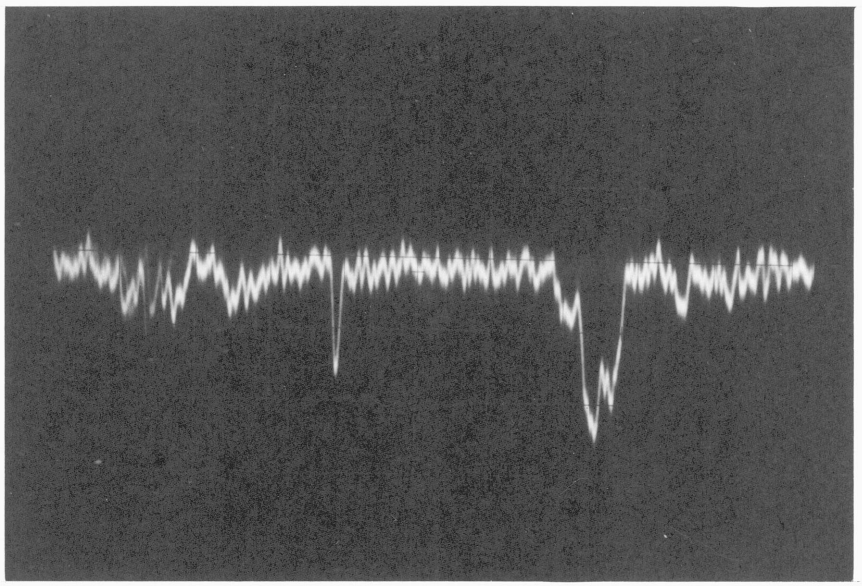


FIGURE 2.2 SCATTERED LIGHT INTENSITY DISTRIBUTION (a) x/d=3, r/d=0.65 (b) x/d=3, r/d=0.3

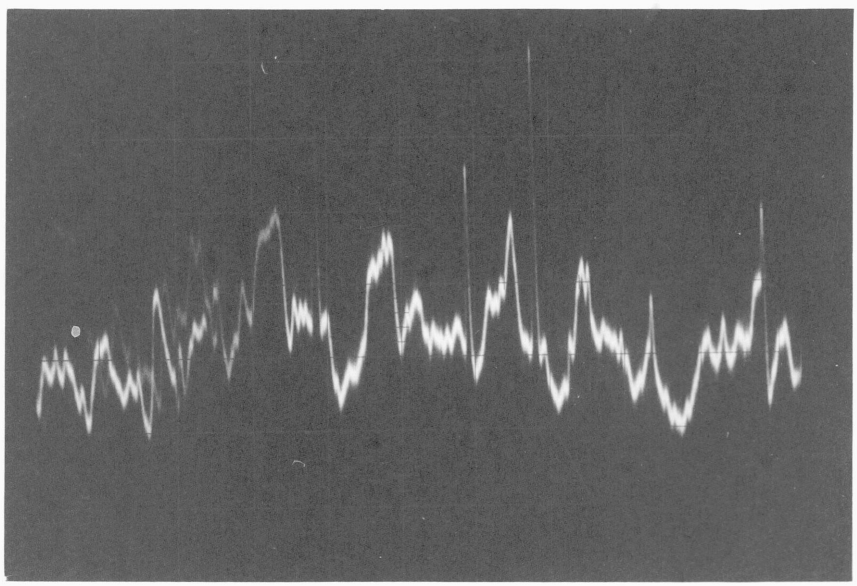
Figure 2.3 Oscilloscope traces of LRS signals



(a) potential core of jet



(b) x/d = 3, r/d = 0



(c) x/d = 6, r/d = 0

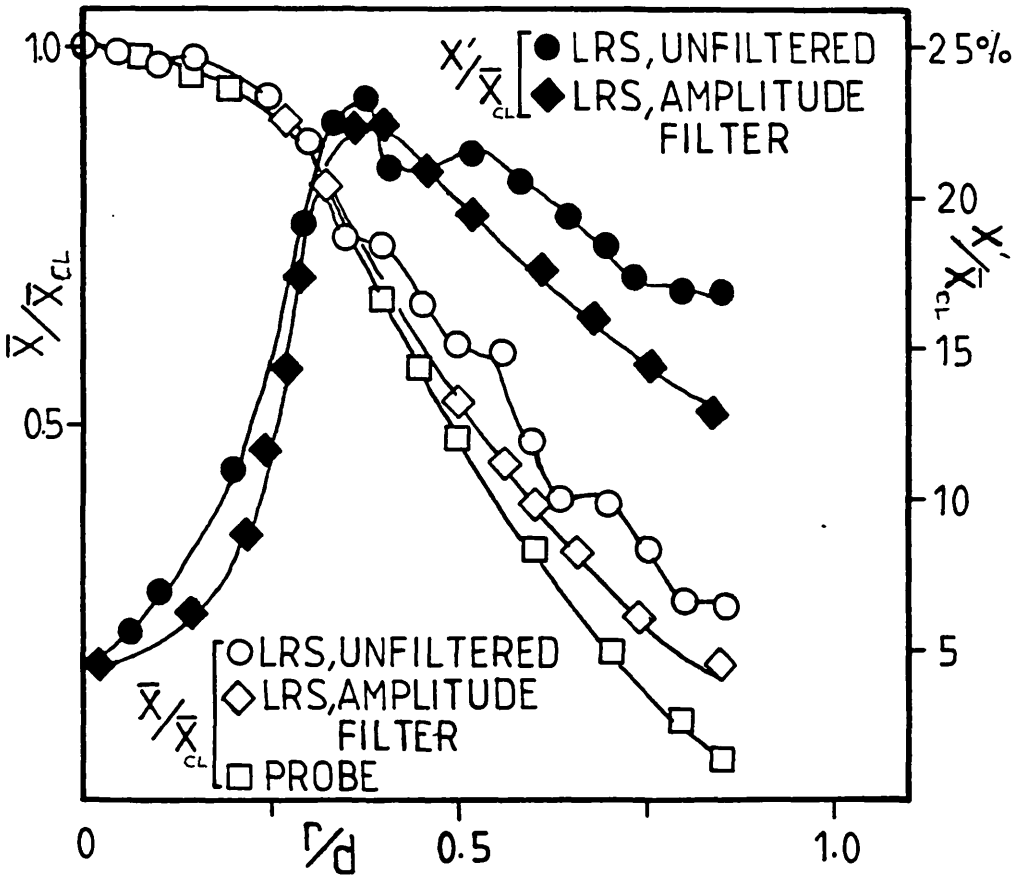


FIGURE 2.4 MEAN AND RMS CONCENTRATION PROFILES ALONG THE JET RADIUS AT x/d=3; COMPARISON OF UNFILTERED, AMPLITUDE FILTERED AND SAMPLING PROBE RESULTS

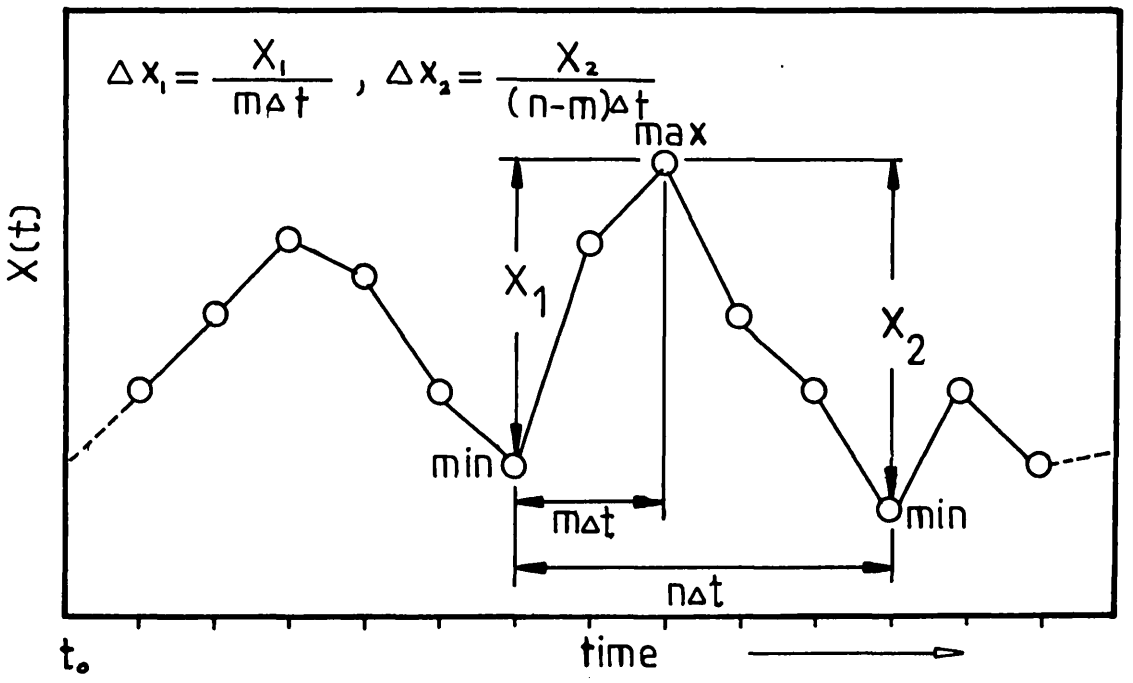


FIGURE 2.5 SCHEMATIC FOR INITIAL RISE FILTER, $\epsilon_o = 0$

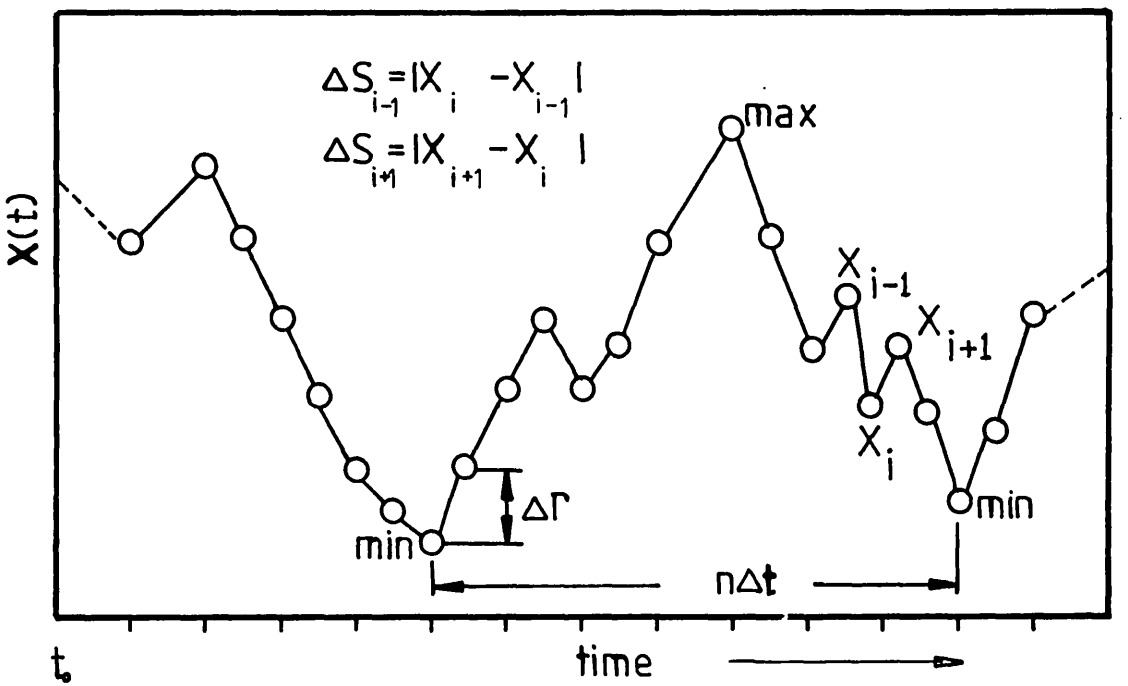


FIGURE 2.6 SCHEMATIC FOR INITIAL RISE FILTER, $\epsilon_o > 0$

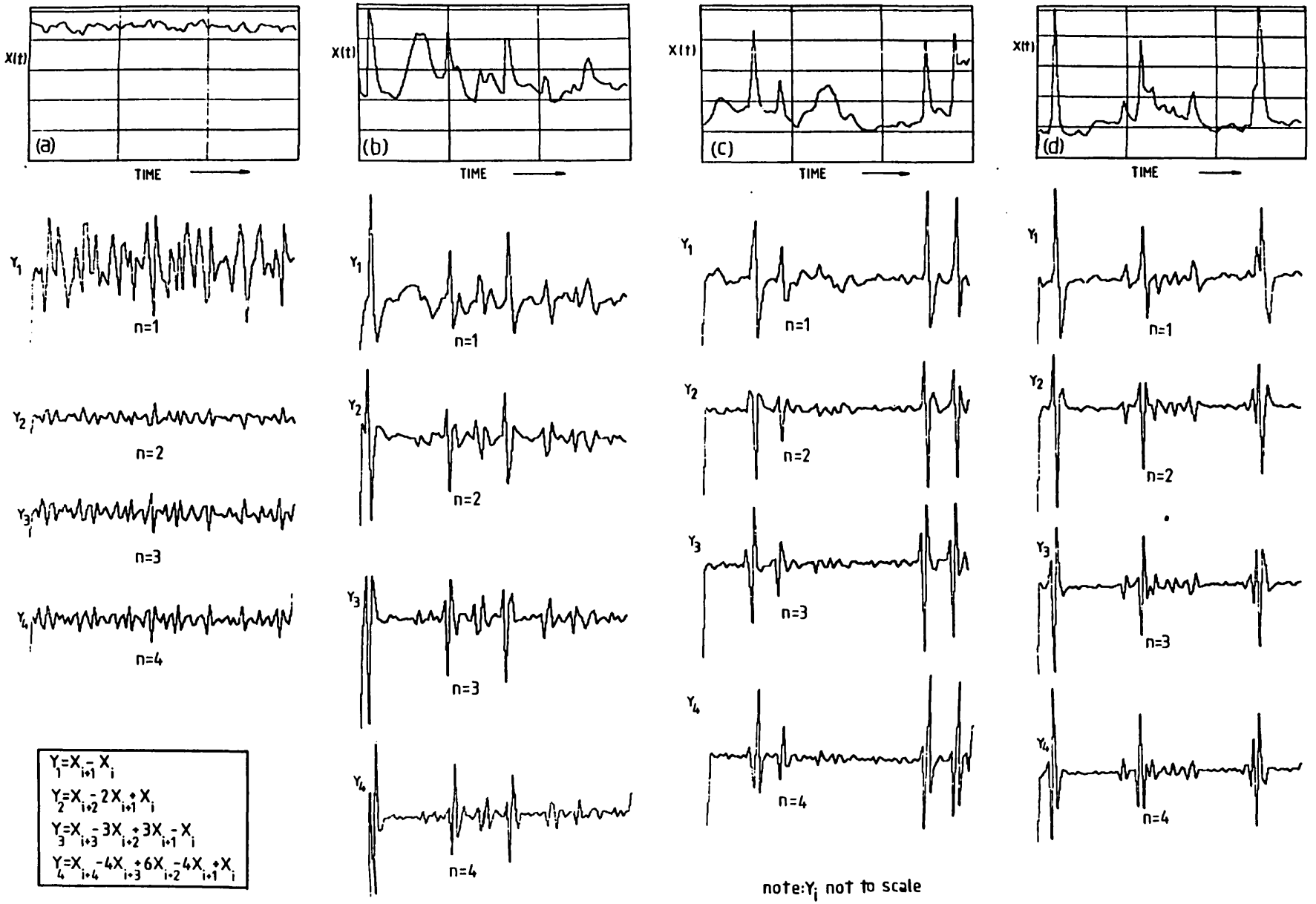


FIGURE 2.7 DIFFERENCE FILTER (with different values of n) APPLIED TO LRS SIGNALS AT (a) jet potential core, x/d=3, r/d=0 (b) x/d=5, r/d=0.4 (c) x/d=18, r/d=0 (d) x/d=3, r/d=0.7

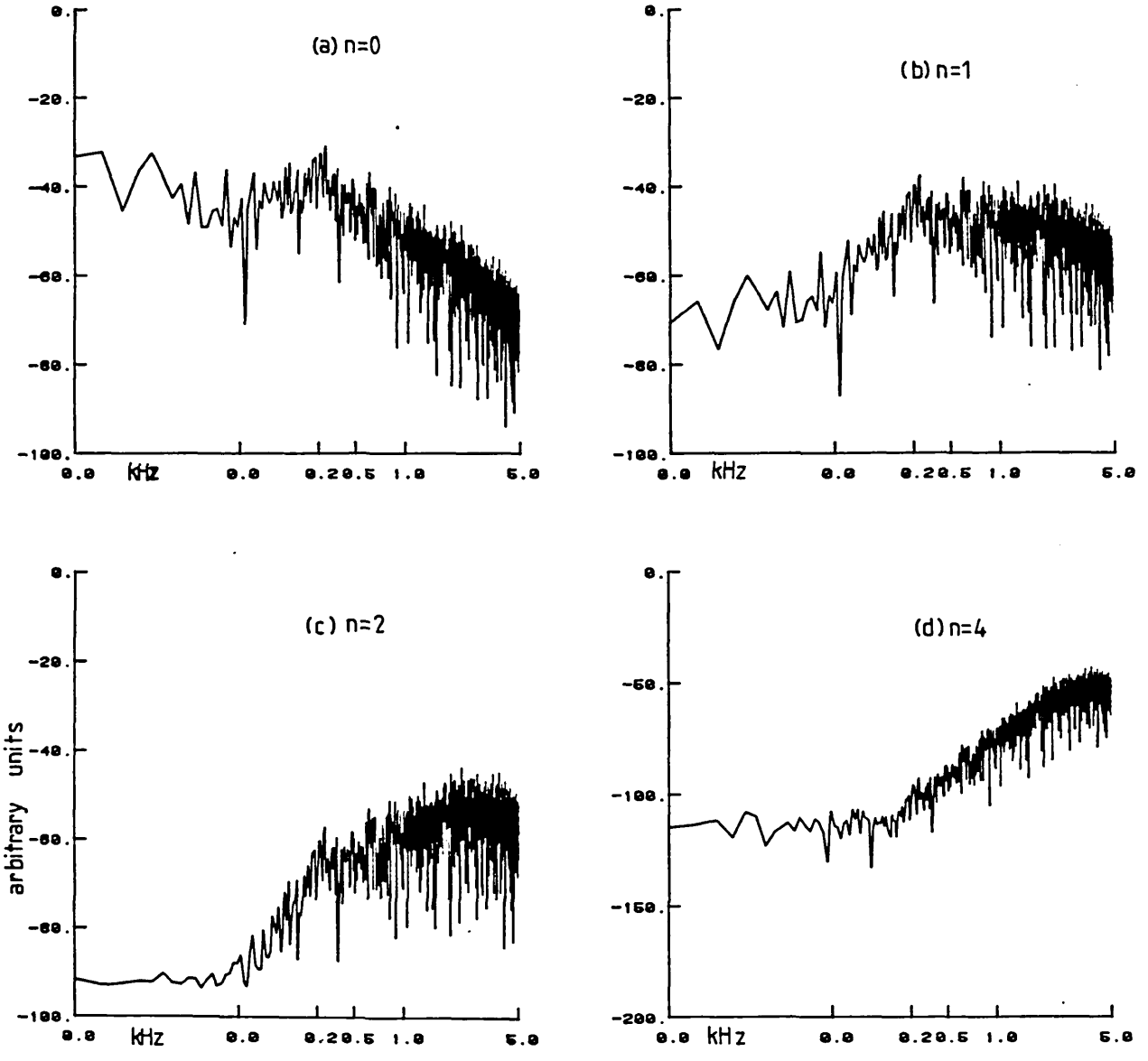


FIGURE 2.8 LRS FREQUENCY SPECTRA AT A JET LOCATION x/d=3, r/d=0.3 WITH THE PARAMETER n SET TO (a) n=0 (b) n=1 (c) n=2 (d) n=4

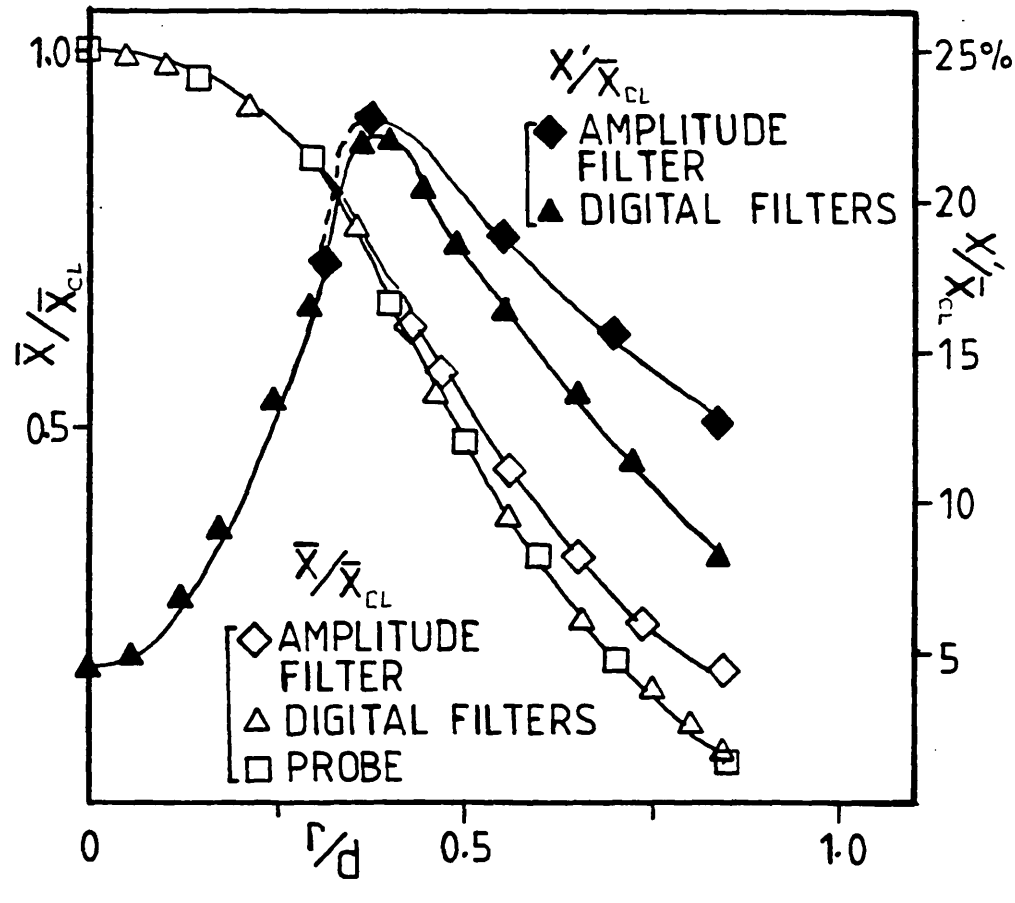


FIGURE 2.9 MEAN AND RMS CONCENTRATION PROFILES ALONG JET RADIUS AT x/d=3, FILTERED RESULTS

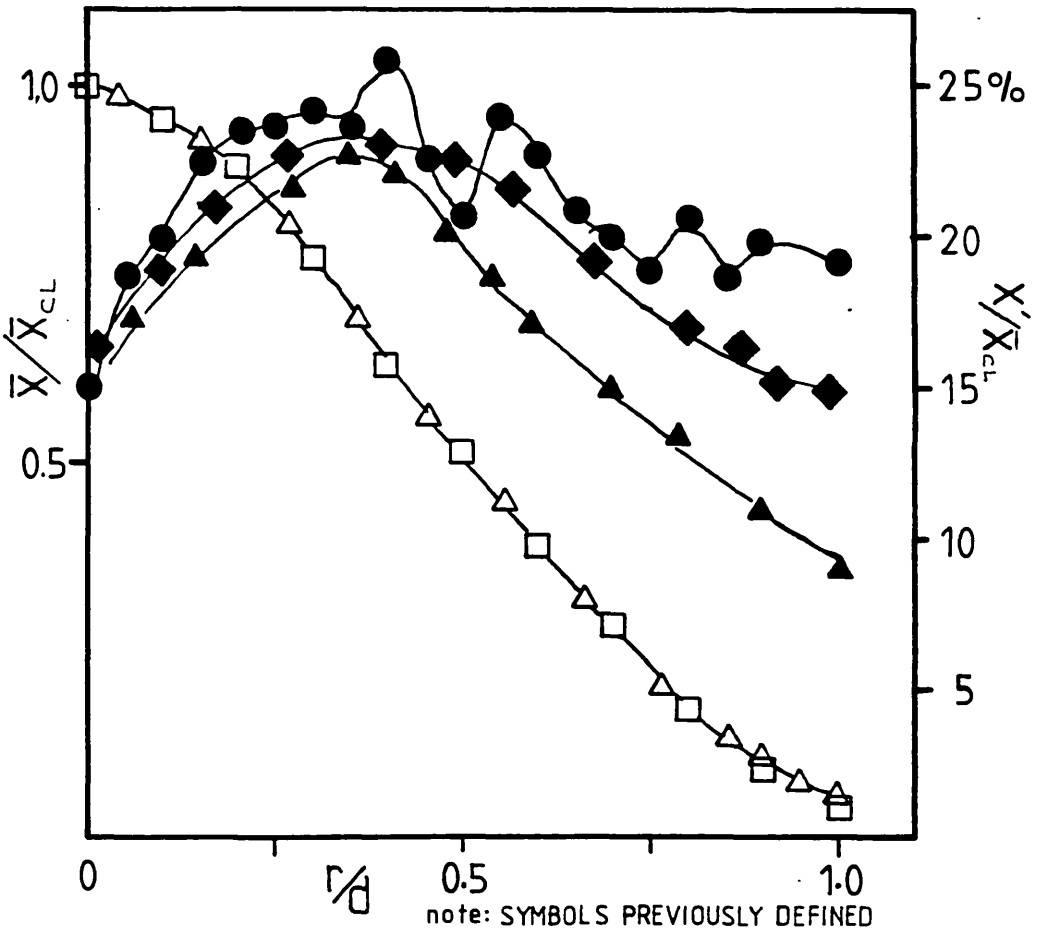


FIGURE 2.10 MEAN AND RMS CONCENTRATION PROFILES ALONG THE JET RADIUS AT x/d=5, FILTERED AND UNFILTERED RESULTS COMPARED

CHAPTER 3 THE NEAR FIELD OF STEADY JETS

3.1 INTRODUCTION

Investigations of non-uniform density jets have been fewer in number than those in equal density jets and considerably less detailed, partly as a result of difficulties associated with measurement techniques. Pressure probes and hot-wire techniques have been used by, for example, Abramovich et al (1969), Sforza and Mons (1978) and Chevray and Tutu (1978) with the second two investigations confined to small density differences. The experiments of Way and Libby (1971) also made use of hot-wire anemometry and reported measurements of velocity and concentration characteristics in a jet of helium rising into air at 15 and 20 diameters from the jet exit; the emphasis was on the development of the measurement technique but the results do show the increase in mixing expected with low density jets. Antonia et al (1975) have used hot-wires in heated jets where the initial density ratio was around 0.94, with emphasis on heat flux and shear stress in the far field of the jet.

More recently, optical techniques, as reviewed in Chapter 2, have been applied to the measurement of scalar quantities in non-uniform density jet flows. Birch et al (1978) used a form of Raman spectroscopy to measure mean and fluctuating levels of concentration in a methane jet in a range from around 5 to 70 diameters although most of the profiles were between 20 and 40 diameters. Techniques based on Rayleigh scattering have also been used to investigate scalar-field properties in jets of non-uniform density, for example by Dyer (1979), Leipertz (1982) and Pitts and Kashiwagi (1984), but the emphasis has again tended to be on the technique development even though Dibble and Hollenbach (1981), Schefer and Dibble (1985) and Pitts (1986) have applied the technique to flames and to isothermal jets of significant density differences with some success.

In this chapter, we are concerned with the details of

free jet flows from the jet exit to around ten diameters downstream and with the differences between a jet of air and a jet of Freon-12 (CCl_2F_2 density 4.2 times that of air)* issuing into still air, see Figure 3.1. A second purpose of this chapter is to provide validation of the Rayleigh scattering technique to the study of a free turbulent jet where, in contrast to previous investigations, the application of Rayleigh scattering to jet flows has been confined to investigations of coflowing jets; due to the problem of particle scatter interference (Chapter 2). The jet is described in the following section together with the measurement techniques which include impact probes and hot-wire anemometry for the measurements in the uniform-density jet and a Rayleigh-scattering technique for the measurement of scalar properties. The results are presented and discussed in the third section which is divided into three sub-sections dealing with averaged quantities and a fourth section concerned with spectral information. In the Freon-12 jet, the averaged quantities are likely to be density weighted and information of the probability density distributions allows the difference between the unweighted and weighted averages to be determined for the case of concentration measurements; a detailed assessment of the density weighted quantities is provided in the Appendix of this chapter. The fourth section of the chapter identifies the more important conclusions, the implications of the results for calculation methods based on averaged equations and the effects of density on the large scale structures formed in the near field.

3.2 FLOW ARRANGEMENT AND MEASUREMENT TECHNIQUES

The jet is identical to that previously used by Durão and Whitelaw (1974) in their comparison of laser velocimeter and hot-wire measurements. It was manufactured from solid plexi-

* The Schmidt number for the Freon-12 jet into air is about 1.4 in contrast to that of 0.2 for the helium jet of Way and Libby (1971)

glass with an area contraction of 16 to a jet-exit diameter of 10mm. Air, or Freon-12, was supplied to the plenum chamber upstream of the contraction and passed through a calibrated rotameter, a drying filter and a length of honeycomb before contracting to the exit plane and issuing into still air. For the present experiments, the jet was directed vertically downwards and surrounded by a metal screen 1m in diameter. The Freon gas was distributed uniformly in the exit plane where the displacement thickness of the boundary layer was 0.27mm with air and less with Freon.

A probe of internal and external diameters of 0.31 and 0.56mm was used to measure total head pressure difference, ΔP, and to withdraw samples of gas to a thermal-conductivity cell for the measurement of mean mole fraction of gas concentration, $\bar{X}$. The static pressure in the jet was assumed to be constant* and equal to the atmospheric value for $x/d > 1$, as suggested by the measurements of Sunyach and Mathieu (1969). Knowledge of the local mean Freon-12 concentration allows the mean velocity ratio to be determined from the equation

$$(U/U_R) = \{(\Delta P/\Delta P_r)\left(1 + X_A(M_A/M_B-1)\right)_r/\left(1 + X_A(M_A/M_B-1)\right)\}^{\frac{1}{2}} \qquad (3.1)$$

which follows directly from Bernoulli's relation between pressure drop, fluid density and velocity. The subscript r defines a reference (i.e. o for the jet exit and CL for any axial location) for the gas A (Freon): the term $\bar{X}_A$ is the mean mole fraction of Freon; and M_A and M_B are the molecular weights of Freon-12 (M_A = 120.9) and of air (M_B = 28.9). This results in an approximation of the time-averaged velocity since $\langle\rho u^2\rangle \neq \langle\rho\rangle\langle u\rangle^2$ and analysis of the difference shows that it includes ratios of triple correlations which are close to zero at the centreline and increase towards the jet half width. When the same probe was used for gas sampling in the Freon-12 jet and in the air jet with a trace of

* Assessments of this assumption are provided in the Appendix to the chapter

helium, the suction rate was arranged to be close to isokinetic so that the measured quantity was not severely influenced by preferential suction of either high or low density gas. The thermal-conductivity cell was used in the manner described by Crabb and Whitelaw (1979) and previous authors, with a precision of approximately $\pm$1.5% of the concentration in the exit plane. In this case, a density weighted quantity is measured and, as will be shown, its difference from the unweighted average can be estimated by comparison with the unweighted values obtained from the optical method (see also Chapter 2).

Hot-wire anemometry was used in the air jet and made use of DISA equipment, including a straight-wire probe, an anemometer (55001) and true rms meter and digital voltmeter. Calibration was performed in the exit plane of the jet and spectral information for the velocity field was obtained with an analogue FFT analyser (Spectral Dynamics model SD340).

The instrumentation required to obtain and process the Rayleigh scattered signals is shown on Figure 2.1. For the present experiments the argon-ion laser operated at a wavelength of 514.5nm and at power levels of around 0.7W. The photomultiplier provided a signal with voltage proportional to the intensity of the scattered light and, after band-pass filtering (5KHz), the signal was converted to digital form and processed in a microcomputer. The measurement software had two main purposes, the first to filter Rayleigh signals from those due to light scattered from sources other than the gas molecules as discussed in the last chapter, and the second to convert the resulting signals into mean values, including correlations, or to pass them to the FFT analyser. A detailed assessment of the measurement uncertainties is provided in the Appendix to this chapter.

3.3 RESULTS AND DISCUSSIONS

3.3.1 Centreline characteristics

Centreline distributions of mean velocity and concentration and the corresponding rms values are shown on Figures 3.2 and 3.3 for air and Freon-12 jets. The mean and rms of the Freon-12 jet concentrations are expressed in terms of mole and mass fraction i.e. by $\bar{X}$ and $\bar{\theta}$, respectively. As can be seen from Figures 3.2 and 3.5, the concentrations measured by the probe and optical techniques are in close agreement (discrepancies less than 2% of the local values). It is expected that these values are close to the unweighted averages. The jet Reynolds number, 16900 in both cases, was chosen after experiments at lower values had shown this to be an asymptotic value in terms of the non-dimensional mean velocity and concentration results. The Froude number of the Freon jet was -224 ($= U_o^2 \rho_{jet}/gd(\rho_{amb} - \rho_{jet})$) where ρ_{amb} and ρ_{jet} denote the ambient and jet fluid density and d and U_o are the jet exit diameter and velocity and, according to the analysis of Chen and Rodi (1980) is sufficient to ensure the absence of buoyancy forces in the present range of measurements.*

The higher density Freon jet decays more slowly as shown by Figure 3.2(a) and, as expected, the ratio of the velocity to concentration is far from constant for the two jets and stems largely from the disparity in the potential core lengths. The growth rates are shown as the reciprocal of the velocity and concentration (Figure 3.2(b)) and it is evident that the air jet spreads more rapidly. For both the air and Freon jets, the velocity growth is less than the concentration growth and the velocity potential core greater. To facilitate comparison of these results with those of others, the centreline dependence of mean mole fraction concentration may be written as

* See also, Gebhart (1979) for a review of buoyancy induced fluid motions and Phillips (1981) on the effect of Froude number on entrainment characteristics

$$\frac{\bar{X}_o}{\bar{X}} = \frac{k_1(x - x')}{r_o} \tag{3.2}$$

where x' is the virtual origin of the mole fraction, k_1 is a constant and r_o is the nozzle radius. A least squares fit to the data for $x/r_o > 20$ leads to values of k_1 and x' of 0.178 and $8.15r_o$ for the Freon-12 jet and 0.457 and $12.8r_o$ for the helium trace in the air jet, respectively. The equation

$$\frac{\bar{\theta}_o}{\bar{\theta}} = \frac{k_2(x - x'')}{r_e} \tag{3.3}$$

includes x" as the virtual origin in mass fraction terms and r_e the effective nozzle radius to account for the density difference between the jet fluid and surroundings. This momentum-scaling concept was introduced by Thring and Newby (1953) with $r_e = r_o(\rho_o/\rho_{amb})^{\frac{1}{2}}$ or, in the present case, $r_e = 2.05r_o$. The value of k_2 was found to be 0.086 and the virtual origin $x'' = 19.78r_o$. Table 3.1 provides an assessment of the influence of density on centreline decay and growth rate based on this and previous experiments: the differences stem mainly from initial conditions. As can be seen, jets of higher density exhibit a more positive location for the mole fraction virtual origin and a more negative location for the mass fraction. Thus, the lighter density jets spread faster with associated higher rms values while heavier density jets exhibit the opposite behaviour. When plotted on a momentum basis, however, the growth rates and centreline decay tend to merge to the same values.*

Figure 3.3 shows the normalised rms of the velocity fluctuations for the air jet and the rms of the concentration for the Freon-12 jet. For comparison purposes, the results

* The validity of this scaling will be limited by the extent of the density difference between the jet and surroundings so that at far enough downstream distance disagreement in collapse of centreline data will result

obtained in an air jet at a Reynolds number of 5800 are also shown and are slightly higher than those at 16900 due in part to the slightly lower values of mean velocity. In both cases the turbulence intensity values $u'/\bar{U}$ tend towards an intensity of 0.25 which is similar to that recorded previously.

The mole fraction un-mixedness, defined as in other works by $X'/\bar{X}$, rises quickly with distance from the nozzle until about 10 jet diameters where it has almost achieved an asymptote of around 0.28 to 0.30. In contrast, the values of the rms of mole fraction concentration, defined by $X'/\bar{X}_o$, reach a maxima of about 0.17 and, when compared to the maximum in the velocity rms, $u'/\bar{U}_o$ = 0.14, makes clear the disparity in potential cores for the velocity and concentration. The maximum un-mixedness in terms of mass fraction $\theta'/\bar{\theta}$ is around 0.19 in contrast to the scalar intensity in the heated jet of Antonia et al (1975) which yielded a value of about 0.26 at 59 diameters. Becker et al (1967) showed a limiting value of $\theta'/\bar{\theta}$ around 0.22 in an air jet and, for jets with lighter density than the ambient, Birch et al (1978) and Pitts and Kashiwagi (1984), found values of $\theta'/\bar{\theta}$ of around 0.28. Also, the heated air jet of Lockwood et al (1980) indicated an asymptote of their temperature fluctuations of 0.21 and corresponds to the case of an initial jet to ambient density ratio of 0.54. The results of Way and Libby (1971), for a helium jet discharging into air (density ratio of 0.14) indicate values of the mass fraction concentration intensity of 0.33 and 0.37 at 15 and 20 diameters, respectively, with values for $u'/\bar{U}$ at these locations of 0.28 and 0.30.

3.3.2 Radial characteristics

The mean profiles for the air and Freon-12 jets, Figures 3.4 and 3.5, indicate that the spread of the jet in the near field ($x/d < 4$) is directly influenced by density ratio. The radial spread of tracer gas in the air jet is similar to that of Freon-12 after about 5 jet diameters and the radial location

corresponding to half the centreline velocity values $(r_{1/2})_u$, is similar for both jets after about 7 diameters. The Freon-12 jet velocity profiles (Figure 3.5) are in all cases fuller than those for air, and similar results were reported by Abramovich et al (1969). The mean mass fraction concentration profile at x/d = 9, Figure 3.5, supports the idea that mass fraction spreads faster than momentum in turbulent jets, as suggested for example by Sforza et al (1978), and does not appear to be density dependent. At x/d > 7 the radial mole and mass fraction distribution can be described by the familiar

$$\frac{\bar{\phi}}{\bar{\phi}_{CL}} = \exp\{-k_3(r/r_{1/2})^{\beta}\} \qquad (3.4)$$

where for $k_3 = \ln 2$ and $\beta = 2$ it is a Gaussian function as used to describe results in the fully developed jet regions; $r_{1/2}$ is the radial location at which the concentration is one-half the centreline value, and ϕ is either the mean mole or mass fraction; and note that a similar form fits the mean velocity results (Figures 3.4 and 3.5). Our constants are slightly different and suggest, in contrast to ligher density jets, that the characteristics of similarity are delayed by the high density ratio (Figure 3.6). The asymptotes (Figure 3.7) of the spreading rate in terms of $r_{1/2}/x$ achieve constant values of 0.071 and 0.099 for mole and mass fraction respectively, for x/d greater than around 10 which, within the experimental uncertainty, are the same as that of Birch et al (1978) for the mass fraction but smaller in terms of mole fraction as usually found, see for example Pitts and Kashiwagi (1984) and Dyer (1979).

The rms of the longitudinal velocity fluctuations $u'/\bar{U}_{CL}$

in the air jet, Figure 3.8, and mole fraction concentration fluctuations of the Freon-12 jet $X'/\bar{X}_{CL}$, Figure 3.9, show a small dependence on Reynolds number away from the centreline and close to the jet exit. The maximum value of the intensity of velocity fluctuations ($u'/\bar{U}_{CL}$) does not exceed 0.18. The intensity of mole fraction concentration $X'/\bar{X}_{CL}$ at x/d = 9 is about 0.29, however, the maximum intensity of the mass fraction fluctuations ($\theta'/\bar{\theta}_{CL}$) is of the same order as the rms velocity intensities, i.e. 0.19. The intensity ratios X'_{max}/X'_{CL} and $\theta'_{max}/\theta'_{CL}$ at x/d = 9 are 1.07 and 1.06, respectively, with the radial location of these maximas at $r/r_{1/2}$ = 0.354; $r_{1/2}$ is the concentration half radius. Pitts and Kashiwagi (1984) report for a similar analysis values of X'_{max}/X'_{CL} = 1.31 at $r/r_{1/2}$ = 0.92 for a methane jet while Birch et al (1978) report $\theta'_{max}/\theta'_{CL}$ = 1.20 at $r/r_{1/2}$ = 0.7, and corresponding findings by Becker et al (1967) for air and Dyer (1979) for propane, are consistent in that jets of heavier gas result in lower values of X'_{max}/X'_{CL} and $\theta'_{max}/\theta'_{CL}$. Some influence of initial conditions (i.e. jets from pipes instead of nozzles) can be expected to influence these $r/r_{1/2}$ values.

3.3.3 Higher moments and probability densities

Results for the skewness and kurtosis of concentration along the jet centreline are in agreement with the trends reported by Birch et al (1978), and Pitts and Kashiwagi (1984). The same variations in skewness at the near exit locations exist up to about 2 potential core lengths. In agreement with these previous authors, the skewness remains negative along the jet centreline and tends toward a nearly constant value of about -0.23 as compared to the value of about -0.35 reported for the methane jet studies of Birch et al and Pitts and Kashiwagi. For heated jets Venkataramani et al (1975) and Lockwood and Moneib (1980) report the centreline skewness

of temperature field to tend to about -0.3 while Antonia et al (1975), at 59 diameters, found a value of about -0.5. It is interesting to note that the trend in the skewness is to increase with increasing axial direction and for the kurtosis to decrease and, as noted by Pitts and Kashiwagi (1984), to date only the results of Lockwood and Moneib (1980) exhibit opposite behaviour. However, while the centreline value for the kurtosis reported by Venkataramani et al (1975), Antonia et al (1975), Birch et al (1978) and Pitts and Kashiwagi (1984) all remain slightly greater than or equal to 3, the present results have a limiting value around 2.3. Pitts (1986) has reported similar values for skewness and kurtosis as here for his heavy density jets, particularly along the similar axial distances ($x/d < 20$) and for the further downstream locations. The smaller skewness of the higher density jets implies lower excursions of the jet density about the mean and towards the lower concentration regions; the lower values of the kurtosis imply that mixing of the heavy jet fluid occurs with less influence away for the mean value.

Measurements of the probability density function of Freon-12 concentration are shown for the jet centreline and two radial locations in Figure 3.10: they were obtained digitally over 1% concentration intervals and normalized according to

$$\int_0^1 P(X)\, dX = 1 \qquad (3.5)$$

The centreline distributions (Figure 3.10(a)) show departures from Gaussian and with negative skewness as noted previously. Venkataramani et al (1975) measured marginal and joint probability distributions of temperature and longitudinal (u) and transverse (v) velocity components in a round heated jet at 15 jet-diameters and

found that the centreline temperature pdf exhibited negative skewness although the pdf's for u and v were more nearly Gaussian. For the pdf's obtained they found that all distributions departed from Gaussian with bimodal temperature distributions in the intermittent regions. The pdf characteristics for the velocity components reported by Ribeiro and Whitelaw (1975) at 57 jet diameters when compared to those of Venkataramani et al (1975) suggest that the basic features of the velocity pdf's are similar at upstream and downstream locations and further support of this is provided by the near field pdf's of u reported by Lau et al (1979).

Birch et al (1978) presented concentration pdf's at about 10 jet diameters and, when compared to the present results at 9 diameters (Figure 3.10(c)), show similar bimodal features are towards the jet edges. The pdf's obtained at 3 jet diameters (Figure 3.10(b)) indicate a much more pronounced bimodal distribution which is consistent with the influence on mixing by the near field periodicity of the large scale structures presumably due to shear layer instabilities. The near field periodicity will be considered further in the following subsection. Similar conclusions involving periodicity of the flow through measures of the pdf in a mixing layer have been reported by Mungall et al (1984).

The work of Dopazo (1975) proposes an analytical pdf approach for a round heated jet but comparison of the results in that work to the experimental findings here and elsewhere, for instance Venkataramani et al (1975), indicates that accuracy is limited. As noted by Pope (1979), Dopazo's model cannot represent large departures from Gaussian and homogeneous behaviour. Improved models have been suggested for example by Pope (1976, 1979), Kollmann (1979) and Givi et al (1984) and appear to better deal with non-Gaussian behaviour. Rigorous testing of the improved models has, however, been limited by lack of measured distributions, in

particular, of fields in reacting and non-reacting flows where density weighted results are obtained.

It is expected that the velocity results are unweighted in the vicinity of the centreline where triple correlations are small and to tend towards weighted averages as $\langle\rho'u'^2\rangle/\langle\rho\rangle\langle U\rangle^2$ increases. The exact values cannot be determined but it is expected that the maximum uncertainty in unweighted mean velocity will be less than 5% and is based on estimates as reported in the Appendix of this chapter. The concentration results obtained by probe and by optical methods should correspond to weighted and unweighted values respectively and it is encouraging to note that the two are similar up to the jet half width with discrepancies up to 3% of unity towards the outer edges. As expected, density weighted values are lower.

3.3.4 Energy spectra

The near field of uniform density jets has been examined by many authors as reviewed in Chapter 1 and the emphasis has been with the nature and magnitude of naturally occurring oscillations and their amplification by external sources.

It is well established that round jets can exhibit preferred frequencies, particularly in the near field and at transitional Reynolds numbers. Hussain (1983), for example, has suggested that the frequencies correspond to Strouhal numbers based on jet exit diameter, d, and velocity ($St_d = fd/\bar{U}_o$) in the range from 0.3 to 0.55 although the preferred mode for the jet and associated stable vortex pairing can occur at higher values. Because the pairing phenomenon is still not fully understood, the velocity and concentration signals obtained both in the uniform and non-uniform density flow were spectrum analysed, using analogue and digital processing, with resolution of better than 5Hz and a uniform

filter bandwidth of 7.2Hz at 3db. Figures 3.11 and 3.12 present energy spectra for the centreline of the air (3.11(a)) and Freon-12 (3.12(a)) jets and show predominant frequencies at the end of the potential cores which correspond to Strouhal numbers of 0.3 and 0.8, respectively. For the non-uniform density jets, spectral information of velocity was obtained with a single hot-wire calibrated in the jet potential core and no attempts were made to further compensate for density effects. This approach yields accurate spectral results for the frequency components although the energy magnitudes are likely to be in error. As a severe test of this, the wire was calibrated in the Freon-12 jet and used in the air jet and vice versa. The spectral results for both jets were similar to those obtained with the wire calibrated for the corresponding density but the energy magnitudes showed some differences.

The broad-band nature of the spectra in the vicinity of the jet exit gives way to the preferred frequency as the vortex structures form; in both cases, however, the preferred frequency has disappeared by 6 diameters indicating the break-up of the structures into the turbulent flow. The fundamental frequency at the jet exit f_o, does not contain the most energy further downstream and at the end of the potential core the first subharmonic, $f_o/2$, tends to become dominant indicating a transfer of energy between the fundamental and the subharmonic. Measurements in the plane three diameters from the exit for the air jet (Figure 3.11(b)) show that the discrete frequencies at the jet exit can be detected consistently up to a radial location of about 0.5d (i.e. towards the region where the maximum in the mean velocity gradient is found and where the intensity $u'/\bar{U}_{CL}$ appear maximum) with similar findings in the Freon-12 jet, Figure 3.12(b). Comparison of the two sets of results shows the dominant frequency of the air jet (at the end of the potential core) to be 2.27 times that of the Freon-12 jet with the Strouhal number 2.67 times smaller. It seems unlikely that the high value of the Strouhal number for the

Freon jet is associated with the stable pairing of vortex rings, as found by Zaman and Hussain (1980) since their investigations were in uniform density jets, and it can be expected that stability characteristics of the jet will be dependent on jet density as well as boundary and initial conditions. This is discussed further below.

It should be noted that, when the air jet was arranged to have the same initial momentum as the Freon-12 jet (i.e. Re ≃ 5850 instead of 16900), the measured frequency was identical to that of the Freon-12 jet and the Strouhal number increased to 0.38. It is noted that a consistent increase in measured frequency resulted with increase in jet velocity and vice versa independent of the jet density. To further test the scaling of frequency with momentum, similar measurements were obtained with helium at the same jet-exit momentum (Re ≃ 2000) and the frequency was again found to be identical with that for air and Freon-12; the corresponding Strouhal number was 0.14. An example of the helium jet spectra is shown on Figure 3.13 for various radii in the 3d plane: as can be seen the dominant frequency can still be observed at 0.8d which confirms the greater spreading when $\rho_{jet}/\rho_{amb} < 1$. Further measurement with the helium jet at Reynolds numbers of 2500, 3000 and 3500 showed that the Strouhal number increased in this range, in contrast to the opposite trend with the air jet but similar to that subsequently determined with Freon-12. Table 3.2 summarises these results and it is clear that for the investigations here, a reduction in jet Reynolds number results in reduction of the dominant frequency independent of jet density. Just as the frequency scale with momentum, the Strouhal number can be shown to scale with the inverse of momentum so that, when defined as

$$St_\rho = \frac{fd}{U} \left(\frac{\rho_{amb}}{\rho_{jet}}\right)^{\frac{1}{2}} \qquad (3.6)$$

the same value is obtained for the helium, air and Freon-12

jets of the same initial momentum within the experimental uncertainty imposed by the small variation in initial boundary-layer thicknesses.

The variation in the shape of the velocity spectra between x/d of zero and four is, in part, due to a variation in the dominant frequency which at the jet exit gives rise to a Strouhal number (St_d) of 0.58 and, at x/d of 4 to a value of 0.30. Durão and Pita (1984) suggest from their air jet measurements that two modes of vortex formation may exist with the preferred mode established by the end of the potential core. The present air jet results are consistent with this conjecture but the results with helium and Freon-12 are not so that density effects may dictate the extent to which multiple vortex pairing can exist. For example, the stability analysis of Anderson and Bejan (1985) for a round jet suggests some agreement with the findings here. Their analysis shows that as the shear layer thickness increases the Strouhal number of the most amplified mode decreases; this observation can be made with our air jet results. With the helium jet a similar condition is observed by considering the rapid spreading of the helium jet resulting in a very fast shear layer growth (consistent, moreover, with the decrease in potential core length for jets of lighter density, see also Pitts (1986)). Thus, for the helium jet, the thick shear layer immediately at the nozzle exit would result in no variations in Strouhal number downstream since the jet preferred frequency would be established very near the exit plane. Finally, in the case of the Freon jet, the slower growth in shear layer thickness along the first four diameters (Section 3.3.2) suggests penetration of disturbances (due to the vortex roll-up at the jet exit) into the centre of the jet to be less possible, as predicted by Anderson and Bejan (1985), and in this case would result in the established frequency at the jet exit shear layer not penetrating into the centreline.

Concentration spectra were obtained from Rayleigh signals from the Freon-12 jet for the same Reynolds numbers as the

velocity spectra and revealed the same dominant frequencies. The periodicity of the flow predicted in part by the pdf results is evident from a typical trace of concentration (LRS) signals as shown in Figure 3.14. An example of the centreline evolution for this scalar spectrum is shown in Figure 3.15 for Re = 16900 with corresponding results along the radial planes in Figure 3.16. The difference in potential core lengths of the scalar and velocity field is evident from Figure 3.15 since the decay of the dominant frequency in the scalar spectrum occurs near to 5 diameters whereas the corresponding behaviour of the velocity spectrum occurs closer to 7 diameters. The radial distributions at x/d = 3 show that the presence of the dominant frequency of the scalar spectrum extends to around 0.65d in contrast to the velocity spectra which lose their dominant frequency at around 0.5d. The lower frequencies found in the heavier density jet, but with the same Reynolds number as lighter jets, suggests that the entrainment of the latter is greater than of the former. Unlike the u-velocity spectrum, the radial location at which the scalar spectrum tends to flatten is not coincident with the radial location of maximum intensity. With the scalar spectrum for the Freon jet, it is interesting to note that along the radial plane at x/d = 1 and 2, a frequency of 660Hz is present towards the outer shear layer (particularly evident at the edges of the potential core as can be estimated from Figure 3.5 and 3.15). Penetration of this frequency characteristic towards the centreline does not result as is consistently shown by Figures 3.15 and 3.16. It is expected that the damping of this frequency results as a consequence of the large density of the jet and associated effects of slow growth of the shear layer, as discussed above, leading to a faster dissipation of the energy of external disturbances than would result with a lighter density jet. If the observed frequency of 660Hz did penetrate towards the centreline at x/d = 1, this would result in a similar trend

between f_o and $f_o/2$ as pbserved with the air jet and discussed above in the velocity spectra results. Similar observations can be made at a lower Reynolds number of the Freon jet (Figures 3.16(f) - (j)) where, in addition, it is observed that at a lower Reynolds number, the distance from the nozzle associated with vortex pairing is increased.

3.4 CONCLUSIONS

The main conclusons which can be extracted from the preceding sections are summarised in the following paragraphs.

Thejet of Freon-12 in air spreads more slowly than jets of lighter gas; quantitative comparisons require consideration of the details of the flow properties in the exit plane of the jet. Adjustment of the abscissa in a manner consistent with momentum scaling, tends to make the velocity and concentration decay rates of the Freon-12 and air jets similar.

The measurement of rms values of velocity and concentration must be interpreted with care in view of the preferred frequencies observed in spectra. They do, however, indicate that the values of mass and mole fraction are smaller with the heavier gas. The probability density distributions show a tendency to be more strongly bimodal in regions where preferred frequencies were found in the spectra in contrast to downstream locations where the mixed jet shows weaker bimodal features. The preferred frequencies associated with u-velocity and concentration measurements were similar, probably associated with vortex pairing and could not be identified further downstream than 7d. The Strouhal number ranges from 0.3 to 0.8 and scales with the inverse of jet momentum.

APPENDIX

MEASUREMENT UNCERTAINTIES

3.1.A Uncertainty in velocity measurements

The mean velocities determined with the total head probe are expected to have uncertainties associated with neglect of static pressure and turbulence fluctuations. In the near field the turbulence is not well defined and there velocity fluctuations are expected to be statistically random and therefore with negligible contribution to uncertainties. In the outer edges of the jet, however, inclusive of the near field and in developed flow regions downstream, velocity fluctuations can be assumed to be normally distributed (Becker and Brown, 1974) and Cho and Becker (1985)) and these can give rise to uncertainties. The longitudinal velocity values as determined by the measurements of total pressure drop ΔP, would be larger than the true velocity by $(1 + \bar{u}'^2/U^2)^{\frac{1}{2}}$. As reported by Bradbury etal (1965,1967), Sunyach and Mathieu (1969) and Cho and Becker (1985), the further neglect of static pressure effects and uncertainty in its accurate measurement , particularly in the near field, can lead to uncertainty of up to 3% in mean velocity and will result in uncertainty in results determined by hot-wire anemometry when calibration of the wire is made with reference to the total head velocity measurements determined with the probe.

When the jet fluid density is different from that of the surroundings, additional errors are introduced due to the effects of density weighting. For variable density flow the total head (Pitot) probe measures the density weighted velocity ρU^2. From first principles the mass average velocity measured with the Pitot probe is a density weighted quantity and is given by

$$\vec{v} \equiv \frac{\int \rho \vec{v}\, d\vec{v}}{\int \rho\, dV} \qquad (3.A.1)$$

where $\vec{v}$ is the velocity vector at a point and ρ the density and dV an element of volume; the mass density ρ is the total density over the volume dV. For a binary gas mixture the mass average velocity is

$$\vec{v} = \frac{1}{\rho}(\rho_A \vec{V}_A + \rho_B \vec{V}_B) = U_{pitot} \tag{3.A.2}$$

where the subscripts A and B denote the two species making up the mixture and $\rho = \rho_A + \rho_B$ the mass density per unit volume of the mixture. If we let $\rho = \bar{\rho} + \rho'$ and $V_i = \bar{V}_i + v_i'$ a time average gives

$$\overline{\rho_i V_i} = \bar{\rho}_i \bar{V}_i + \overline{\rho_i' v_i'}$$

and

$$\overline{\bar{\rho}+\rho'} = \bar{\rho}, \text{ since } \bar{\rho}' = 0$$

Thus (3.A.2) becomes (dropping the vector symbol)

$$\bar{U}_{pitot} = \frac{(\bar{\rho}_A \bar{V}_A + \overline{\rho'_A v'_A}) + (\bar{\rho}_B \bar{V}_B + \overline{\rho'_B v'_B})}{\bar{\rho}_A + \bar{\rho}_B} \tag{3.A.3}$$

At present, it is not possible to measure the individual species velocities and thus the quantity represented by the Pitot probe measurements is the total time average $\langle \rho U^2 \rangle$ and is not equal to $\langle \rho \rangle \langle U \rangle^2$. From Bernoulli's law

$$\Delta P = \frac{1}{2} \rho U^2 \tag{3.A.4}$$

and this result can be conveniently used in a non-dimensional form. For a reference state (o) and any other arbitrary state the ratio of ΔP can be formed as

$$\frac{\Delta P}{\Delta P_o} = \frac{\rho U^2}{\rho_o U^2} \tag{3.A.5}$$

and since the left hand side represents the ratio of $<\rho U^2>/<\rho U^2>_o$ we obtain

$$\frac{U}{U_o} = \{\rho_o/\rho \frac{<\rho U^2>}{<\rho U^2>_o} \}^{\frac{1}{2}} \tag{3.A.6}$$

where the density ratio ρ_o/ρ can be determined under the assumption of ideal gas behaviour from the measured mole fractions X_j and molecular weights M_j of species A and B. Since the conservation of mass requires $X_A + X_B = 1$ and with the ratio ρ_o/ρ after rearrangement being given by

$$\rho_o/\rho = \frac{\left(1 + X_A(M_A/M_B - 1)\right)_o}{\left(1 + X_A(M_A/M_B - 1)\right)} \tag{3.A.7}$$

and to within the first order of approximation, the ratio (3.A.6) can be determined to define the velocity ratio of species A, $(U/U_o)_A$; strictly speaking (3.A.5) is a measure of (3.A.3).

Considering the problem of density in terms of Favre (1969) decomposition with

$$\tilde{U}^2 = \frac{\overline{\rho U^2}}{\bar{\rho}} = \frac{\bar{\rho}\bar{U}^2 + \overline{\rho' u'^2}}{\bar{\rho}} = \bar{U}^2 + \frac{\overline{\rho' u'^2}}{\bar{\rho}} \qquad (3.A.8)$$

then from (3.A.6) and (3.A.8) we obtain

$$\left(\frac{U}{U_o}\right)_A = \left(\frac{\bar{\rho}_o}{\rho_\infty} \frac{(\bar{\rho}\bar{U}^2 + \overline{\rho' u'^2})}{(\bar{\rho}\bar{U}^2 + \overline{\rho' u'^2})_o}\right)^{\frac{1}{2}} \qquad (3.A.9)$$

and in this case the triple correlations would require measurement and with local density to determine

$$\left(\frac{U}{U_o}\right)_A = \left\{\frac{\bar{U}^2}{\bar{U}_o^2}\left(\frac{(1 + (\overline{\rho' u'^2}/\bar{\rho}\bar{U}^2))}{(1 + (\overline{\rho' u'^2}/\bar{\rho}\bar{U}^2))_o}\right)\right\}^{\frac{1}{2}} \qquad (3.A.10)$$

Provided $\overline{\rho' u'^2}/\bar{\rho}\bar{U}^2 << 1$ the conventional average and mass average are approximately the same.

Analysis of the limited data on correlation measurements of velocity and scalars as reported by Stanford and Libby (1974), Pope (1979) and Starner (1983, 1985 and 1986) indicates that mean velocity results in the variable density jet of Freon-12 are unweighted in the vicinity of the centreline where triple correlations are small and to tend towards weighted values with maximum uncertainty of about 5% as the triple correlations increase. If the effects of density are neglected the effect on mean velocity profiles is to obtain measured quantities with the Pitot probe that underestimate the true velocity when the jet density is greater than the surroundings, Figure 3.A.1, and to overestimate the true velocity when the jet density is less than the surroundings,

these conclusions are clear from Equation 3.A.6.

With the hot-wire measurements, uncertainty of up to 3% can be expected near the edges of the jet where the velocity is low and the errors there are expected to be influenced in addition by uncertainties in the pitot probe measurements used to calibrate the wire, Yavuzhurt (1984). Neglecting static pressure effects leads to uncertainties in mean velocity as discussed in Section 3.3.A below.

3.2.A Uncertainties in concentration measurements

For measurements made with the concentration probe an analysis shows that a density weighted quantity is measured for concentration C and with a similar results as obtained with velocity between the Favre average $\tilde{C}$ and time averaged $\bar{C}$ concentration,

$$\frac{\tilde{C}}{\bar{C}} = 1 + \frac{\overline{\rho' C'}}{\bar{\rho}\,\bar{C}} \qquad (3.A.11)$$

The result (3.A.11) holds as a first approximation for a constant suction velocity. When $\overline{\rho' C'}/\bar{\rho}\bar{C} \ll 1$, then $\tilde{C} \sim \bar{C}$ and results for conditions of isokinetic sampling.

The concentration levels determined with both the optical and probe techniques are mole fraction (i.e. percent by volume) quantities. In the case of the probe measurements a sensitive katharometer (Taylor Servomex MK158) was used and had the ability to sustain high suction flow rates and these could be adjusted as required. The katharometer was calibrated for mixtures of known concentration of Freon-12 in air and for helium in air and with uncertainty in full scale of .001mV with full scale for Freon being 320mV and for helium 1100mV. For helium the calibration was linear for volume concentrations of less than 5%. For the Freon the calibration was non-linear

and in this case the calibration data were fit to a power curve

$$\bar{C} = \Sigma\, a_i v^{\alpha_i} \qquad (3.A.12)$$

with the coefficients a_i and exponents α_i determined to provide .995 correlation, v is the voltage.

The effects of density weighting were estimated for the use of different size probes and suction flow rate and were determined to be very sensitive variables. Instrumentation sensitivity was sufficient to detect .01% gas concentrations. When a large intake diameter is used for the probe high fluctucations result and if additionally the suction velocity is greater than that of the stream being measured the lighter component gas in the mixture will be preferentially sampled. When the probe intake velocity is adjusted to be less than that of the measured stream the heavier component is drawn in. These results can be seen from the equation for gas and probe tip concentrations

$$C_{probe} = \frac{\bar{C}_{gas}\,\bar{\rho}\bar{U}_s + \overline{C'_{gas}(\rho U_s)'}}{\overline{\rho U_s}} \qquad (3.A.13)$$

where U_s is the suction velocity. Figure 3.A.2 shows typical sensitivity (slope) of calibration curves determined for Freon-12 and air mixtures as a function of probe size, katharometer input voltage and suction velocity (volumetric intake). Figures 3.A.3 and 3.A.4 present measurements of mean concentration for the jet centreline and along two radial planes, respectively, and make clear the influence of probe size as discussed above. With a larger probe but, under isokinetic

sampling, overprediction of mean concentration can result by as much as 20% of unity in the present isothermal case. When differences in concentration are small (Figures 3.A.2 and 3.A.4(b)), the difference between density weighted and unweighted values decrease but can be as high as 10% of unity.

With the particular probe size used for the measurements reported in the chapter (and by comparison to results as in Chapter 2 to the time averaged LRS results), uncertainties in mean concentration are expected to be 2% in the inner jet regions and with maximum uncertainty towards the edges of the jet of about 3%.

3.3.A Uncertainty due to neglect of static pressure

For the round jet, the static pressure variation across the jet can result from contributions of mean and rms velocity. The influence of velocity fluctuations is greater than the mean velocity and particularly the radial fluctuations of velocity. Thus, the resulting time-averaged momentum equation along the radial direction is given by

$$\frac{1}{\rho}\frac{\partial \bar{P}}{\partial r} + \frac{\partial \bar{v}}{\partial r}^{,2} + \frac{\overline{v'^2} + \overline{w'^2}}{r} = 0 \qquad (3.A.14)$$

and can be integrated across the jet to give

$$\bar{P} + \rho\overline{v'^2} + \rho\int_0^\infty \frac{\overline{v'^2} - \overline{w'^2}}{r}\,dr = P_s \qquad (3.A.15)$$

where $\bar{P}$ is the stagnant (total) pressure at a point and P_s the static pressure at the same point. At the jet centreline, the

integral term is zero from considerations of symmetry and thus

$$\bar{P} - P_s = -\rho\overline{v'^2} \tag{3.A.16}$$

Away from the centreline the additional term of the integral contributes but as indicated from measurements in round jets $\overline{v'^2} \sim \overline{w'^2}$ so that neglect of $\overline{v'^2} - \overline{w'^2}$ will introduce only a negligible error in contrast to $\rho\overline{v'^2}$.

The ideal response of the Pitot probe is

$$\bar{P}_p - P_s = \frac{1}{2}\rho\bar{U}^2 \tag{3.A.17}$$

where $\bar{P}_p$ (i.e. $\bar{P}$) is the time-averaged total pressure sensed by the probe. Taking the ambient pressure as reference instead of the local static pressure (P_s) at the measurement point gives

$$\bar{P}_p - P_{amb} = (\bar{P}_p - P_s) + (P_s - P_{amb}) \tag{3.A.18}$$

or

$$\bar{P}_p - P_{amb} = \frac{1}{2}\rho\bar{U}^2 - \rho\overline{v'^2} \tag{3.A.19}$$

The result (3.A.19) indicates the measured velocity using a Pitot probe with the reference pressure as the ambient leads to overprediction of the true velocity. For $\bar{U}^2 >> \overline{v'^2}$, $\bar{P}_p - P_{amb} \sim \bar{P}_p - P_s$; however, the quantities are not exact and as suggested by measurements of $\overline{v'^2}/\bar{U}^2$, $\bar{P}_p - P_{amb}$ can lead to differences in $\bar{U}$ from (3.A.17) by as much as 3% greater. It is important to note that when turbulence levels are low

the difference between static and ambient pressure will be greatest and thus assuming $\bar{P}_p - P_{amb} \sim \bar{P}_p - P_s$ will tend towards the amount of largest error for the measurements, for example, as can result for measurements in the potential core.

The 5% uncertainty (Section 3.1.A) for the mean velocity results of the Freon jet take into account the static pressure neglect; in addition to uncertainties in the density estimates and triple correlations, equation (3.A.10). For the air jet, the mean velocities have an estimated uncertainty of about 3% and the rms values about 5%. The effect of neglecting the static pressure correction, as noted above, is to overpredict mean velocities determined with the Pitot probe. The contribution to the mean velocity uncertainty is $(\partial U/\partial P_s)\Delta P_s \sim \frac{1}{2}U\ \overline{(\Delta P_s/\bar{P}_s)^2}^{\frac{1}{2}}$. If correction of the static pressure variations were made, the uncertainty in mean and rms velocities would be less than 1% and 3%, respectively. The uncertainty in the mean velocity of the Freon jet would be about 2.5% to 3%, influenced by variations in $\rho' u'^2$.

TABLE 3.1 Influence of density ratio on mean flow

Reference	ρ_{jet}/ρ_{amb}	k_1	x'/r_o	k_2	x''/r_o	Re
Becker et al (1967)	1.0	0.093	4.8	0.093	4.8	54000
Birch et al (1978)	0.55	0.090	3.5	0.125	11.6	16000
Dyer (1979)	1.52	0.114	5.1	0.090	0.3	9790
Pitts et al (1984)	0.55	0.083	-7.5	0.112	-2.0	4130
Present work	4.17	0.178	8.1	0.086	-9.78	16900

TABLE 3.2 Summary of velocity spectra results for air, helium and Freon-12

Jet fluid	ρ_{jet}/ρ_{amb}	Re	f(H_z)	St_d	St_ρ
Helium	0.136	2000	330	0.14	0.38
		2500	450	0.15	0.41
		3000	595	0.16	0.43
Air	1.00	5850	330	0.38	0.38
		8450	400	0.32	
		16900	750	0.30	
Freon-12	4.17	5860	85	0.59	0.29
		16900	330	0.80	0.38

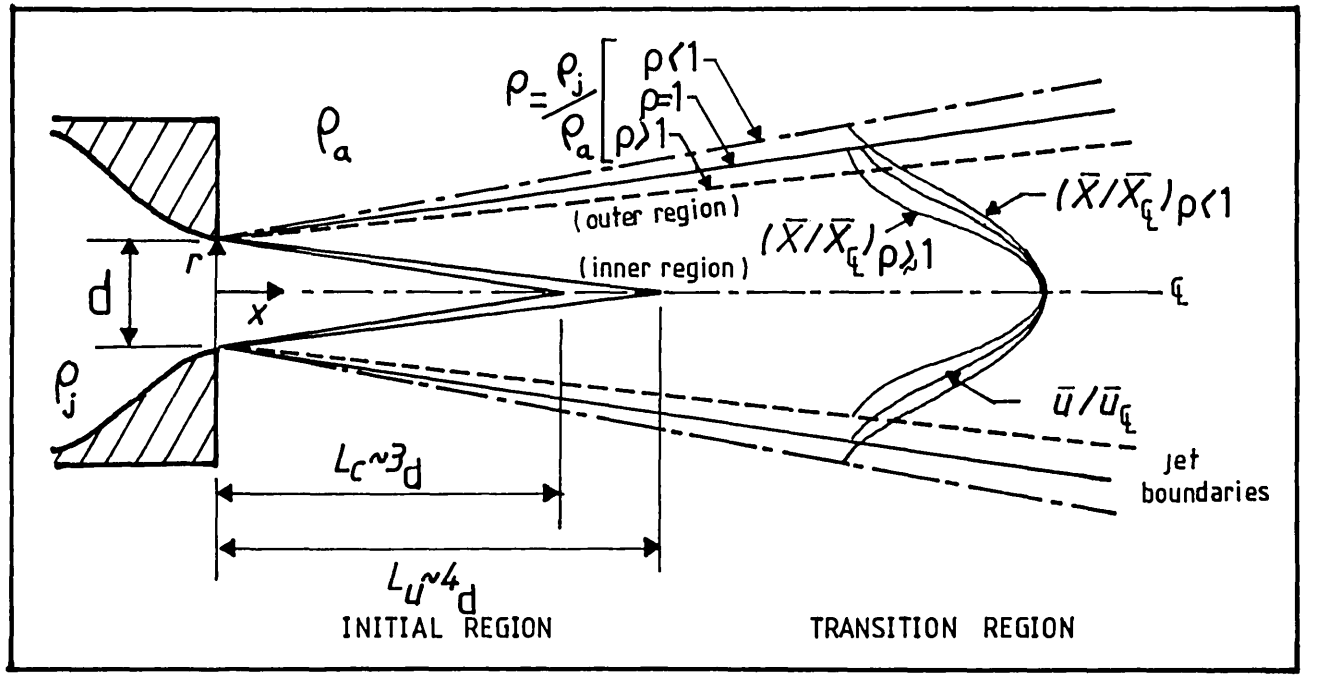


FIGURE 3.1 SPREADING OF JETS; Lc and Lu DESIGNATE THE TYPICAL CONCENTRATION AND VELOCITY POTENTIAL CORE LENGTHS, RESPECTIVELY

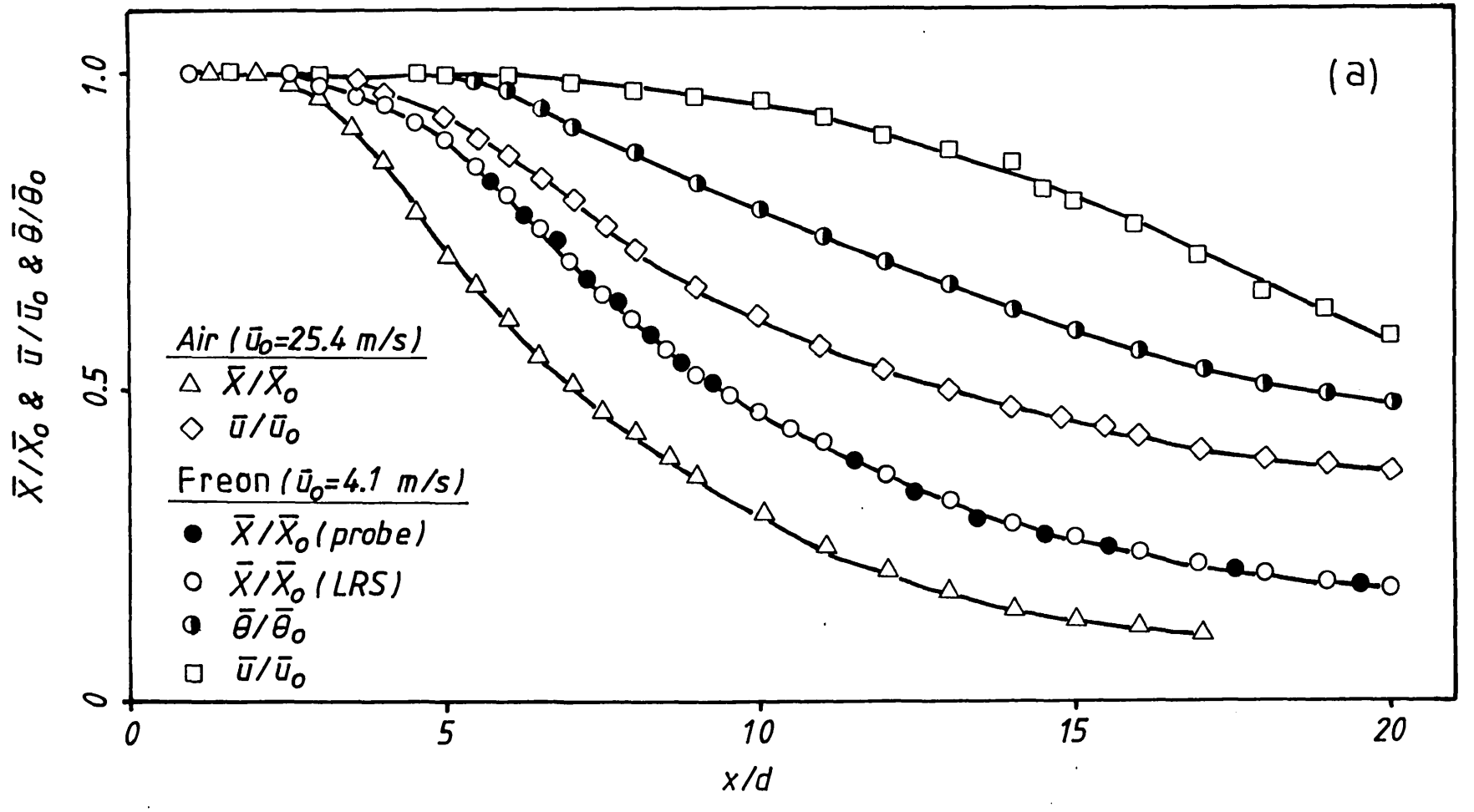


FIGURE 3.2 CENTRELINE DISTRIBUTIONS OF MEAN VELOCITY AND CONCENTRATION

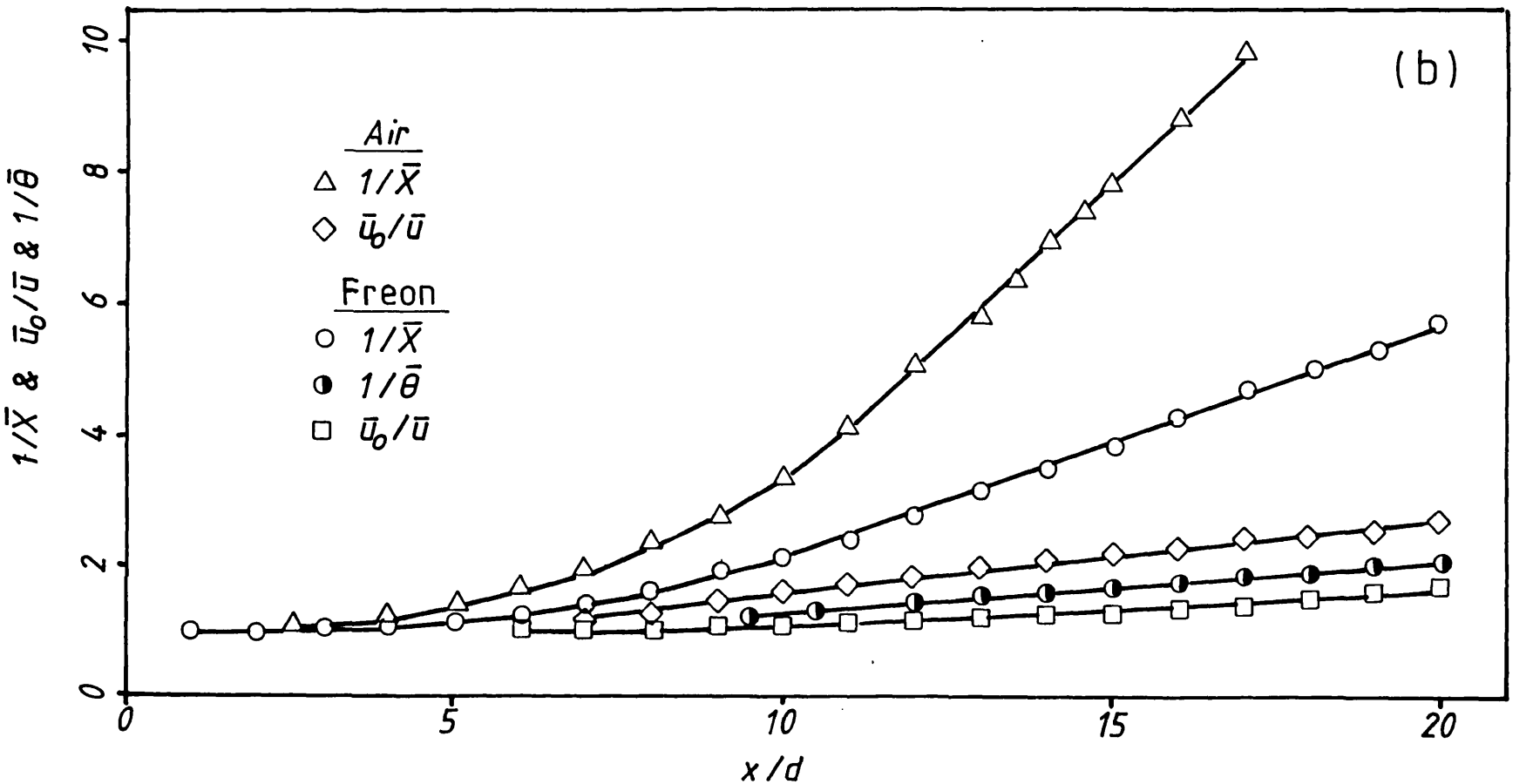


FIGURE 3.2 continued

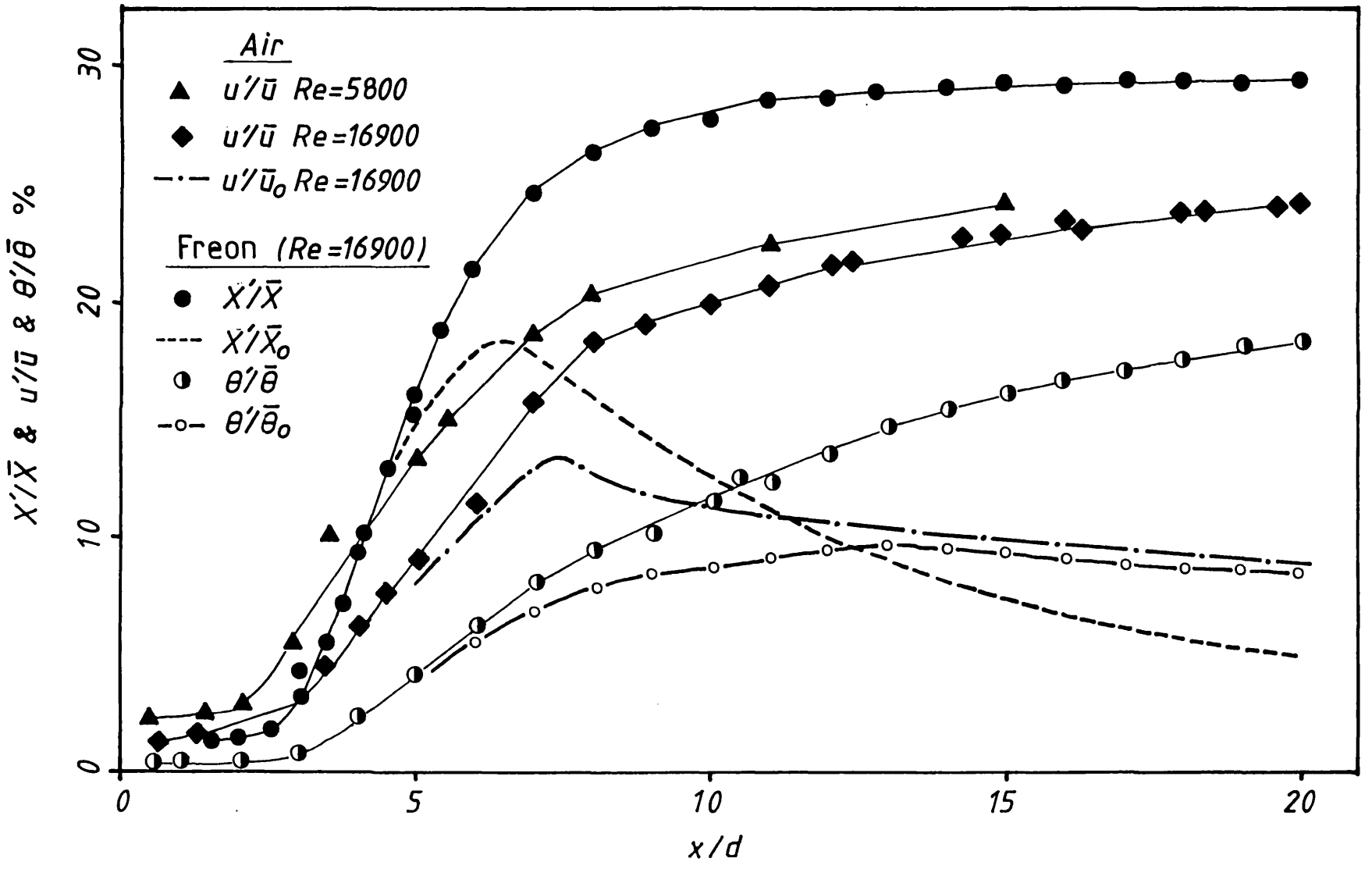


FIGURE 3.3 CENTRELINE DISTRIBUTIONS OF THE RMS OF VELOCITY AND CONCENTRATION SIGNALS

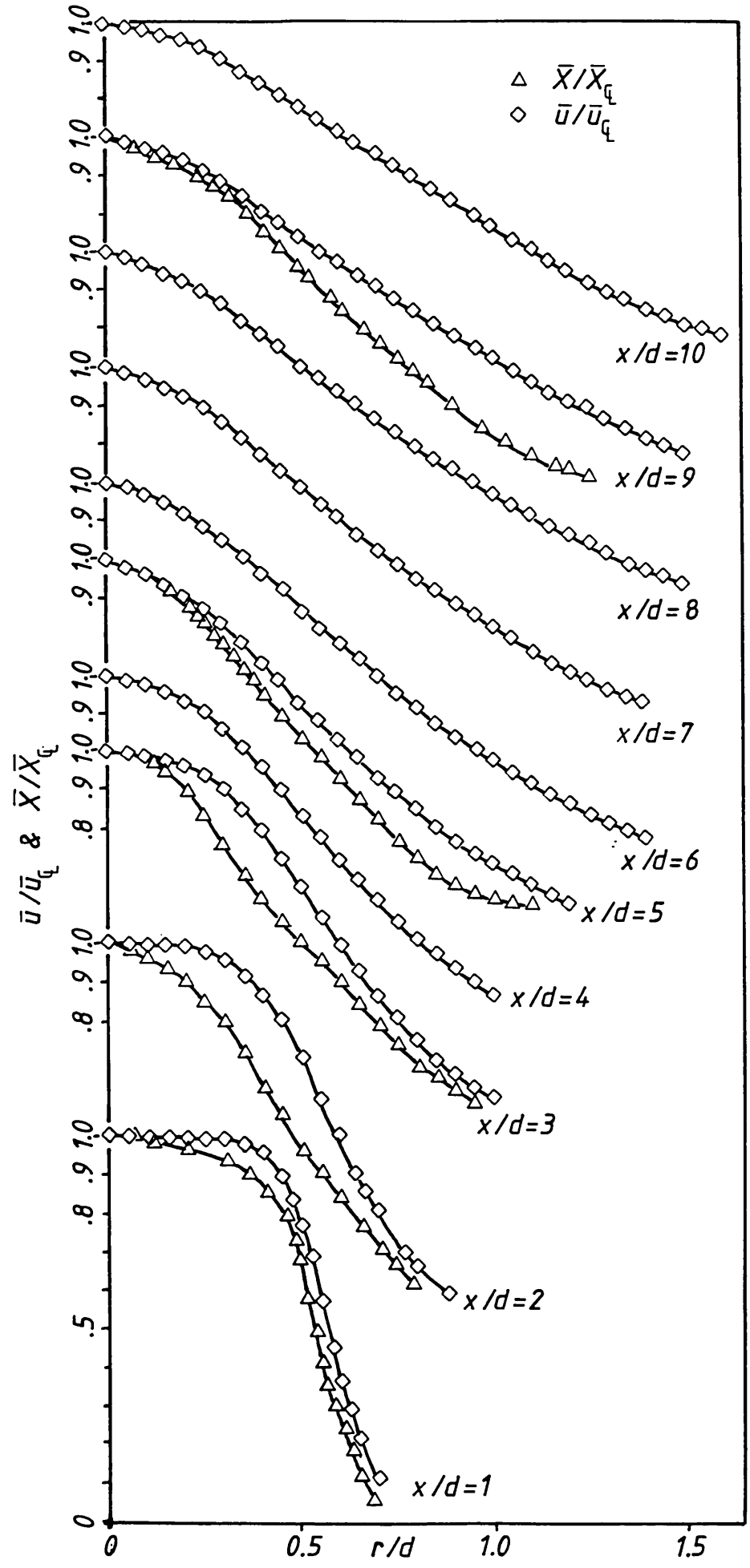


FIGURE 3.4 RADIAL PROFILES OF MEAN VELOCITY AND HELIUM TRACE CONCENTRATION FOR AIR JET WITH RE=16, 900

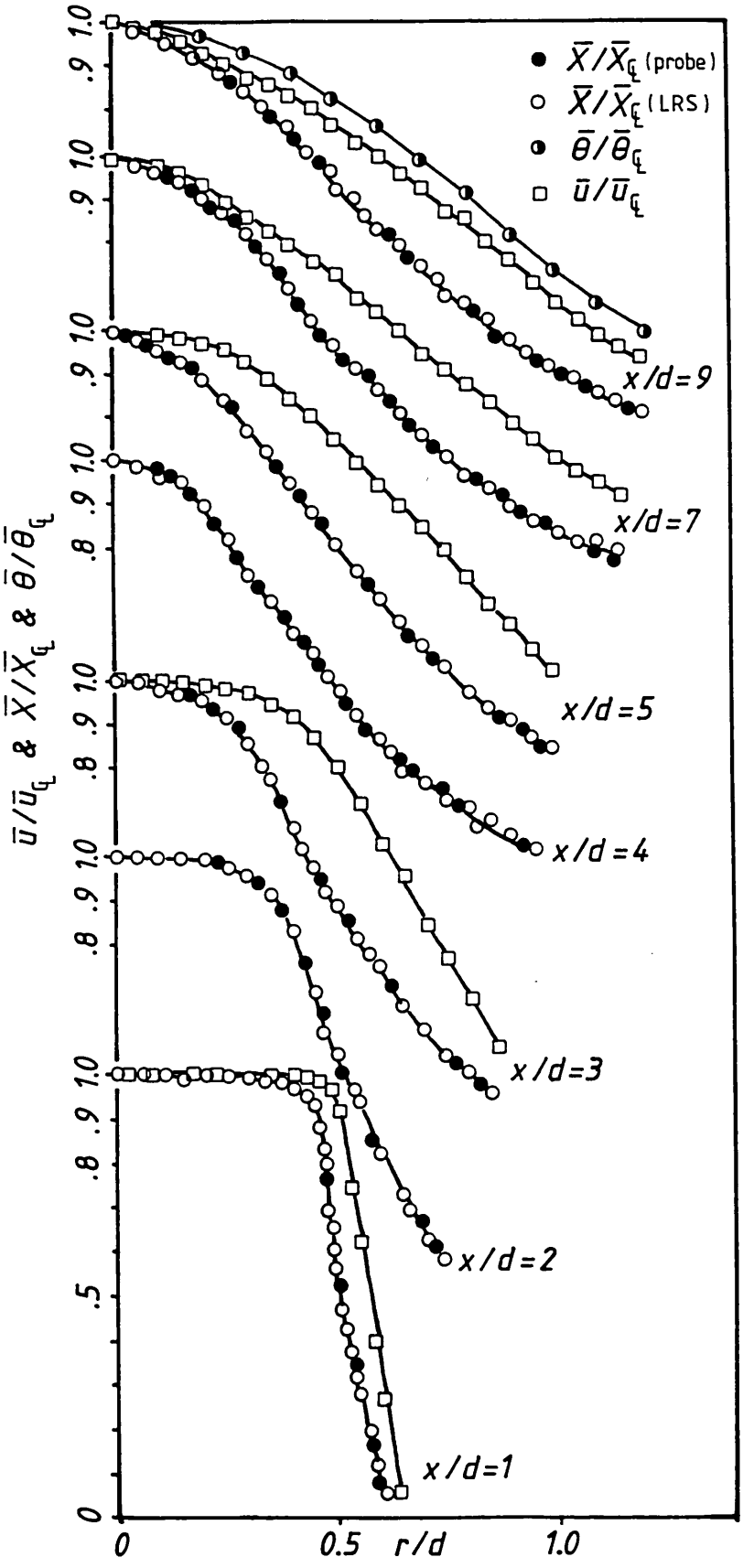


FIGURE 3.5 RADIAL PROFILES OF MEAN VELOCITY AND CONCENTRATION FOR FREON-12 JET WITH RE=16900

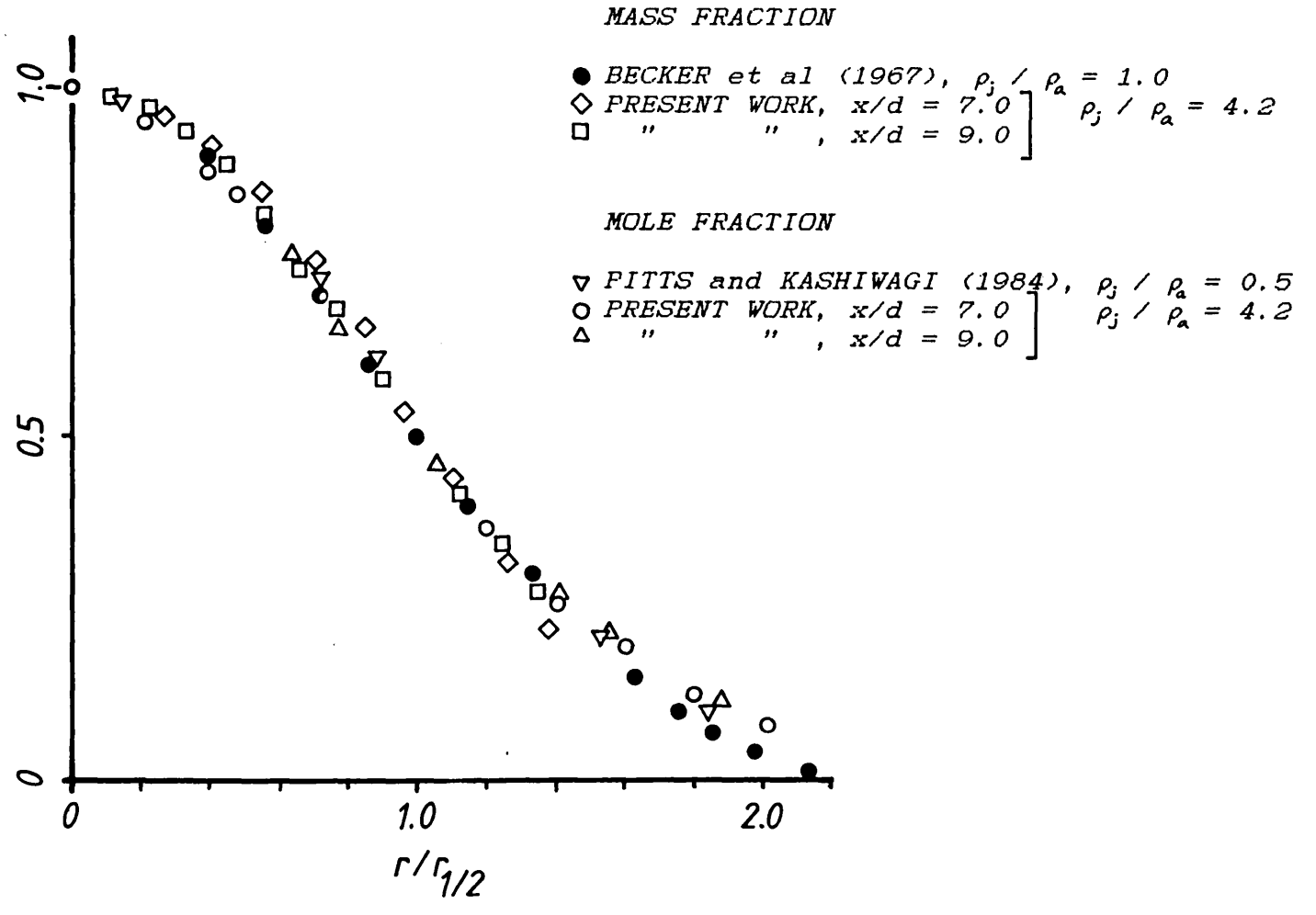


FIGURE 3.6 SIMILARITY IN MEAN PROFILES OF CONCENTRATION (note that the same similarity characteristics result with the mean velocity profiles)

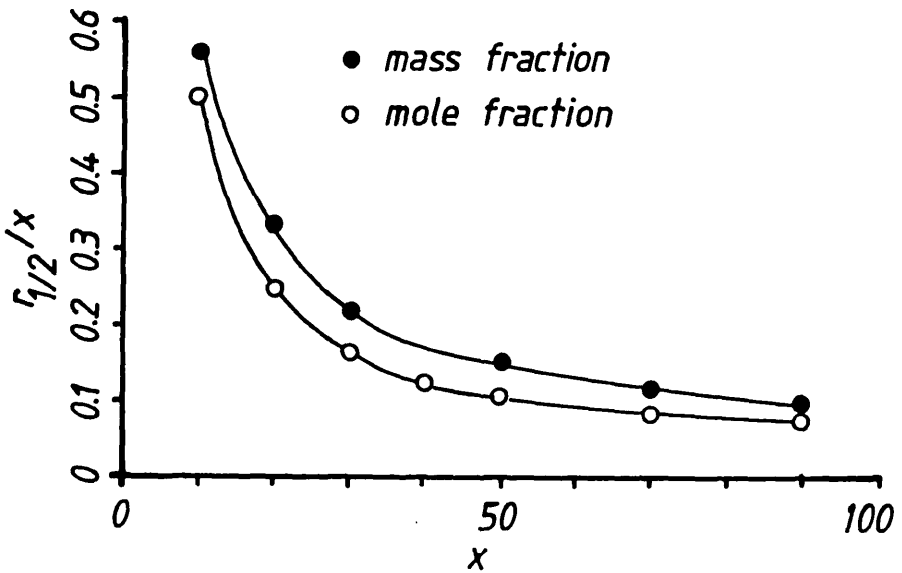


FIGURE 3.7 AXIAL CHARACTERISTICS OF MASS AND MOLE FRACTION SPREAD

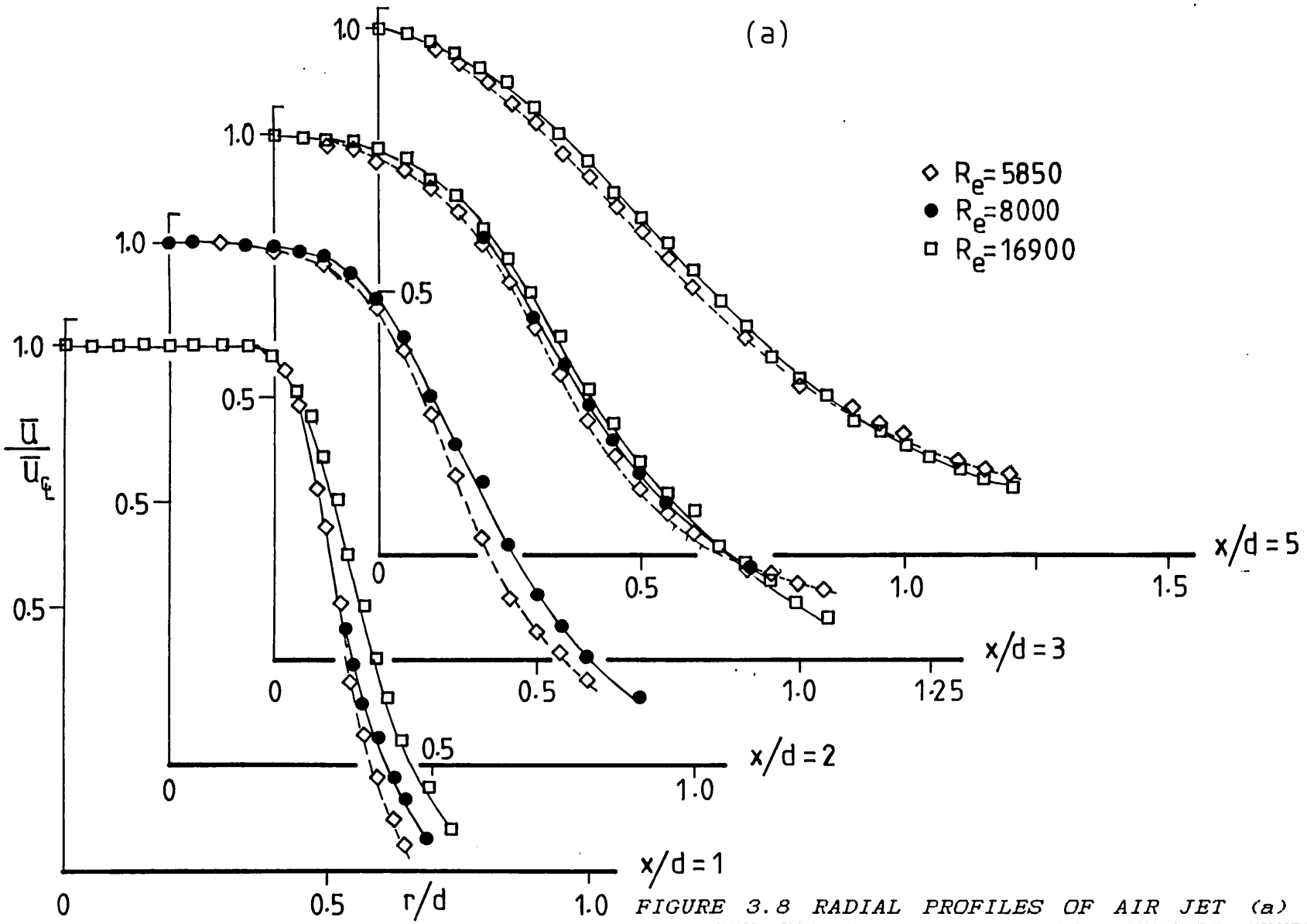
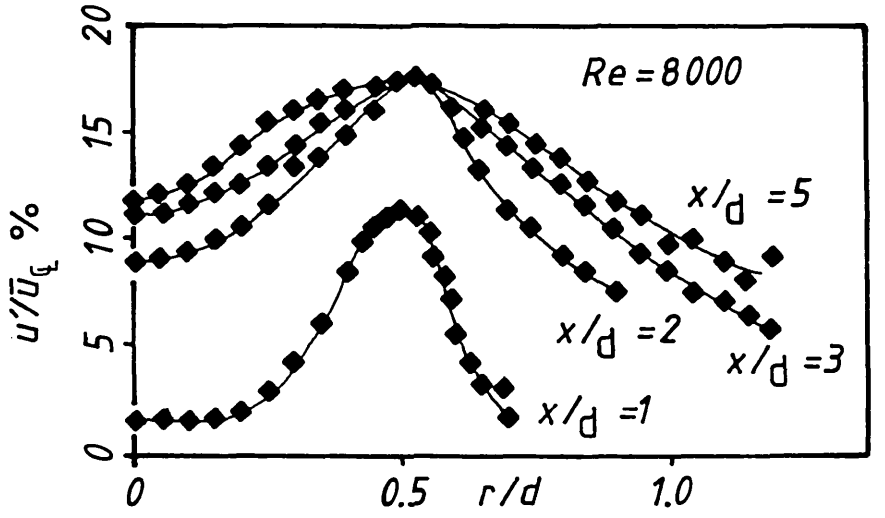
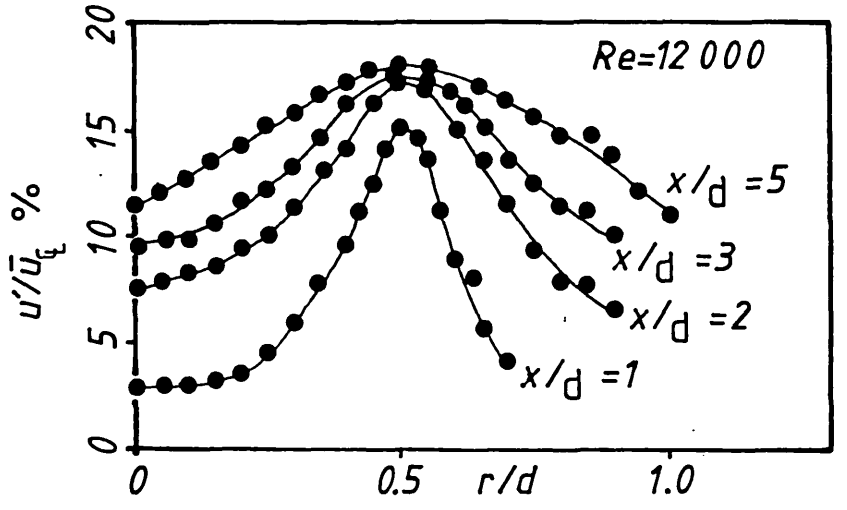


FIGURE 3.8 RADIAL PROFILES OF AIR JET (a) MEAN and (b) RMS VELOCITY SIGNALS AT DIFFERENT REYNOLDS NUMBERS (note that at Re=5850, the air jet has the same exit momentum flux $\rho\bar{U}d^2$ as the FREON-12 jet at Re=16,900)



(b)



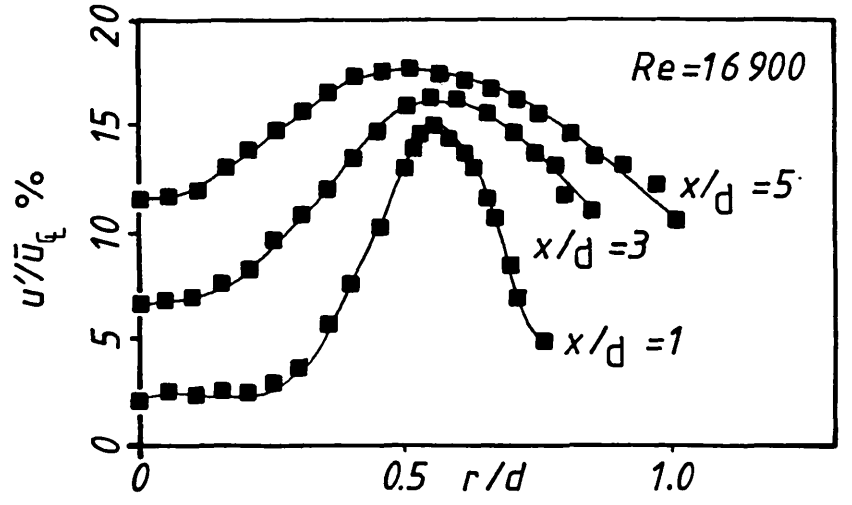


FIGURE 3.8 continued

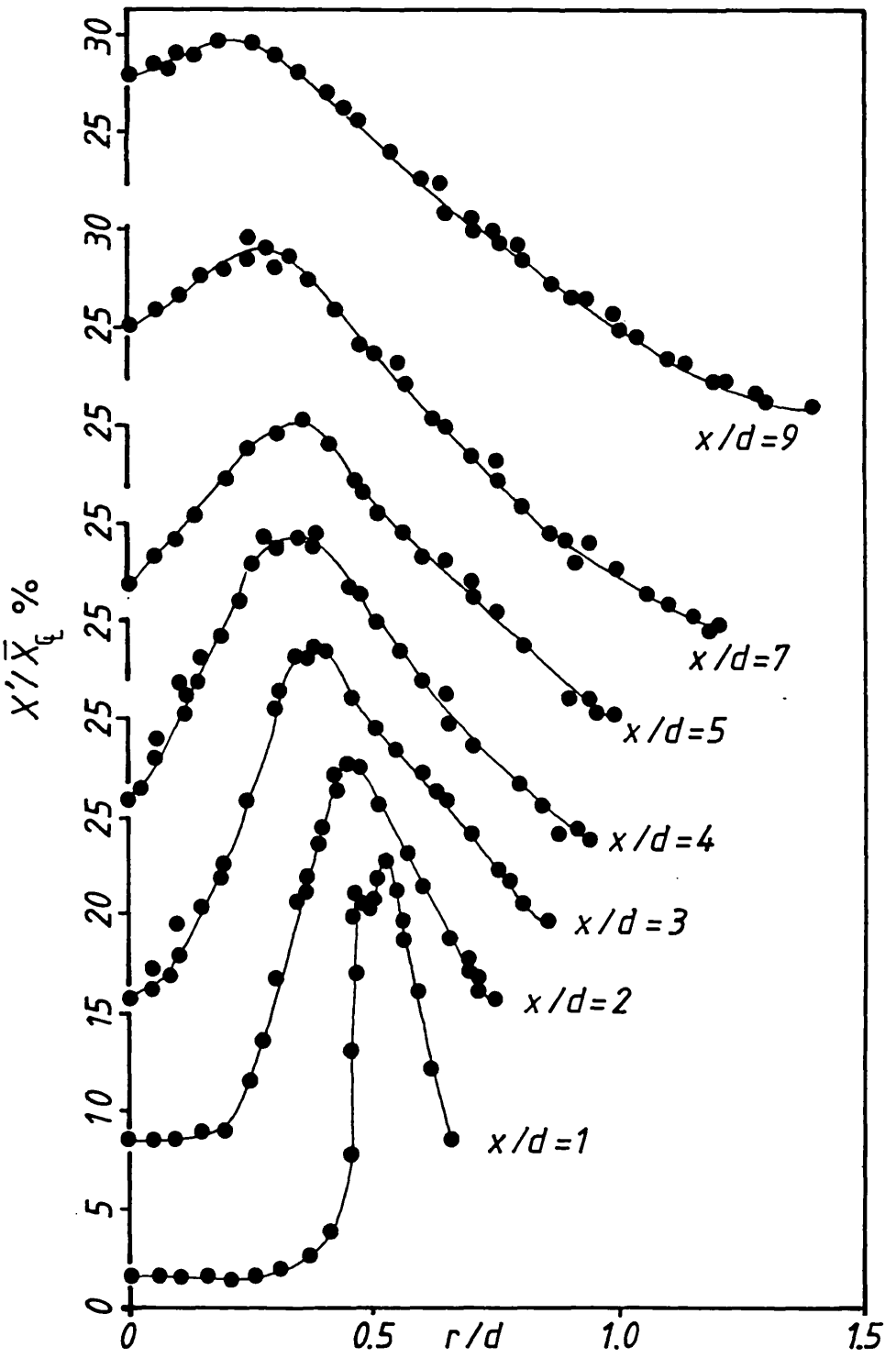


FIGURE 3.9 RADIAL PROFILES OF THE RMS OF CONCENTRATION SIGNALS FOR FREON-12 JET WITH Re=16,900

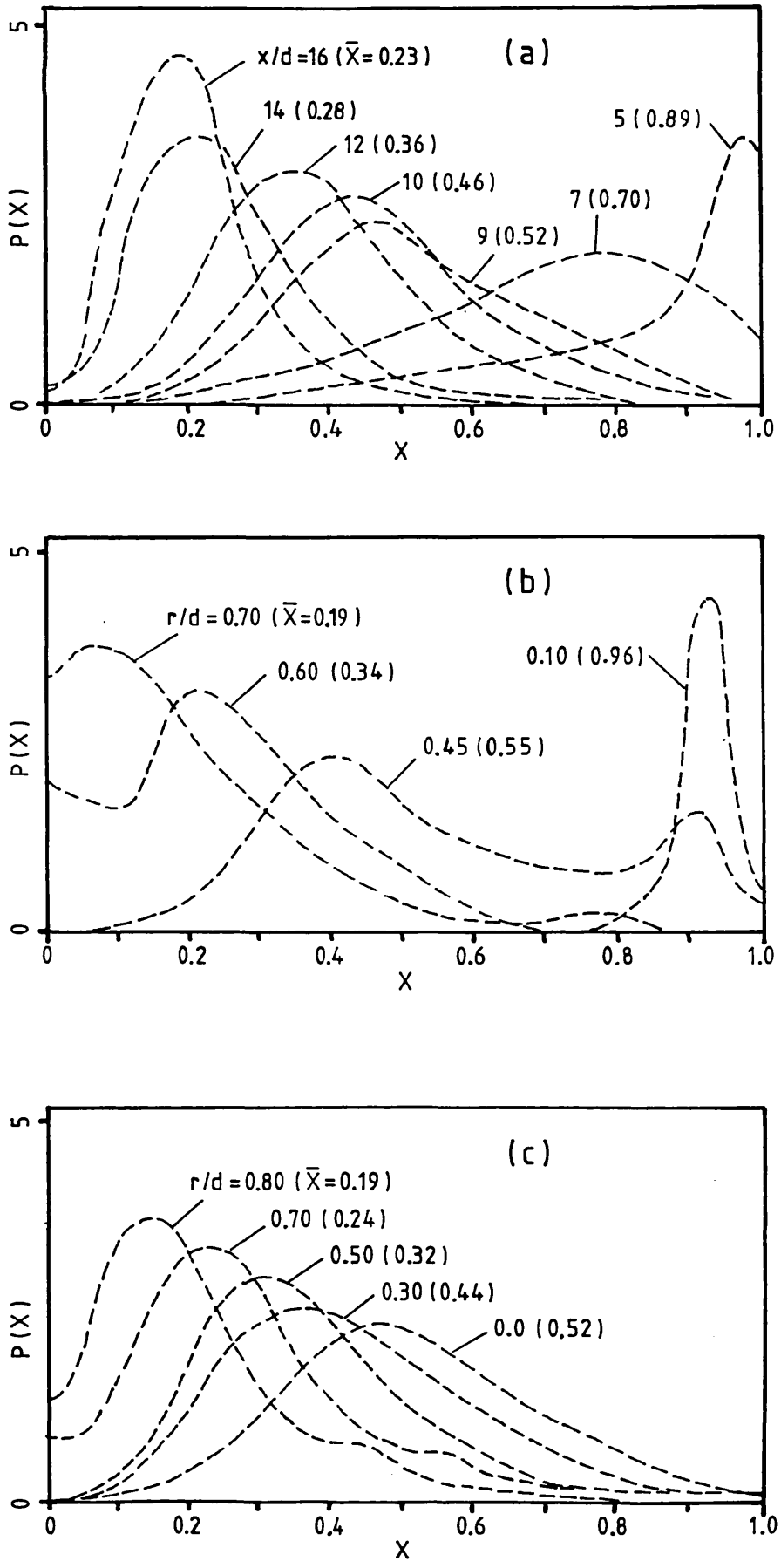


FIGURE 3.10 PROBABILITY DENSITIES FOR FREON-12 JET, Re=16,900 (a) CENTRELINE, (b) x/d=3.0 and (c) x/d=9.0

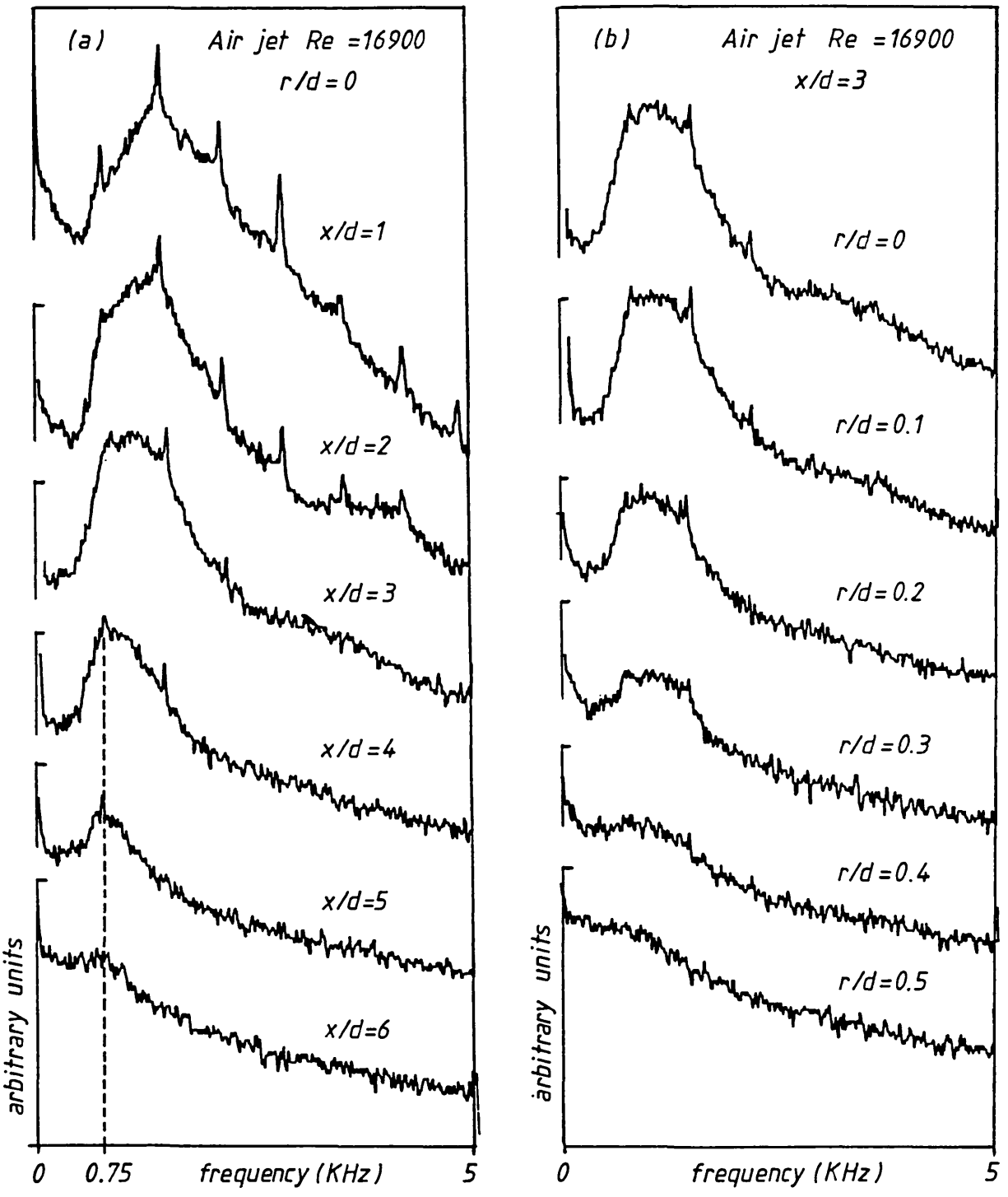


FIGURE 3.11 SPECTRA OF u-VELOCITY FLUCTUATIONS IN AIR JET (a) CENTRELINE and (b) x/d=3.0

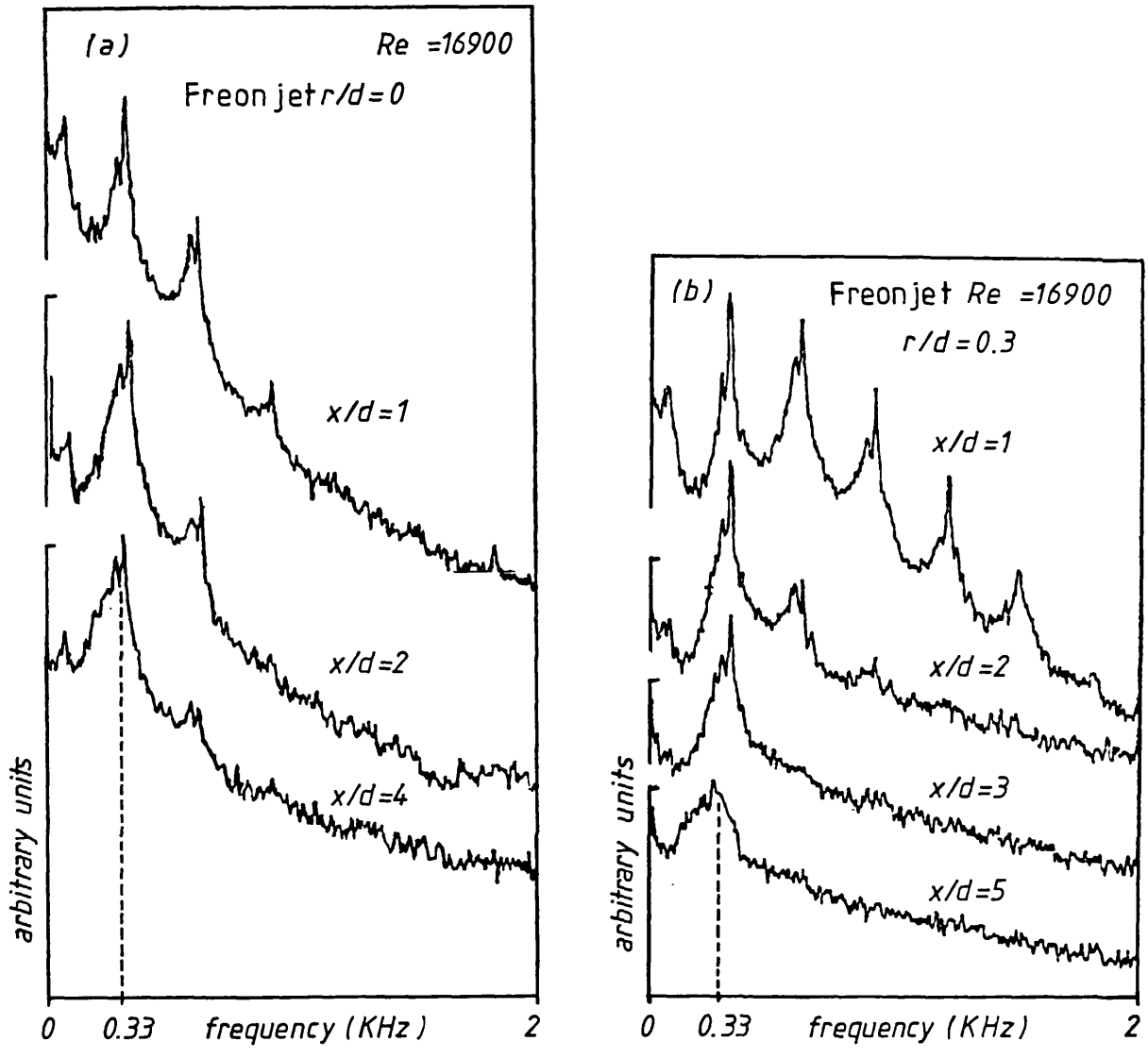


FIGURE 3.12 SPECTRA OF u-VELOCITY FLUCTUATIONS IN FREON-12 JET (a) CENTRELINE and (b) x/d=3.0

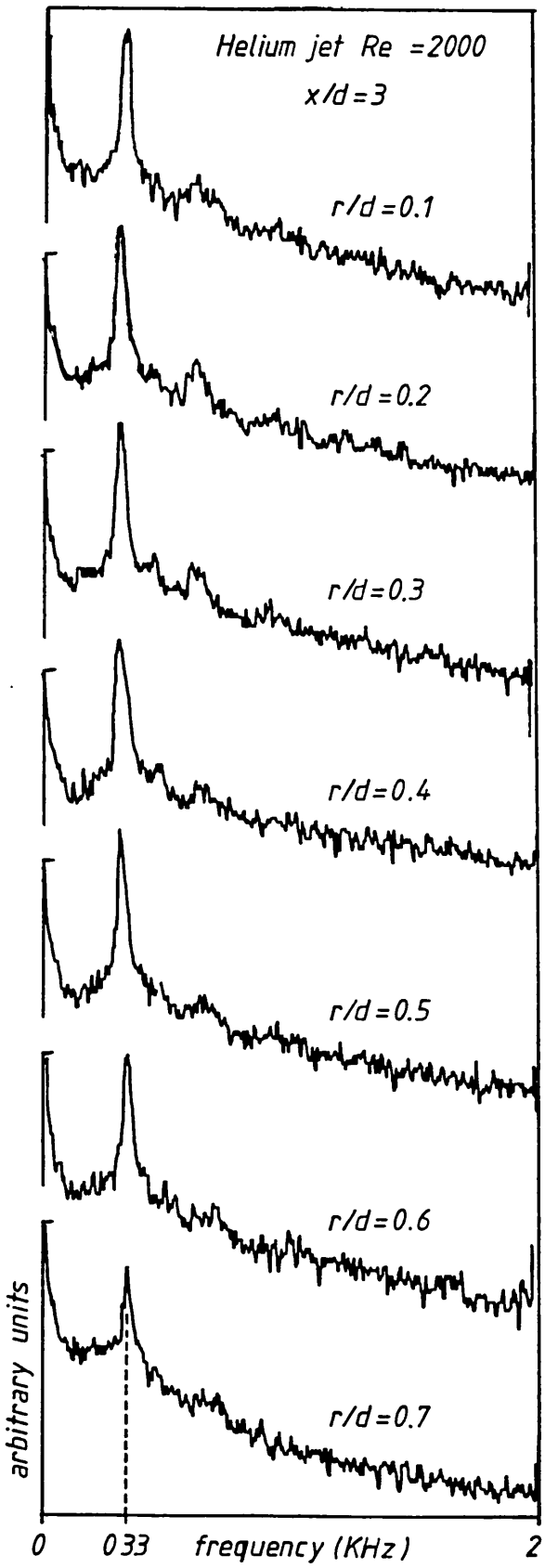


FIGURE 3.13 SPECTRA OF u-VELOCITY FLUCTUATIONS IN HELIUM JET ALONG THE PLANE AT x/d=3.0

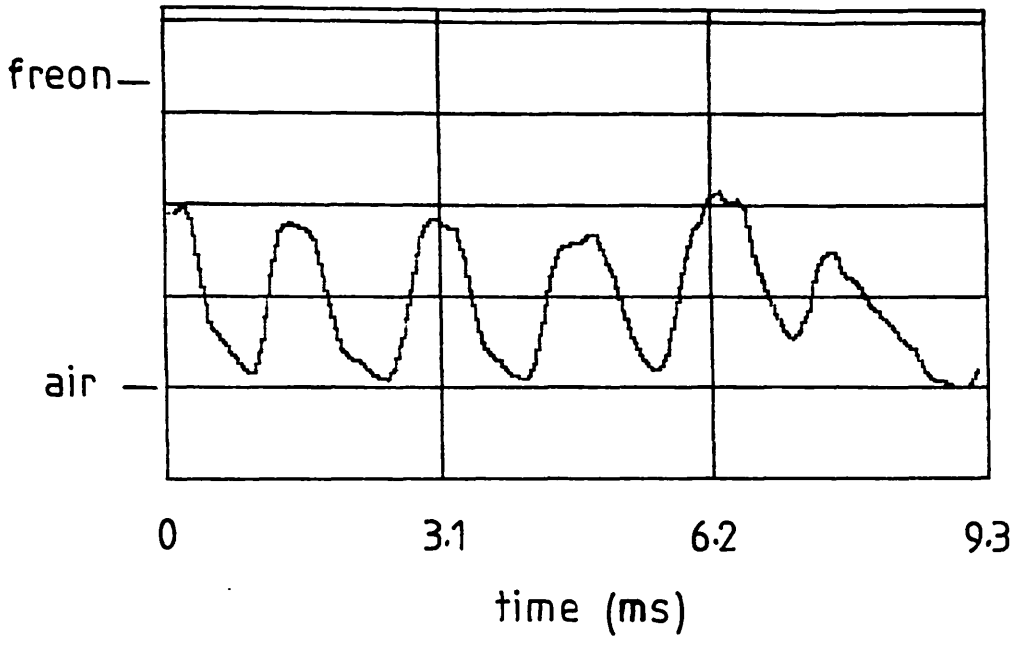


FIGURE 3.14 TYPICAL LRS SIGNALS OF CONCENTRATION WERE PERIODIC BEHAVIOUR IS EXHIBITED BY THE FLOW (x/d=3.0, r/d=.35): FREON-12 JET WITH Re=16,900.

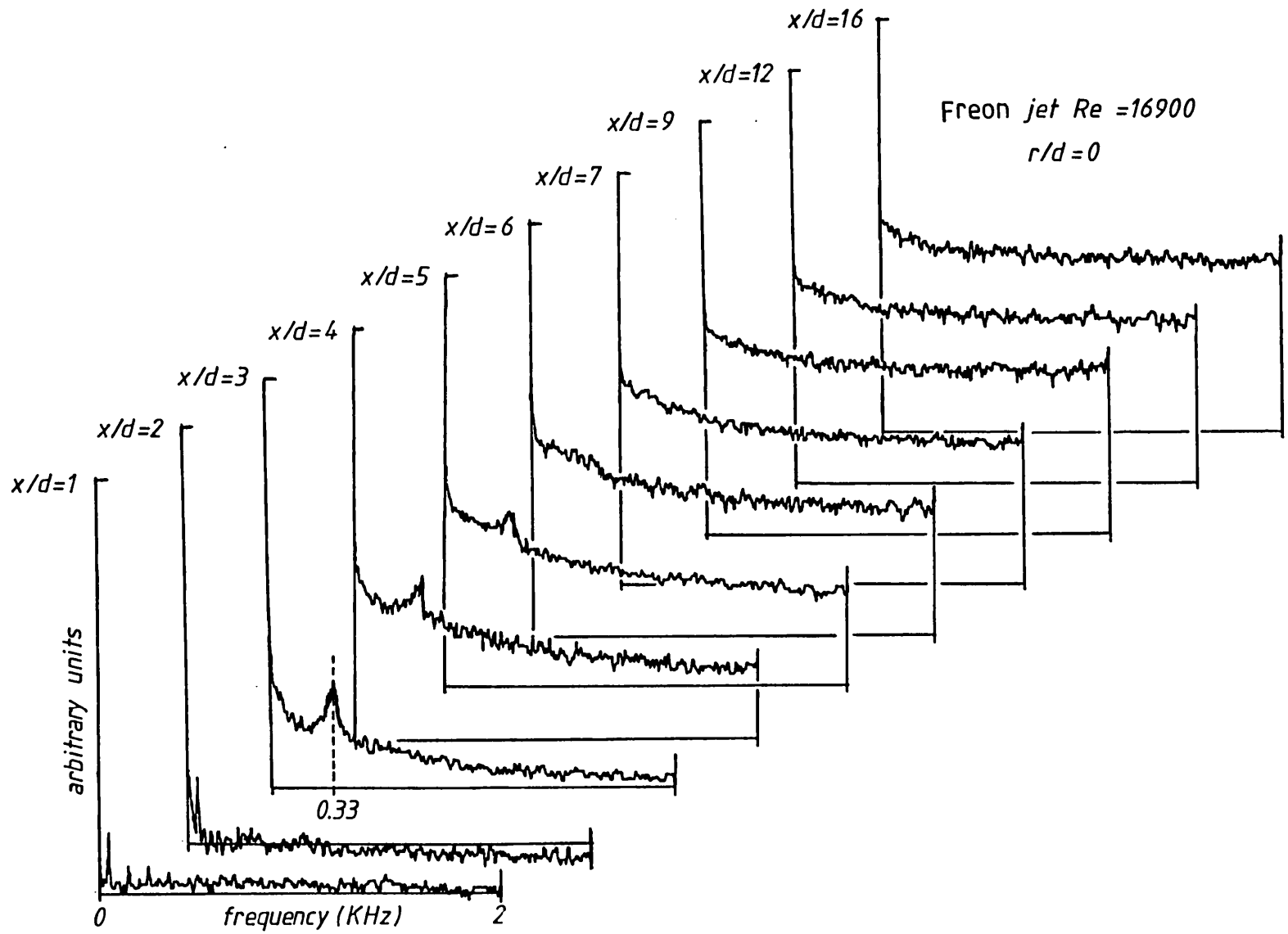


FIGURE 3.15 CENTRELINE EVOLUTION OF SPECTRA OF CONCENTRATION FLUCTUATIONS: FREON-12 JET WITH Re=16,900

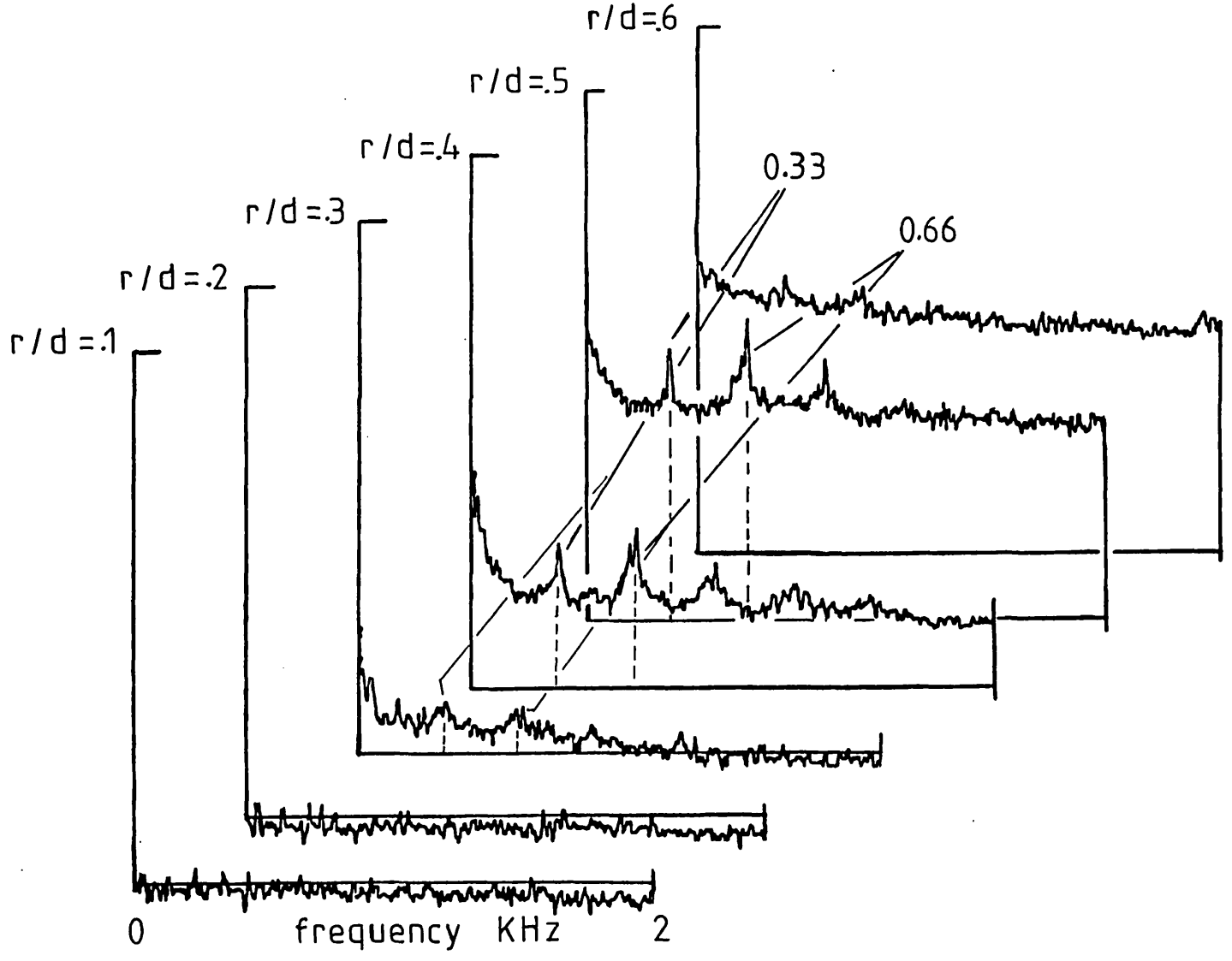


FIGURE 3.16 RADIAL SPECTRA OF CONCENTRATION FLUCTUATIONS OF FREON-12 JET (a) x/d=1.0, Re=16,900

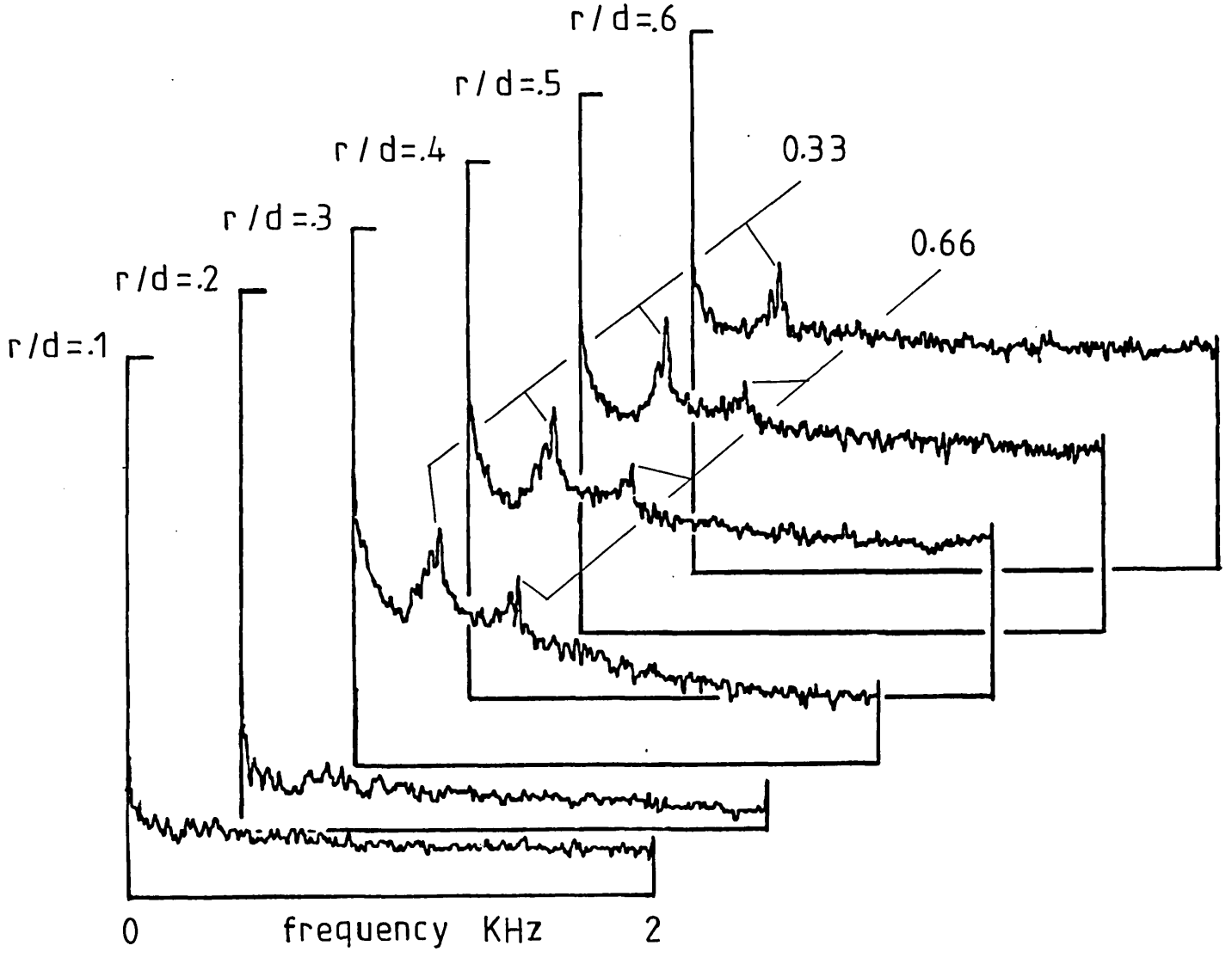


FIGURE 3.16 (b) x/d=2.0, Re=16,900

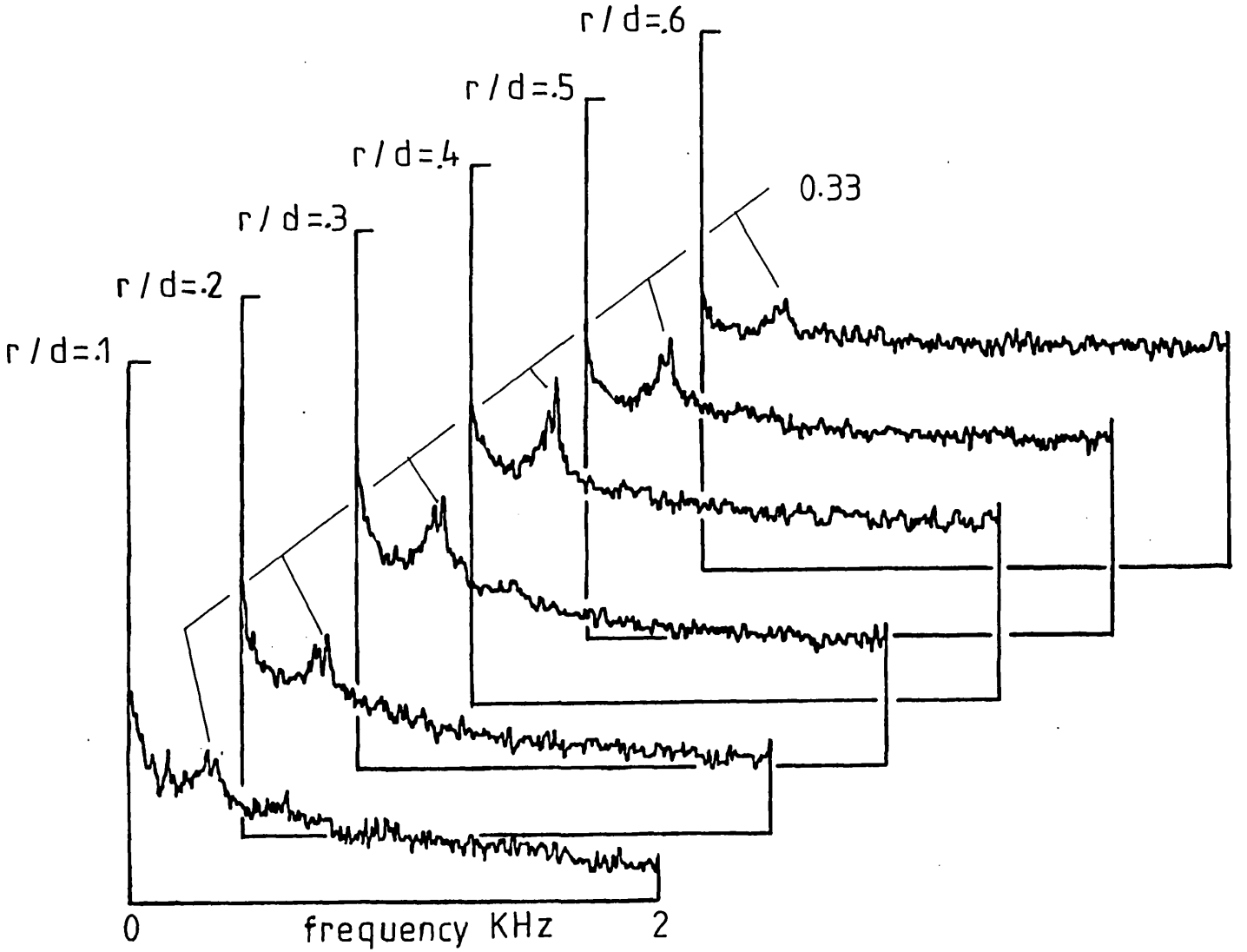


FIGURE 3.16 (c) x/d=3.0, Re=16,900

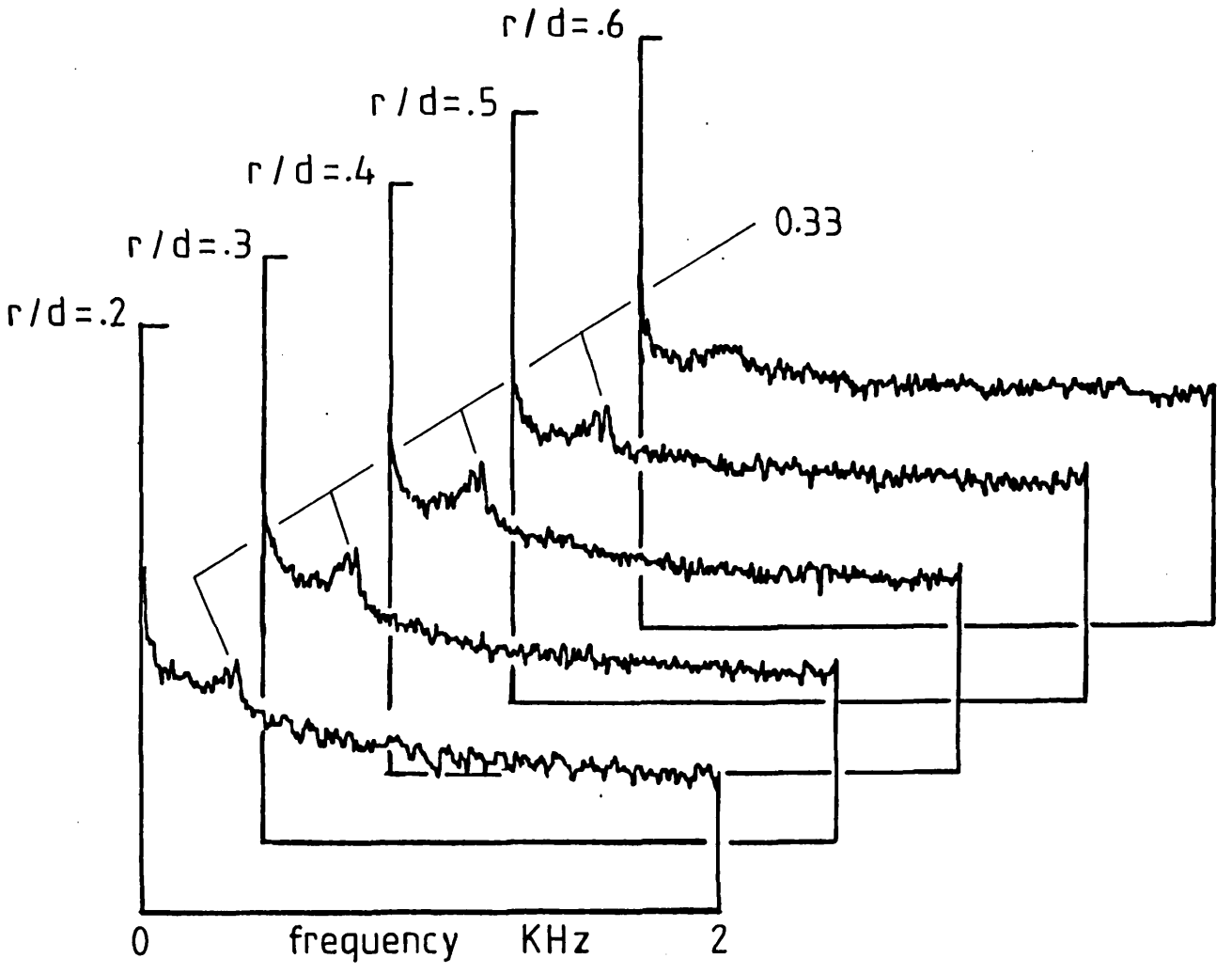


FIGURE 3.16 (d) x/d=4.0, Re=16,900

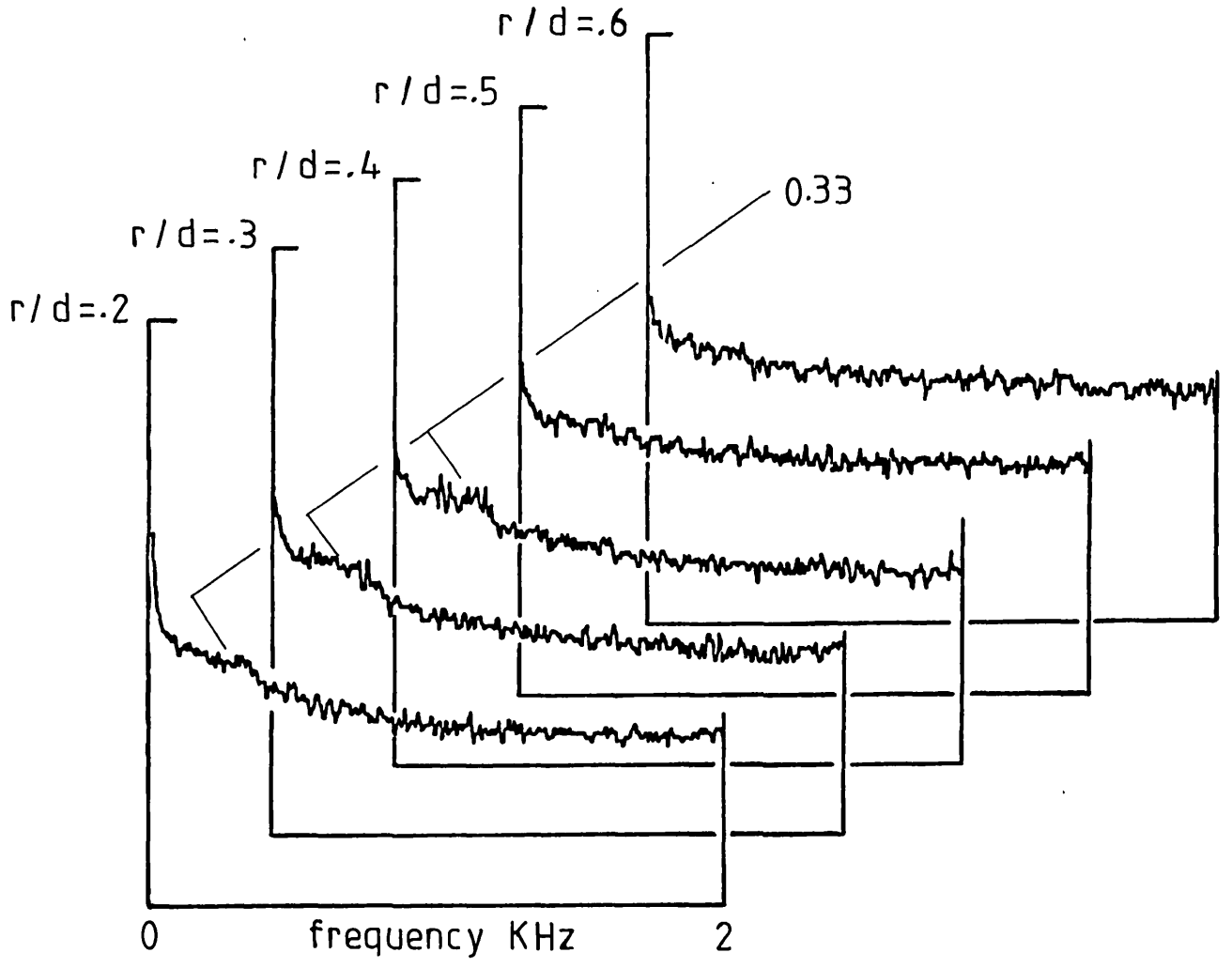


FIGURE 3.16 (e) x/d=5.0, Re=16,900

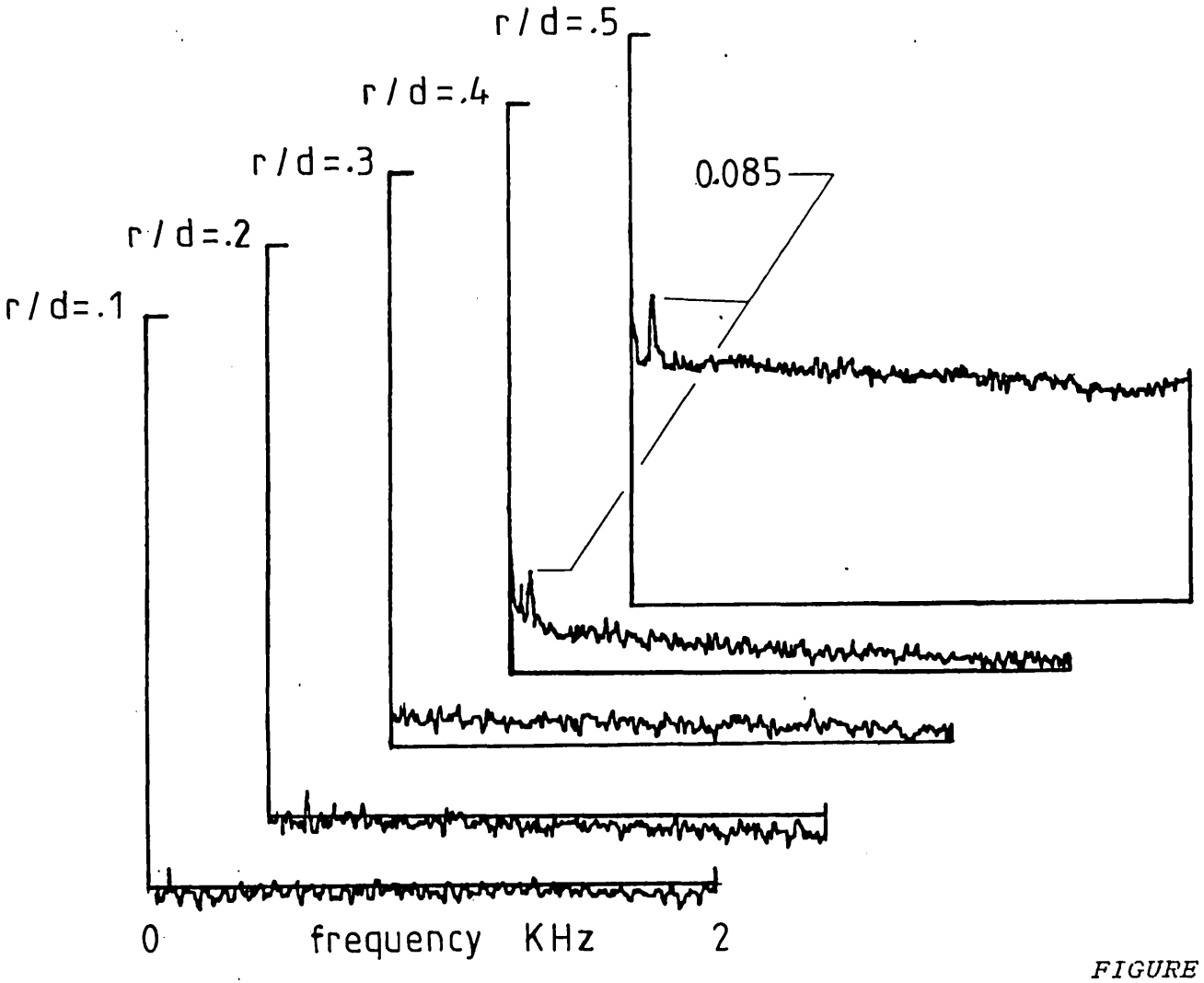


FIGURE 3.16 (f) x/d=1.0, Re=5860

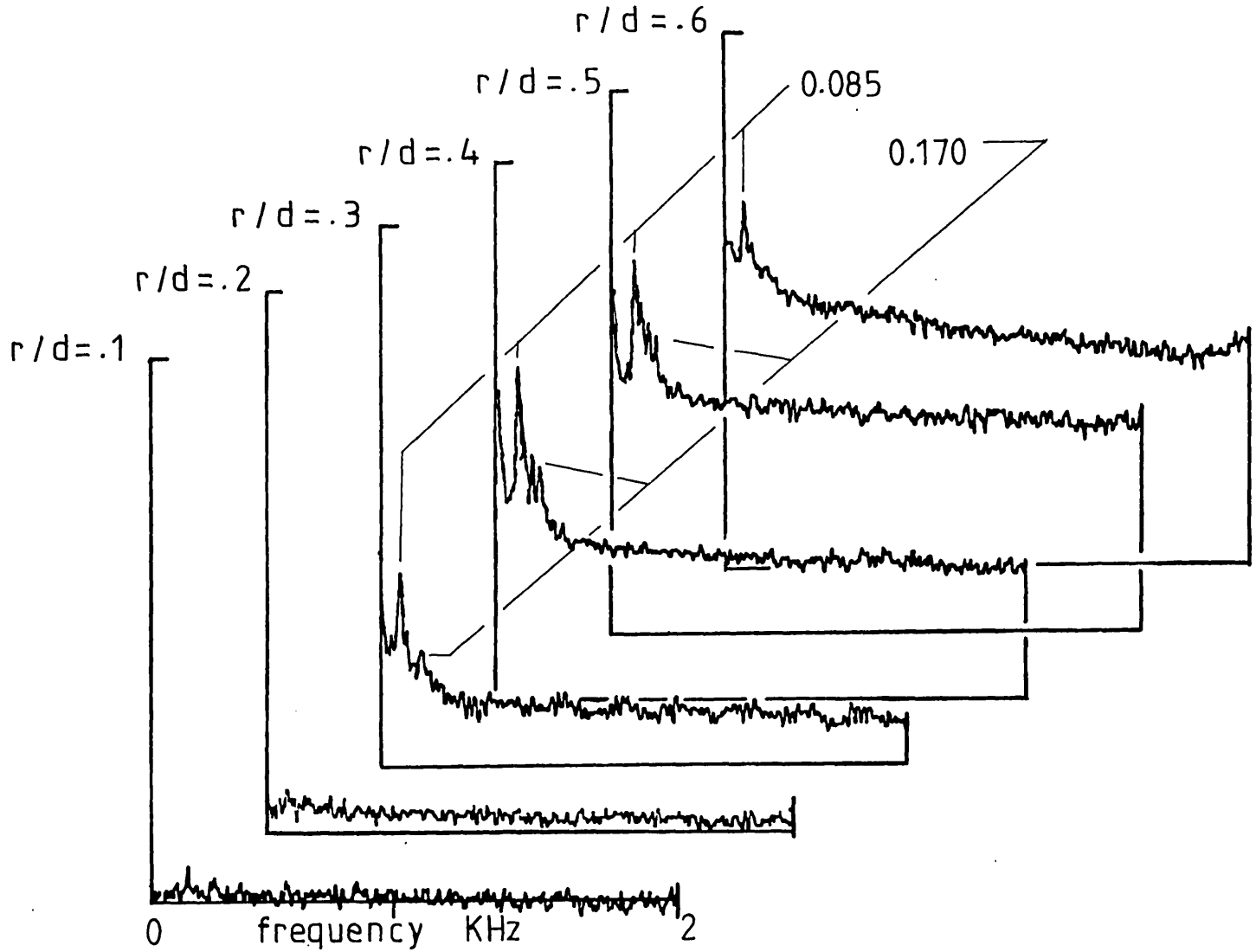


FIGURE 3.16 (g) x/d=2.0, Re=5860

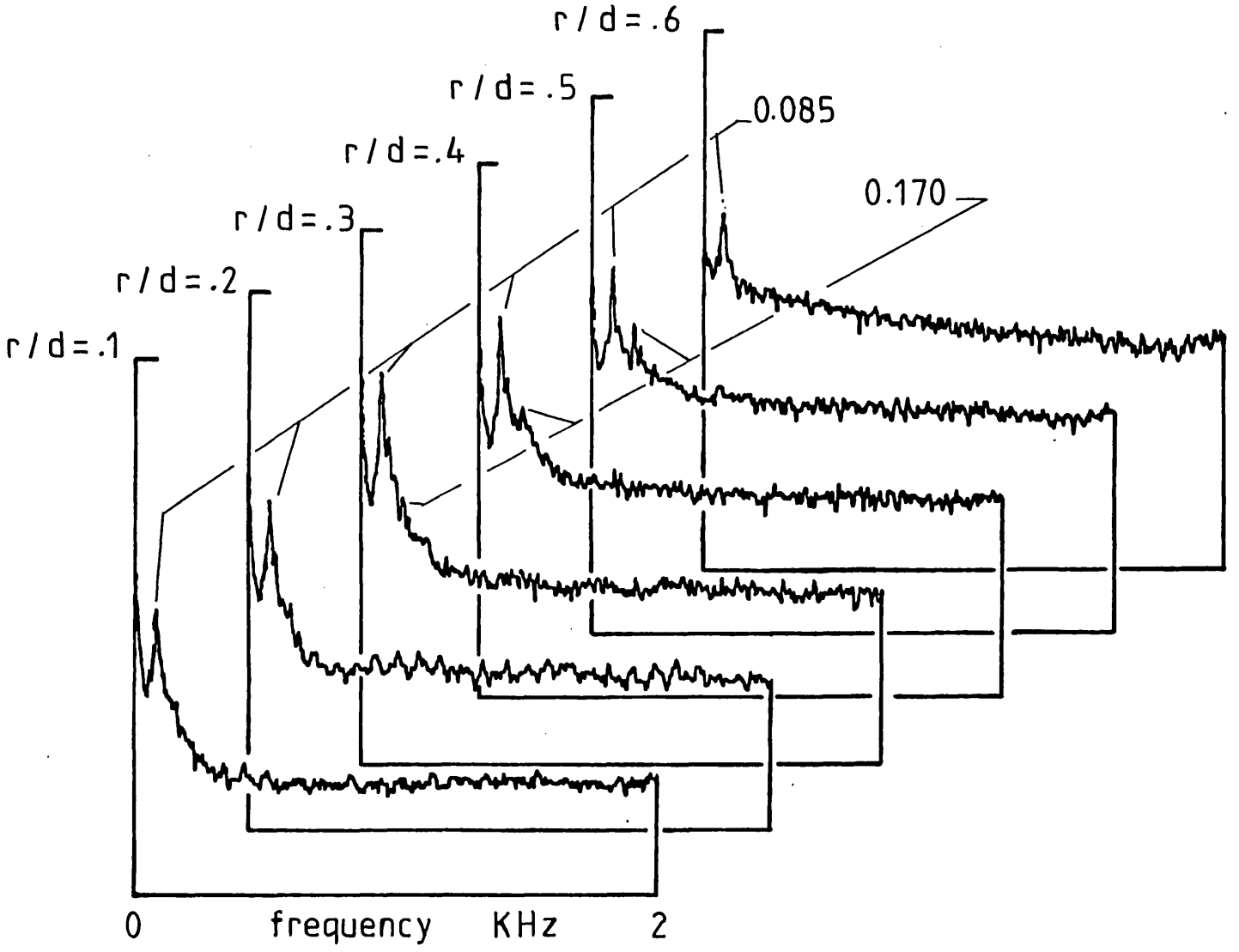


FIGURE 3.16 (h) x/d=3.0, Re=5860

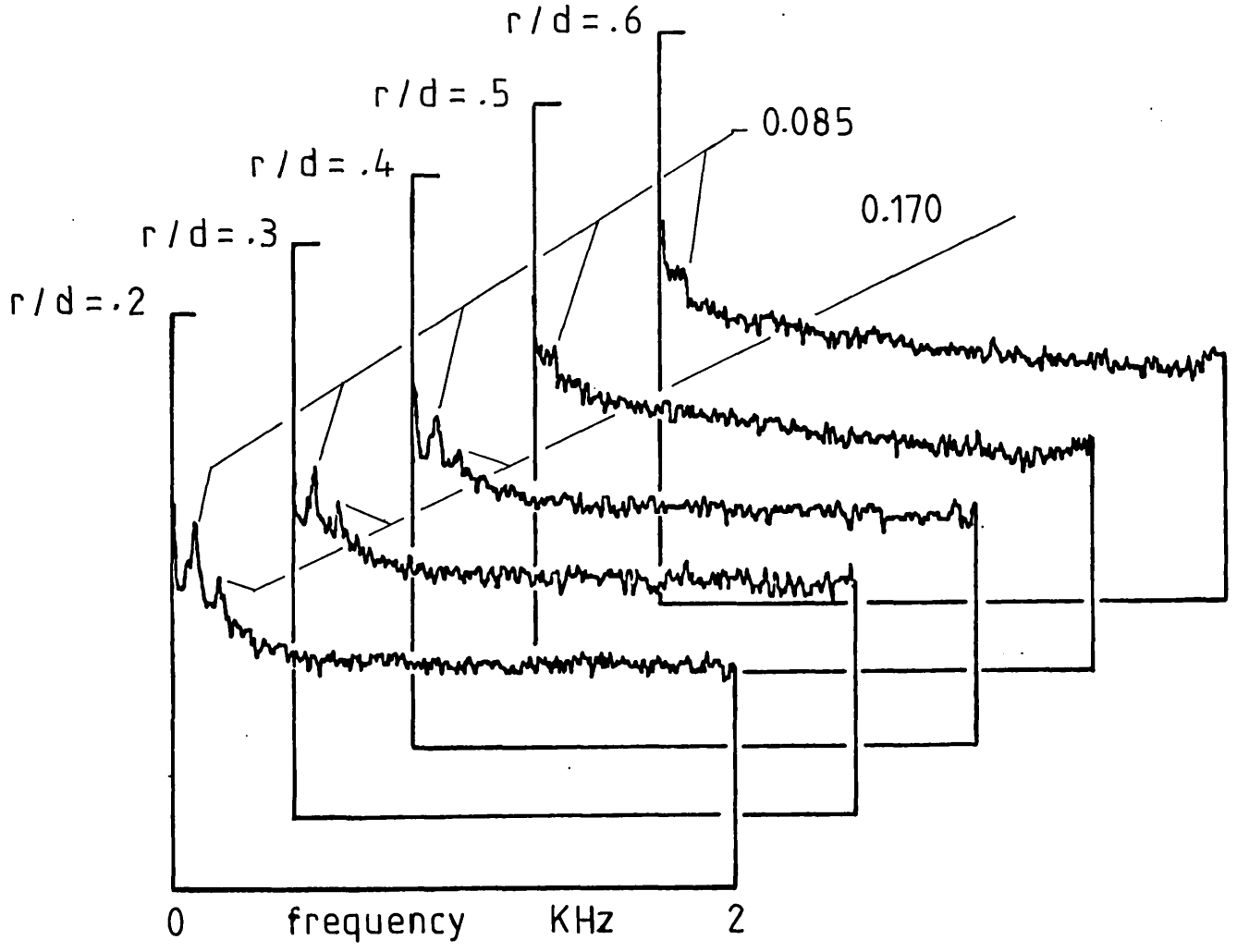


FIGURE 3.16 (1) x/d=4.0, Re=5860

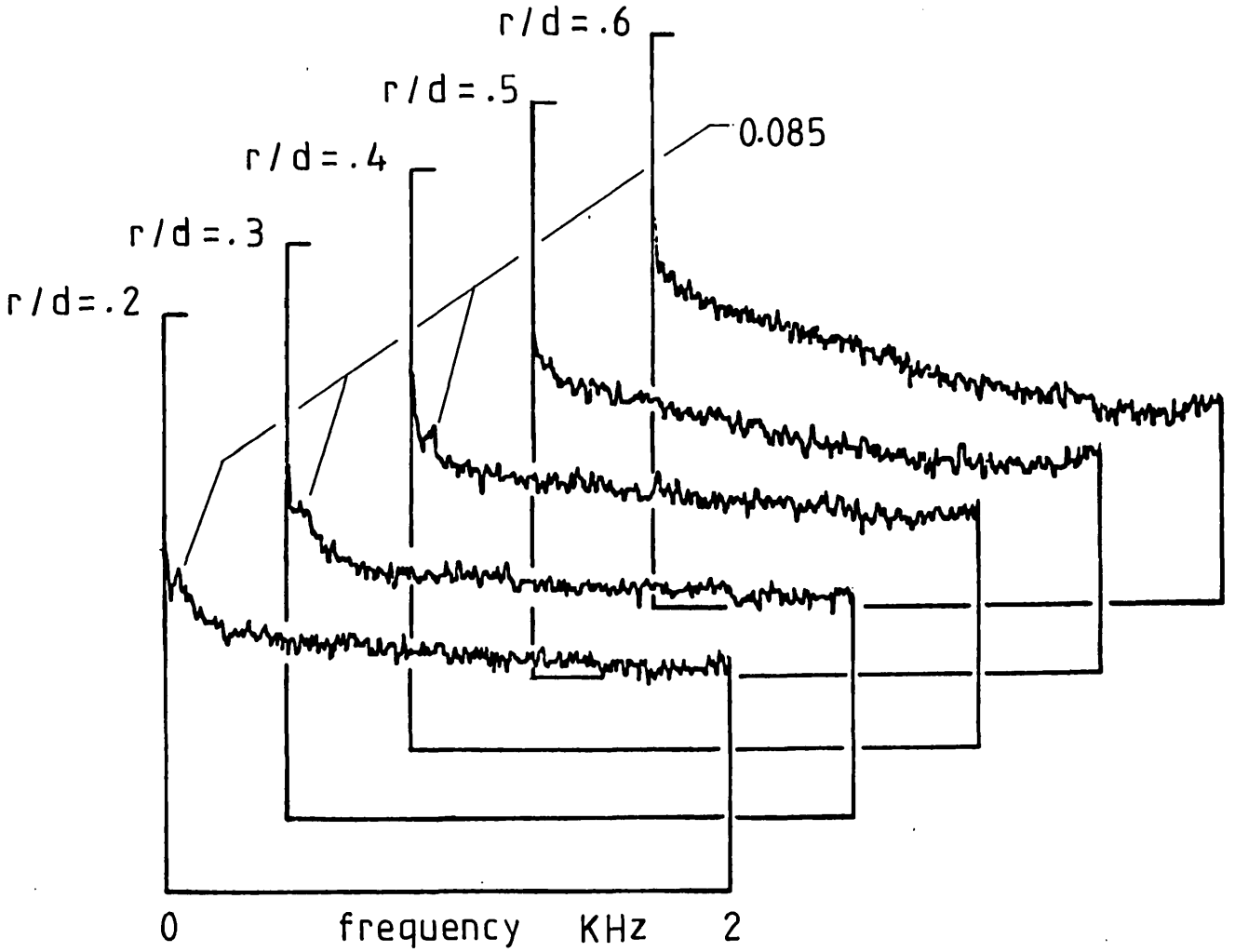


FIGURE 3.16 (j) x/d=5.0, Re=5860

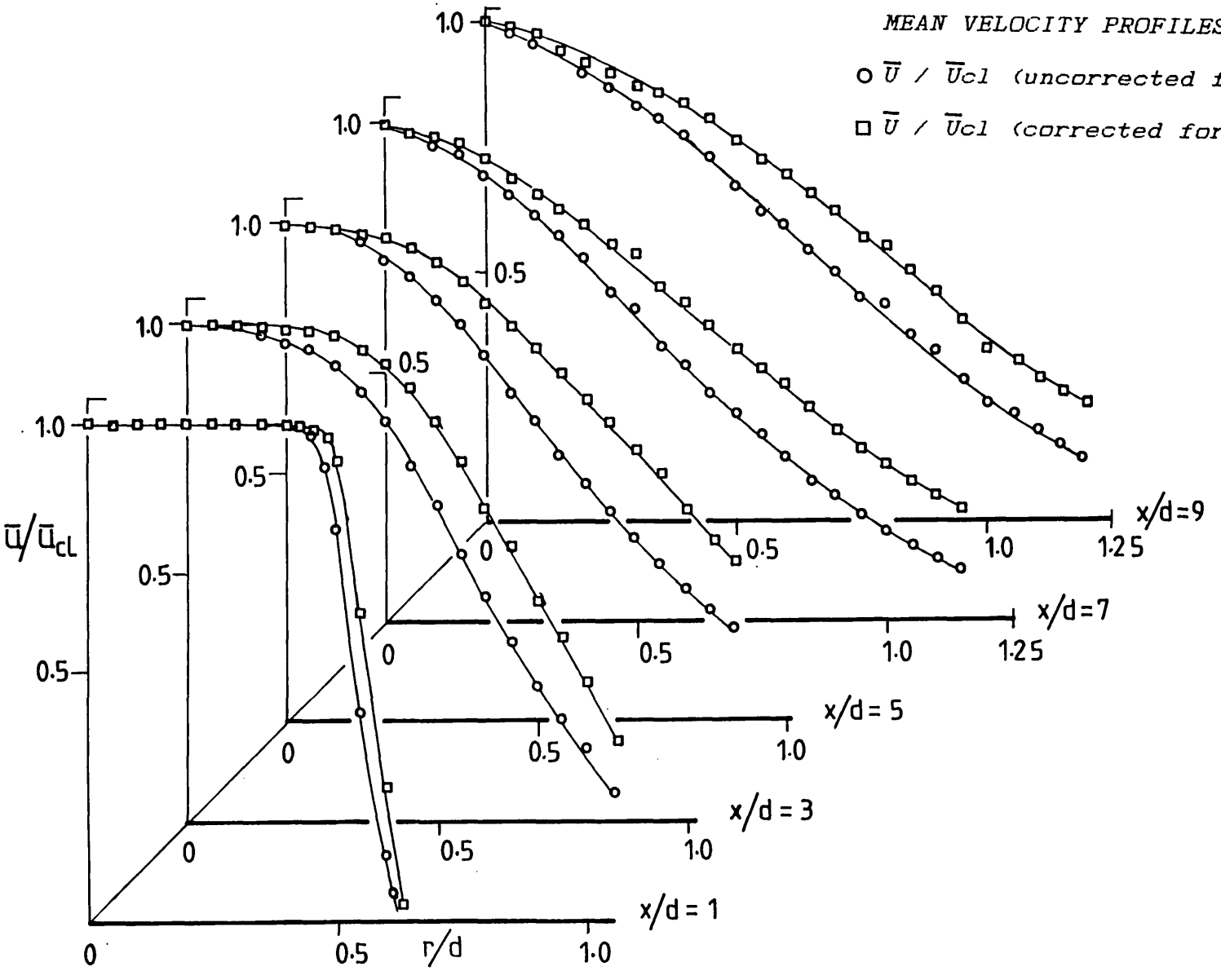


FIGURE 3.A.1 COMPARISON OF MEAN VELOCITY DETERMINED WITH PITOT PROBE CORRECTED AND UNCORRECTED FOR LOCAL DENSITY: FREON-12 JET, Re=16,900

Symbol	Probe	Probe size i.d. (mm)	Volumetric intake ml/min	Katharameter setting bridge voltage (volts)
○	1	0.310	100	7.5 (high input)
●	1	0.310	250	7.5
□	1	0.310	100	5.0 (low input)
◇	2	0.685	100	5.0
◆	2	0.685	100	7.5
◇	2	0.685	250	7.5
◆	3	1.20	250	7.5

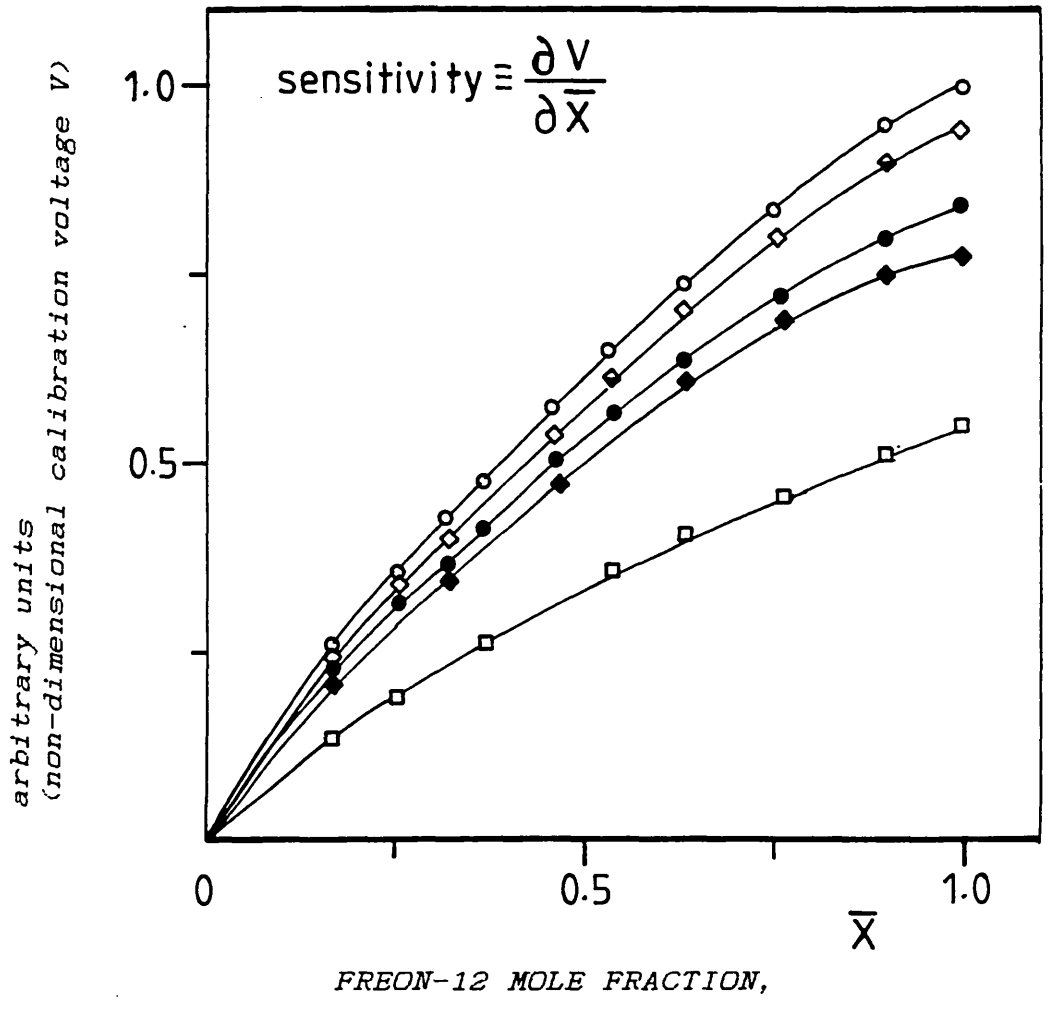


FIGURE 3.A.2 SENSITIVITY OF PROBE CONCENTRATION MEASUREMENTS TO VARIABLES OF PROBE SIZE, KATHAROMETER VOLTAGE AND PROBE SUCTION RATE

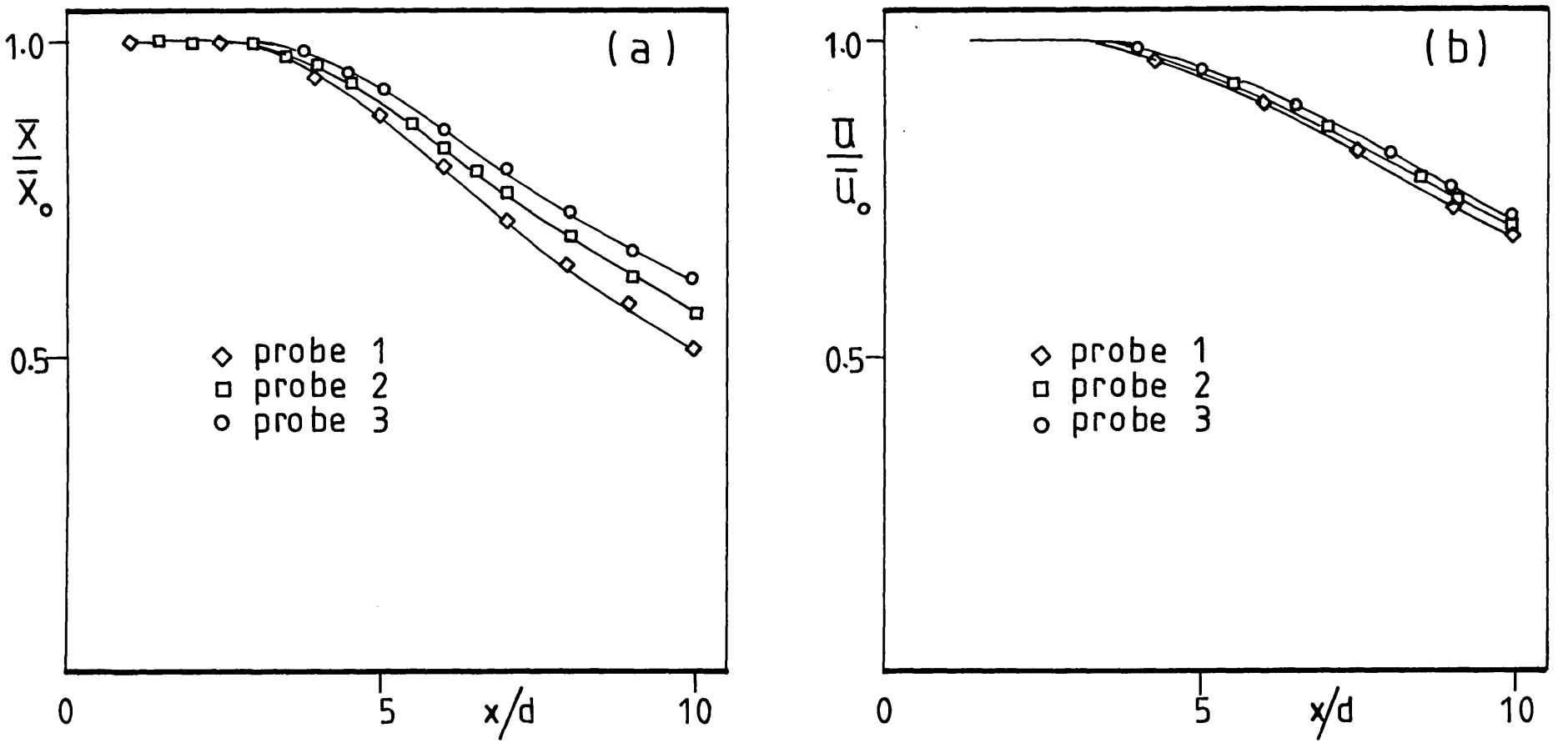


FIGURE 3.A.3 EFFECTS OF PROBE SIZE ON MEASURED (a) MEAN CONCENTRATION (mole fraction) and (b) MEAN VELOCITY (Pitot probe results shown uncorrected for local density): FREON-12 JET, Re=16,900

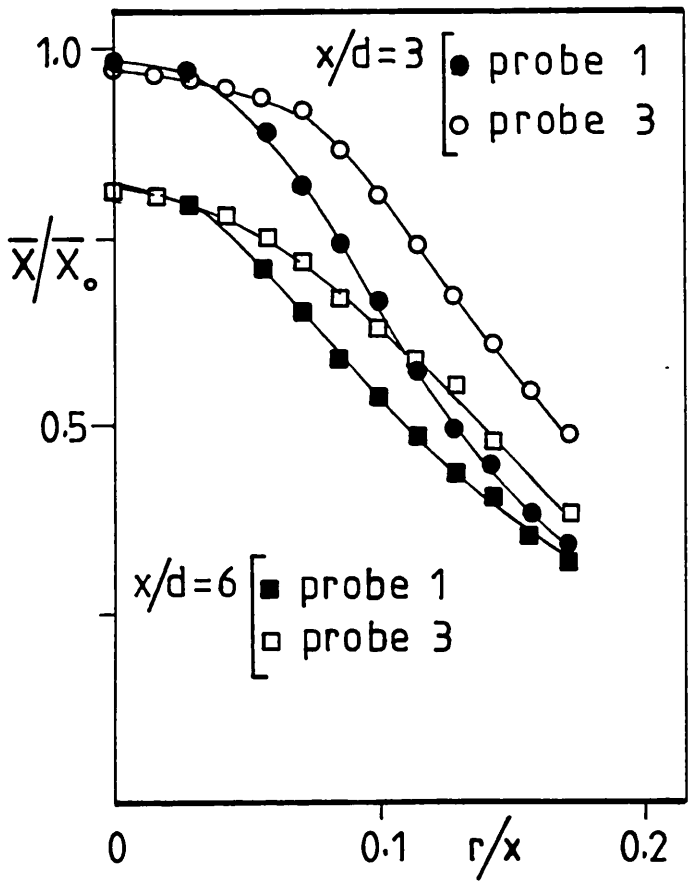


FIGURE 3.A.4 MEAN CONCENTRATION RADIAL PROFILES MEASURED AT TWO LOCATIONS TO DEMONSTRATE EFFECTS OF DENSITY WEIGHTING IN REGIONS OF HIGH TURBULENCE AND WITH LOW AND HIGH LEVELS OF MEAN CONCENTRATIONS. AS CAN BE SEEN, THE PROFILES AT x/d=6, INDICATE THAT TOWARDS THE JET EDGES THE WELL MIXED JET FLUID LEADS TO REDUCED DISCREPENCIES PARTICULARY WITH RESPECT TO THE INFLUENCE OF PROBE SIZE AND PROBLEMS OF PREFERENTIAL DENSITY SUCTION.

CHAPTER 4 NON-COMPRESSING MODEL ENGINE

4.1 INTRODUCTION

Knowledge of internal combustion engines can be assisted by experimental investigations and by theoretical and predictive methods. The latter require the support of measurements and the two together can be developed to quantify the influences of isolated parameters. Experimental studies involving the effects of injection pressure, combustion chamber configuration, intake valve geometry and swirl intensity in fired direct injection Diesel and motored model Diesel engines have been reported by Kamimoto et al (1980), Bicen (1983), Vafidis and Whitelaw (1984) and Bicen, Vafidis and Whitelaw (1985). The emphasis has been on the study of the pre-combustion air motion, particularly as influenced by engine geometry and compression ratio.

The further problem of the interaction of the high pressure, high momentum two-phase fuel spray with the swirling air in the combustion chamber of Diesel and stratified-charge engines is a complex mixing process and quantification of droplet size and velocity near the fuel injector is difficult and, at present inaccurate. To circumvent many of the experimental problems associated with in-cylinder measurements, simulations have been made of the fuel injection process. Steady gas jet simulations have been reported, for instance, by Adler and Lyn (1969), Melton (1971), Morris and Dent (1976), Witze (1980), Turns and Rau (1982) and Tanabe et al (1982) with measurements on centreline and radial gas velocities and gas concentration fields. The difficulty of making quantitative measurements of velocity and concentration in liquid fuel sprays has resulted in studies to improve the understanding of the liquid atomization process and there, the importance of nozzle design on the spray angle and droplet size have been

characterised, for example, by Radcliffe (1953), Bergwerk (1959), Reitz and Bracco (1979) and Wu et al (1983). The work reported by these authors has made use of steady flow rigs to study liquid jets issuing into high pressure and high temperature ambient gases and as resulting from the typical nozzle configurations used in Diesel engines. Studies involving details of the penetration of liquid fuel sprays, break-up length of the liquid jet (and transition to spray) and the empirical correlations of the various parameters of injection backpressure, liquid to ambient density ratio and nozzle length to diameter ratio have been reported on by Wakuri et al (1960), Dent (1971), Hay and Jones (1972), Lafrance (1977) and Reitz and Bracco (1979, 1982) with the results from these studies making clear, among other things, the significant dependence of the resulting spray characteristics on density ratio between the injected fuel and surrounding ambient. More realistic studies have included the transients of the liquid fuel injection process and have been reported by Sinnamon et al (1980) and Takuchi et al (1983) and attempts to measure droplet velocity using laser velocimetry close to the nozzle of a Diesel fuel injector (where a dense liquid core is known to exist) have been reported by Wu et al (1983). However, experimetnal difficulties and the large errors resulting in the measurements near the edges of their liquid jets make it clear that obtaining conclusive quantitative results must await further developments in experimental techniques; Dyer (1985) and Witze and Dyer (1986) have reviewed the state-of-the art of experimental techniques for engine flow studies.

The effects of bulk fluid motion on fuel spray burning, flame propagation and flame development in Diesel and

spark ignition engines has been characterised in purpose built research engines and combusting bomb chambers as reported by Witze et al (1984), Yule and Bolado (1984), Hanson and Thomas (1984), Barker et al (1985) and Kalghatgi (1985). From these studies, indications are that the initial induction characteristics of the bulk air motion play a dominant role on the consequent combustion process and that the influence of induction swirl, in particular, is significant. Detailed studies of the swirl influence in simulated gas-liquid mixing and the in-cylinder air motion of reciprocating engines have been reported on by Tishkoff et al (1979), Lohmann et al (1979), Witze and Vilchis (1981), Vafidis (1984), Fansler (1985) and Bopp and Whitelaw (1985) and show that swirl imparted on the intake air leads to the formation of three-dimensional flow strucutres which remain present through to the end of the compression process and these accelerate air/fuel mixing.

The important conclusion which can be drawn from the works which have been referenced above is that up to present, the information of the instantaneous in-cylinder quantities of velocities, species concentrations and temperature fields is still limited and that progress continues to be made; the measurements made up to the present have been in most instances of velocity fields. Measurements of the scalar properties associated with the turbulent air/fuel mixing and consequent combustion process have received considerably less attention partly because of the related experimental difficulties although recent studies have reported the use of optically based techniques such as Raman spectroscopy, laser-excited fluorescence and Rayleigh scattering for the measurement of species concentration, temperature and density, but the emphasis has been on technique development; see, for example, Smith (1980), Cole and Swords (1980) and Arcoumanis et al (1984).

In the present chapter laser Rayleigh scattering and laser velocimetry have been used to determine the velocity and scalar characteristics of the simulation of air/fuel mixture as a function of fuel injection timing, piston geometry, induction swirl and nozzle geometry within the non-compressing model Diesel engine for which velocity characteristics have already been reported by Bicen (1983). A more detailed investigation of the scalar characteristics is reported in the next chapter where a compressing engine is used to more realistically represent the air/fuel mixing process. The goal of the present chapter, therefore, is to characterize the velocity and concentration fields of a simulated fuel jet and to demonstrate the application of the experimental techniques. The flow configuration and instrumentation is described in the next section. The third section of the chapter presents and discusses the results and the fourth section summarizes the more important conclusions.

4.2 EXPERIMENTAL SYSTEM

4.2.1 Flow configuration

A line diagram of the model Diesel engine is shown in Figure 4.1 with its geometric characteristics listed in Table 4.1. The engine cylinder was made of plexiglass to provide optical access and the piston was driven in simple harmonic motion by a crank and motor arrangement at a speed of 200rpm $\pm$1%. A single valve was centrally located and flush with the cylinder head forming a 4mm annular opening for both the intake and exhaust flow. Since the valve was permanently open the engine was operating without compression which facilitated the application of the Rayleigh scattering technique without the added difficulties associated with the time-varying density field during compression. Swirl was induced by 60

degree vanes located in the inlet port to give a swirl number of 1.73 and an air filter was incorporated as shown in Figure 4.1 to minimise the presence of dust particles during the Rayleigh scattering measurements; the filter used could control particle intake in the range up to 2μm.

The simulated fuel (Freon-12 vapour) was injected through a nozzle bored concentrically with the valve. The nozzle geometries, as shown in Figure 4.2, were employed to allow investigation of the effect of initial jet angle on mass and momentum transport. The piston geometries comprised a flat and re-entrant (bowl-lipped) piston. Freon-12 was selected due to its high relative to air scattering cross-section (17.9 times that of air) which allowed adequate time and space resolution to be obtained. Moreover, the density ratio between Freon-12 and air (4.2) was similar to that of vapourised Diesel fuel and, as a result, a better simulation the air/fuel mixing process was achieved; for example, gasified n-dodecane, $C_{12}H_{26}$, results in a fuel-to-air density ratio of 5.8.

The injection process was controlled by an Angar model 008 solenoid valve electronically activated by a gating system interfaced with a microcomputer. The injection and measurement timings were synchronized in the manner described in Appendix C. Freon was supplied to the solenoid from a pressurized bottle through a flow circuit which included a microfilter (Balston 93) to filter impurities in the gas greater than 1μm. The backpressure to the solenoid was kept constant at 0.377MPa.

The injection characteristics are summarized in Table 4.2 and are similar to those of the simulation study by Johnston (1979). The jet exit velocities for nozzles A and B were 30.7 and 25.8m/s, respectively, which corresponds to Reynolds numbers of 42800 and 40200 based on nozzle diameter and Freon-12 density at atmospheric conditions. The jet time constant τ_j, which is defined as the ratio of nozzle radius, r_o, to the jet exit velocity u_j ($\tau_j = r_o/u_j$) and according to Witze (1980) characterises the behaviour of impulsively started jets, was 111μs for nozzle A and 151μs for nozzle B.

4.2.2 Experimental techngues

Concentration measurements:

The in-cylinder mole fraction distribution of Freon-12 was measured with the laser Rayleigh scattering system described in detail in Chapter 2. In the present investigations the argon-ion laser was operated at 0.7W and 514.5nm. The output voltage from the photomultiplier was lowpass filtered at 4KHz, digitized by a 12-bit A/D convertor at a rate of 30KHz and then sampled at 10KHz by a microcomputer. Measurements were initiated at 31 degrees before TDC and carried out over a 5 degree (4.2ms) crank angle window. Data were collected over no less than 100 engine cycles with injection terminated in-between cycles to prevent accumulation of the Freon-12 vapour inside the engine cylinder. The cycle data was graphically displayed and only cycle data free from particle scatter interference was transferred to a hard disk for post-data processing after deconvolution of background light intensity and shot noise effects (details are provided in Appendices A and C); also see discussion in Section 4.3.1.

Velocity measurements:

A laser Doppler anemometer, shown in Figure 4.3, was used in the dual-beam forward scatter mode to measure the injected "fuel" velocity field. The principal characteristics of the optical system are summarized in Table 4.3. The voltage output from the photomultiplier was amplified and filtered prior to its input (A) to a frequency counter which was externally triggered (C) by the measurement pulse from the gating system. Every time the signal was exceeding the preset threshold of the counter, a pulse was sent to channel (B) of the scope to porvide means of monitoring the part of the Doppler burst which

provided the frequency information. The start and stop times of Freon-12 injection, as well as the measurement window, were software controlled through the microcomputer interfaced to both the frequency counter and the gating system. For the 5 degree window employed,* a sample size of 2000 was obtained and averaged to provide ensemble mean and rms velocities with a statistical uncertainty of less than 1%.

Both the Freon-12 flow through the nozzle and the air flow through the valve were seeded by a glycerol/water solution which was atomised by a blast type atomiser to provide a satisfactory particle size and arrival rate.

The optical arrangements for both the LRS and LDA were mounted on a traversing lathe bed allowing movement of the optics relative to the fixed engine; resolution in traverse position was 0.025mm.

4.2.3 Measurement uncertainties

The possible sources of error in Rayleigh scattering measurements in connection with the engine flow are described in detail in Appendix A and will not be repeated here. The presence of particles and the uncertainty introduced by their signal interference with Rayleigh scattered light has also been discussed in Chapter 2. Since errors were still present in the measured mean and rms concentration from shot noise and background light, noise was deconvoluted from the Rayleigh signal following the procedure of Pitts and Kashiwagi (1984) after which the uncertainty in the mean concentration was estimated to be 5% with a maximum uncertainty of 10% in the rms of the concentration fluctuations. The uncertainty in the present work,due to the effect on the signal by the plexiglass surface, is accounted for in these values and is discussed in detail in Appendix B.

The most important source of error in the velocity measurements was velocity-gradient broadening due to the non-

linear and steep velocity gradients present at the edges of the transient Freon jet. It is estimated that this error source can introduce uncertainties up to 10 and 15% in the mean and rms velocities, respectively.

4.3 RESULTS AND DISCUSSION

The mean and rms Freon-12 jet velocity and concentration results are presented in Figure 4.4 through 4.13 in the form of instantaneous distributions and centreline and radial profiles. The centreline and radial profiles were obtained by ensemble averaging data over a 5 degree crank angle window centred at 28.5 degrees before the top-dead-centre (TDC) position of the piston (Figure 4.4 shows two in-cycle temporal ensembles). The in-cycle characteristics on which the spatial ensemble results were based (Figures 4.7 - 4.13) are represented on the axis of the exit plane and at downstream locations by Figures 4.5 and 4.6, respectively. The results of these figures show in-cycle (instantaneous) traces of Freon concentration and exhibit similar characteristics to those reported by Tanabe et al (1982) in their study of the transient concentration in a hydrogen jet. The scalar characteristics of Figures 4.5 and 4.6 (and those of Tanabe et al, for instance) further show that these are similar to those for typical instantaneous velocity traces as reported, for example, by Witze (1980) and Tanaka (1984). Wong (1986) has also obtained similar instantaneous velocity traces for the particular nozzles of the present investigations. The ensemble averages of velocity and concentration are based on averaging along the plateau (steadying) region after the initial transient rise, Figure 4.4. The decrease in jet fluid concentration with increased axial distance from the nozzle is made clear by Figure 4.6, which is also typical of the resulting characteristics with increased radial distance away from the centreline.

The ensembled centreline results for velocity and concentration have been made non-dimensional by normalizing mean values by the corresponding values at the first measured location of velocity (U_o) and mole fraction (X_o). The rms of the velocity and concentration fluctuations have been normalized by their local mean values; in the case of the concentration results, this normalizing represents the un-mixedness as discussed in Chapter 3. For the radial profiles, mean and rms quantities along the measured radial planes have in all cases been normalized by the respective mean centreline velocity or concentration at the plane of the measurements. The axial coordinate is x/d where x is the axial distance and d the nozzle diameter and the radial coordinate is r/d where r is the radial distance measured away from the centreline.

4.3.1 Centreline distributions

Figures 4.7 and 4.8 show centreline distributions for nozzles A and B with a flat piston and Figure 4.9 for nozzle B with the re-entrant piston. The results for the centreline decay of the transient fuel jet show consistently that different decay rates exist for the velocity and concentration field; the latter being greater than the former. The axial velocity decay is very slow and is indicative of the high momentum-dominated jet flow but the concentration decays much faster and confirms similar observations made in steady jet flows and is independent of the density ratio between the jet fluid and that of the ambient; similar results in steady jets have been documented by Sforza and Mons (1978) and are also shown by the results of the steady jet measurements in Chapter 3. That the rate of decay along the centreline of these transient jets appears nearly constant is in part due to the normalizing quantities used and is explained below.

Differences between results for the two nozzles are clear in that the decay of nozzle B is slightly greater than that of nozzle A. The non-dimensional results of mean concentration values are based on normalization by the first measured point which, in the case of these concentration measurements, was limited by the proximity of the LRS laser beam to the nozzle exit. The face diameter of nozzle B was greater than that of nozzle A and since both nozzles were made of brass the background light due to reflection differed in both cases; greater for nozzle B and it was significant in terms of the effect on the LRS signal. Through experience gained at a later stage, this problem was circumvented by painting all interior components of the model engine with non-reflective black paint which minimized and equalized reflections. The greater decay of the jet from nozzle B is to be expected due to the larger diffusing angle over nozzle A and in the present case is supported by the measure of radial spread (discussed in the next sub-section) for both the velocity and concentration fields.

Comparison of the mean values of velocity and concentration obtained with a re-entrant piston and a flat piston, shows that the effect of the fuel jet impingement on the flat piston leads to increased mixing and suggests that the increased penetration distance (in the case of the re-entrant geometry) alters the jet centreline velocity more than the centreline concentration decay. Differences in the radial characteristics of concentration do result, however, and these are discussed below. The increase in centreline velocity of the fuel jet results from the jet flow moving towards the smaller diameter entry of the piston bowl, Figures 4.8 and 4.9.

The centreline concentration rms $X'/\bar{X}$ shows that the unmixedness of injected fuel is less with the flat piston case than with the re-entrant piston. This is made clear by the faster asymptotic behaviour shown with the impinging jet on the flat piston where constant levels of $X'/\bar{X}$ of about 6% result at

closer distance to the nozzle than those obtained with the re-entrant geometry. The velocity rms $u'/\bar{U}$ shows similar trends for both piston types, with slightly lower values resulting near the re-entrant piston due to the local increase in the normalizing value of mean velocity, $\bar{U}$. The consistently higher levels of $u'/\bar{U}$ obtained near the jet exit plane are in agreement with the higher turbulence intensities reported for pulsating jets relative to steady jets; see, for example, Binder and Favre-Marinet (1973). Witze (1980) reports similar values for the $u'/\bar{U}$ exit values as found here ($\sim$12%). It cannot be said, however, that exit values of $u'/\bar{U}$, as referred to here, and in other impulsively started jet studies, are associated with a location in the velocity potential core since a potential core is difficult to define due to the finite opening and closing times of the solenoid (Bremhorst and Harch (1979)). The problems in defining a potential core in impulsively started jets have been discussed at some length by Witze (1980) and we agree with his conjecture, that a well defined potential core, in the sense of steady jets (see, for example, discussions in Chapter 3), may at times not exist in impulsively started jets if the on-time for the jet is very short. *

Difficulties are also expected in defining a potential core for the concentration field. For the measurements reported in the present chapter, the concentration rms values X' were defined relative to X'_o by assuming that the rms value obtained at the first centreline measurement location $(X'_o)_{CL}$ was that associated with the mole fraction "potential core" and that $(X'_o)_{CL}$ should theoretically be zero. Thus, the quantified values for $(X'_o)_{CL}$ were considered as noise and deconvoluted from the downstream values X'_d by $\{(X'_d - (X'^2_o)_{CL}(\bar{X}/\bar{X}_o)\}^{\frac{1}{2}}$ in order to obtain the values of X'; see also, Arcoumanis et al (1984). As a post-prognosis, this definition of X' is not necessary, since the assumption that the first measurement location is associated with the mole fraction potential

* In the present case the jets result from opening the solenoid for 7ms leading to a total transient jet time of $\sim$ 17ms, Figures 4.4 - 4.6

core is not accurate. The relative values of X' are thus different from the true rms by the term $(\bar{X}_o'^2)_{CL}(\bar{X}/\bar{X}_o)$. The magnitude of $X'/\bar{X}$ cannot, therefore, be compared directly to the magnitude of $u'/\bar{U}$. In fact when the results of the concentration measurements of the next chapter and those of Chapter 3 are considered, the magnitude of $X'/\bar{X}$ values tend to be greater than $u'/\bar{U}$ as should be expected from the steady jet results (Chapter 3) and from other concentration measurements reported for impulsively started jets (for instance, Tanabe et al (1982)). There the centreline scalar intensities are consistently greater than those of the longitudinal velocity intensities.

Since the measurements made here were quantified on-line, the exact values of $X'/\bar{X}$ cannot be presented but on the basis of the results of Chapters 5 and 6 estimates can be made and these show that the values for $X'/\bar{X}$ in the proximity of the piston should be about 25% (in contrast to the 10% levels shown in Figures 4.7, 4.8 and 4.9) and that near the exit plane of the nozzles, $X'/\bar{X}$ should be about 12% to 14% for nozzles A and B, respectively. The spatial distribution of $X'/\bar{X}$ is correctly shown with respect to the trend of increasing values of $X'/\bar{X}$ with downstream distance.

4.3.2 Radial distributions

Radial distributions for mean and rms velocity and concentration for nozzles A and B with a flat piston and with fuel-injection initiated at 40 degree BTDC are shown in Figures 4.10 and 4.11. Figures 4.12 and 4.13 show radial results for mean and rms concentration for the case of nozzle A with the re-entrant piston and with fuel injection initiated at both 40 degree BTDC and at 10 degree ATDC. The main difference in radial characteristics between the flat and re-entrant piston

is in mean spread with only slight differences resulting between the rms distributions and this is shown by comparison of Figures 4.10, 4.12 and 4.13. Differences in mean spread also result as a function of injection timing as the results of Figures 4.12a and b show. With fuel injection initiated at 10 degree ATDC, a wider mean profile results and is independent of piston configuration. This is partly expected from the radial pressure exerted on the jet when the piston motion is towards the jet in contrast to when the piston is moving away. Independent of injection timing, a larger radial spread in mean concentration results with the re-entrant piston; similar influences of the piston geometry are found for measurements made in the compressing engine of the next chapter and a more complete discussion is provided there explaining the causes and effects of piston type on fuel spread with the additional variable of dissimilar nozzle geometries. The influence of nozzle geometry is made clear by the mean velocity and concentration results of Figures 4.10 - 4.11 where the greater spread of the fuel jet results with the larger diffusing angle of nozzle B. The most important feature of these results is the differences between the spread of the velocity field and concentration field and the differences between the region of maximum shear $\partial\bar{U}/\partial r$ (associated with the maxima in the velocity rms) and of maximum concentration gradient. As shown by Figures 4.10 and 4.11, the concentration gradients $\partial\bar{X}/\partial r$ attain their maxima at radial locations r/d which are greater than those for the velocity; consistently the concentration rms maximas are at larger r/d values. At the near exit location (Figures 4.10a and 4.11a) the scalar rms exhibits much greater change between the centreline level and the radial maxima than the velocity rms, with the latter more gradually increasing to its maxima. It is interesting to note that the rms characteristics of velocity and concentration of these transient jets are similar to the trends of the steady jet results of Chapter 3. As noted in the above discussions for the centreline results, comparison of magnitudes for the concentration and velocity

rms cannot be made directly. However, the ratio of maximum rms to centreline rms for the velocity and concentration (i.e. X'_{MAX}/X'_{CL} and u'_{MAX}/u'_{CL}) tends to about 1.25* in contrast to those for the concentration which show that X'_{MAX}/X'_{CL} tends towards values of 1.8 for the same near exit locations. Further downstream the quantities u'_{MAX}/u'_{CL} are less but with the mole fraction rms ratio remaining greater.

Table 4.4 presents a summary of the radial results of mean concentration spread in terms of the characteristic parameter $r_{1/2}/r_o$, where $r_{1/2}$ is the radial location at which the concentration reaches one-half its centreline value. Results are shown for the influence of nozzle and piston geometry and injection timing. It is clear that with nozzle B having a larger initial angle, greater spread of fuel results into the cylinder as values of $r_{1/2}/r_o$ indicate. Moreover, with a re-entrant piston the $r_{1/2}/r_o$ values are also shown to increase and the effect of piston geometry remains consistent independent of initiation timing of fuel injection. Differences are small near the piston in $r_{1/2}/r_o$ values between the results obtained with the different nozzles and a flat piston.

4.4 CONCLUSIONS

The main conclusions which can be drawn from the in-cylinder investigation of the velocity and "fuel" concentration fields are as follows:

1. The transient gas jet of Freon-12, like the steady turbulent jets of Chapter 3, revealed a scalar field which spread and decayed more rapidly than the vector field.

2. Both the spread and decay of velocity and concentration had a marked dependence on nozzle geometry. The larger the initial angle the greater the fuel spread.

* This value is typical for the velocity results obtained with different nozzles

3. Independent of the initiation time of fuel injection, greater mean spread of fuel concentration results with a re-entrant piston over a flat piston but with the rms intensities less influenced. With injection timing at 10 degrees ATDC and independent of piston geometry, greater spreading of mean concentration results and with differences in the characteristics of radial rms distribution, however, the maxima of rms intensity remain similar in all cases.

4. Impingement of the fuel jet on the flat piston leads to faster and more uniform mixing as indicated by levels of the mole fraction un-mixedness. With the re-entrant piston, the increased penetration distance delays the impingement process resulting in slower mixing as indicated by higher levels of mean velocity and concentration and the slower development of asymptotic behaviour of the velocity and concentration rms centreline distributions.

5. The application of an intensity based experimental technique such as LRS requires great care. With this proviso, the experience gained in the present investigations justifies the application of LRS to the simulation study of air/fuel mixing in reciprocating engines, as described in the following chapter.

TABLE 4.1 Geometric characteristics of model Diesel engine

Bore, mm	75
Stroke, mm	60
Clearance (TDC), mm	30
Intake/exhaust valve	
Diameter, mm	34
Seat angle, degree	30

TABLE 4.2 Injection characteristics

Injection timing, deg. BTDC	40
Injection duration, degree	17.5
Injection mass, kg/s x 10^3	
Nozzle A	1.41
Nozzle B	1.48

TABLE 4.3 Characteristices of laser Doppler anemometer

Half angle of intersecting beams, deg	6
Fringe spacing, μm	3
Diameter of intersection region at e^{-2} intensity, μm	125
Length of intersection region at e^{-2} intensity, μm	1190
Number of stationary fringes	41
Frequency shift, MHz	variable up to 6

TABLE 4.4 Influence of nozzle and piston geometry and injection timing on jet spread

Nozzle	Flat Piston		Re-entrant Piston	
	x(mm)	$r_{1/2}/r_o$	x(mm)	$r_{1/2}/r_o$
I Injection initiated at 40° BTDC				
A	6	1.176		
	12	1.282	12	1.324
	18	1.364		
	24	1.530		
	27	1.90	27	2.20
B	8	1.210		
	12	1.346		
	16	1.394		
	24	1.842		
	28	2.0		
II Injection initiated at 10° ATDC				
A	12	1.353	12	1.471
	24	1.676		

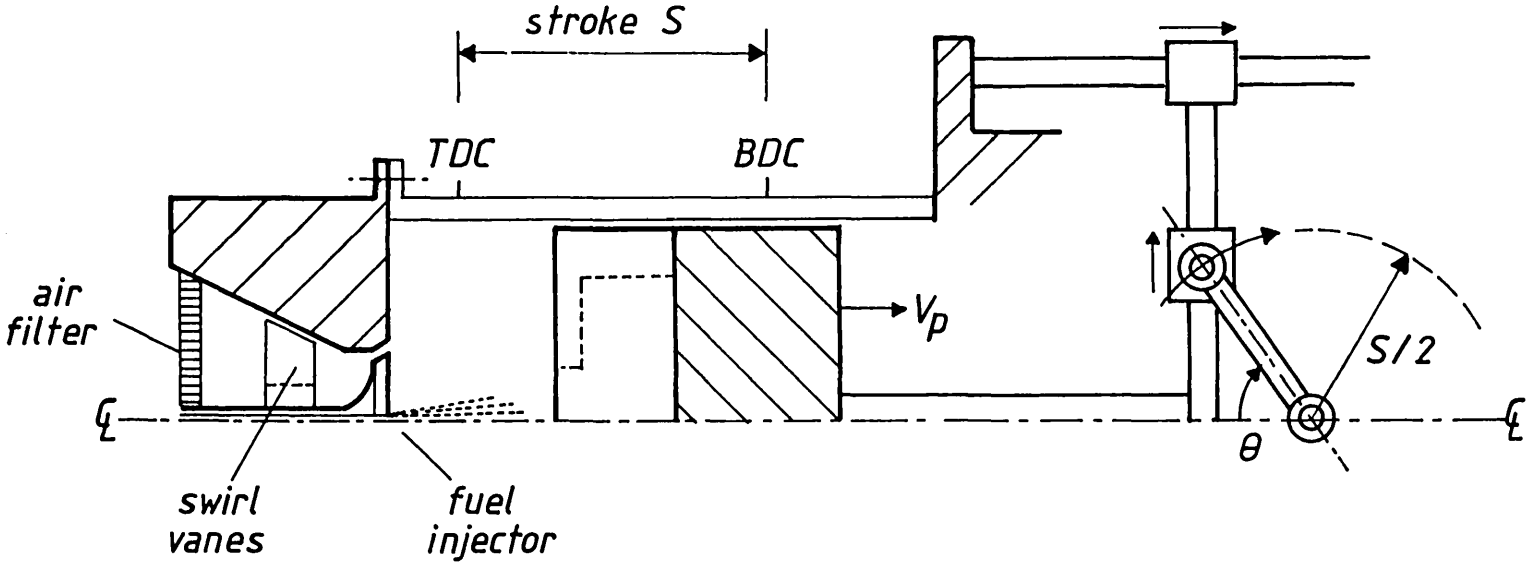


FIGURE 4.1 LINE DIAGRAM OF MODEL ENGINE

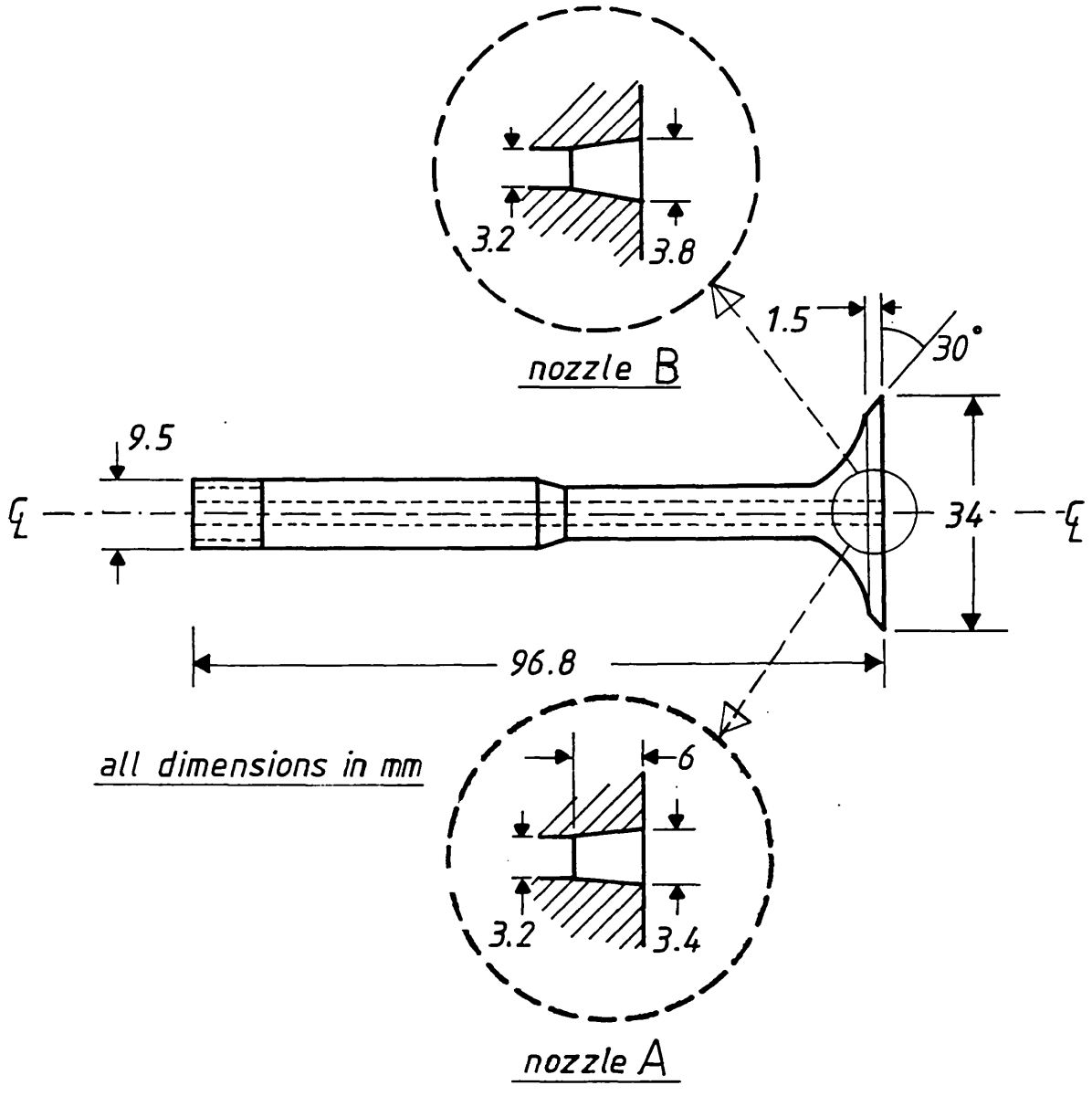


FIGURE 4.2 NOZZLE GEOMETRIES

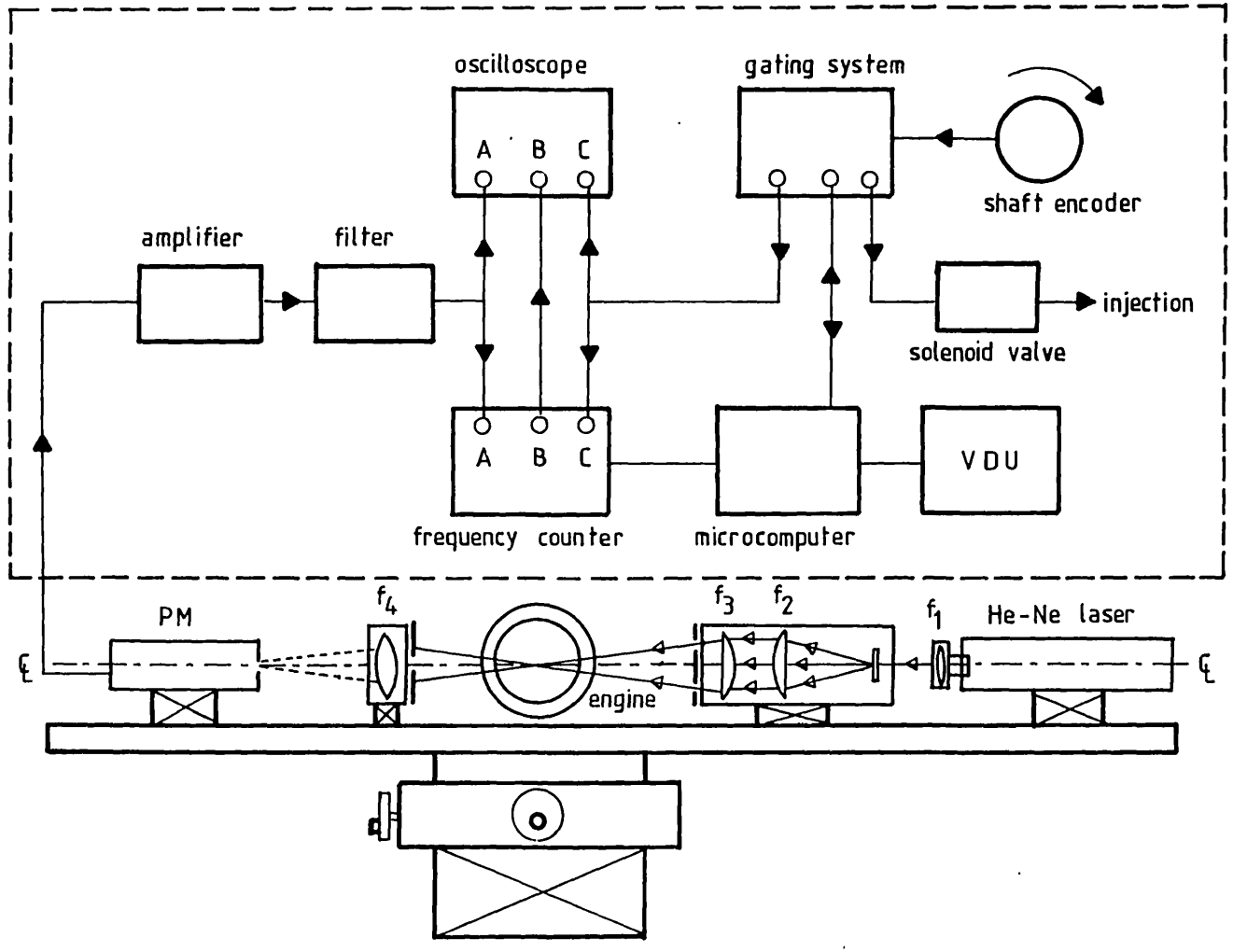


FIGURE 4.3 LINE DIAGRAM OF LDA SIGNAL PROCESSING AND OPTICAL ARRANGEMENTS

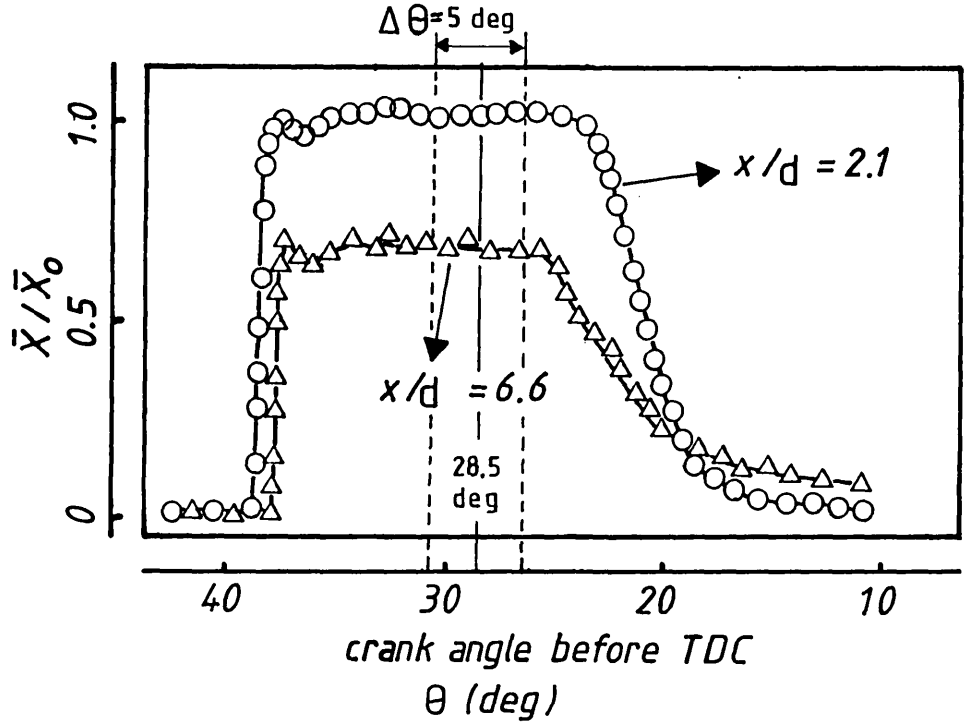


FIGURE 4.4 TIME-AVERAGED CONCENTRATION OF IN-CYCLE FUEL INJECTION AT TWO AXIAL LOCATIONS

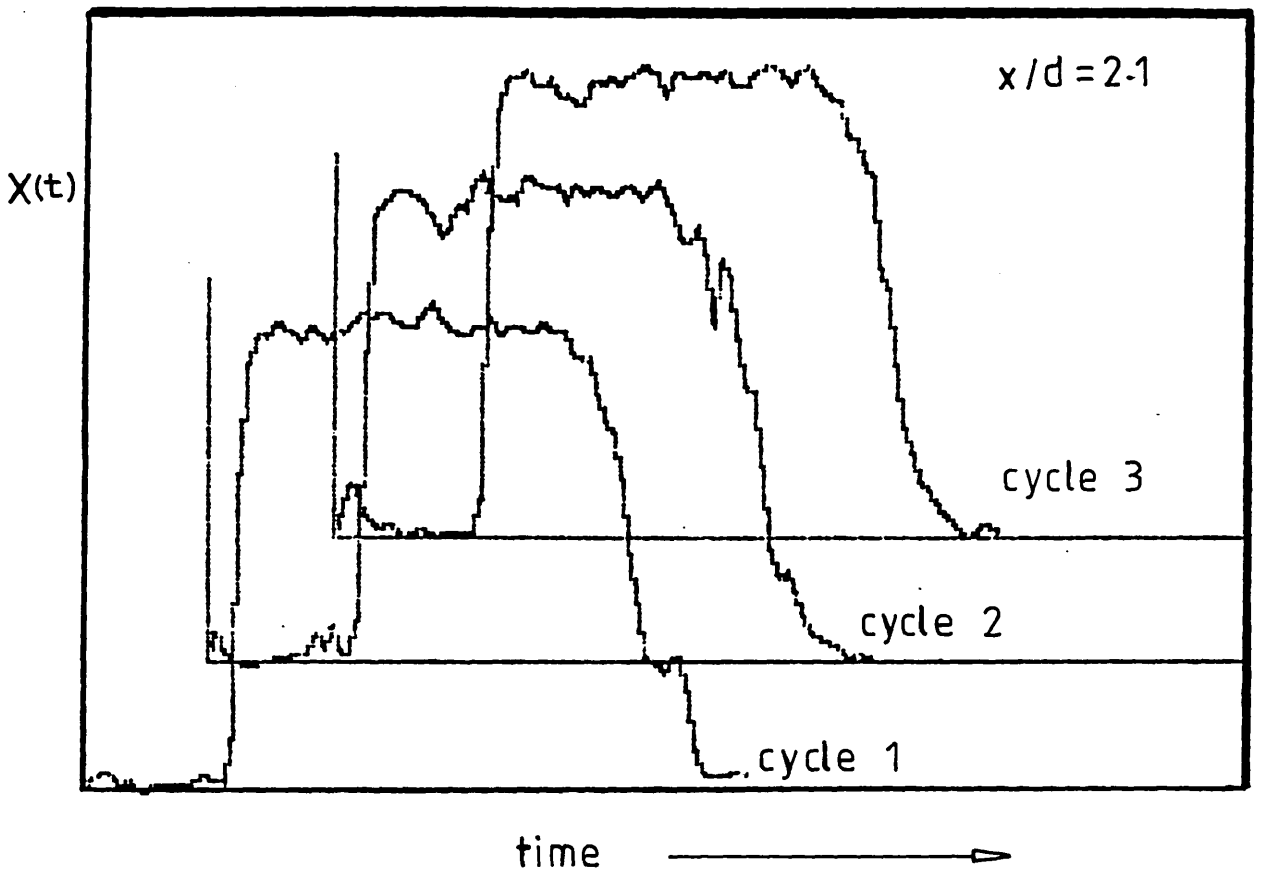


FIGURE 4.5 INSTANTANEOUS FREON CONCENTRATION AT THE NOZZLE EXIT FOR THREE CONSECUTIVE JET FIRINGS; NOZZLE A, FLAT PISTON

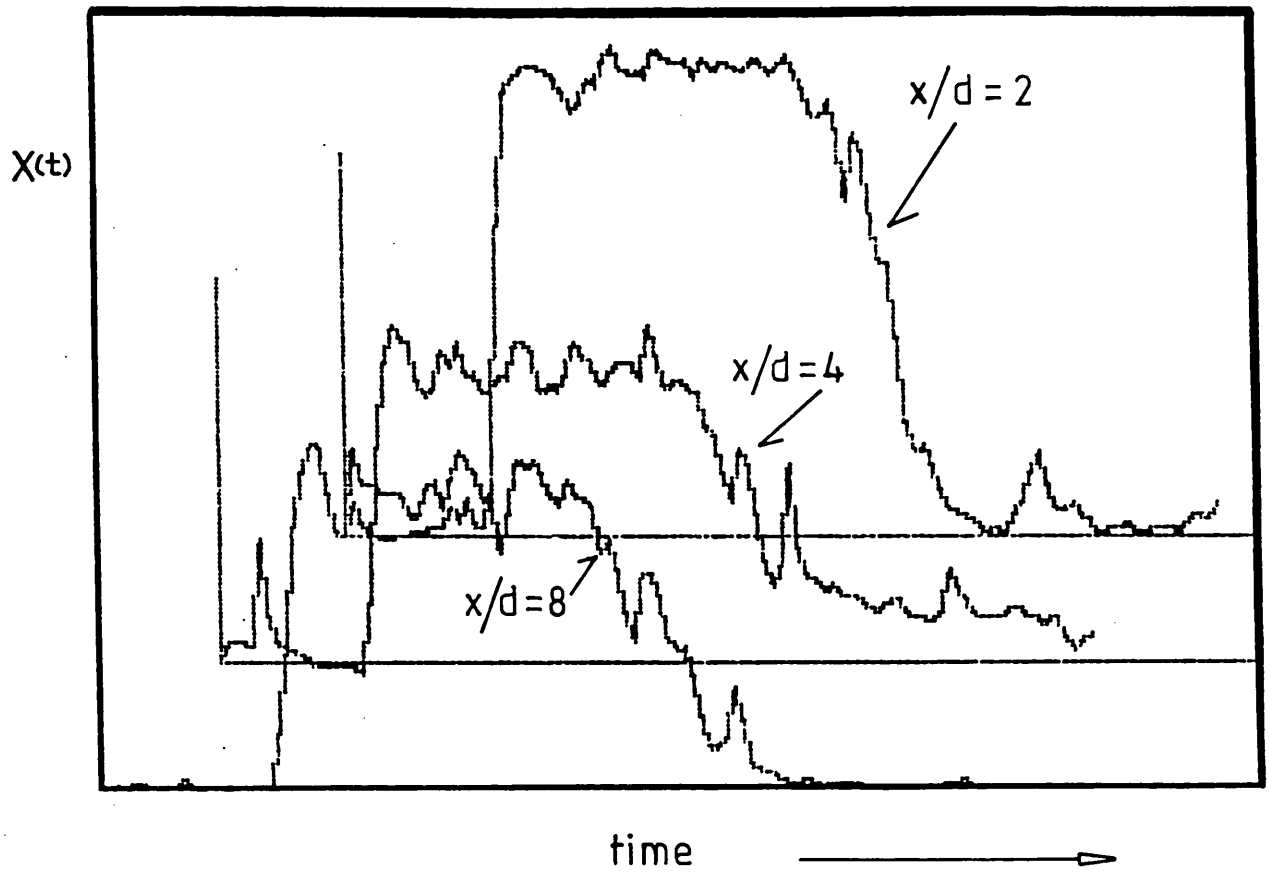


FIGURE 4.6 IN-CYCLE CONCENTRATION AS A FUNCTION OF DISTANCE FROM THE NOZZLE ALONG THE CENTRELINE: NOZZLE A, FLAT PISTON

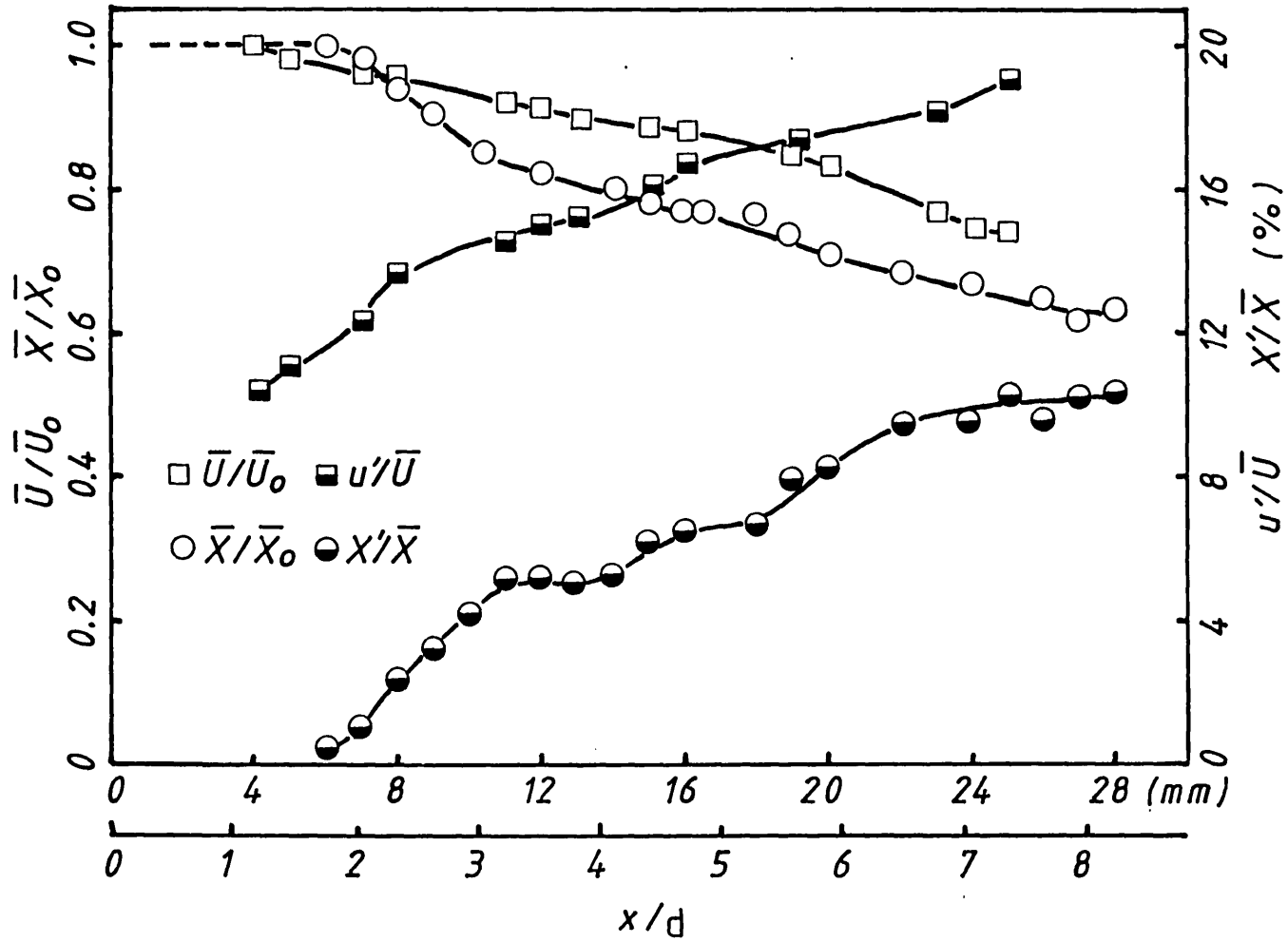


FIGURE 4.7 CENTRELINE DISTRIBUTIONS OF MEAN AND RMS CONCENTRATION AND VELOCITY; NOZZLE A, FLAT PISTON

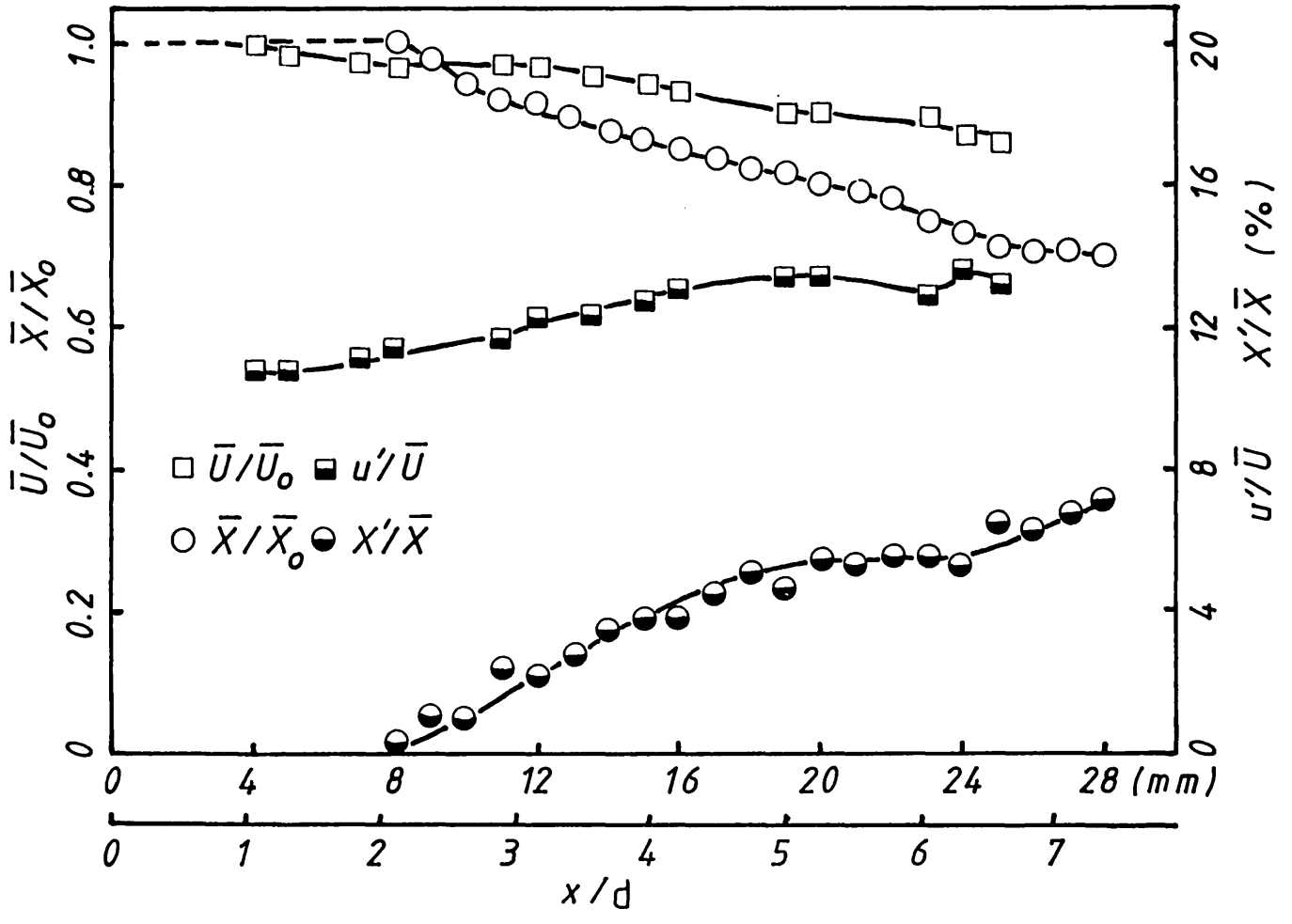


FIGURE 4.8 CENTRELINE DISTRIBUTIONS OF MEAN AND RMS CONCENTRATION AND VELOCITY; NOZZLE B, FLAT PISTON

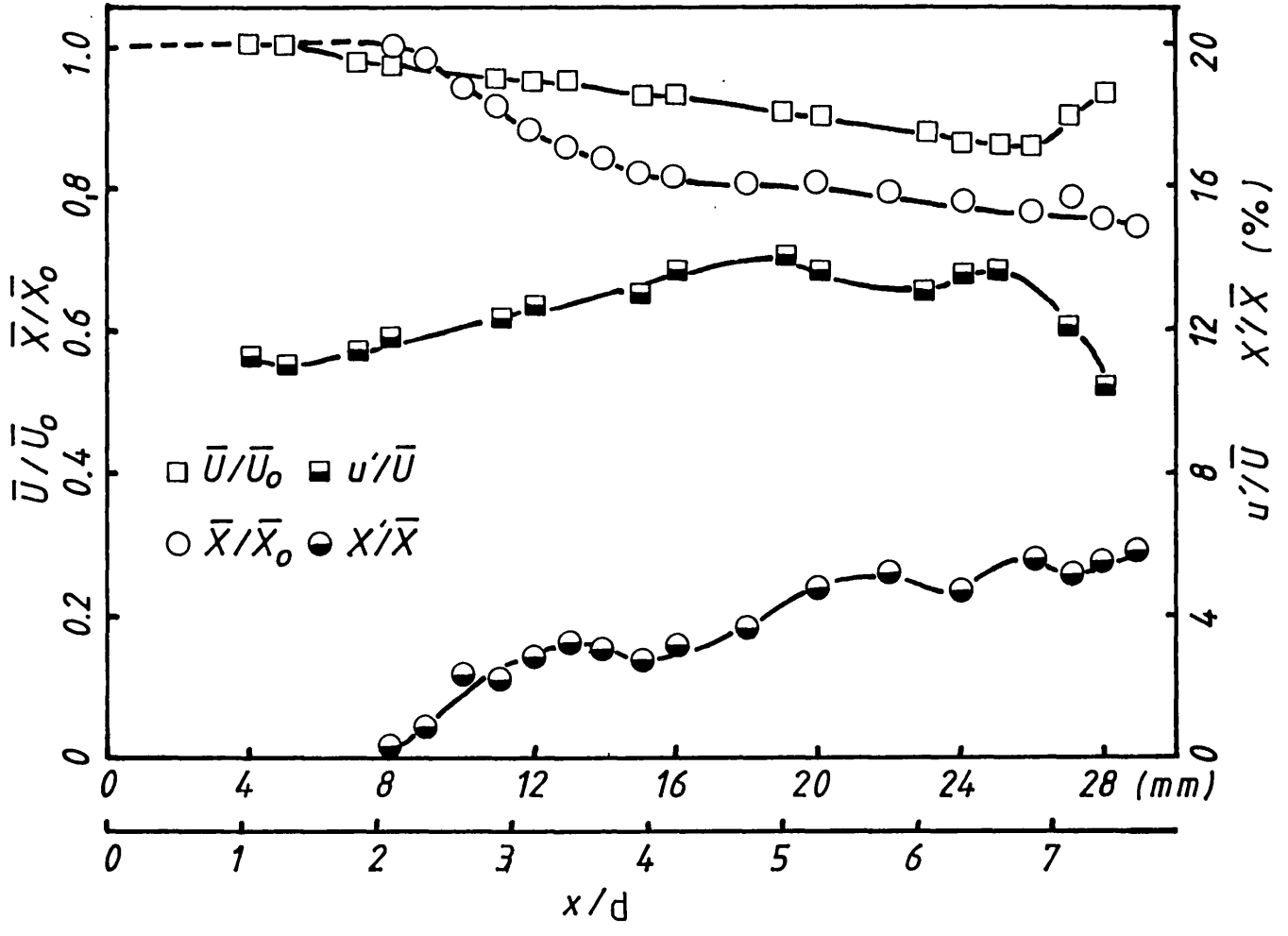


FIGURE 4.9 CENTRELINE DISTRIBUTIONS OF MEAN AND RMS CONCENTRATION AND VELOCITY; NOZZLE A, RE-ENTRANT PISTON

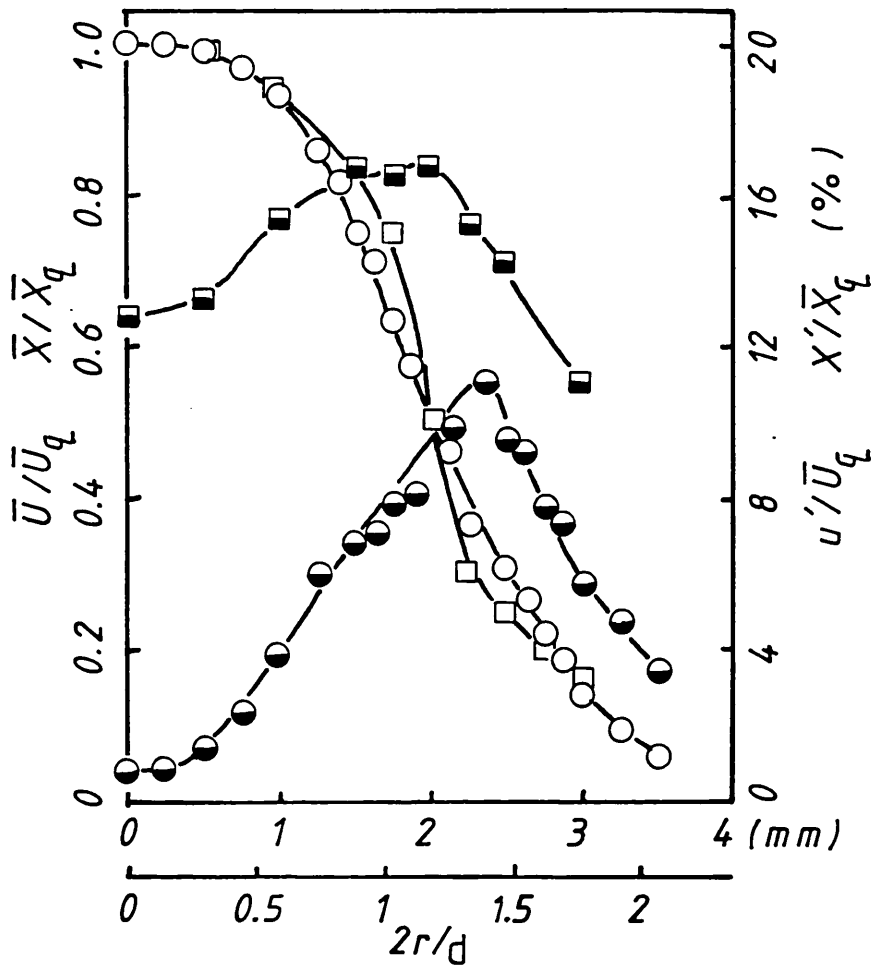


FIGURE 4.10(a) RADIAL DISTRIBUTIONS OF MEAN AND RMS CONCENTRATION AND VELOCITY AT x/d=2; NOZZLE A, FLAT PISTON

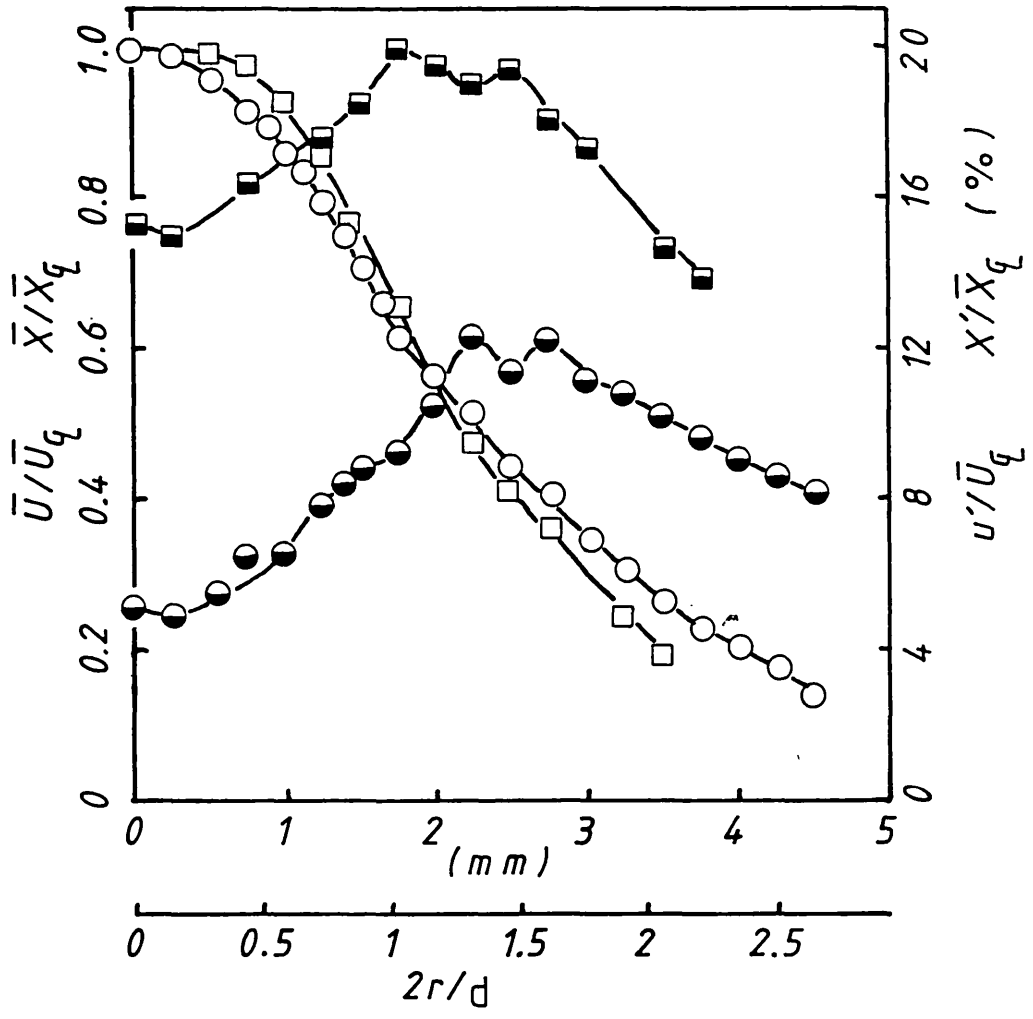


FIGURE 4.10(b) RADIAL DISTRIBUTIONS OF MEAN AND RMS CONCENTRATION AND VELOCITY AT x/d=4; NOZZLE A, FLAT PISTON

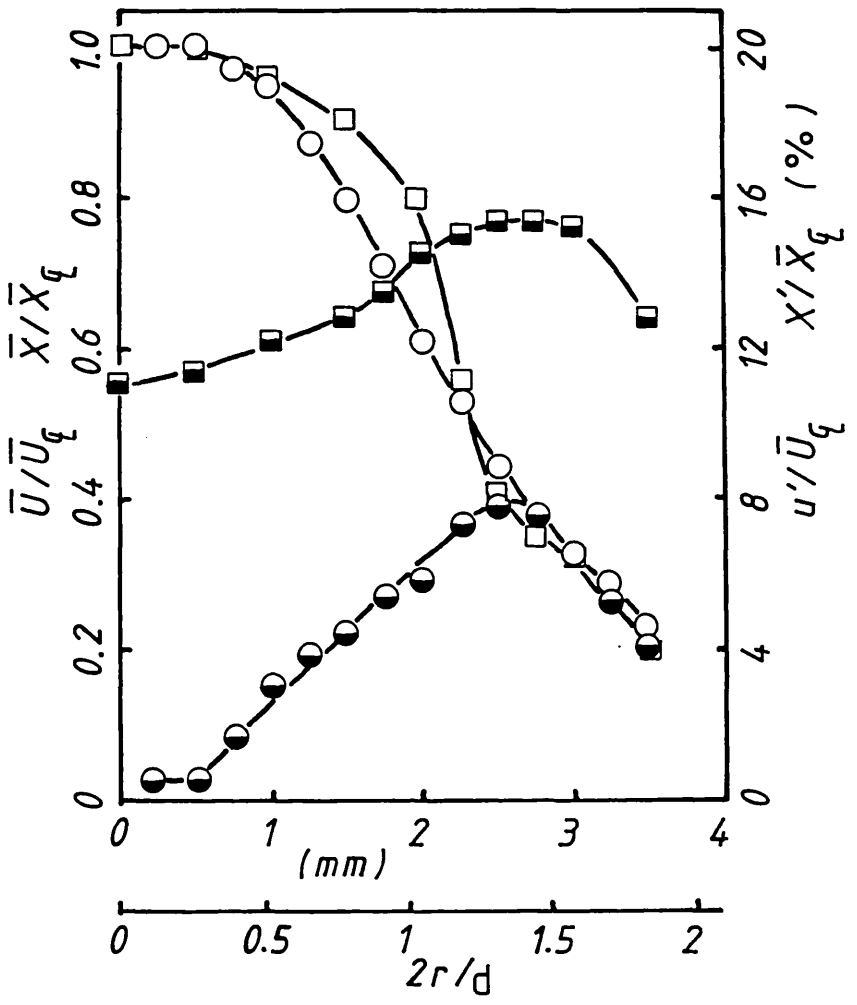


FIGURE 4.11(a) RADIAL DISTRIBUTIONS OF MEAN AND RMS CONCENTRATION AND VELOCITY AT x/d=2; NOZZLE B, FLAT PISTON

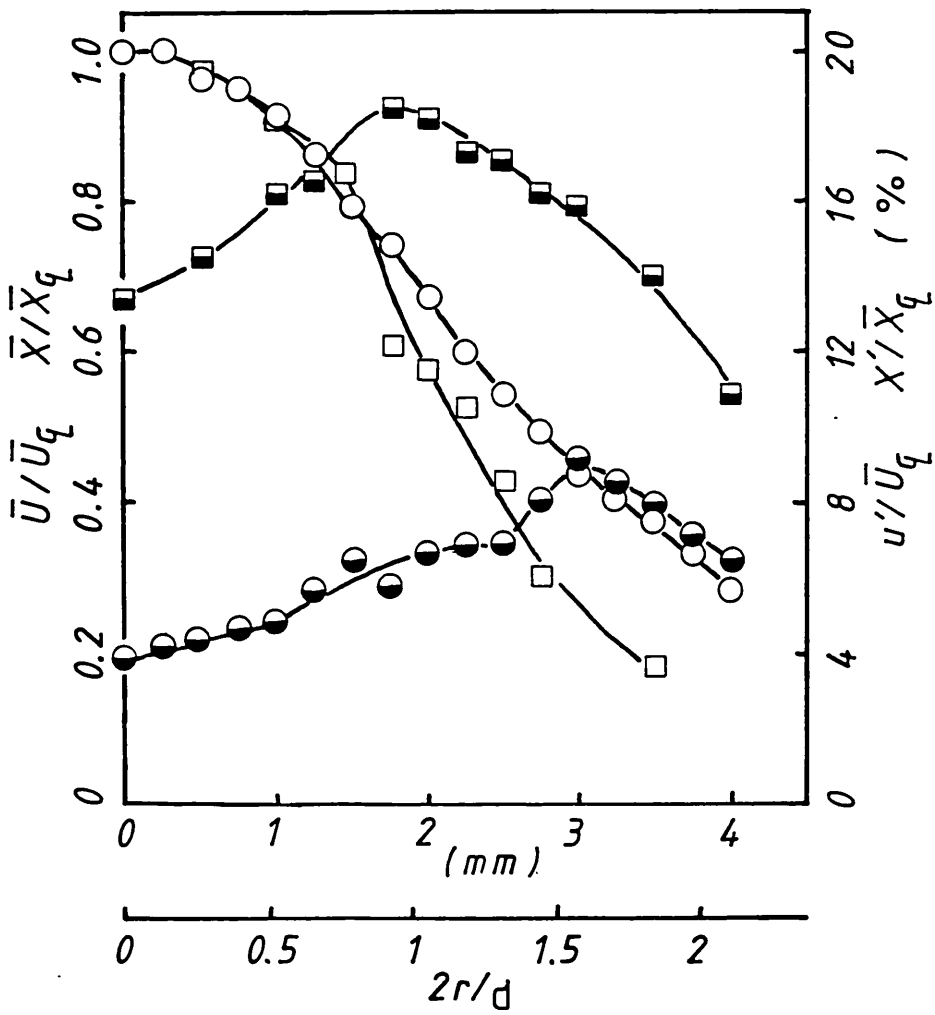


FIGURE 4.11(b) RADIAL DISTRIBUTIONS OF MEAN AND RMS CONCENTRATION AND VELOCITY AT x/d=4; NOZZLE B, FLAT PISTON

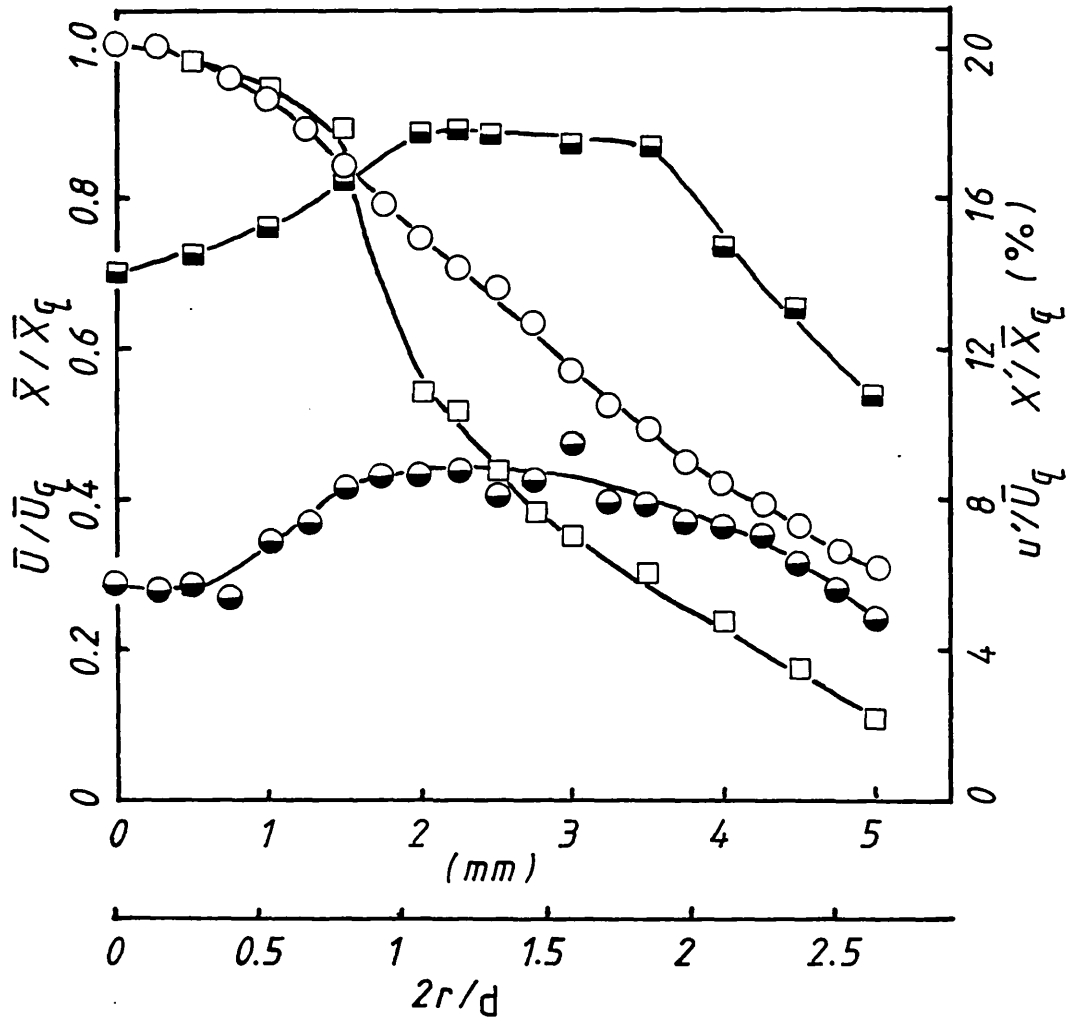


FIGURE 4.11(c) RADIAL DISTRIBUTIONS OF MEAN AND RMS CONCENTRATION AND VELOCITY AT x/d=6; NOZZLE B, FLAT PISTON

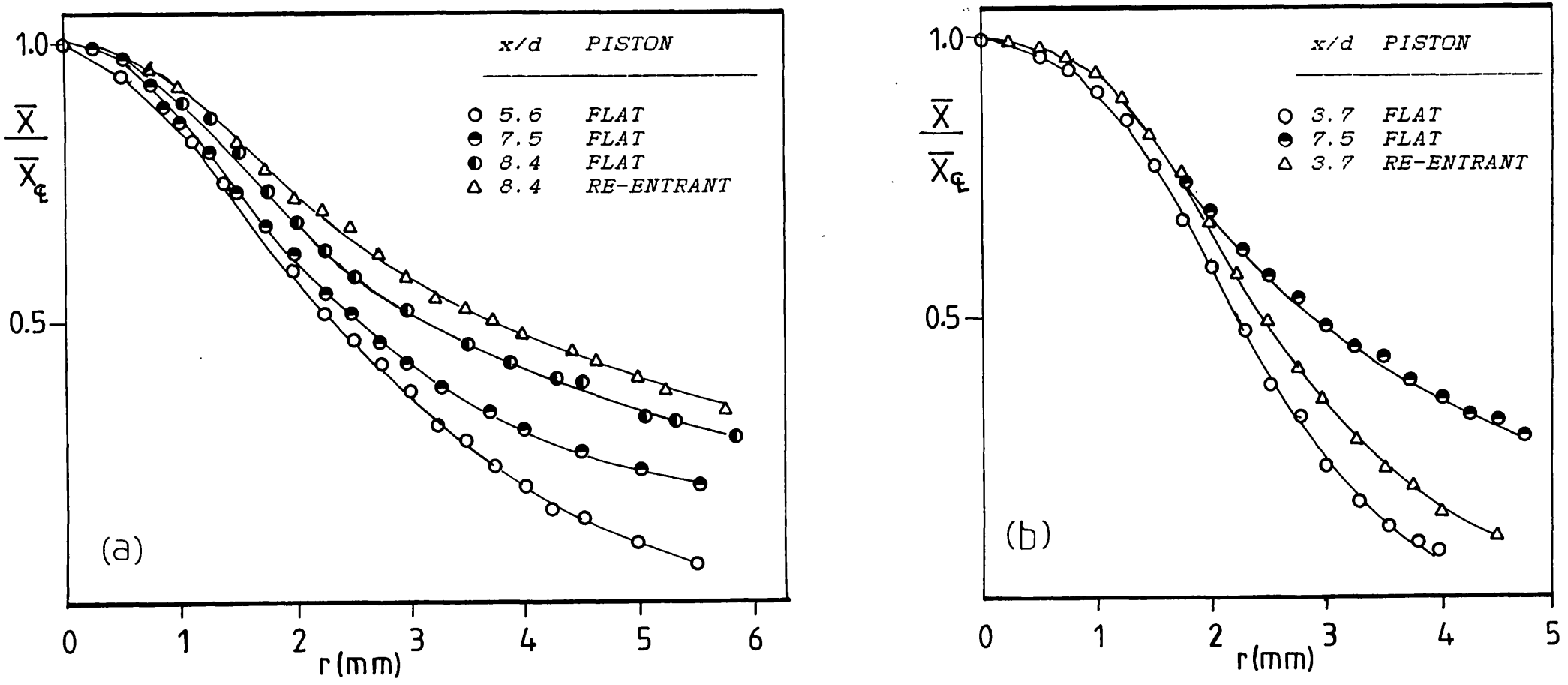


FIGURE 4.12 RADIAL PROFILES OF MEAN CONCENTRATION (NOZZLE A) AS INFLUENCED BY PISTON GEOMETRY (a) FUEL INJECTION INITIATED AT 40 deg. BTDC and (b) FUEL INJECTION INITIATED AT 10 deg. ATDC

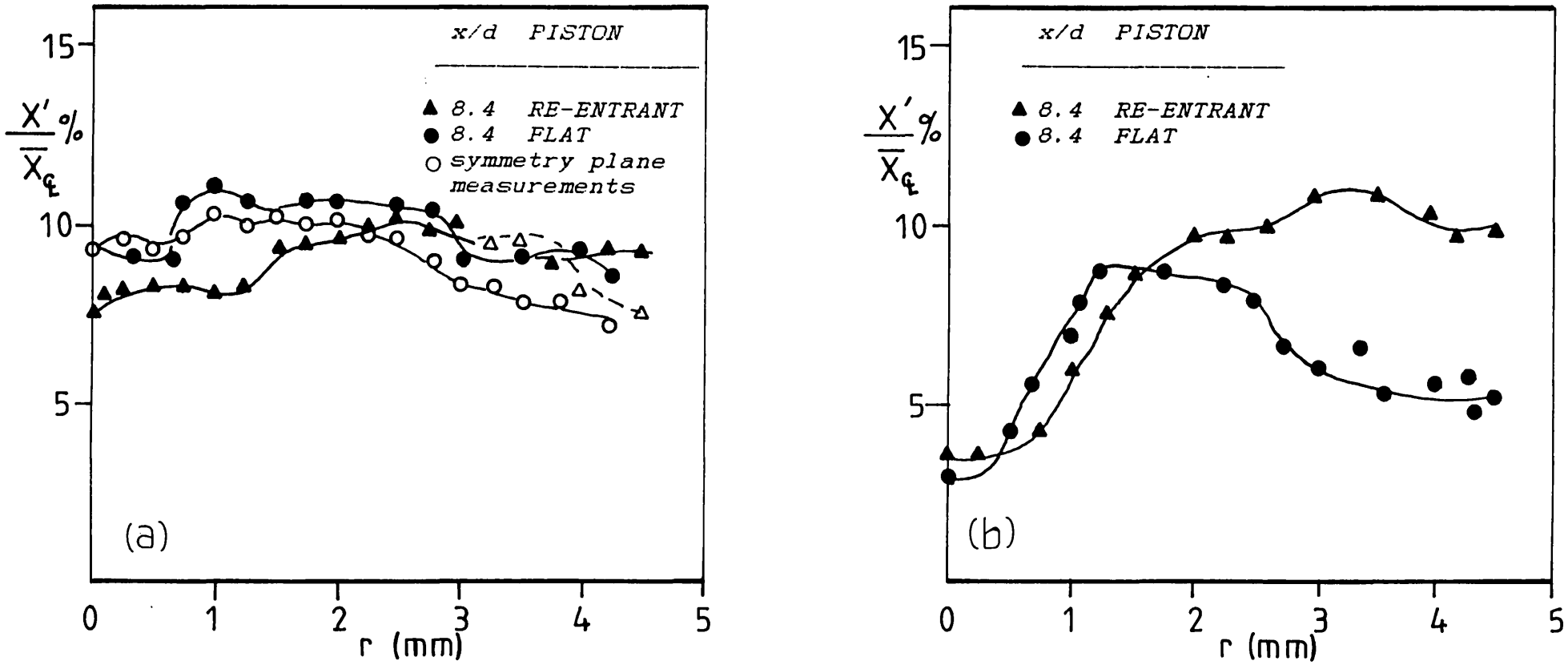


FIGURE 4.13 RMS CONCENTRATION AS INFLUENCED BY PISTON GEOMETRY (a) FUEL INJECTION INITIATED AT 40 deg. BTDC and (b) FUEL INJECTION INITIATED AT 10 deg. ATDC

CHAPTER 5 COMPRESSING MODEL ENGINE

5.1 INTRODUCTION

This chapter presents experimental results of the simulated fuel-injection process carried out in the presence of compression in a motored model Diesel engine similar to that reported in Chapter 4 but where measurements were obtained in the absence of compression. Laser Rayleigh scattering was employed to quantify the in-cylinder mole fraction of simulated injected fuel and laser Doppler anemometry was used to measure the exit plane velocity for the fuel jet from different nozzle geometries. The investigations have been made with the engine operating at compression ratios of 3.5 and 6.7 and with and without induction swirl. The effect of piston geometry has also been investigated with the use of flat, cylindrical bowl and re-entrant (bowl-lipped) pistons.

The flow configuration and experimental system is described in the next section. The results obtained with the engine operating at a 3.5 compression ratio are presented in section 5.3 and those obtained at a compression ratio of 6.7 in section 5.4. The more important conclusions are reported in section 5.5.

5.2 EXPERIMENTAL SYSTEM

5.2.1 Flow configuration

The operating characteristics of the plexiglass model engine are summarized in Tables 5.1 and 5.2 for the 3.5 and 6.7 compression ratio (CR) cases respectively. The in-cylinder pressure field and a detailed characterization of the in-cylinder air-motion and velocities have been reported by Vafidis (1986). For the 3.5 CR measurements, Freon-12 vapour was used to simulate fuel as noted in Chapter 4 because of its high density relative to air ($\rho_{Freon}/\rho_{air} \sim 4.2$) and the

large Rayleigh scattering cross-section of Freon-12 molecules relative to air ($\sigma_{Freon}/\sigma_{air}$ = 17.9). For the investigations made in the 6.7 CR case, the low vapour pressure of Freon-12 made its use unsuitable and an alternative gas SF_6 (sulfur hexa fluoride) was used. SF_6 was chosen because it too has a large density relative to air ($\rho_{SF_6}/\rho_{air} \sim 5.1$) and its Rayleigh scattering cross-section is also relatively high ($\sigma_{SF_6}/\sigma_{air} \sim 6.7$). The simulating fuel was injected through a nozzle inserted in the centre of a single axisymmetric valve, which was operated by a dual cam and rocker mechanism and used for both the intake and exhaust flow during the four stroke engine cycle. Measurements were obtained with the four nozzles* shown in Figure 5.1. Control of the fuel injection and synchronization of all real-time information was carried out in the same manner as in the non-compressing engine investigations and is described in Appendix C.

Fuel was injected and measurements carried out in every second four stroke cycle so as to avoid accumulation of the injected fuel vapour. The injection characteristics are summarized in Table 5.3 and are similar to those of the non-compressing engine studies. The injector system comprised a solenoid valve (Angar Model 008), a 3.2mm diameter hole along the axis of the valve stem and one of the four nozzles mounted flush with the valve face. The backpressure was maintained constant to define the same pressure drop across the nozzles at both the 3.5 and 6.7 CR (ΔP = 0.101 MPa) and the injection time was 16.7ms, corresponding to approximately 20° of crank angle. A gated laser velocimeter (see Chapter 4) was used to determine the exit-plane velocities. For the Freon, with injection into atmospheric air, these were 37.7, 30.9, 57.0 and 85m/s with nozzles A, B, C and D, respectively, and imply Reynolds numbers of 52600, 48200, 23400 and 17600. With injection into the compressing engine, these values were reduced to approximately 17.5, 14.0, 38.0 and 64.0m/s, with

* The diverging nozzle geometries were chosen to similarly investigate the effect of initial jet angle but with injection of the fuel jets into a compressing engine (in contrast to a non-compressing engine). The converging nozzles were chosen since their size and characteristics are more typical of actual geometries in Diesel injectors.

corresponding Reynolds numbers of 81800, 74400, 53100 and 44750; the in-cylinder mass of Freon injected for nozzles A, B, C and D was 45.6, 45.6, 8.57 and 3.7mg. Since the acoustic velocity for the Freon and SF_6 was greater than 150m/s, the nozzles did not choke. A check of the SF_6 velocities showed that these scaled by the square root of density ratio between Freon and SF_6 (as expected from Bernoulli's law), thus, $U_{SF_6} \sim 0.91 U_{Freon}$ and was constant since ΔP was constant for all the cases investigated. The corresponding injected mass values of SF_6 were about 0.86 times that of Freon.

The in-cylinder pressure associated with the 3.5 compression ratio reduces the jet exit momentum to around 0.55 of that at atmospheric pressure and that with the 6.7 compression ratio to about 0.38. The implications of reduced momentum for similar operating conditions (backpressure and injection timing as used at atmospheric conditions) are increases in mixing and spread of the jet equivalent to an upstream shift in its virtual origin. This is due in part to the increase in density of the in-cylinder air which leads to a faster rate of decrease in the initial jet momentum* and results in faster jet spread and decay. It is interesting to note that Reitz and Bracco (1982) reported similar increases in jet spread and decay for their liquid jets issuing into pressurized surroundings and this has also been observed by Siebers (1985) in his work with liquid fuel jets injected into a simulated engine environment prior to combustion. Similar observations have been reported for investigations at critical pressure and temperature for atomising liquid jets, see Newman and Brzustowski (1971), and for steady gas jets by Birch et al (1978) and Pitts and Kashiwagi (1984). The momentum of the present jets are slightly lower than reported for the non-compressing investigations of Chapter 4 but still higher than that of Johnston (1979).

* Equivalent to the effect of decreasing the density ratio between the fuel and air

5.2.2 Optical and signal processing systems

The in-cylinder mole fraction distribution of Freon-12 was measured with the laser Rayleigh scattering system described in Chapter 2. A line diagram of the optical arrangement and signal instrumentation is shown in Figure 2.1. In the present investigations the argon-ion laser was operated at 1.0 W and 488nm. The output from the photomultiplier was bandpass filtered (4KHz cut-off) and input to the data acquisition system through an A/D converter at a rate of 30KHz; sampling was carried out by software with a maximum rate of 16KHz. A second signal from a pressure transducer was sampled simultaneously with the photomultiplier output. Variations in engine speed, in-cylinder pressure at the start of injection and peak cycle pressure were monitored in each cycle and were consistent within 1% and 0.001 MPa, respectively. Freon (or SF_6) was used to fill the engine cylinder at the beginning of each experiment to check for systematic errors as would be indicated by differences in scattering intensity ratio between fuel and air (I_{fuel}/I_{air}) relative to theoretical values; discussed further below.

5.2.3 Sources of error and uncertainties

The sources of error in laser Rayleigh (LRS) scattering measurements have been documented in detail in Appendix A, additional sources in the present application include variations in cylinder pressure and gas temperature. In addition, droplets may give rise to scattered light which has to be distinguished from the molecular (Rayleigh) scattered light.

For a binary mixture at constant temperature and pressure, a Rayleigh signal is based on variations in the effective total mixture scattering cross-section and thus, mole fraction. In the engine, the time-varying process requires that the signal be analysed at the instantaneous thermodynamic state at which scattering occurs. Calibration measurements under both static and time-varying conditions made with concentrations of Freon-12 and air of 20%, 40%, 60% and 80%, confirmed the

expected linearity between pressure and intensity in the case of the 3.5 CR engine.

The static measurements were made with a pressure vessel having optical access while the time varying results were obtained with the engine running; for the latter, the head was covered with a polyethylene bag and provision made for the intake gas to be varied. To ensure that the mixture concentration did not change, the scatter intensities before and after running of the engine were determined and found to be within $\pm$0.5% of the expected values. Comparison of the static and time-varying results showed rms deviations of less than 1.5% and these were attributed to the sudden rise in gas temperature during compression which was small in the 3.5 CR measurements.

The temperature influence on the LRS signal was large for the engine operated at a 6.7 compression ratio and interpretation of the signal followed from calibrations as reported in Appendix A, section A.3. An example of the time varying calibrations for the 3.5 CR engine with Freon-12 is shown in Figure 5.2 (see also, Figure A.2).

Systematic checks were made during the measurements to ensure that the scatter intensity ratio between pure Freon and air remained constant (16 $\pm$ 0.05). This ratio is slightly lower than the commonly reported value of 17.9 and due to impurities in the Freon; note that $I_{Freon}/I_{air} = \sigma_{Freon}/\sigma_{air}$ where I is the detected Rayleigh scatter intensity of the respective gases deconvoluted from noise. Similar checks were made when the SF_6 gas was used and results there indicated better agreement between the expected scattering ratio and that measured (i.e. $\sigma_{SF_6}/\sigma_{air} = 6.7$).

Scattering from solid particles (e.g. room dust) was readily identified and removed when the intensity values were greater than that of pure fuel gas. When particle intensities fell below this maxima, the digital filtering techniques described in Chapter 2 were used and resulted in a mean uncertainty of around 1.5% and about 3% for the rms.

The measured pressure-influenced signal intensities were corrected to atmospheric value according to the equation

$$I_g(\theta) = \frac{(I_g(\theta,P) - I_B)}{P} \qquad (5.1)$$

where $I_g(\theta)$ is the equivalent instantaneous gas mixture scatter intensity at 1 atm, I_B the averaged optical background at the measurement location (detected using helium), and P the absolute pressure at the crank angle θ. It was possible in most instances to set $I_B = 0$. The transient temperature error, introduced into the measured pressure, is around 0.005 bar and can be combined with the overall uncertainty in the pressure measurements to give a maximum error in the quantified mole fraction of less than 1%, assuming that in-cycle temperature effects are negligible. The more general form for the scatter intensity of the fuel/air mixture accounting, in addition, for the influence of temperature as occurs in the 6.7 CR investigations, shows that neglecting temperature effects can lead to as much as 12% of unity uncertainty.

The photon count rate estimates in the present case N_p (Appendix A.2) along with the cut-off frequency Δf = 4KHz, define a signal to noise ratio (SNR) = $(N_p/2\Delta f)^{\frac{1}{2}}$ of about 233 or a relative uncertainty given by 1/(SNR) of 0.45%. For the pure air signal the relative uncertainty is about 2% and the corresponding SNR is 51. At the pressures of the measurements, the SNR values are improved by a factor of about $(P)^{\frac{1}{2}}$ thus, the effects of photon statistics on higher statistical moments (i.e. variance, skewness and kurtosis) are very small. Moreover, electronic shot-noise effects at pressures as found in the engine should be about 1% but, since the mole fractions are defined relative to atmospheric conditions (equation (5.1)), shot-noise uncertainty is more likely to be about 2%. Having obtained the corrected signal values for the Rayleigh scattering

intensities ($I_g(\theta)$) the mean mole fraction is related to the ensemble of the signal intensities by

$$\frac{\bar{X}}{\bar{X}_o} = \frac{\bar{I}_g}{\bar{I}_{go}} \tag{5.2}$$

where the subscript (o) refers to a reference state and the normalized rms intensity is given by

$$\frac{X'}{\bar{X}_o} = \frac{\overline{(I_g'^2)}^{\frac{1}{2}}}{\bar{I}_{go}} \tag{5.3}$$

and $\overline{(I_g'^2)}^{\frac{1}{2}}$ represents the rms of the signal after deconvolution of shot-noise effects and photon statistics. The results of the next section as respresented by equations (5.2) and (5.3) have an estimated uncertainty in mean concentration (5.2) of less than 3% with a maximum uncertainty in the rms of the concentration fluctuations (5.3) of 7%. When there are influences of temperature on the LRS signal, corrections following the discussions in Appendix A must be applied or uncertainties increase to 10% and 15%, respectively, for the mean and rms values; at 6.7 CR the uncertainties are 5% and 10% for mean and rms.

The ensembled mole fractions do not lead directly to mean mass fractions as they would under constant temperature and pressure conditions where the mass fraction $\bar{Y}$ is approximated by

$$\bar{Y} = \frac{(\alpha+1)X}{\alpha X+1} + \ldots \tag{5.4}$$

with $\alpha = (\rho_j/\rho_o - 1)$ and ρ_j and ρ_o the density of the jet and surroundings, respectively. In the engine flow $\rho = \rho(P,T)$ and

$\bar{X}$ is the average mole fraction centred at some crank angle θ over the interval $\Delta\theta$, In the limit of $\Delta\theta \to 0$ the mean mass fraction would be:

$$\bar{Y}(\theta) = \frac{(\alpha(\theta) + 1)\bar{X}}{\alpha(\theta)X + 1} + \ldots \qquad (5.5)$$

and $\alpha(\theta) = (\rho_j(\theta)/\rho_o(\theta) - 1)$ where $\rho = \rho(P(\theta),T(\theta)) = \rho(\theta)$ is the corresponding gas density defined at a state $P(\theta)$, $T(\theta)$. With the assumption of ideal gas behaviour for both the fuel and air, $\rho_j(\theta)/\rho_o(\theta) = M_j/M_o$ where M is the molecular weight of the gases and thus $\bar{Y}$ is accurate to within the approximation of equation (5.4). Values of $\bar{Y}$ have been obtained in terms of $\alpha(\theta)$ for both ideal and actual gas behaviour of the fuel and air and indicate that an underestimation of 4% is present at low values of $\bar{X}$, while the underestimations are within 2% at larger values of $\bar{X}$; we note that the higher order terms associated with equation (5.4) will introduce further errors at the lower values of $\bar{X}$. Similar analysis of the mass fraction fluctuating intensities, $Y' = f(X')$, indicates that they can be underestimated by up to 10%.

5.3 RESULTS FOR 3.5 CR ENGINE

Results for the Freon concentration field are presented in Figures 5.3 through 5.17 in the form of temporal distributions and centreline and radial concentration profiles. The ensemble averaged in-cycle fuel concentrations for three nozzles are shown in Figure 5.3. These were obtained at the same axial location (x = 5mm) on the centreline and indicate the faster decay and mixing expected with the initially lower mass of injected fuel of nozzle C and the greater mixing of nozzle B relative to nozzle A due to the increased diffusion angle of

nozzle B. The decay in centreline concentration distributions with downstream distance is represented by Figure 5.4.

The results of Figure 5.3 and 5.4 are based on instantaneous fuel-injection signals over 10^4 engine cycles and examples for nozzle A at a centreline location of x/d = 2.47 (x = 8.4mm) are shown in Figure 5.5; both the pressure-influenced signal (Figure 5.5(a)) and corrected signal (Figure 5.5(b)) are shown. The start time of injection is consistent for each cycle and the measured injection duration is effectively constant (16.7ms).

The results of Figure 5.5 may be compared with the non-compressing results of Figure 5.6 and confirm that the penetration of the jet into compressed air is less than that in atmospheric air with increased jet decay and spread as expected from steady-flow results such as those of Chapter 3.

The spatial distributions of the mean and rms of the concentration fluctuations of Figure 5.7 to Figure 5.17 are based on ensemble averages over a 10 degree crank angle window $\Delta\theta$ centred at 21 degrees before TDC and, as can be seen from the downstream results indicated by Figure 5.4, this averaging window consistently defines a region of characteristic behaviour for the fuel injection process. Averaging was also carried out with a 5 degree window centred at 21 degrees before TDC and comparison with the 10 degree results showed no differences. The choice of a 10 degree window improved the data acquisition rate and permitted more statistically accurate results to be obtained.

In the following sub-sections discussion of results is presented first in terms of general characteristics of centreline and radial profiles followed by more detailed discussions of the effects of nozzle and piston geometry and swirl. The final sub-sections analyse the fuel jet spread and scaling of the centreline and radial profiles.

5.3.1 Centreline characteristics

In Figure 5.7 results are presented for the mean and rms mole fraction concentration corresponding to three nozzles and with a flat piston and for nozzle A with a cylindrical bowl-piston geometry; the mean values are normalised by the exit concentration $\bar{X}/\bar{X}_o$, where $\bar{X}_o = 1$ is the exit mole fraction. The mean concentration characteristics of Figure 5.7(a) indicate results similar to those of free steady-jets where rapid initial decay of concentration is followed by a more gradual decay rate. The large distance represented by the ratio of piston clearance to nozzle diameter suggests that similar behaviour of centreline concentration decay as found for free jets should exist; similar observations have been made for the centreline velocity field of impinging jets as reported for example by Gutmark et al (1978) and Amano and Brandt (1984). Analysis of the results of Figure 5.7(a) show that the initial decay of concentration for nozzle C is greatest and that when the penetration distance is increased, as results with a bowled-piston, the initial decay is decreased as compared to the results for nozzle A with a flat and cylindrical bowled-piston indicate. Thus, a decrease in piston clearance leads to faster decay because of faster jet impingement onto the piston face. Further analysis shows that the downstream decay of mean concentration is greater for the larger diffusion nozzles A and B over that which results for the convergent nozzle C. A detailed comparison of these centreline results is provided below by considering the differences in their spread rates. Towards the downstream region near the piston, the mean concentration levels for nozzle A and B become more independent on upstream conditions. The concentration levels, however, remain higher for nozzles A and B due to the greater mass of fuel initially injected over nozzle C.

The rms distributions of Figure 5.7(b) are presented in terms of the local rms divided by the local mean concentration, $X'/\bar{X}$, and this is referred to as unmixedness as discussed in

Chapter 3. As can be seen, the initial rise in $X'/\bar{X}$ tends, with respect to the amount of mixing achieved, to a constant type behaviour. The distance from the nozzle at which the constant behaviour begins to occur is influenced by the degree of mixing and associated rate of concentration decay. It is observed that with the lower mass of injected fuel associated with nozzle C, mixing is more rapid for fuel with air and results in the fastest constant behviour and lowest levels of $X'/\bar{X}$. In contrast, the case of nozzle A with the bowled-piston (which results in the slowest mixing due in part to the increased penetration distance) indicates a slower growth towards constant behaviour in the characteristics of $X'/\bar{X}$. Moreover, the increased spread and thus mixing of the fuel jet from nozzle B over nozzle A, due to the increased diffusing angle of nozzle B, also shows a consistent trend in the resulting behaviour of $X'/\bar{X}$. Normalising the local values of the rms X' by the exit mean mole fraction (i.e. $\bar{X}_o = 1.0$) shows, as expected, that values of $X'/\bar{X}_o$ decrease with distance from the nozzle with values for nozzle A and B tending towards 9% rms and those for nozzle C to around 3%. These values suggest, when compared to similar results obtained in the non-compressing engine that the effect of compression through increase of the in-cylinder air density results in decreased penetration of the fuel jet and increased mixing, in particular, as lower values of $X'/\bar{X}_o$ result near the piston and indicate a more homogeneous air-fuel mixture.

5.3.2 Radial characteristics

Radial profiles of mean and rms concentration for nozzles A, B and C, obtained with a flat piston are shown in Figures 5.8, 5.9 and 5.10, respectively. The mean radial distributions are normalised by the centreline value of concentration. These radial profiles show that the rate of decay $\partial\bar{X}/\partial r$ decreases

with downstream distance as indicated by the broadening of mean profiles and is consistent with the variations in mole fraction close to the cylinder axis. The rms quantities tend toward a maximum and then decrease with the ratio $\dot{X}'_{max}/X'_{CL}$ not exceeding 1.15, although, in steady jets this ratio can be as high as 1.35 for jets having a density less than the surroundings. The present results indicate that the increased rate of momentum decay (due to the increase in air density) and the transient nature of the fuel jets, can lead to a result of more intensive mixing for an initially heavier density fuel jet. In addition, examination of the probability density distributions (pdf) of the ensembled values of the mole fraction showed that they were skewed towards the lower values, in a manner consistent with pdf's for the velocity characteristics of steady jets or the concentration characteristics of the steady jet of Chapter 3. The larger diffusing angle of nozzle B over nozzle A results in greater spread for nozzle B which associates itself with the increased mixing evident in the results of Figure 5.7 and thus reduced spread rates result downstream as indicated by analysis for the spread rate for nozzles A and B; note that with nozzles A and B the same mass of fuel is injected.

5.3.3 Effect of nozzle type and piston geometries

The bowl-lip piston with nozzle A (Figure 5.11a) results in a mean concentration of 0.90 at x/d = 2.35 (x = 8mm), similar to that obtained with a flat piston, and with both pistons the mean concentration level decays to about 0.4 near the piston. In contrast, nozzle C with a bowled-lip piston (Figure 5.12a) leads to a mean concentration of about 0.45 at x/d = 5 (x = 5mm) which, in contrast to nozzle A, gradually decays towards the entrance of the piston until it reaches an asymptote of about 0.20 beyond x/d = 25 (or x = 25mm). More-

over, with nozzle A, mean concentration is higher with a bowled piston geometry but the opposite behaviour is observed with the nozzle C results; the nozzle B results are consistent with those of nozzle A and those for nozzle D are consistent with nozzle C. For nozzle C, the centreline rms, X', normalised by the mean exit concentration $\bar{X}_o$ is about 5% at x/d = 5 and as shown by Figure 12b decreases gradually downstream to a value of 1.5% near the piston. With nozzle A (Figure 5.11(b)) the centreline value of $X'/\bar{X}_o$ rises quickly from 6% to a maximum of around 12.5% and decreases gradually to around 10% near the piston. The low rms values for nozzle C near the piston suggest well mixed fuel and air and are consistent with the rapid initial mixing of injected fuel with nozzle C.

Figures 5.13 and 5.14 show the radial profiles for mean concentration for nozzles A and C at x/d = 2.35 and x/d = 5, respectively. For nozzle A (Figure 5.13a), the jet spread is greatest with the flat piston as expected from the increased mixing associated with impingement on the piston; for the bowled pistons the jet has to penetrate into the bowl before increased mixing results. These trends in radial spread reverse in the case of nozzle C (Figure 5.14a). With the convergent nozzle C and D, the squish generated by the bowl-lip piston increases the extent of fuel mixing before the fuel jet penetrates into the bowl. These trends agree with the observations of Witze (1980), who showed that the larger the time constant of a transient jet, the greater the inertia of the leading vortex relative to forces impeding its progress.

The rms values tend to be slightly lower with the bowl-lip piston for both nozzle types (Figures 5.13b and 5.14b) and due probably to the squish effect introduced by the bowl-lip geometry and the resulting increase in air entrainment. The in-cylinder flow field velocity measurements of Vafidis (1986) confirm that differences do exist in the cylinder velocity field due to the piston configuration; lower rms levels are observed with bowl-piston geometries.

5.3.4 Effects of swirl

Centreline distributions in the presence of swirl (Figures 5.11 and 5.12) show that the swirl increases the decay rate of mean mole fraction. In the case of nozzle A with a bowl-lip piston (Figure 5.11a), the mean concentration near the nozzle at x/d = 2.35 is reduced to 0.49 of the exit value in the absence of swirl and the percentage difference is almost constant at higher values of x/d. Similar results are indicated on Figure 5.11a for the flat piston with and without swirl. With the flat piston geometry, the combined effects of impingement lead to fast centreline concentration decay as indicated by levels of mean concentration as low as 5% near the piston. With the added effect of swirl, momentum is transferred to the air which is entrained into the fuel jet with consequent reduction in the fuel jet penetration rate. Similar effects were observed by Sinnamon et al (1980) in their experimental and calculation results. Characterisation of squish and swirl effects on the air-motion in cylinder assemblies has been made, for example, by Witze (1980), Vafidis (1984) and Fansler (1985). The general indications are that the complex interaction of swirl with squish has an effect as found here on the extent of the jet penetration and spread. Moreoever, the three dimensional flow structures known to remain through TDC can be expected to dominate the air-fuel mixture dynamics and different induction swirl levels may be expected to result in different mixing strengths. The effect of swirl can also be viewed as resulting in an increase in shear of the jet boundary thus accelerating its radial growth.

The radial distributions of mean concentration (Figures 5.13a and 5.14a) indicate that, independent of piston and nozzle geometry, an increase in jet spread results in the presence of swirl; the differences which result are observed to be greater with the bowled piston geometries. With a bowl-lip piston, the diffusing nozzle A gives rise to a character-

istic jet spread (defined by $r_{1/2}/d$) of the order of 3.6 times greater than that in the absence of swirl and in increase of the order of 1.26 times found with the flat piston; $r_{1/2}$ is the radial distance at which the mean radial concentration is one-half the centreline value at the same axial location.

The rms intensities defined by $X'/\bar{X}_{CL}$ obtained with the diffusing nozzles (nozzle A and B) do not exceed 18% (Figure 5.13b). The rms quantities tend to increase with radial distance but the near nozzle value of X'_{max}/X'_{CL} does not exceed 1.3 and this value is similar to the value of 1.31 obtained by Pitts and Kashiwagi (1984) in their steady methane jet investigation. In the presence of swirl, the radial rms distribution are similar for both piston types (Figures 5.13b and 5.14b) in contrast to when swirl is absent where the rms distributions are more clearly influenced by piston geometry.

The convergent nozzle C (Figure 5.12b) indicates maximum centreline rms levels $X'/\bar{X}_{CL}$ of near 10% in the case of a flat piston with swirl but a slightly lower value results with a bowl-lip piston geometry ($\sim$8%). For all the nozzles with flat and bowled piston geometries, the centreline rms intensities clearly exhibit characteristics in the presence of swirl which are significantly different than in the absence of swirl (see Figures 5.11b and 5.12b). The effects of swirl lead to an interaction of the in-cylinder vortex structure which is absent without swirl at TDC.

5.3.5 Fuel jet spread and decay

The growth rates of the fuel jets along the centreline are shown as the reciporcal of the mean mole fraction concentration (Figure 5.15) and it is evident that the fuel jet spreads most rapidly in the presence of swirl as noted above. A comparison of the results can be made by describing the centreline decay in terms of the decay law

$$\frac{\bar{X}_o}{\bar{X}} = \frac{k_1(x - x_o)}{r_o} \qquad (5.6)$$

with x_o the virtual origin of the mole fraction, k_1, a constant and r_o, the nozzle radius. A least squares fit to the linear regions of the data obtained with the different parameters of these investigations provide the results summarised in Table 5.4. The spray type nozzles have the most negative values for the virtual origins but their spread rates as defined by the values of k_1 are less than those corresponding to the larger nozzles. This effect results from the faster development of the jet from these nozzles and corresponds to the very gradual decay expected when the flow is developed. The initial decay rate of the spray nozzles is greatest as is clear from the results of Figures 5.11 and 5.12 but their subsequent decay rate is not and is consistent with the findings of the centreline rms results which indicate about 4% rms in the piston proximity in contrast to the value of 10% for the larger nozzle. Similar observations can be made with respect to the k_1 values resulting for the cases involving swirl and a bowl-lip piston geometry.

For nozzles A and B, and in the absence of swirl, a larger decay rate is indicated for the bowl-lip piston over the flat piston and this follows from the observed increase in mixing associated with impingement. For nozzles A and B with a flat piston, the decay rate is similar. The fastest decay rate occurs for a flat piston geometry with swirling air motion. In contrast, for nozzles C and D, although similar decay rates exist between the two when a flat piston is used, the decay rate for nozzle C is greater than that of nozzle D with a bowl-lip geometry. These trends are consistent with those expected from the combined differences in the time constants and initial fuel mass injected. For nozzle B, the time constant increases

relative to nozzle A and thus more initial decay is expected for nozzle A with subsequent reduction along the linear region; nozzle B has a lower initial decay rate which subsequently increases. The same observations can be made about nozzles C and D where, in addition to a decrease in the time constant for nozzle D over nozzle C, the lower initial mass injected with nozzle D further results in initial differences in mixing and decay. It is interesting to note that for the case when a bowl-lip piston geometry is used and in the absence of swirl $(k_1)_A/(k_1)_B \sim r_a/r_b$ and similarly $(k_1)_C/(k_1)_D \sim r_c/r_d$. In contrast, with the flat piston, the ratios of the spreading rates, $(k_1)_A/(k_1)_B$ and $(k_1)_C/(k_1)_D$ is of order unity.

The radial spread of the fuel jets can also be characterised by a form similar to Equation (5.6) in terms of the half-width $r_{1/2}$; with $r_{1/2}$ as defined above. The form of $r_{1/2}$ as a function of axial distance x is given by

$$r_{1/2} = k_2(x - x_o^r) \tag{5.7}$$

where k_2 is a constant and x_o^r is the mole fraction virtual origin defined by the results $r_{1/2}/r_o$ versus x/r_o. From the simultaneous conservation of momentum and nozzle fluid concentration, x_o^r should equal x_o and thus $X_{CL}(r_{1/2}/r_o) = k_2/k_1$ = constant, see for example Becker et al (1967), Sforza and Mons (1978) and Lockwood and Moneib (1980). These relations apply when self-preservation is reached, as results from the asymptotic behaviour of steady jets indicate, but analysis of our results show that they do not apply. Within the limited comparison that can be made, the virtual origin defined by Equation (5.7) shows a shift to a more positive location than that defined by Equation (5.6). This has also been observed by Bremhorst and Watson (1981) in their velocity field measurements in a pulsed core jet where

the virtual origin defined by the centreline velocity spread was more positive. For transient jets, the conservation of momentum does not hold at any cross-section of the jet as it does in steady jets. The value of k_2 is greater than k_1 and the ratio k_2/k_1 is much greater than usually reported for steady jets; k_2/k_1 defines the ratio of growth of the mean concentration half-width to that of the mean concentration decay of the centreline. These observations are in agreement with findings in transient and impulsively started jets, where it is known that entrainment, growth and decay are greater than for steady jets. We note that the trends in radial spread as determined by the time constants, nozzle geometry and piston configuration remain in consistent agreement with those determined for the centreline behaviour. It remains, however, to quantify the features with nozzles where, for example, transient fuel jets issue from multiple hole injector nozzles and at high compression ratios.

An analysis of the results in terms of mass fractions indicates the same trends observed with the mole fraction for spread and decay. From the mass and mole fraction results, it is observed that with the bowl piston geometry, the ratio of the spread constant k_1 between any two nozzles is equivalent to the ratio of the radius r_o of the nozzles. Similar findings were not made for the flat piston results and an explanation must await further studies.

In the case of the bowl piston, the jet penetration is not influenced by the impingement effect as results with the flat piston and thus the spread and decay characteristics can be expected to be different. The scaling of spread rates with the jet time constants is also observed and is not too surprising since, as discussed in detail by Witze (1980), τ_j is a similarity parameter for transient jets (the investigations there made with free jets of equal density to the environment). With the bowl piston geometry, the increased depth for penetration is indirectly representative of the free jet condition.

Comparison of radial spread in terms of $(r_{1/2}/r_o)$ and physical and dimensionless axial distance (x and x/r_o) for all parameters investigated is presented in Table 5.5. As shown, the convergent nozzles give rise to the greatest spread $(r_{1/2}/r_o)$ in terms of physical distance from the nozzle exit and implies that the extent of mixing near the nozzles plays an important role in the fuel jet spread achieved downstream. The spread for the smallest nozzle is about four times that of the larger nozzles in the flat piston case and about 9.6 times greater with the bowl-piston geometries. The dimensionless characteristics, however, are dependent upon τ_j and consistent trends are observed with those reported elsewhere (eg. Witze (1980) and Reitz and Bracco (1979)). Most interesting is that the predicted behaviour of our gaseous jet as influenced by nozzle criteria, is similarly predicted for high pressure, atomising liquid jets and sprays.

5.3.6 Effects of scaling and similarity characteristics

Since the piston geometry defines different characteristic axial lengths for a fixed compression ratio, an attempt was made to characterise the axial coordinate for the centreline concentration decay in terms of the distance defined from the nozzle to the full depth available for the fuel jet to penetrate, H ; this is the distance between the nozzle and the piston face in the case of the flat piston or the inner depth of the bowl. Since the fuel injection takes place near TDC of compression, H was defined at TDC. Figure 5.16 shows that different trends to those with the normalisation by the nozzle diameter result for the mean concentration decay. The decay of mean concentration with the bowl-lip piston geometry and nozzle A is represented as greater although the initial mean concentration levels are nearly the same as those with the flat piston. With the convergent nozzles (C and D), the

jet decay is less influenced by piston geometry since the inertia of the jets from these nozzles is less than those from the diffusing nozzles and they tend toward their asymptotic behaviour physically much closer to the nozzle and are thus less influenced by downstream conditions.

The radial distributions of mean mole fraction concentration are presented in Figure 5.17 for the four nozzles and two of the piston geometries in the absence of swirl; the radial coordinate chosen here is $r/r_{1/2}$. It is noted that when swirl is induced during the intake stroke the radial profiles starting very near the nozzle quickly tend towards flat distributions and suggests that the interaction of swirl with the fuel jet promotes uniform mixture close to the nozzle. As shown in Figure 5.17, use of the radial coordinate $r/r_{1/2}$ tends to collapse all the results to a curve which can be characterised in terms of the Gaussian function

$$\frac{\phi}{\phi_{CL}} = \exp\left(k_3 (r/r_{1/2})^{\beta}\right) \qquad (5.8)$$

where $k_3 = -\ln 2$ and $\beta = 2$ are the values reported for fully developed steady jets. The Equation (5.8) also represents the similarity for the mass fraction results. Bremhorst and Watson (1981) have reported the same result (5.8) for the radial velocity distributions of their pulsed jets and also found similarity in their rms distributions. No similarity of the rms profiles could be established in the present case since the profiles were strongly influenced by piston geometry and the presence of swirl.

5.4 RESULTS FOR 6.7 CR ENGINE

In this section measurements of the mole fraction concentration of SF_6 are presented and were obtained in the engine operated at a compression ratio of 6.7 and in the absence of swirl; emphasis is on characterizing the effect of compression ratio on the air/fuel mixing process. The measurements were made with the nozzles A and C and with a flat and re-entrant piston. Because of the change to SF_6 for measurements in the 6.7 CR engine (due to the low vapour pressure of the Freon-12), measurements have also been made with SF_6 and the engine operating at a 3.5 CR to facilitate comparisons of the effects of compression ratio. Moreover, assessment of the effects of fuel density can also be made by comparison of results obtained in the 3.5 CR engine using Freon-12 and SF_6. The influence of compression ratio on the spatial distribution of injected fuel is represented in terms of the centreline and radial profiles presented and discussed in the next two sub-sections. The influence on the temporal characteristics, in terms of the fuel jet autocorrelation function, is discussed in a third sub-section.

5.4.1 Centreline distributions

Figure 5.18 presents values of mean and rms concentration obtained with nozzle A, a re-entrant and flat piston at 3.5 CR and with nozzles A and C and a flat piston at 6.7 CR; the mean and rms values are normalized by the exit plane concentration as $\bar{X}/\bar{X}_o$ and $X'/\bar{X}_o$, respectively, where $\bar{X}_o = 1$. Comparison of the nozzle A results at 3.5 CR with SF_6 and Freon-12 (Figures 5.18(a) and 5.11(a)) shows that the effect of piston geometry is is independent of fuel density. When the flat piston is used, jet impingement on the piston face leads to increased

mixing over the re-entrant case where, as noted in Section 5.3, impingement was delayed by the increased penetration. With a flat piston, the concentration decays in a similar manner with both the SF_6 and Freon-12 with the same mean concentration levels ($\bar{X}/\bar{X}_o \sim 0.3$) being reached near the piston. For the SF_6, since the mass of fuel injected is slightly lower than with Freon, see section 5.2, the initial decay of SF_6 is greater than results with Freon in the case of the re-entrant piston but similar mean concentration levels ($\bar{X}/\bar{X}_o \sim 0.45$) are reached near the entrance to the bowl. A greater influence of fuel density, on the rms of the concentration, is shown by Figures 5.11(b) and 5.18(b) with the absolute rms levels $X'/\bar{X}_o$ for the SF_6 5% greater than those resulting for the Freon jet. This indicates higher unmixedness for the heavier fuel near the nozzle and is consistent with the observed slower development of asymptotic behaviour in heavier density steady jets, see Chapter 3. Further downstream the density influence on X' is less and with similar rms levels ($X'/\bar{X}_o \sim 0.10$) resulting near the piston for both the SF_6 and Freon-12 jets.

The effect of compression ratio can be seen by comparing the results obtained for nozzle A with a flat piston at 3.5 CR and 6.7 CR, Figure 5.18(a). With the higher compression ratio, a much faster initial decay of concentration results as shown by mean levels near the nozzle exit and the corresponding mean levels are about one-half of those obtained with the engine oeprated at 3.5 CR. The downstream decay (independent of the nozzle) is nearly uniform, and unlike the 3.5 CR results, differences between the mean levels obtained with nozzles A and C are very small with the same rate $\partial\bar{X}/\partial x$ indicated for the jets from both these nozzles. In contrast, at the lower compression ratio of 3.5, the role of nozzle size (and thus the resulting mass of injected fuel) was significant. For example, the lower mass of fuel injected with nozzle C led to more rapid mixing of the fuel

jet near the nozzle with very low and uniform levels of mean and rms concentration being achieved (see Figures 5.11 and 5.12). At the higher compression ratio of 6.7, the further decrease in density ratio between the injected fuel and in-cylinder air leads to similar results for both nozzles even though a greater mass of fuel is consistently injected with nozzle A (Figure 5.18). The implications are that mixing of fuel with air at the nozzle exit is important in defining the subsequent mixture characteristics and that mixing is more influenced by compression ratio so that there is less influence of nozzle geometry.

The air/fuel mixture uniformity is made clear by the low rms intensities with similar characteristics resulting for both nozzles as shown in Figure 5.18(b).

5.4.2 Radial distributions

Figures 5.19, 5.20 and 5.21 present radial profiles of mean and rms concentration of SF_6 for nozzle A with a flat and re-entrant piston at 3.5 CR and for nozzles A and C with a flat and re-entrant piston at 6.7 CR. The mean results are normalized by the centreline value as $\bar{X}/\bar{X}_{CL}$ and the rms intensities by the corresponding centreline rms, X'/X'_{CL}.

As noted above with the centreline results, a greater mass of fuel is injected with the Freon than with SF_6 for the constant operating conditions of the fuel injection system. The exit momentum, however, is similar with the momentum of the SF_6 jet being only about 8% greater. As the results of this section will show, it is the differences in injected mass of fuel (in addition to compression ratio) which affect the air/fuel mixing process. Figure 5.19 shows results for the radial mean and rms concentration obtained with Freon-12 and SF_6 and with the engine operated at 3.5 CR.

Comparison of the mean profiles (Figures 5.19(a) and (c)) shows that the radial spread of SF_6 is greater than with Freon. This increase in radial mean spread with associated decrease in mean centreline values (Section 5.4.1 and Figure 5.18) indicates that more fuel is present in the outer regions of the SF_6 jet and is a consequence of the faster mixing which results when the amount of fuel injected is decreased. It is noted that the differences in injected mass do not have to be significant (for instance, as occurs with the use of nozzle C, section 5.3.3). In the present case a slight reduction in injected mass of 12% leads to the immediate result of increasing fuel spread of the heavier SF_6.

The rms results of Figure 5.19(b) and (d) also make clear that a greater extent of radial fuel spread results when the mass of injected fuel is decreased (thus improving the downstream mixture homogeneity). From Figures 5.19(b) and (d) the radial location at which the rms maxima occurs is greater with the SF_6 jet. As represented by the near nozzle results obtained at x = 5 and 8mm, the rms ratio X'/X'_{CL} is greater for the SF_6 (Figure 5.19(b)) than results with Freon (Figure 5.19(d))and similar trends were shown by the centreline rms results of Figures 5.11(b) and 5.18(b). Further downstream, however, the increased radial spread of SF_6 remains but with the levels of X'/X'_{CL} for SF_6 tending towards unity along the entire radial plane in contrast to the results obtained with Freon where the levels and characteristics of X'/X'_{CL} remain similar to those resulting upstream (i.e. X'tending towards a maxima and then decreasing).

With the re-entrant and flat piston a consistent trend is established with respect to the maxima in radial rms intensities. Defining r_{max} as the radial location at which X'/X'_{CL} becomes maximum and with $r_{1/2}$ as previously defined, the values for $r_{max}/r_{1/2}$ obtained with a flat piston are greater than those obtained with a re-entrant piston and follows (independent of fuel density and mass of fuel injected) in consistent agreement with the detailed discussions of Section 5.3. For

example, at the axial location x = 8mm, with a flat piston $r_{max}/r_{1/2}$ is equal to 0.783 and 0.851 for Freon and SF_6, respectively, while with a re-entrant piston the corresponding values are 0.567 and 0.474. These greater values of $r_{max}/r_{1/2}$ with the flat piston indicate more rapid spread results.

The effects of fuel density and amount of fuel injected also show separate effects. With the re-entrant piston the increased penetration distance is representative of a free jet and is supported in part by the analysis of Section 5.3.5. For the SF_6 jet (and a re-entrant piston), $r_{max}/r_{1/2}$ tends to be less than with Freon and as the results of Chapter 3 show, this is expected with the heavier density of SF_6. With the flat piston geometry the same effect of fuel density was not found and this is to be expected since there impingement on the upstream mixing characteristics is important, as discussed in Section 5.3.3.

When the compression ratio is increased from 3.5 to 6.7, the fuel jet radial spread increases in a manner which is consistent with the centreline results. Comparison of Figures 5.20(a) and 5.19(a) makes clear the differences in radial spread with the effect of higher compression ratio and, particularly with a flat piston, leads to a rapid homogeneous mixture as indicated by the flat concentration profiles of Figure 5.20(a). The growth of the jet is represented by comparison of the radial profiles at 6.7 CR (Figure 5.20(a)) which, in contrast to similar profiles obtained with the engine operated at a 3.5 CR (Figure 5.8(a)), shows that the values of $r_{1/2}/r_o$ are different, and a summary is provided below. The effects of nozzle geometry remain consistent at the higher compression ratio as shown by comparison of results obtained with nozzle A and C (Figure 5.20 and 5.21). The differences in radial spread of the two nozzles (as characterized by $r_{1/2}/r_o$) are less at the higher compression ratio, see Figures 5.13(a), 5.14(a), 5.20(a) and 5.21(a). Similar findings for the combined effects of com-

pression ratio and nozzle geometry were shown with the centre-line results of Section 5.4.1.

The rms results shown by Figure 5.20(b) and 5.21(b) support the findings in the mean radial profiles and centre-line profiles that an increase in compression ratio leads to increased mixing through faster centreline decay, particularly at the nozzle exit, with increased radial growth leading to more rapid air/fuel mixutre distribution. As shown by Figure 5.20(b), X'/X'_{CL} increases with radial distance near the piston for the jet from nozzle A in contrast to the opposite behaviour shown from distributions resulting with nozzle C (Figure 5.21(b)). With the larger nozzle A the increased rate of radial spread of fuel leads to greater mixing intensity at a further radial distance before the profiles of X'/X'_{CL} can become uniform. With the greater mass of fuel injected with nozzle A, differences in the fuel mixing dynamics are expected as discussed in Section 5.3.5.

A summary of results obtained with the SF_6 fuel jet at 3.5 CR and 6.7 CR is provided in Table 5.6 and facilitates comparison of the similar results obtained with Freon-12 at 3.5 CR (Table 5.5) and at 0 CR (Table 4.4). Clearly, a consistent trend appears through influence of the in-cylinder air density ρ_{air}; the characteristic spread $r_{1/2}/r_o$ consistently increases for a given nozzle geometry and with differences in $r_{1/2}/r_o$ also remaining consistent between different nozzles. The effect of ρ_{air} on $r_{1/2}/r_o$ and with different piston geometries is also consistent but some dependence on fuel density (combined with the mass of fuel injected) can result in variations of $r_{1/2}/r_o$ for the same nozzle geometry.

5.4.3 Temporal characteristics (autocorrelations)

In steady flow investigations the autocorrelation

function $R(\tau)$ obtained from fluctuating concentrations at a fixed point can provide detailed information of the temporal characteristics of the mixing process. In the air/fuel mixing process of the engine, the flow is transient and non-stationary and implies that the statistical properties which can be determined are dependent on the time t_o at which measurements start and the time at which they stop, t_f. As discussed in Section 5.3, the averaging window $\Delta\theta$ used to measure data for the ensemble quantities was chosen so that the beginning and duration of $\Delta\theta$ occurred in a region of quasi-steady behaviour of the fuel injection process (Figure 5.4). Assessment of the temporal characteristics must, however, be based on the total time interval of the transient fuel injection process and, according to results such as those of Figures 5.4 and 5.5, implies that a single definition of the start and stop of the measurement time cannot be applied.

Based on instantaneous results such as those of Figure 5.5, but for individual engine cycles, the start time t_o of the autocorrelation function has been defined as the time associated with the maxima in initial rise of fuel concentration and the stop time t_f as the time when the concentration has decayed to a level of less than 3%. On average, the times t_o and t_f correspond to 330 and 356 crankangle degrees, respectively, after the start of an engine cycle. Details of the calculation procedures for the autocorrelation function of these transient and non-stationary fuel injection characteristics follow from the methods used for similar processes as reported by Bendat and Piersal (1971, Chapter 10, pp 356-360). Below, the autocorrelation of individual (instantaneous) cycle data is represented by $R(\tau)$ while the ensemble autocorrelations (based on a minimum of 100 engine cycles) are represented by $\langle R(\tau) \rangle$; as usual both $R(\tau)$ and $\langle R(\tau) \rangle$ are defined in the interval ± 1.0 and an estimate of the confidence limits follows from analysis as reported by Bendat and Piersal (1971) and Chatfield (1984, Chapter 4).

Figure 5.22 presents results for the ensembles $\langle R(\tau) \rangle$ for nozzle A obtained with the engine operating at 3.5 and 6.7 CR with flat and re-entrant pistons. The time lag τ is the same for all cases (100μs) and with differences in the correlation times clearly indicating that the temporal characteristics of the air/fuel mixing process are strongly dependent on engine and nozzle geometry and compression ratio. Comparison of Figures 5.22(a) and (b) shows the increase in correlation time at the higher compression ratio which is due in part to the faster mixing and lower rms levels found at higher compression ratio in contrast to the higher mean and rms at the lower compression ratio. The short correlation times for the 3.5 CR measurements (Figure 5.22(a)) are indicative of greater randomness in the air/fuel mixing process. Similar observations can be made for the effect of piston geometry (Figures 5.22(b) and (c)) where again the dependence shown by the mean and rms results on flat and re-entrant geometries (Section 5.3) are indicated by the results here of $\langle R(\tau) \rangle$; faster and more uniform mixture results with a flat piston than with a re-entrant geometry.

The interesting result represented by Figures 5.22(a) - (c) is that the correlation time decreases with downstream distance in contrast to the opposite behaviour known to exist in steady jets; see Birch et al (1978) and Pitts and Kashiwagi (1984). This results from the definition of the correlation time which in the present case is associated with a transient interval. When the correlation time is confined to the interval of quasi-steady behaviour, a similar trend in correlation time results for the transient and steady jets. Figure 5.22(d) shows a typical example for nozzle A with a re-entrant piston. A long correlation time is indicative of a strong characteristic in the time series and in the present case this is associated with the characteristic defined by

a concentration plateau and then decay. Further downstream the trend weakens; see, for example, Figures 5.4 and 5.6.

Single cycle autocorrelations $R(\tau)$ are shown in Figures 5.23(a) and (b) for measurements made with the re-entrant piston and nozzle A at 3.5 and 6.7 CR. They indicate larger cyclic variance results in the air/fuel mixing process at a lower compression ratio. For the higher compression ratio it was shown (Section 5.4.2) that the air/fuel mixing process is improved over that achieved at a lower compression ratio (for similar geometry and fuel injection conditions) and the results of Figure 5.23(a) are consistent with those findings. Comparison of Figures 5.23(b) and (c) for the single cycle results of $R(\tau)$ with a flat and re-entrant piston are also consistent in that the influence of piston geometry is predicted in a similar manner as by the mean and rms ensembles. Improved mixing due to impingement on the flat piston face results as shown in the decreased cyclic variance for the flat piston results of $R(\tau)$ (Figure 5.23(c)).

The variables investigated here are seen to influence the temporal characteristics of the air/fuel mixing process in the engine. The autocorrelation function is very sensitive to the effects of engine geometry and compression ratio. The transient and non-stationary behaviour of the fuel injection process does not result in similar characteristics for the autocorrelation as in steady jets where $R(\tau)$ can be fit to an exponential of the form exp (-t/T) where T is the integral time scale. Moreover, cyclic variance in the air/fuel mixing process leads to variations in the autocorrelation which are strongly influenced by the level of mixing achieved with a given engine configuration.

5.5 CONCLUSIONS

The investigation of the influence of compression ratio,

nozzle geometry, piston configuration, induction swirl and fuel density on the in-cylinder concentration field of a simulated fuel in a model engine operated in a four stroke cycle and motored at 200 rpm revealed the following:

1. Nozzle design plays a predominant role and the characteristics of the air/fuel mixture can be predicted in terms of the time constants, τ_j. The convergent (spray) nozzles lead to a more rapid initial decay with associated lower rms values and greater characteristics spread $r_{1/2}/d$ than the diffusing nozzles. Nozzles with larger τ_j and with correspondingly larger momentum and Reynolds numbers lead to slower decay and higher rms levels in contrast to the opposite behaviour shown by the spray nozzles with smaller τ_j and lower Reynolds number. These results suggest that the extent of initial mixing of fuel with air is important in controlling rapid mixture throughout the cylinder.

2. The squish effect induced by the re-entrant piston configuration also plays a dominant role in the air/fuel mixing process but to a lesser extent than that of the nozzle design. When squish is induced by the re-entrant piston geometry, the fuel jet decays more slowly in the case of the diffusing nozzles but more rapidly with the spray nozzles. This interaction appears to be coupled to the initial inertia and momentum characteristics of the fuel jet.

3. Induction swirl increases air entrainment and results in faster and more uniform air/fuel mixtures. The combined effects of swirl and squish is to reduce the mean centreline fuel concentration levels by about 50% and 20% with the diffusing and convergent nozzles, respectively. In the presence of swirl, the rms distributions in both the centre-line and radial directions are uninfluenced by piston geo-metry although differences do remain between the nozzle types.

4. In the absence of swirl, the fuel jets exhibit similarity in the radial mean concentration distributions independent of nozzle geometry and piston geometry but no similarity was found in the rms distributions. With swirl, flat concentration profiles very near the nozzle exit imply uniform mixtures of fuel and air.

5. The effect of increasing the compression ratio is to further increase the air/fuel mixing rate in a manner which remains consistent with the above findings for the nozzle and piston geometry. The achievement of faster mixing at the nozzle exit is important and reduces the differences in the mean and rms characteristics resulting from the use of different nozzles. Non-dimensional parameters show a consistent effect to result for the jet density as in steady jets.

6. The autocorrelation function is very sensitive to the influences of engine variables and predicts characteristics of the air/fuel mixing process in the same manner as results with the measurement of mean and rms concentration. The additional information provided by the autocorrelations is on cyclic variance of the temporal characteristics and requires care in interpretation.

TABLE 5.1 Characteristics of the model engine (3.5 CR)

Speed rpm	200
Compression ratio	3.5
Bore mm	75.8
Stroke mm	94
Connecting rod length mm	363.5
Intake-exhaust valve	
Diameter mm	33
Seat angle degree	45^{o}
Valve lift (max) mm	8
Flat piston	
Diameter mm	75
Clearance at TDC mm (H)	36
Piston Bowl	
Diameter mm	49
Depth mm	23
Effective clearance at TDC mm (H) (nozzle to bottom of bowl)	59
Piston re-entrant (bowl-lip)	
Diameter mm	43
Depth mm	23
Lip thickness mm	8
Entry diameter mm	16.5
Effective clearance at TDC mm (H) (nozzle to bottom of the bowl)	59

TABLE 5.2 Characteristics of the model engine (6.7 CR)

Speed	200
Compression ratio	6.7
Bore, mm	75.8
Stroke, mm	94
Connecting rod length, mm	363.5
Intake-exhaust valve	
Diameter, mm	33
Seat angle, degree	45
Valve lift (max), mm	8
Flat piston	
Diameter, mm	75
Clearance at TDC, mm (H)	16

TABLE 5.3 Injection characteristics

Injection pressure MPa	0.55
Injection timing deg. BTDC	38
Injection during deg.	24

TABLE 5.4 Influence of nozzle geometry, piston geometry and induction swirl on mean flow

Nozzle	τ_j (us)	Piston	Swirl	k_1	x_o/r_o
A	196	Flat	No	0.120	- 9.49
A		Bowl-lip	No	0.179	- 1.16
A		Flat	Yes	0.591	+ 3.79
A		Bowl-lip	Yes	0.321	- 3.18
B	274	Flat	No	0.114	-12.79
B		Bowl-lip	No	0.221	- 0.55
C	26.6	Flat	No	0.049	-36.64
C		Bowl-lip	No	0.063	-26.34
C		Flat	Yes	0.114	-19.99
C		Bowl-lip	Yes	0.090	-17.78
D	7.9	Flat	No	0.041	-57.31
D		Bowl-lip	No	0.025	-129.30

Note: τ_j is the time constant as defined in Chapter 4, $\tau_j = r_o/u_o$, which for a given nozzle in the present investigations is a constant

TABLE 5.5 Influence of nozzle geometry, piston geometry and induction swirl on jet spread

Nozzle	Flat Piston		Bowl-lip Piston	
	x(mm)	$r_{1/2}/r_o$	x(mm)	$r_{1/2}/r_o$
I Absence of Swirl				
A	5	0.822		
	8	1.352	8	0.793
	10	1.730		
	15	2.116	15	1.882
	27	3.440	22	2.940
B	5	0.894	5	0.578
			10	0.920
	15	2.070	15	1.578
C	5	1.3	5	1.9
	10	3.2	10	4.3
	15	3.7	15	5.1
D	8	4.2	8	5.0
	12	5.4	12	7.6
II Presence of Swirl				
A	8	1.704	8	2.852
C	-	-	5	5.3

TABLE 5.6 Influence of nozzle geometry, piston geometry and Compression ratio on jet spread (absence of swirl

Nozzle	Flat Piston		Re-entrant Piston	
	x(mm)	$r_{1/2}/r_o$	x(mm)	$r_{1/2}/r_o$
I 3.5 CR				
A			5	1.617
	8	1.382	8	1.675
			12	1.823
			22	3.029
II 6.7 CR				
A	5	2.617	5	1.50
	8	3.235		
C	5	2.50	5	2.30
	8	3.40		

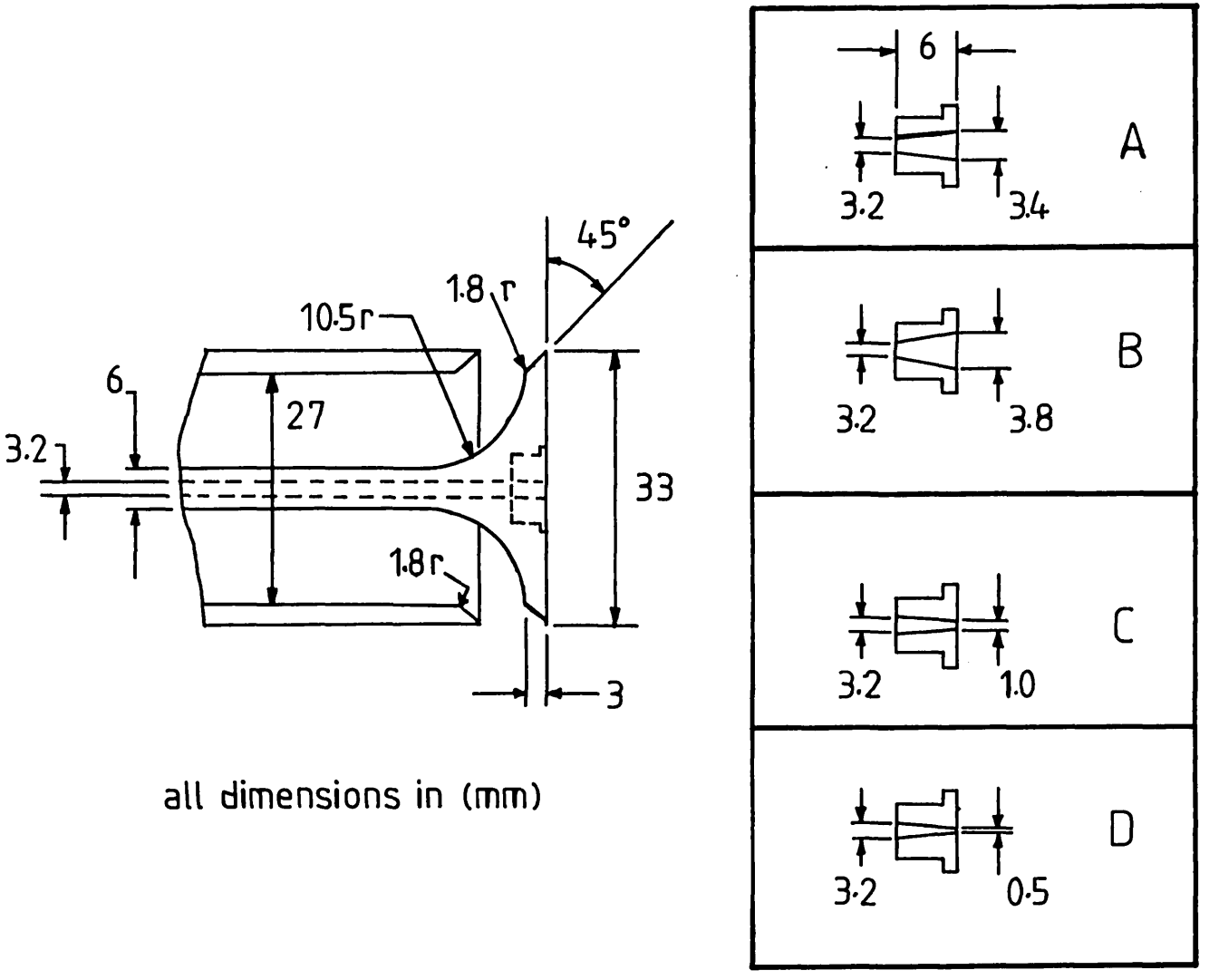


FIGURE 5.1 NOZZLE GEOMETRIES

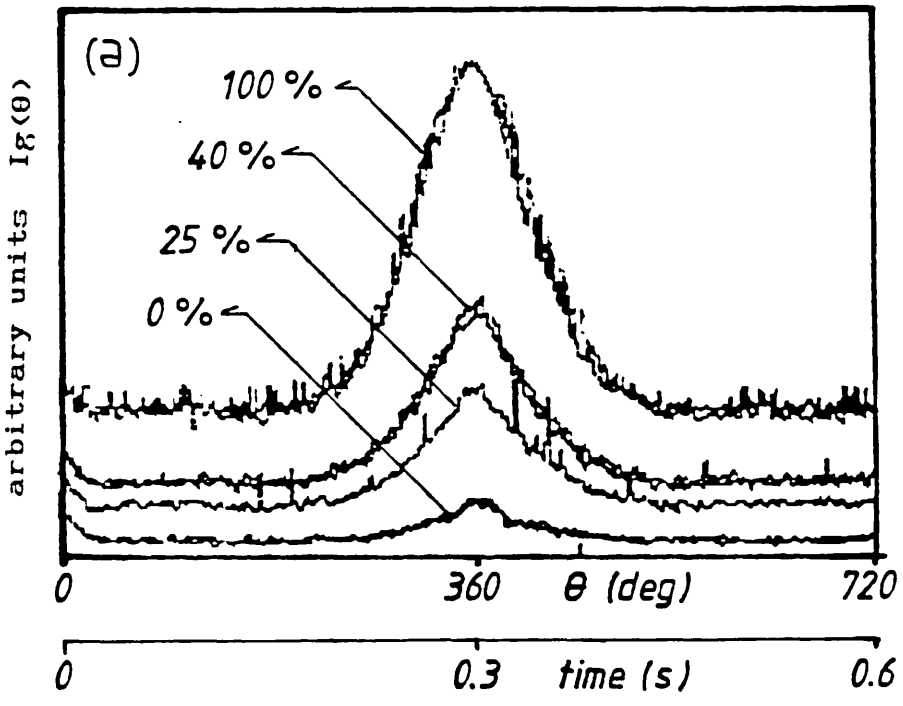
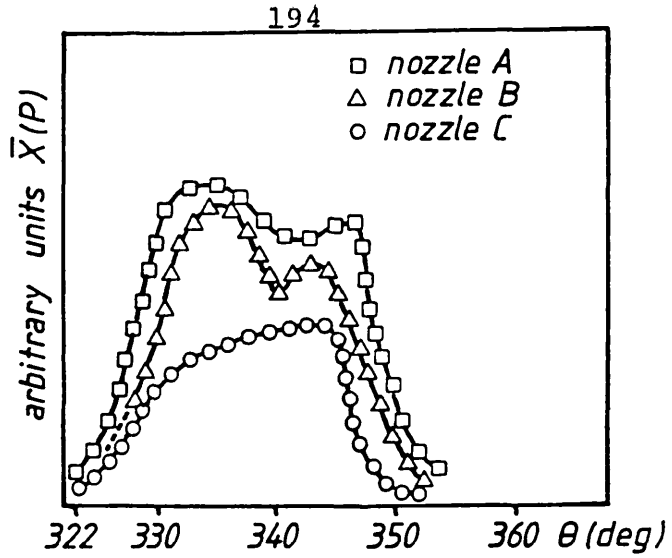


FIGURE 5.2 IN-CYLINDER CALIBRATION OF LRS SIGNALS FOR VARIABLE COMPOSITIONS OF FREON-12 PERCENT IN AIR: COMPRESSION RATIO 3.5



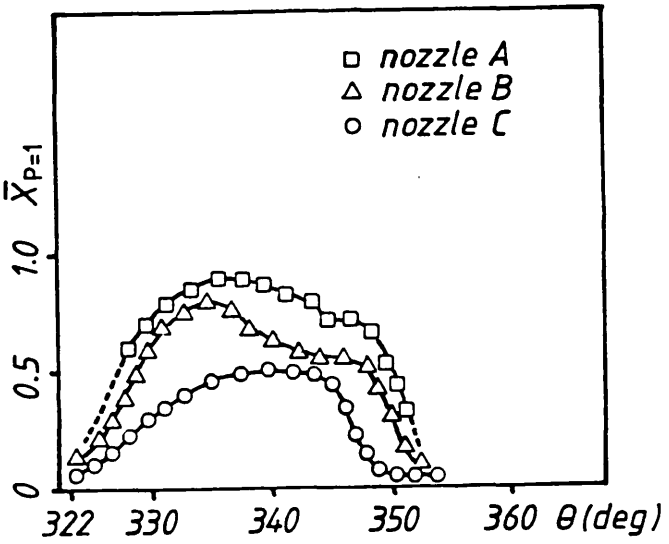


FIGURE 5.3 TIME-AVERAGED CONCENTRATION OF IN-CYCLE FUEL INJECTION AT EXIT PLANE OF DIFFERENT NOZZLES (a) SIGNALS INFLUENCED BY PRESSURE (b) CORRECTED FOR PRESSURE INFLUENCE

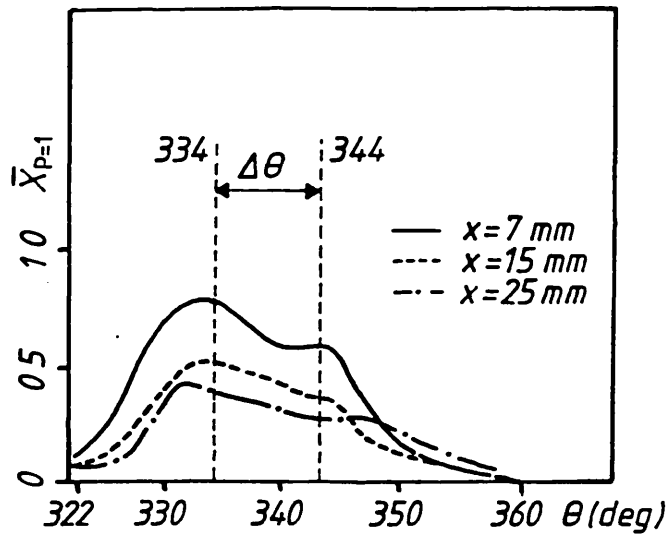
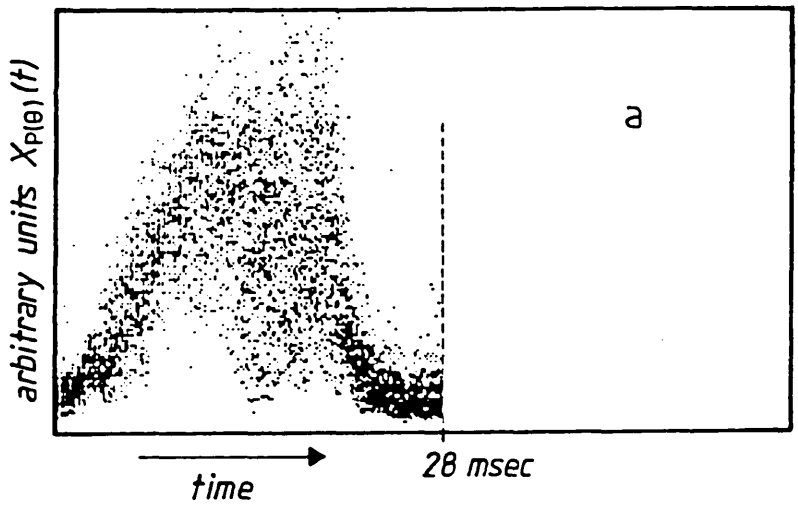


FIGURE 5.4 TIME-AVERAGED CONCENTRATION OF IN-CYCLE FUEL INJECTION AS A FUNCTION OF DISTANCE FROM THE NOZZLE ALONG THE CENTRELINE: NOZZLE A, FLAT PISTON



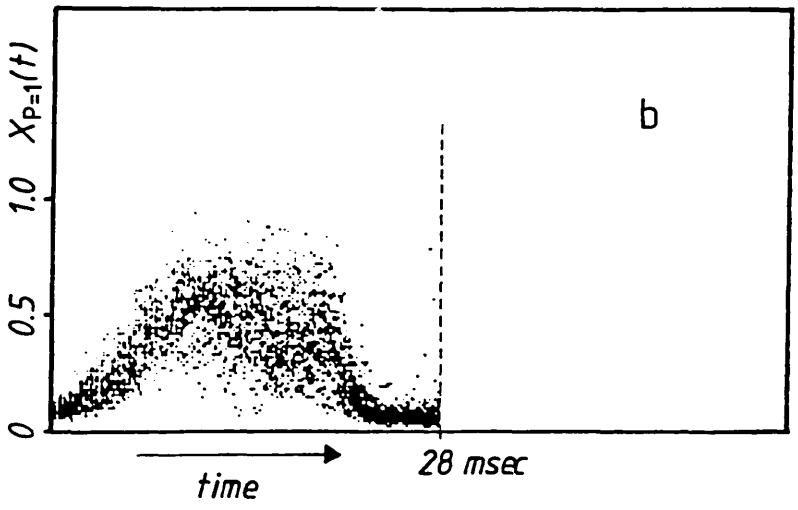


FIGURE 5.5 INSTANTANEOUS FREON-12 CONCENTRATION AT x/d=2.47 (x=8mm): NOZZLE A, FLAT PISTON (a) SIGNALS INFLUENCED BY PRESSURE (b) CORRECTED FOR PRESSURE INFLUENCE

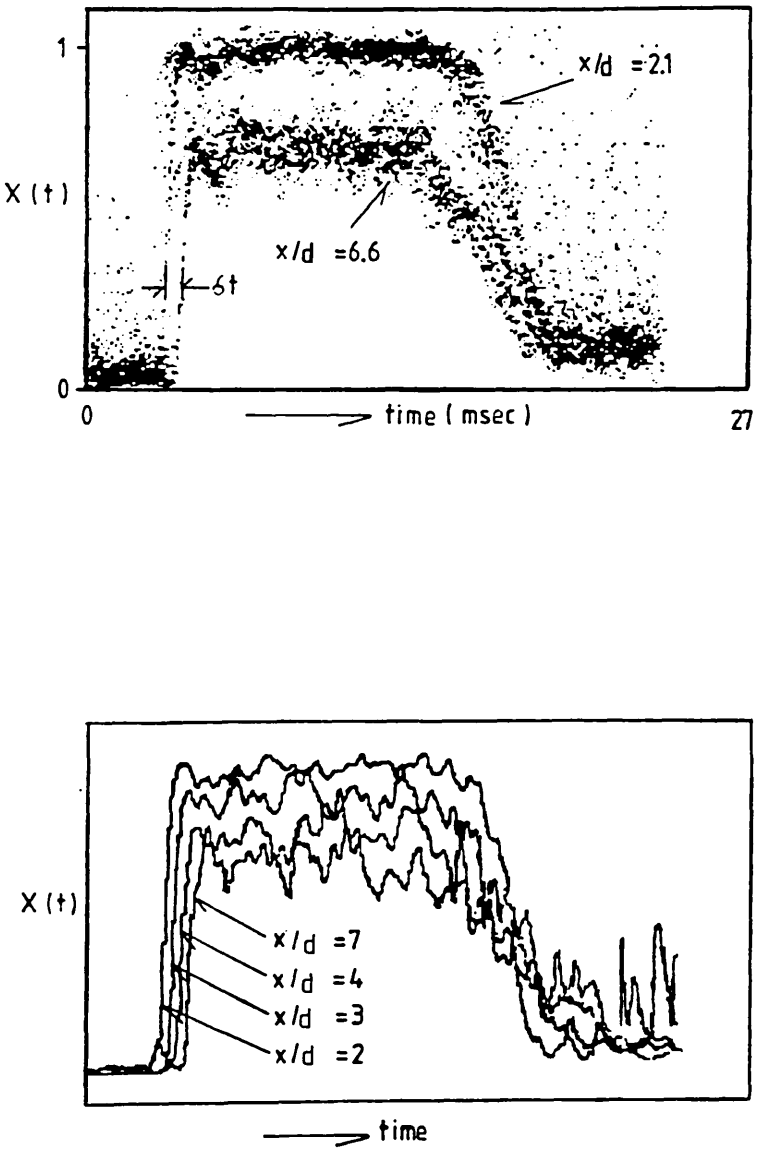


FIGURE 5.6 INSTANTANEOUS FREON CONCENTRATION (in the absence of compression) AS A FUNCTION OF DISTANCE FROM THE NOZZLE ALONG THE CENTRELINE: NOZZLE A, FLAT PISTON

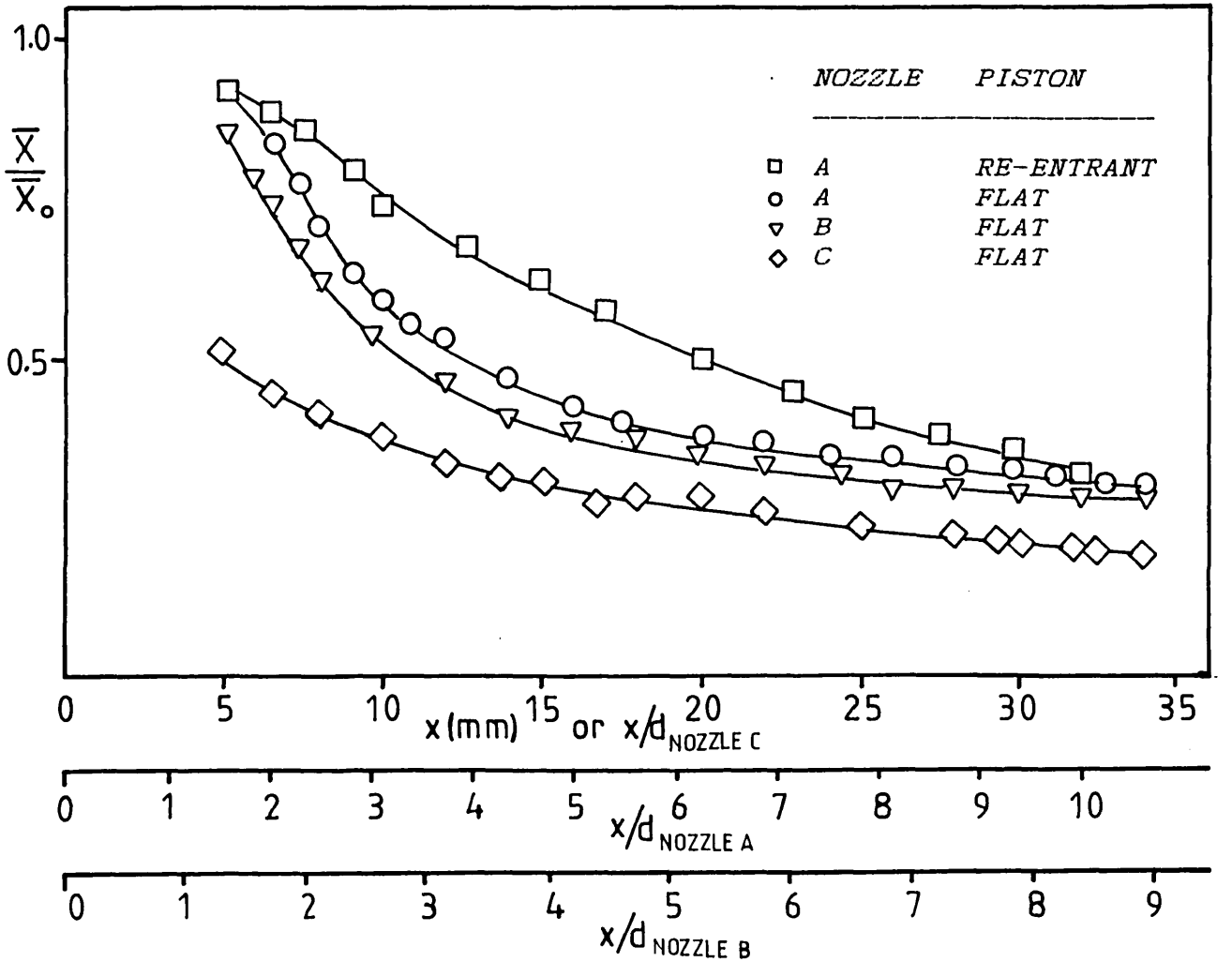


FIGURE 5.7(a) CENTRELINE DISTRIBUTIONS OF MEAN CONCENTRATION AS INFLUENCED BY PISTON AND NOZZLE GEOMETRY (absence of swirl)

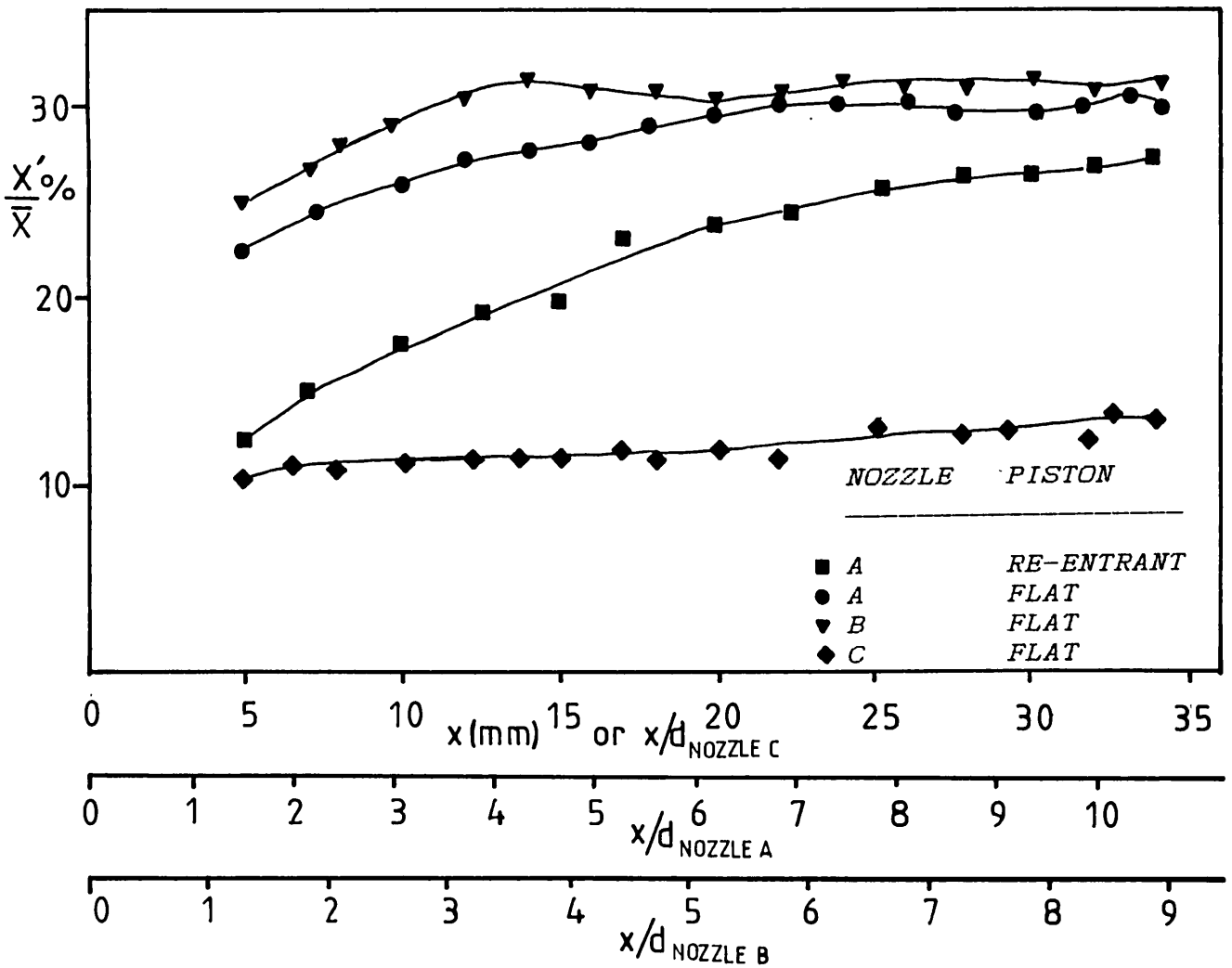


FIGURE 5.7(b) CENTRELINE DISTRIBUTIONS OF RMS CONCENTRATION AS INFLUENCED BY PISTON AND NOZZLE GEOMETRY (absence of swirl)

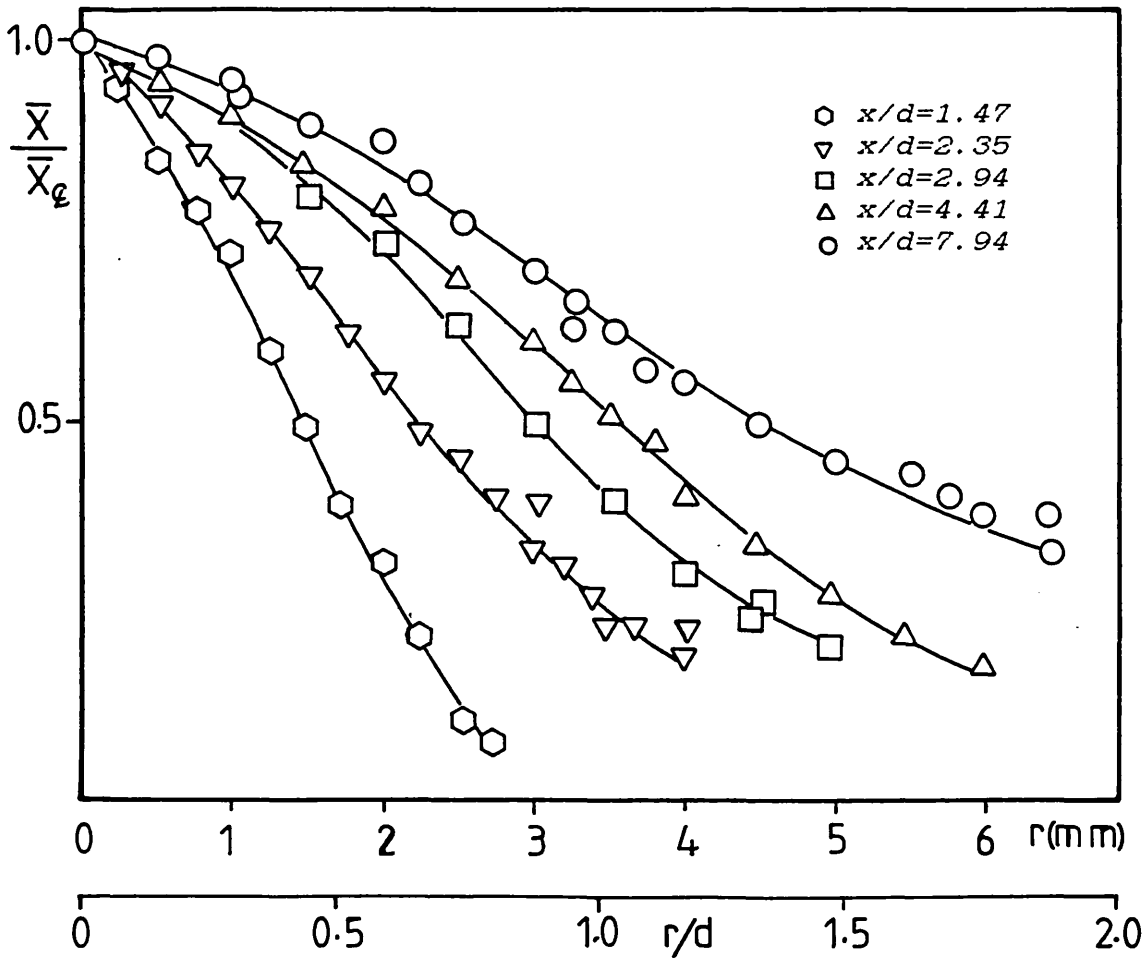


FIGURE 5.8(a) RADIAL DISTRIBUTIONS OF MEAN CONCENTRATION: NOZZLE A, FLAT PISTON (absence of swirl)

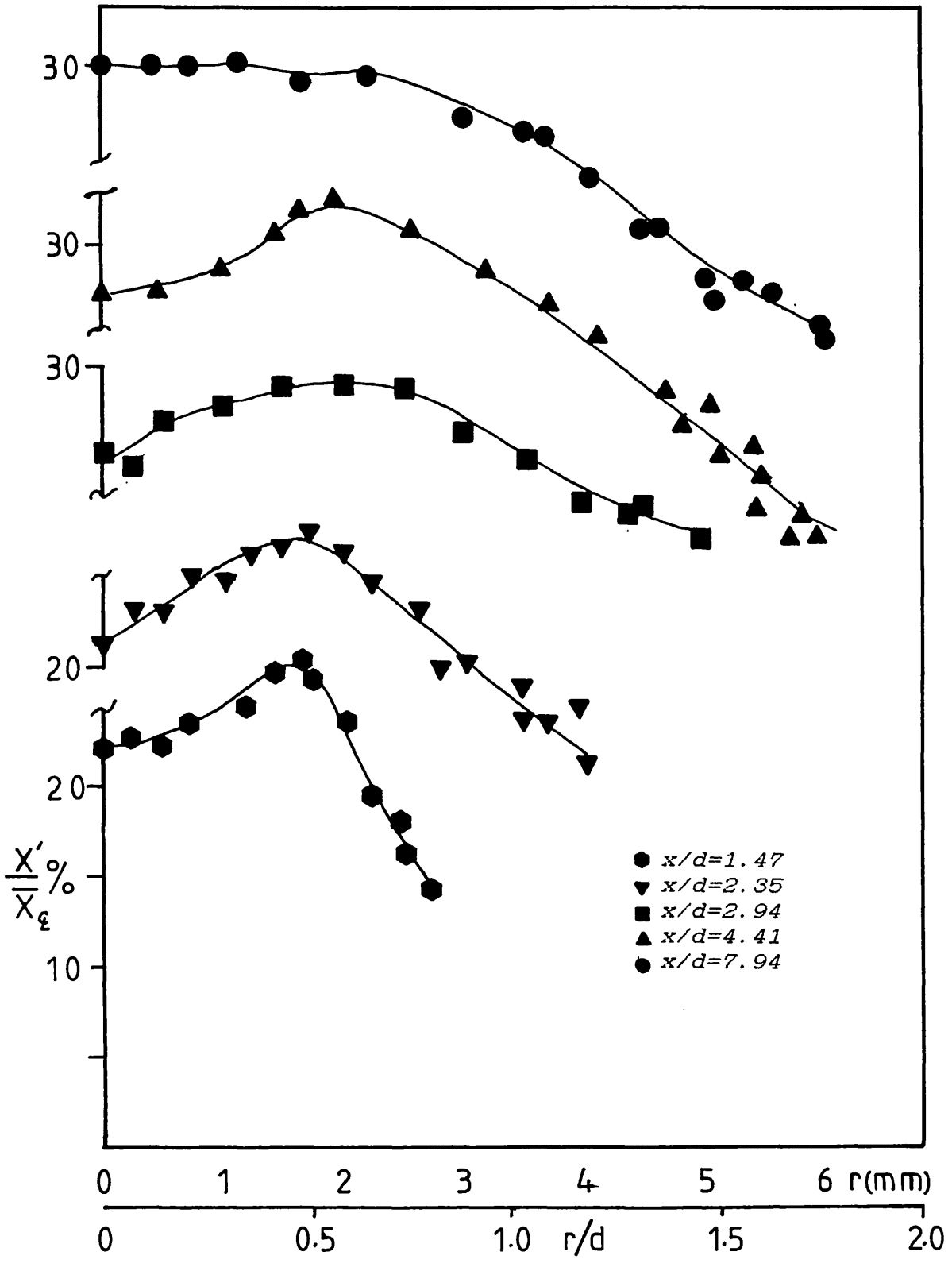


FIGURE 5.8(b) RADIAL DISTRIBUTIONS OF RMS CONCENTRATION: NOZZLE A, FLAT PISTON (absence of swirl)

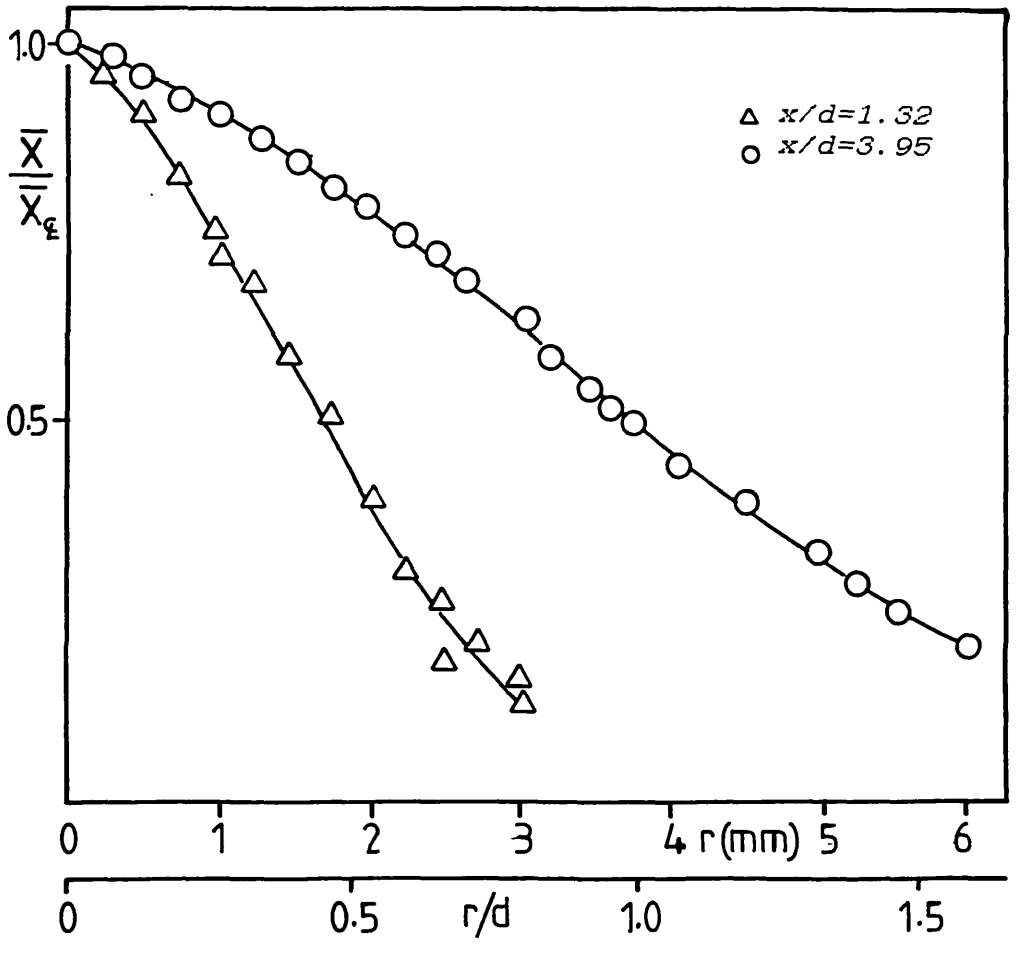


FIGURE 5.9(a) RADIAL DISTRIBUTIONS OF MEAN CONCENTRATION: NOZZLE B, FLAT PISTON (absence of swirl)

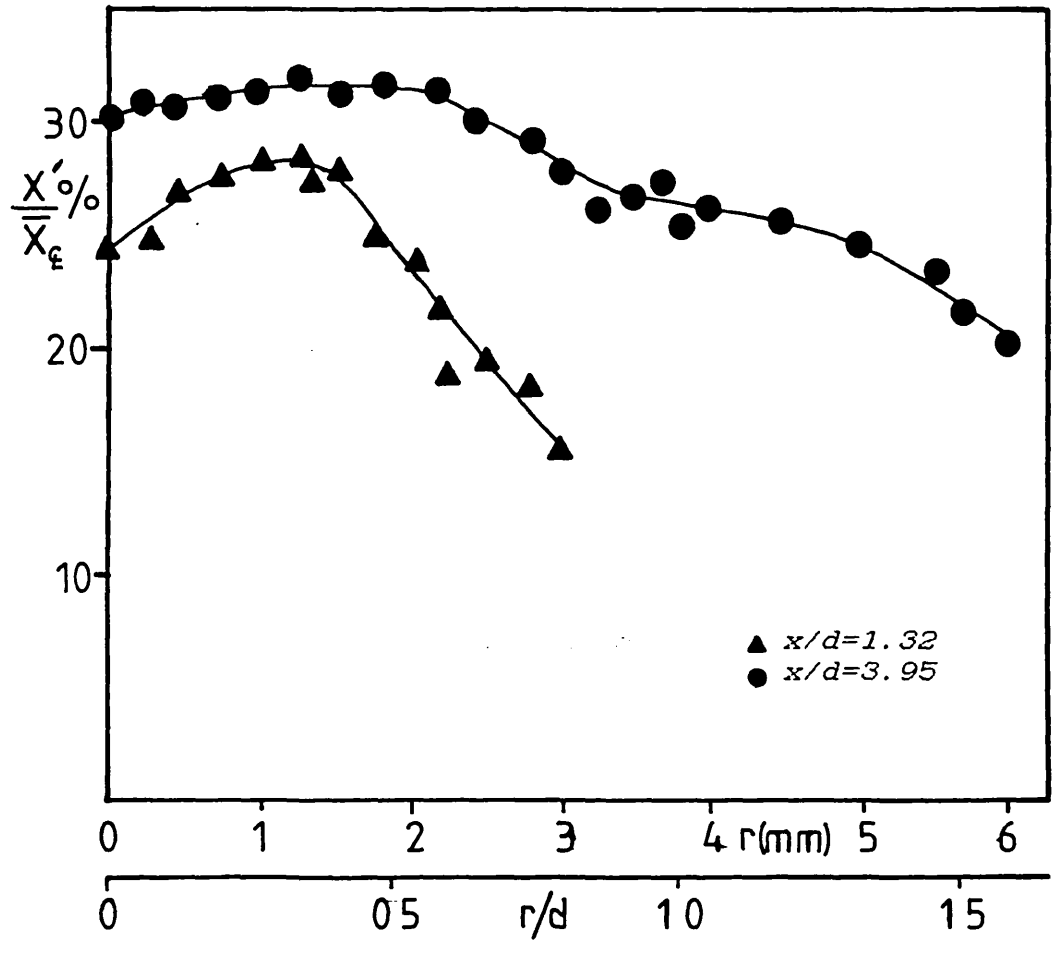


FIGURE 5.9(b) RADIAL DISTRIBUTIONS OF RMS CONCENTRATION: NOZZLE B, FLAT PISTON (absence of swirl)

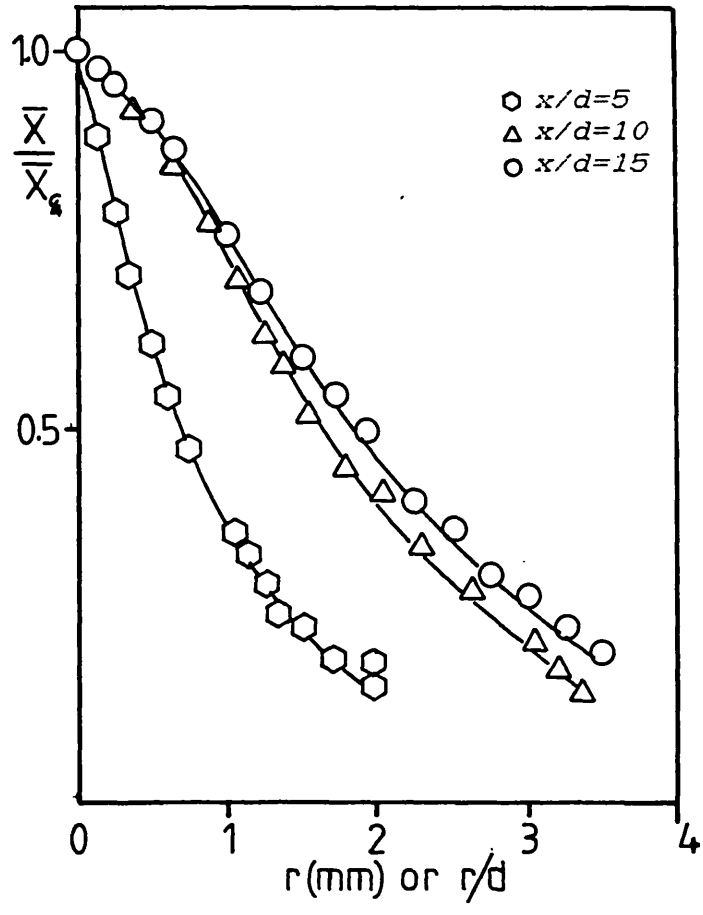


FIGURE 5.10(a) RADIAL DISTRIBUTIONS OF MEAN CONCENTRATION: NOZZLE C, FLAT PISTON (absence of swirl)

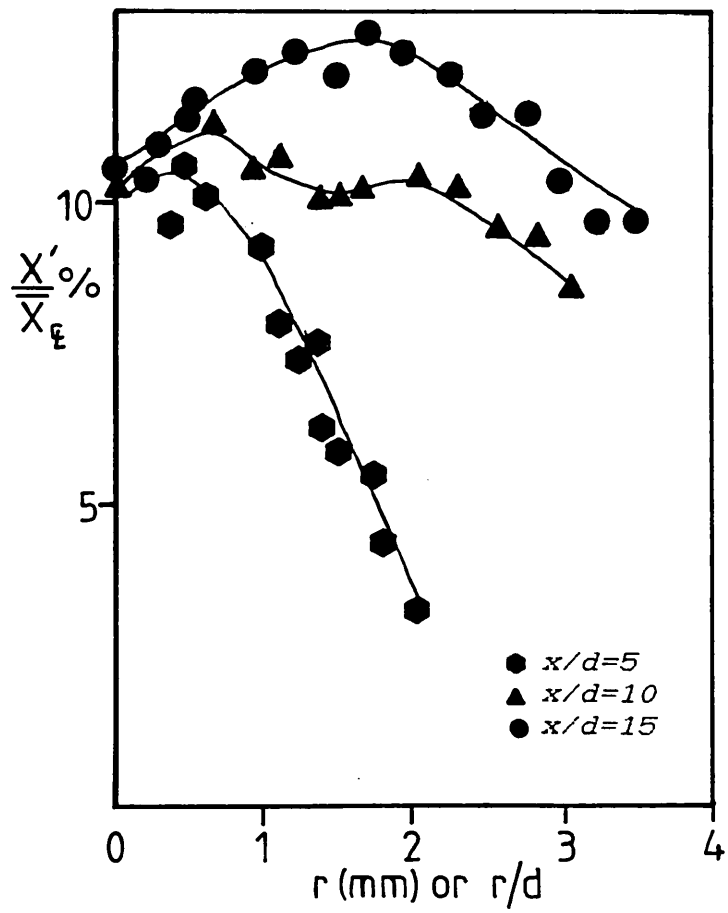


FIGURE 5.10(b) RADIAL DISTRIBUTIONS OF RMS CONCENTRATION: NOZZLE C, FLAT PISTON (absence of swirl)

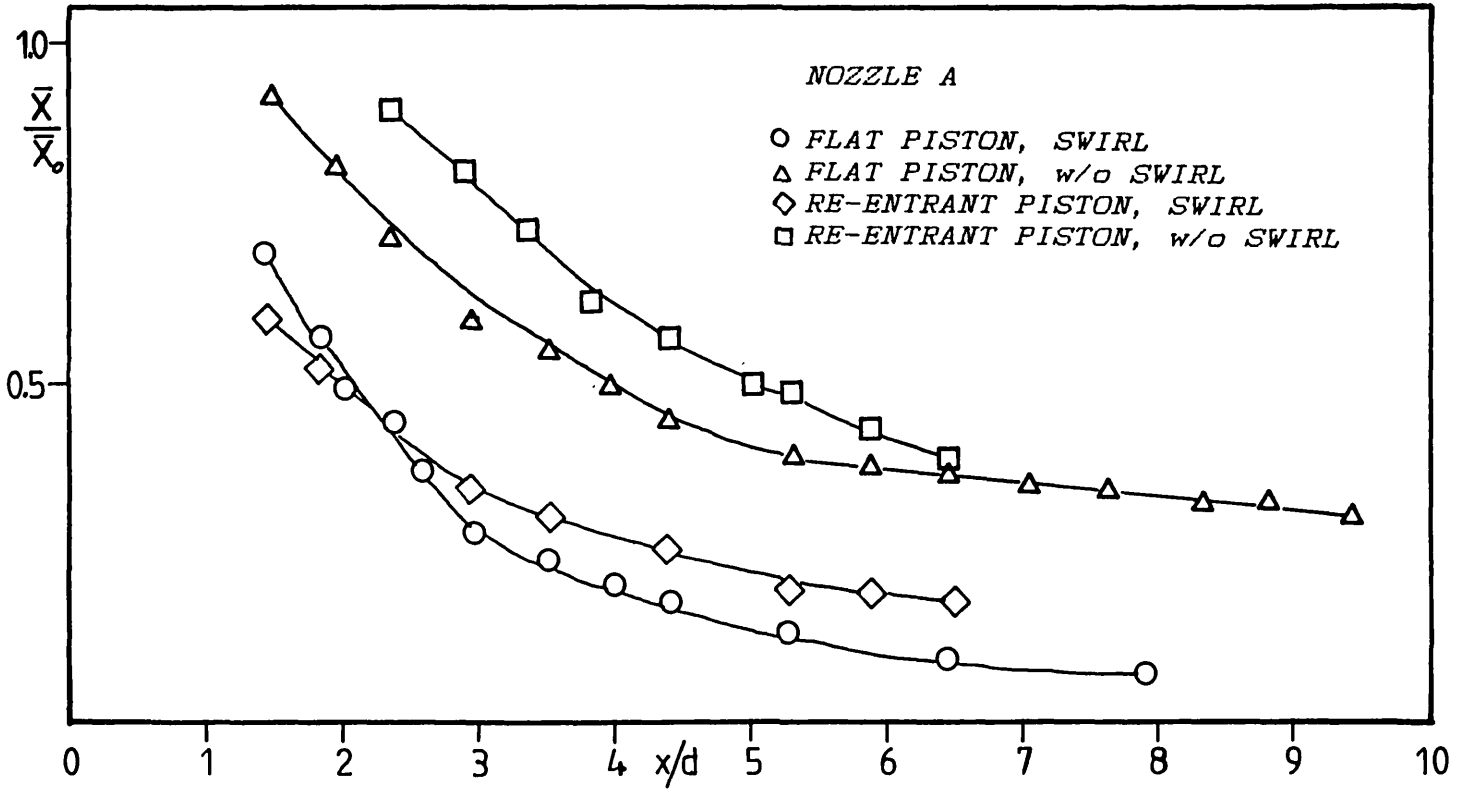


FIGURE 5.11(a) CENTRELINE DISTRIBUTIONS OF MEAN CONCENTRATION AS INFLUENCED BY PISTON GEOMETRY AND INDUCTION SWIRL: NOZZLE A

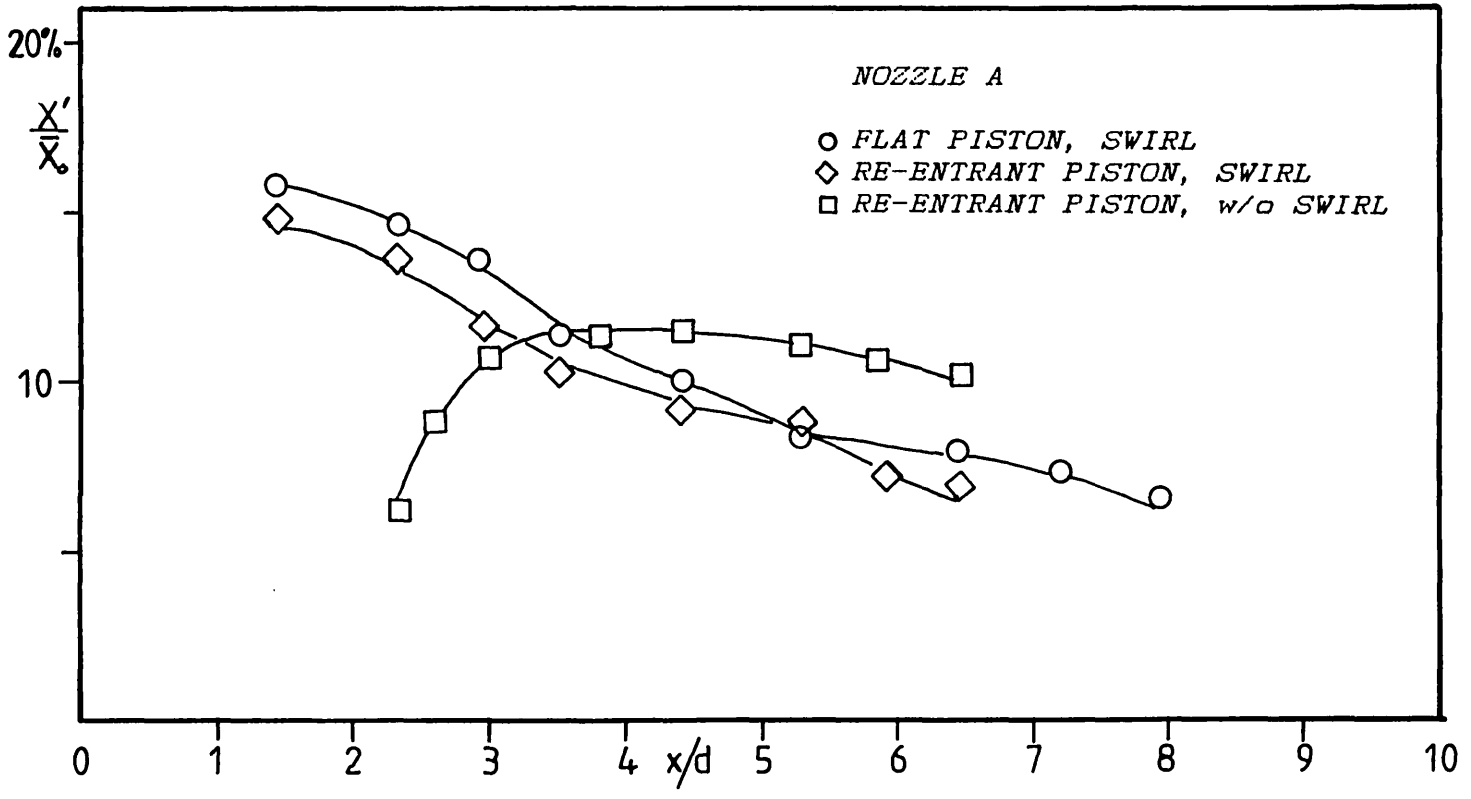


FIGURE 5.11(b) CENTRELINE DISTRIBUTIONS OF RMS CONCENTRATION AS INFLUENCED BY PISTON GEOMETRY AND INDUCTION SWIRL: NOZZLE A

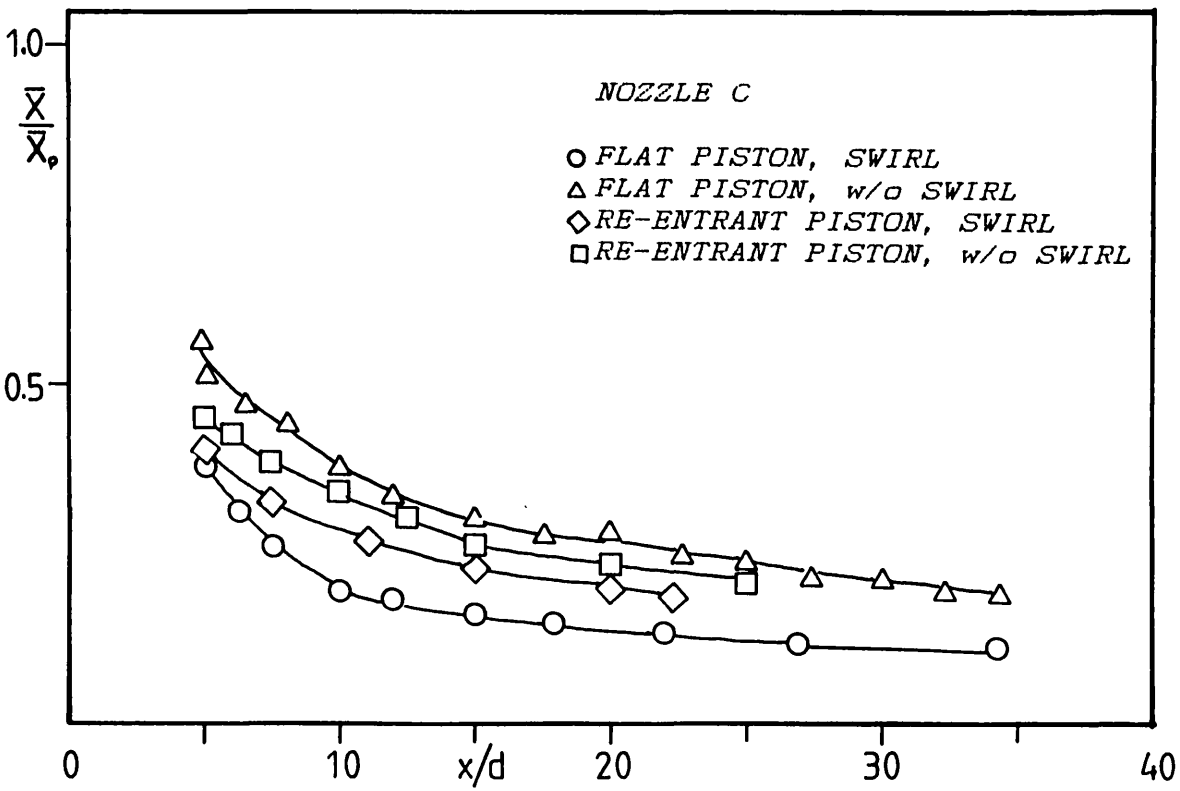


FIGURE 5.12(a) CENTRELINE DISTRIBUTIONS OF MEAN CONCENTRATION AS INFLUENCED BY PISTON GEOMETRY AND INDUCTION SWIRL: NOZZLE C

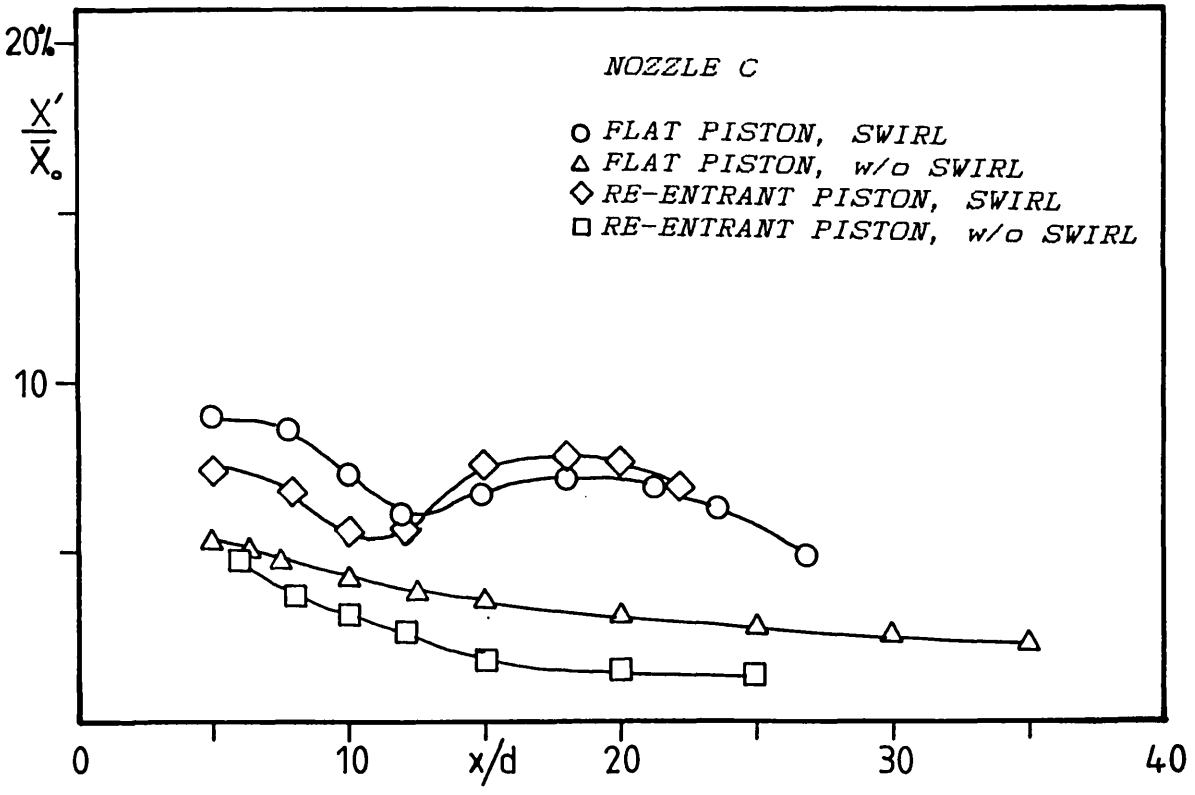


FIGURE 5.12(b) CENTRELINE DISTRIBUTIONS OF RMS CONCENTRATION AS INFLUENCED BY PISTON GEOMETRY AND INDUCTION SWIRL: NOZZLE C

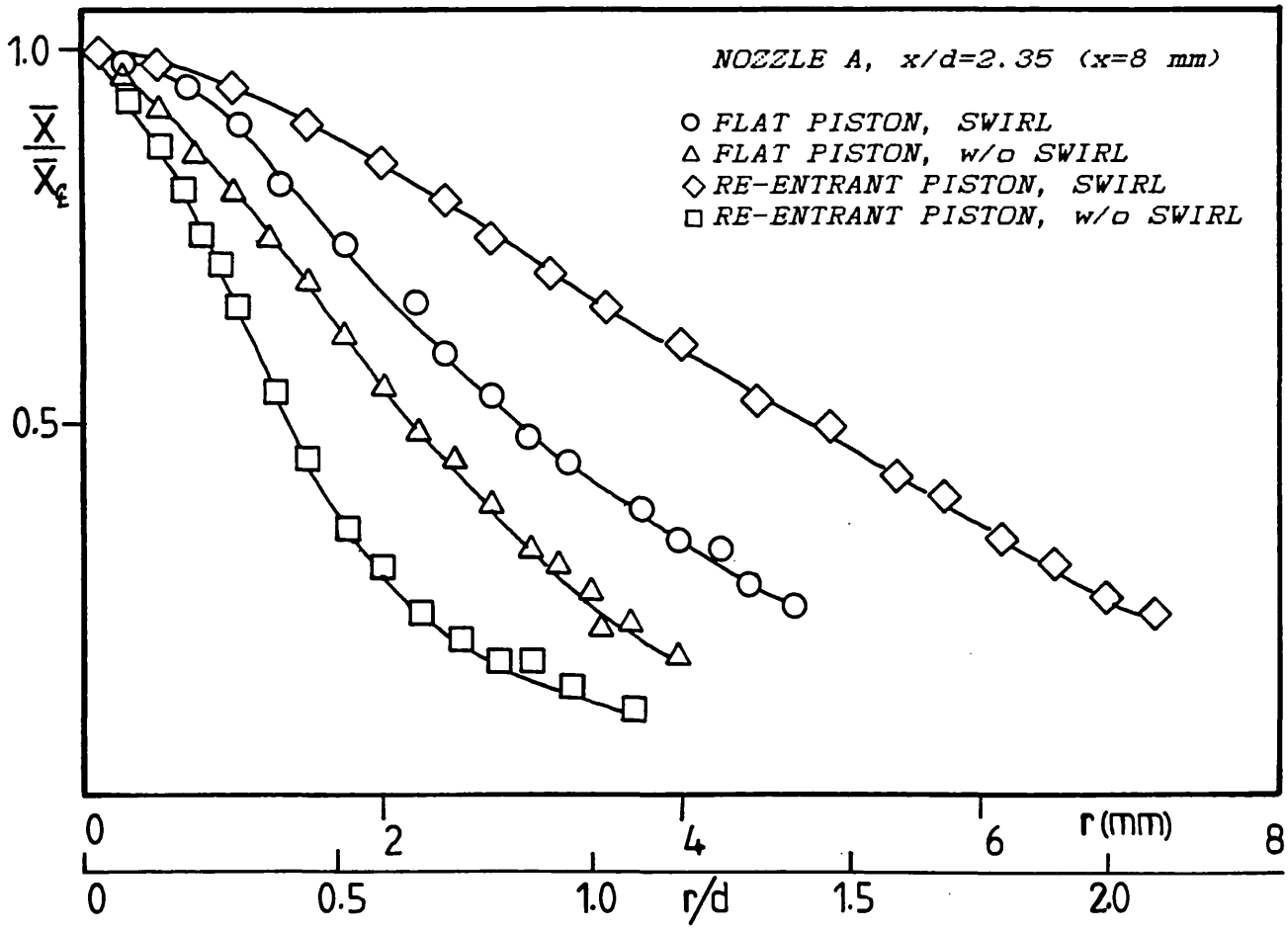


FIGURE 5.13(a) RADIAL DISTRIBUTIONS OF MEAN CONCENTRATION AS INFLUENCED BY PISTON GEOMETRY AND INDUCTION SWIRL: NOZZLE A

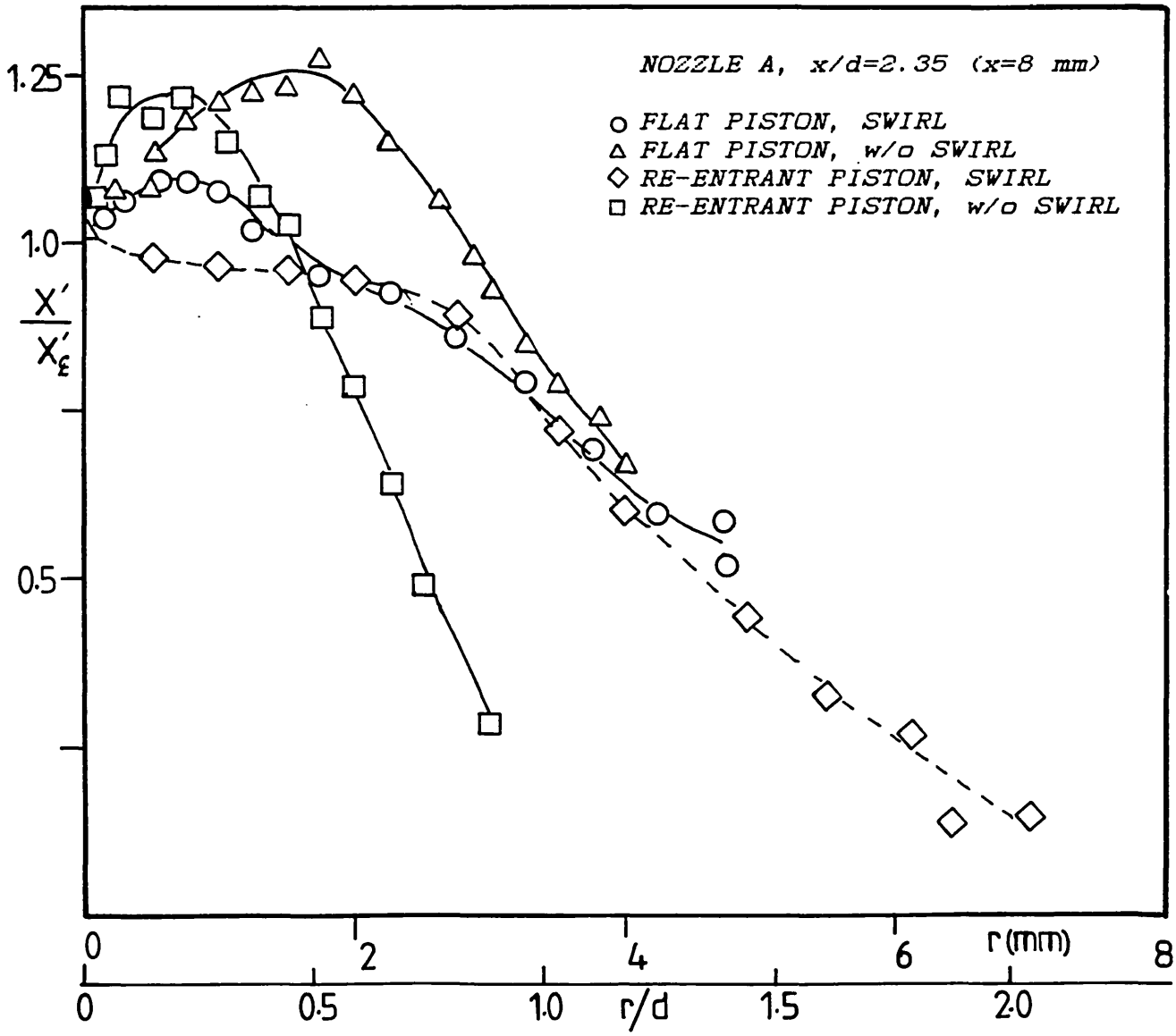
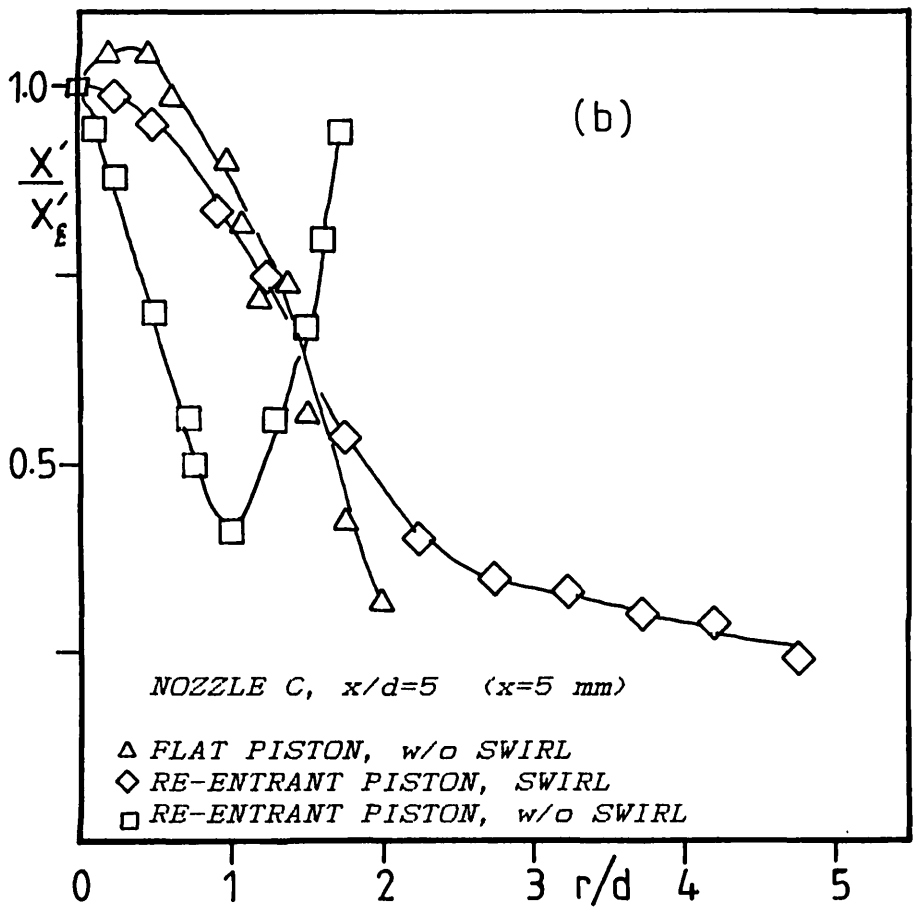


FIGURE 5.13(b) RADIAL DISTRIBUTIONS OF RMS CONCENTRATION AS INFLUENCED BY PISTON GEOMETRY AND INDUCTION SWIRL: NOZZLE A



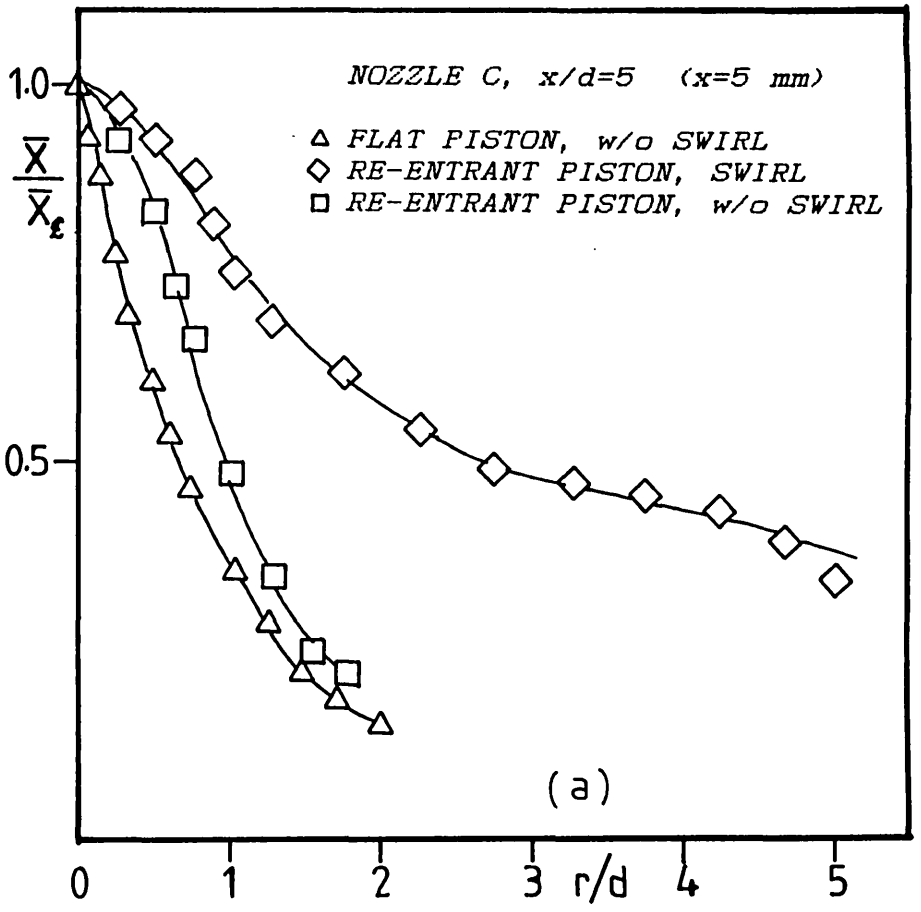


FIGURE 5.14 RADIAL DISTRIBUTIONS OF (a) MEAN and (b) RMS CONCENTRATION, AS INFLUENCED BY PISTON GEOMETRY AND INDUCTION SWIRL: NOZZLE C

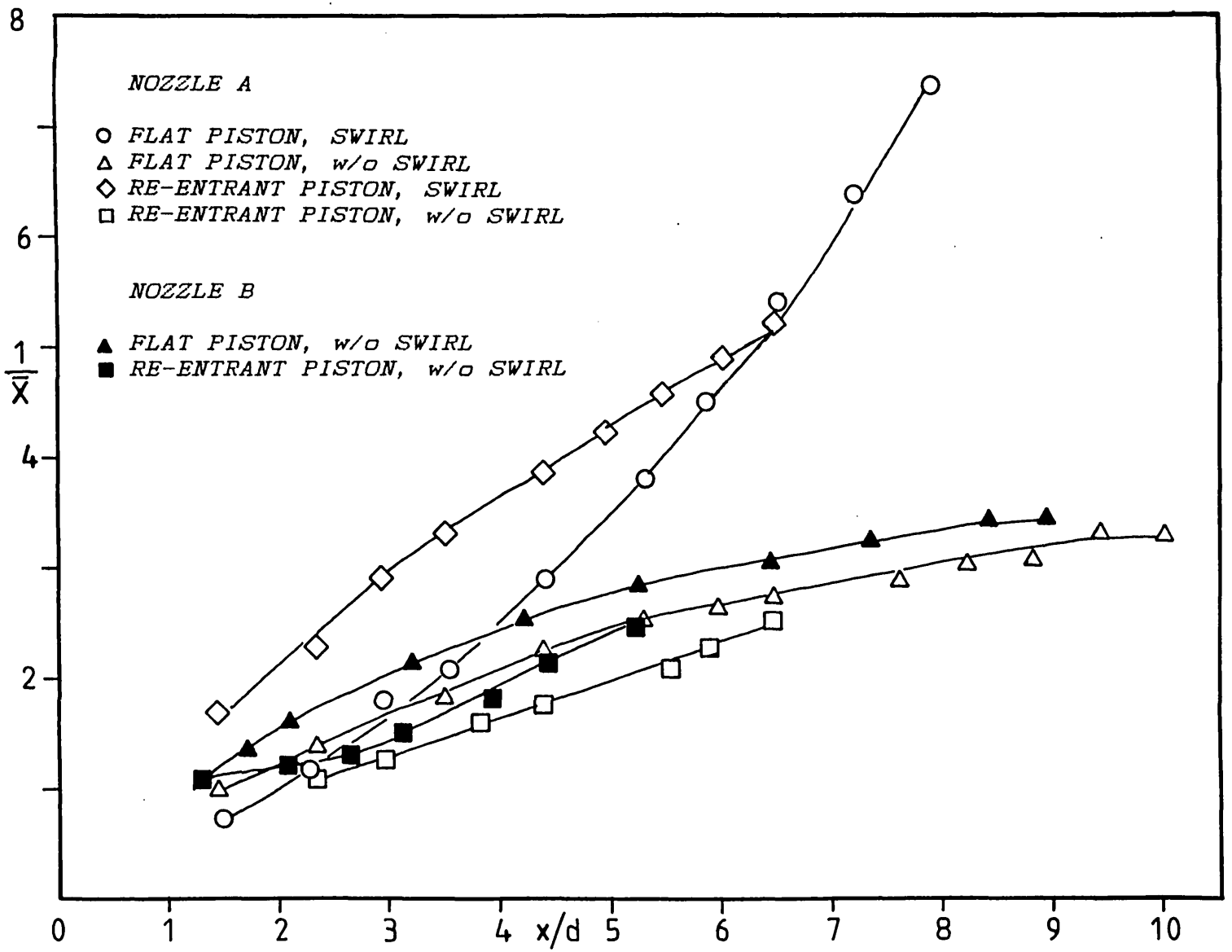


FIGURE 5.15(a) GROWTH RATES OF FUEL JETS AS INFLUENCED BY NOZZLE AND PISTON GEOMETRY AND INDUCTION SWIRL: NOZZLES A & B

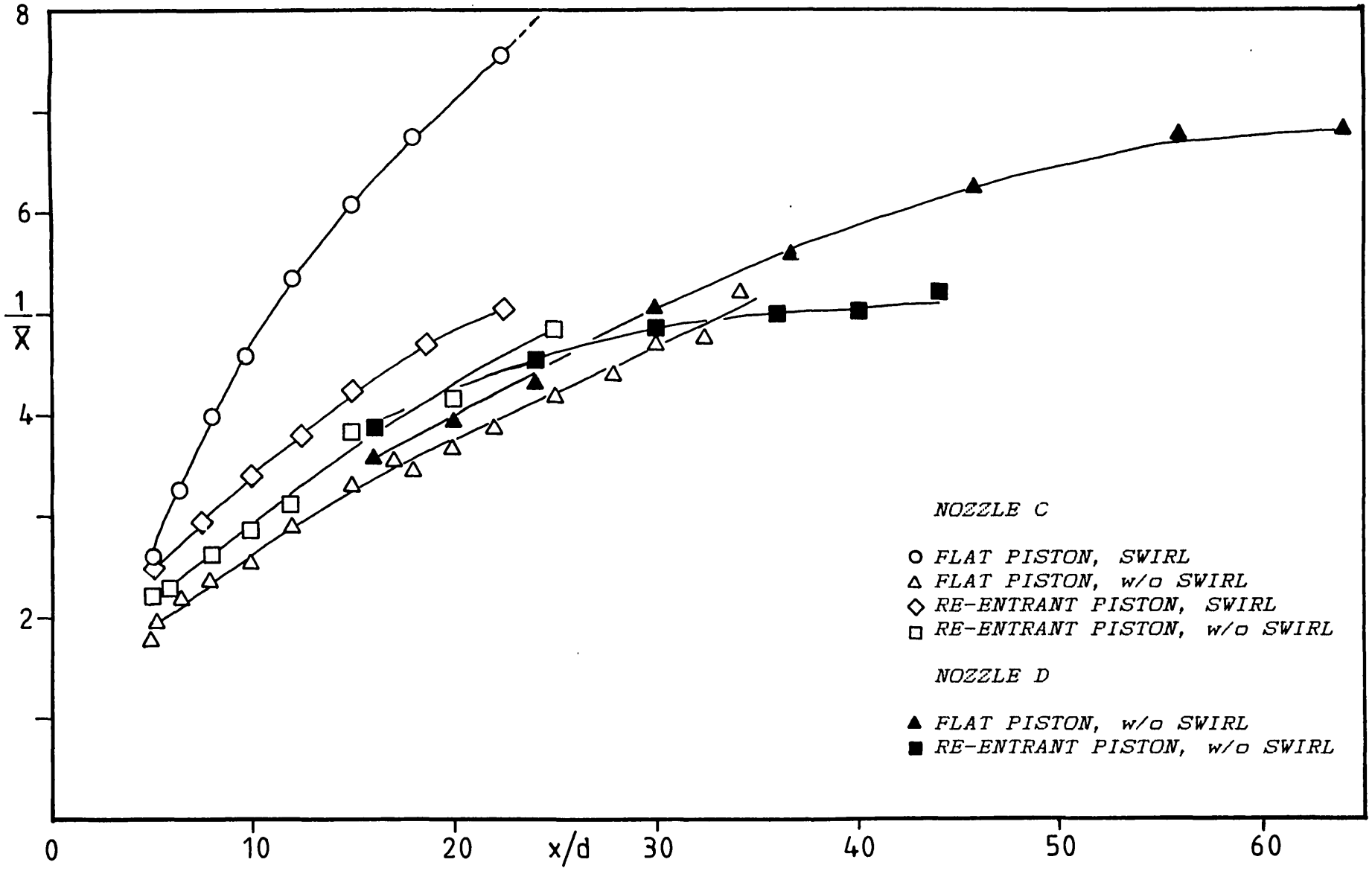


FIGURE 5.15(b) GROWTH RATES OF FUEL JETS AS INFLUENCED BY NOZZLE AND PISTON GEOMETRY AND INDUCTION SWIRL: NOZZLES C & D

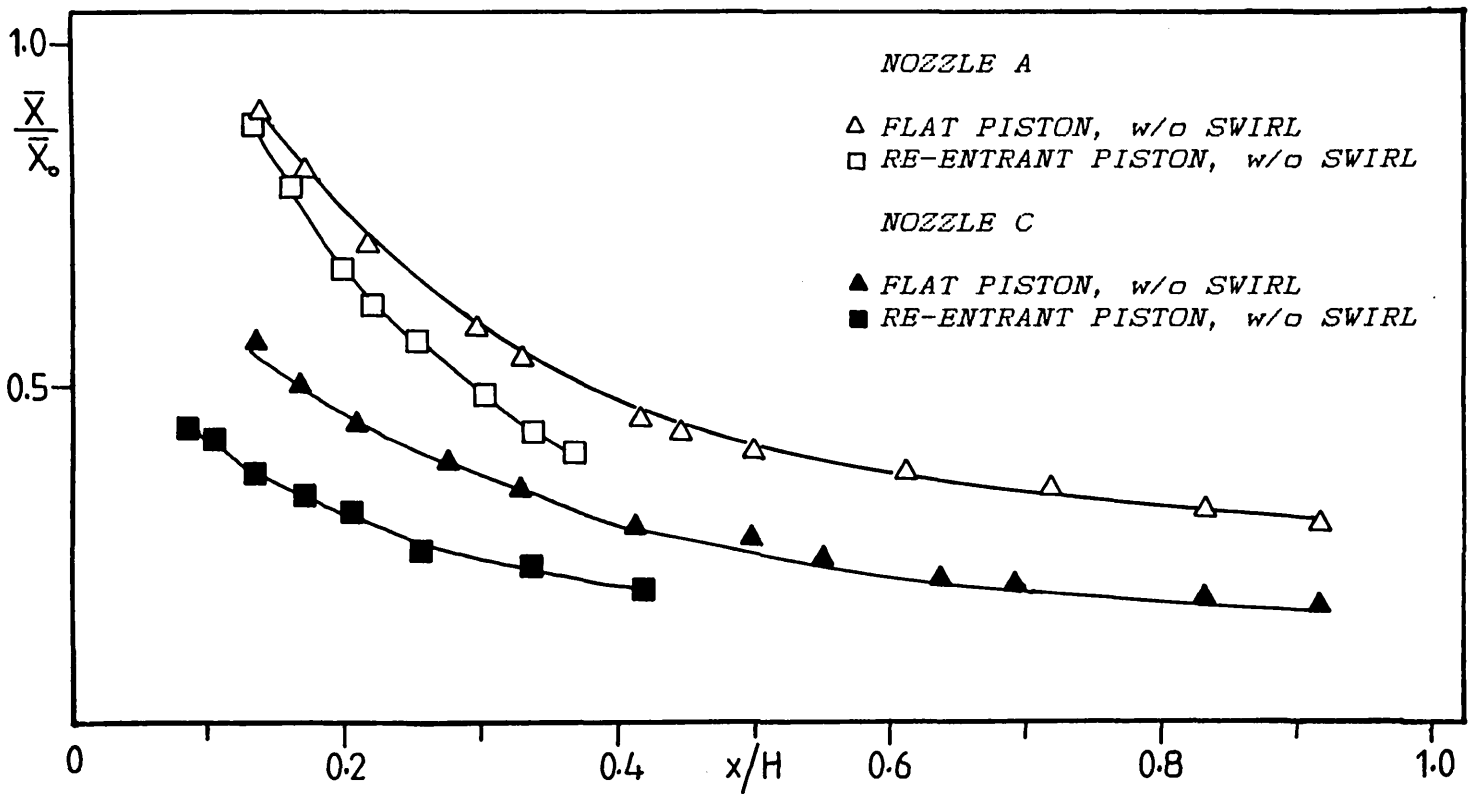


FIGURE 5.16 CENTRELINE DISTRIBUTIONS OF MEAN CONCENTRATION WITH NOZZLES A and C AGAINST x/H AS THE AXIAL CO-ORDINATE

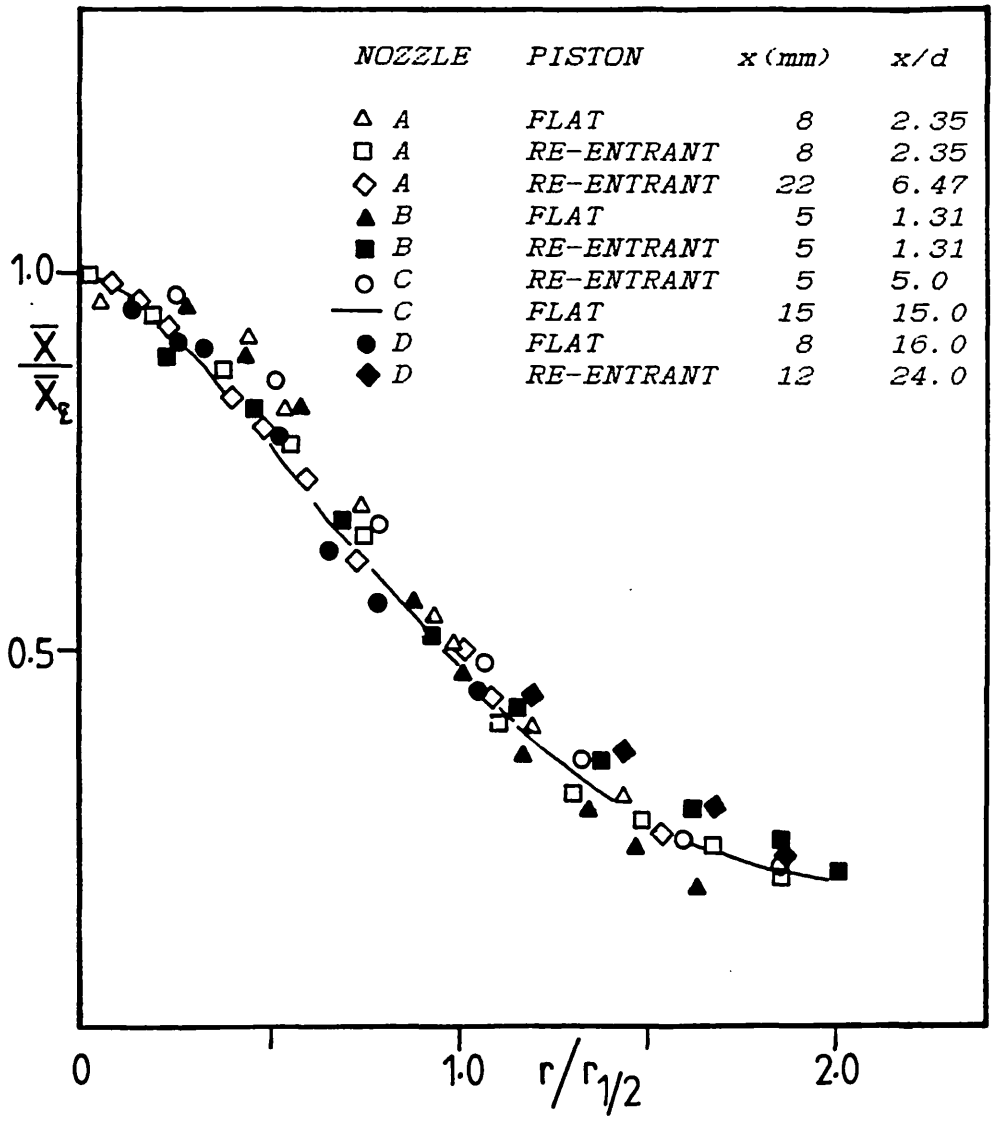


FIGURE 5.17 SELF-SIMILAR PROFILES OF THE RADIAL DISTRIBUTIONS OF MEAN CONCENTRATION WITH NOZZLES A, B, C and D

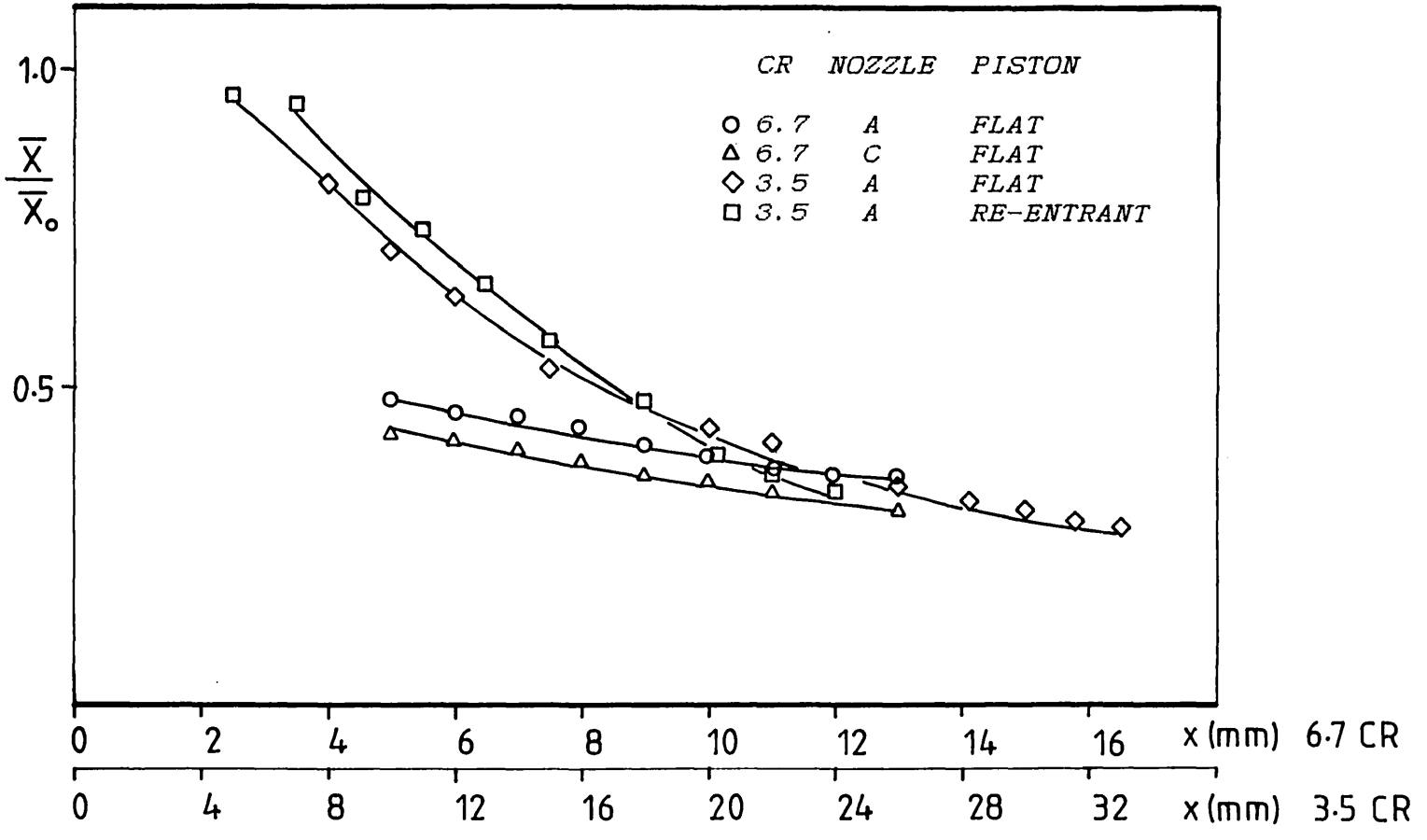


FIGURE 5.18 (a) CENTRELINE DISTRIBUTIONS OF MEAN CONCENTRATION AS INFLUENCED BY GEOMETRY AND COMPRESSION RATIO (absence of swirl)

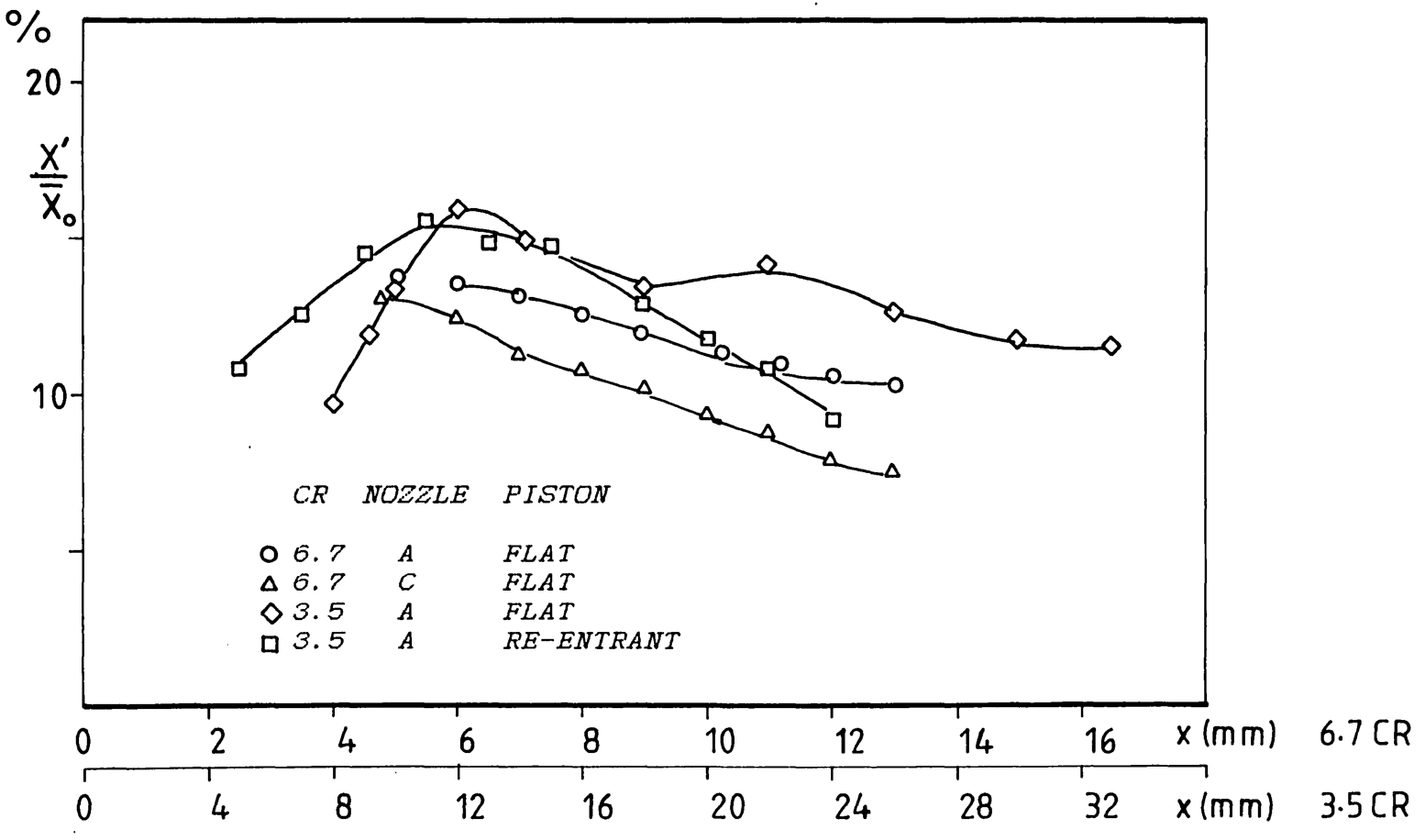


FIGURE 5.18(b) CENTRELINE DISTRIBUTIONS OF RMS CONCENTRATION AS INFLUENCED BY GEOMETRY AND COMPRESSION RATIO (absence of swirl)

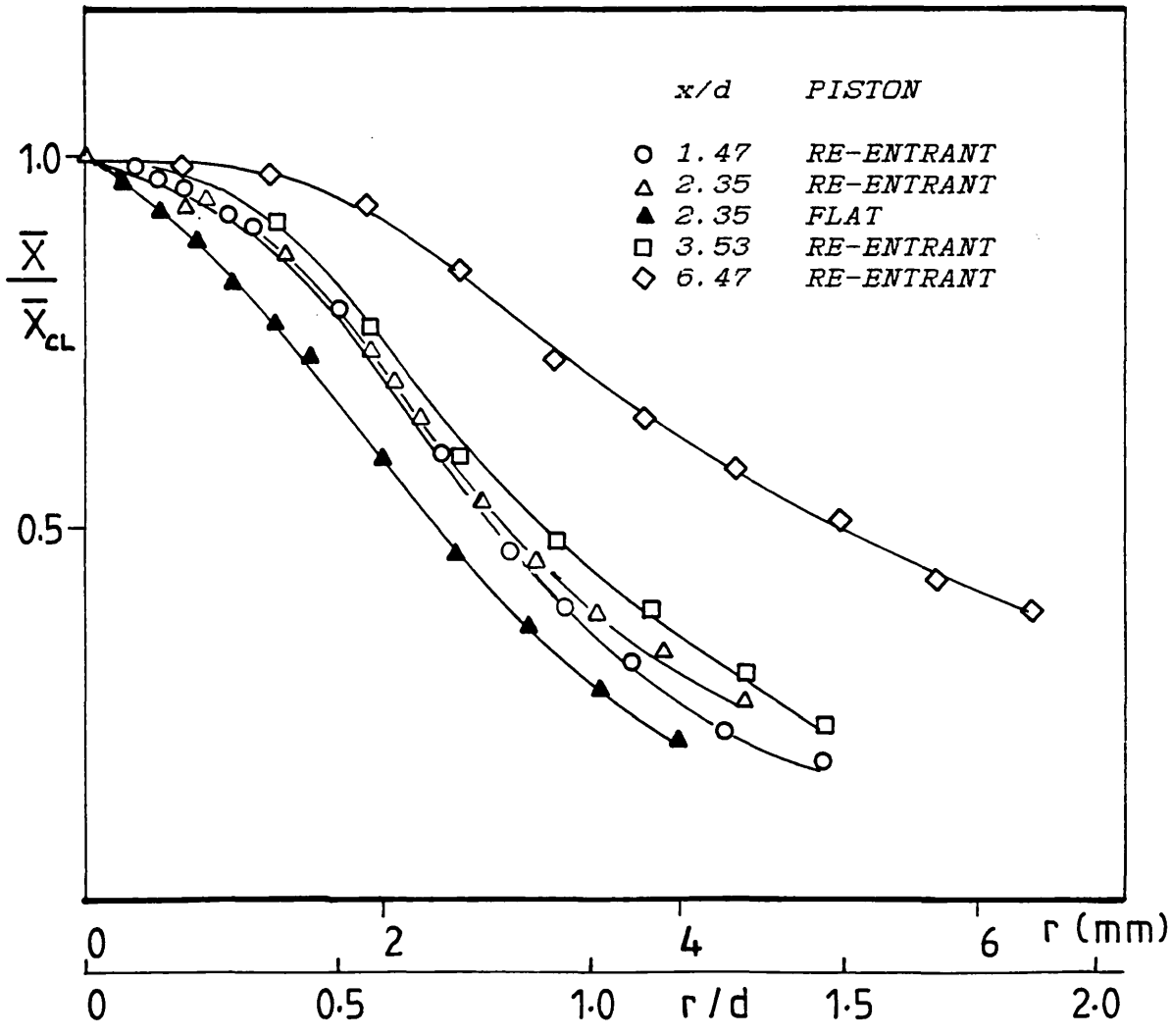


FIGURE 5.19(a) RADIAL DISTRIBUTIONS OF MEAN CONCENTRATION AS INFLUENCED BY PISTON GEOMETRY FOR COMPRESSION RATIO 3.5 WITH NOZZLE A AND SF_6 (absence of swirl)

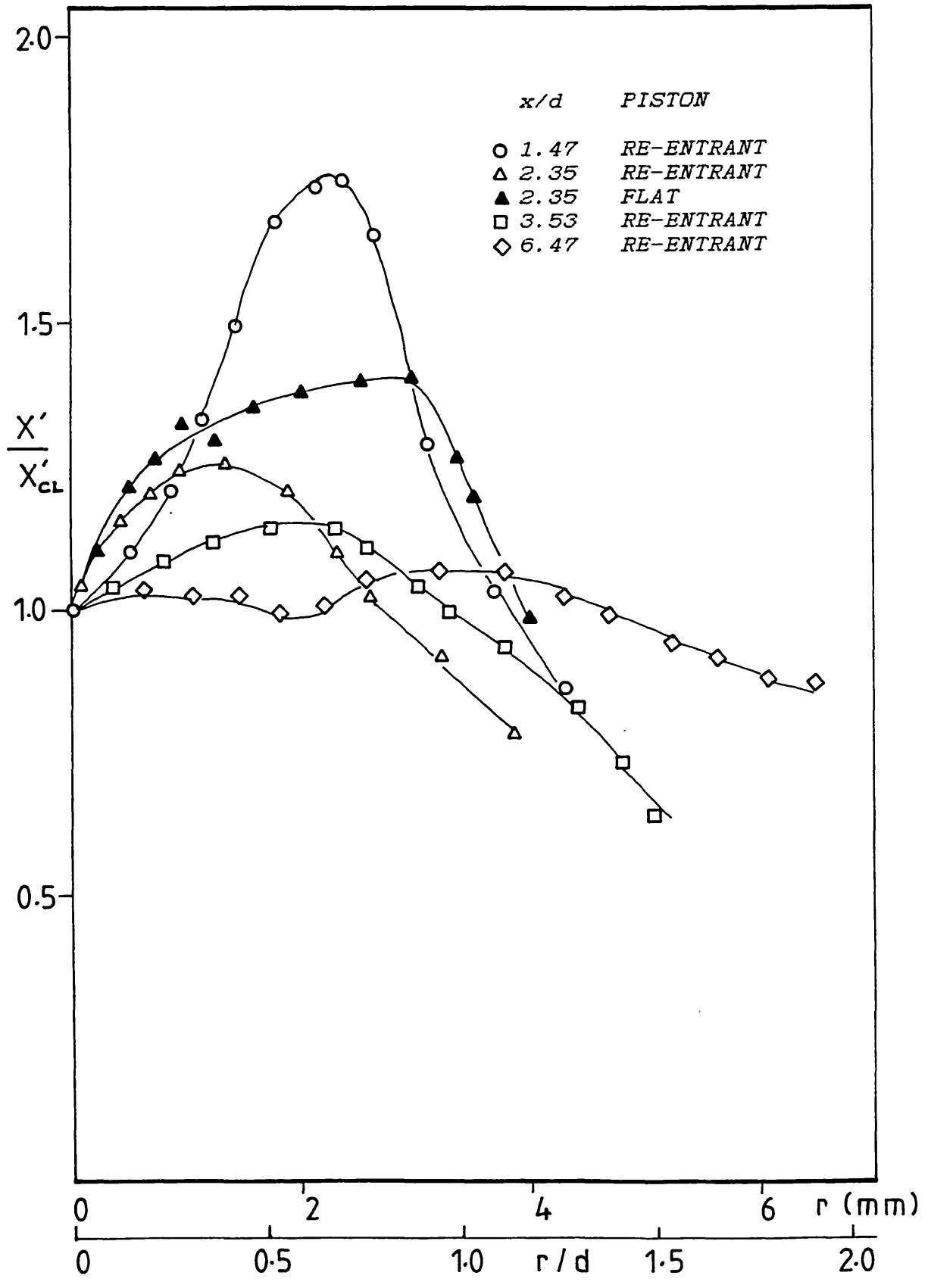


FIGURE 5.19(b) RADIAL DISTRIBUTIONS OF RMS CONCENTRATION AS INFLUENCED BY PISTON GEOMETRY FOR COMPRESSION RATIO 3.5 WITH NOZZLE A AND SF_6 (absence of swirl)

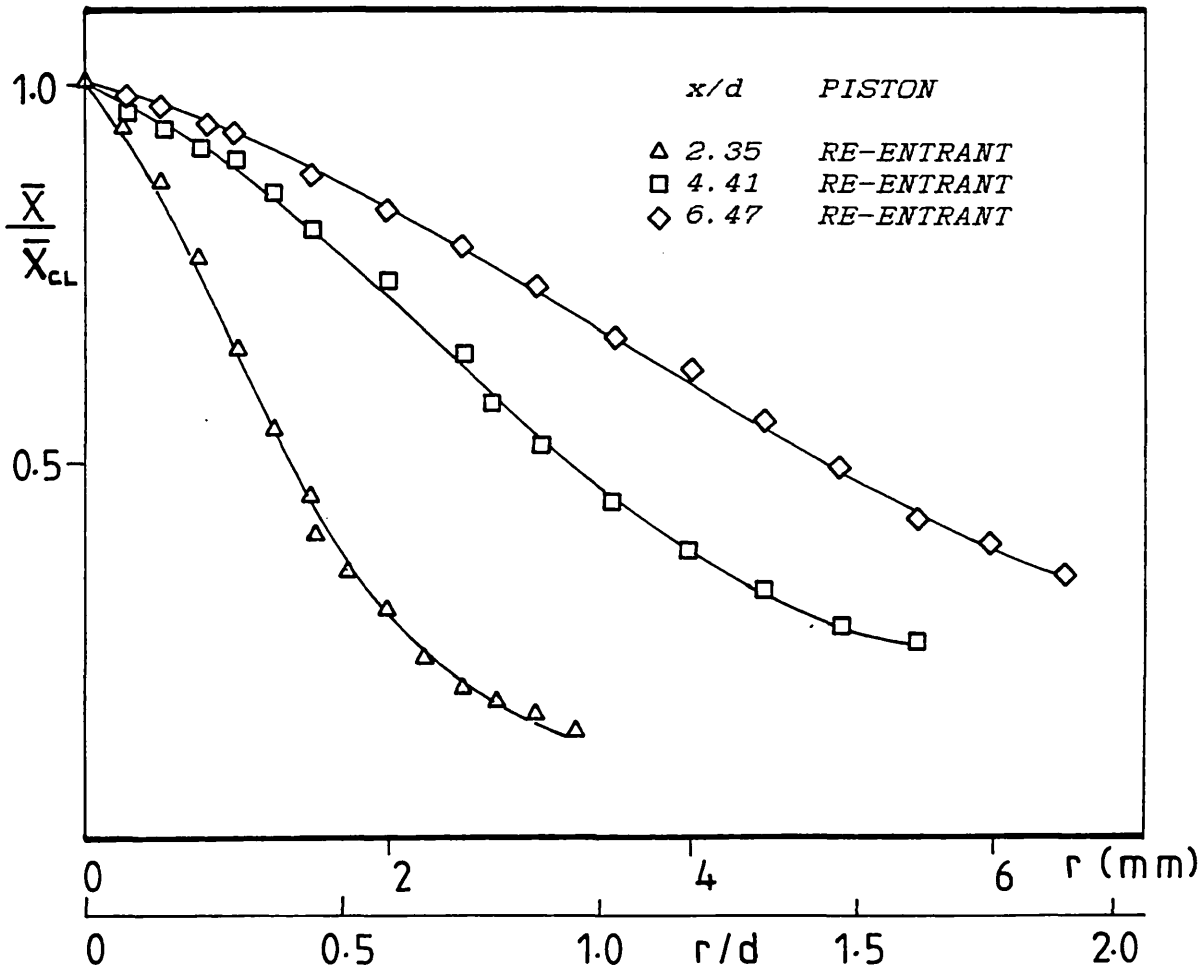


FIGURE 5.19(c) RADIAL DISTRIBUTIONS OF MEAN CONCENTRATION AS INFLUENCED BY PISTON GEOMETRY FOR COMPRESSION RATIO 3.5 WITH NOZZLE A AND FREON-12 (absence of swirl): see FIGURE 5.8(a)

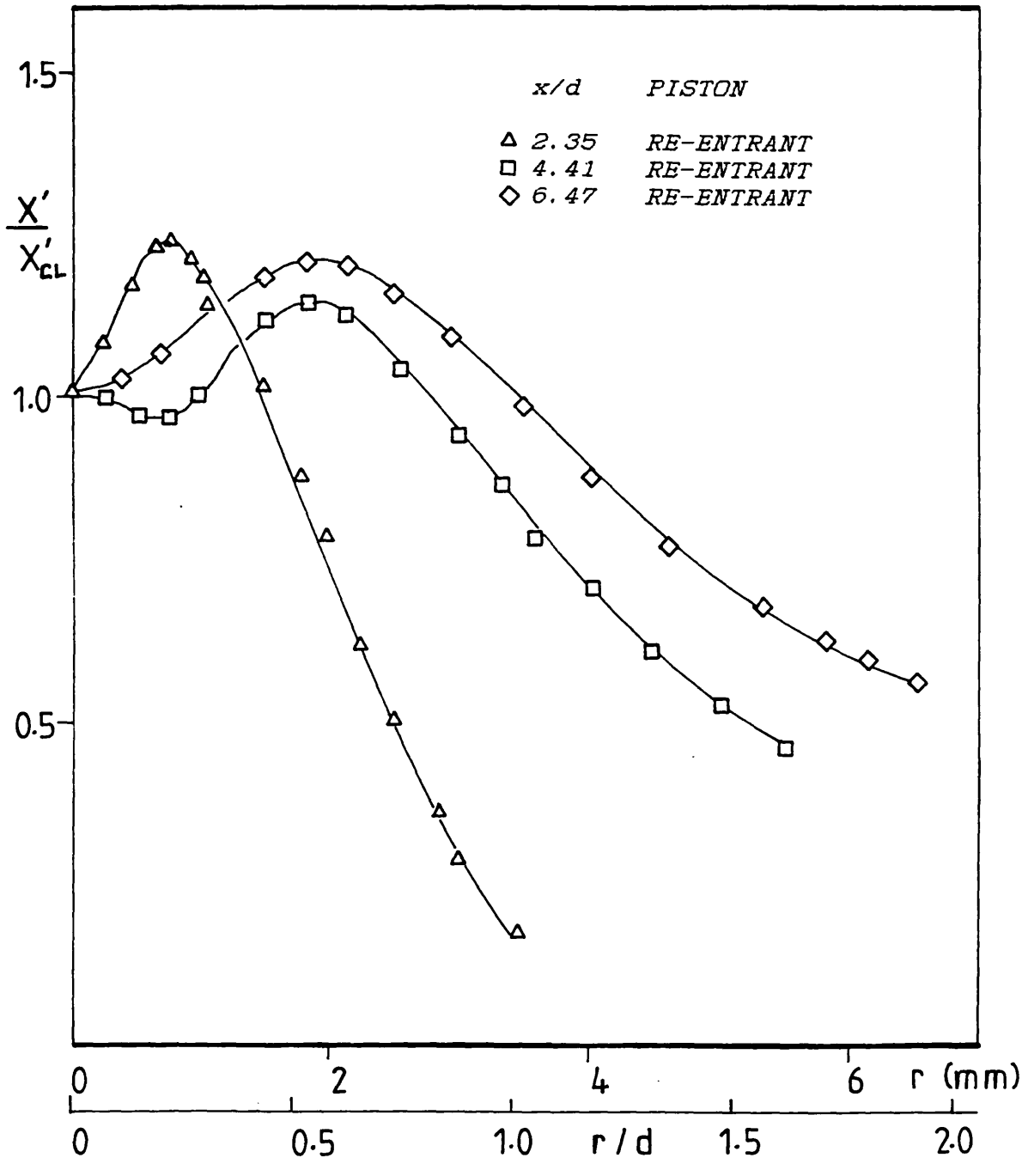


FIGURE 5.19(d) RADIAL DISTRIBUTIONS OF RMS CONCENTRATION AS INFLUENCED BY PISTON GEOMETRY FOR COMPRESSION RATIO 3.5 WITH NOZZLE A AND FREON-12 (absence of swirl): see FIGURE 5.8(b)

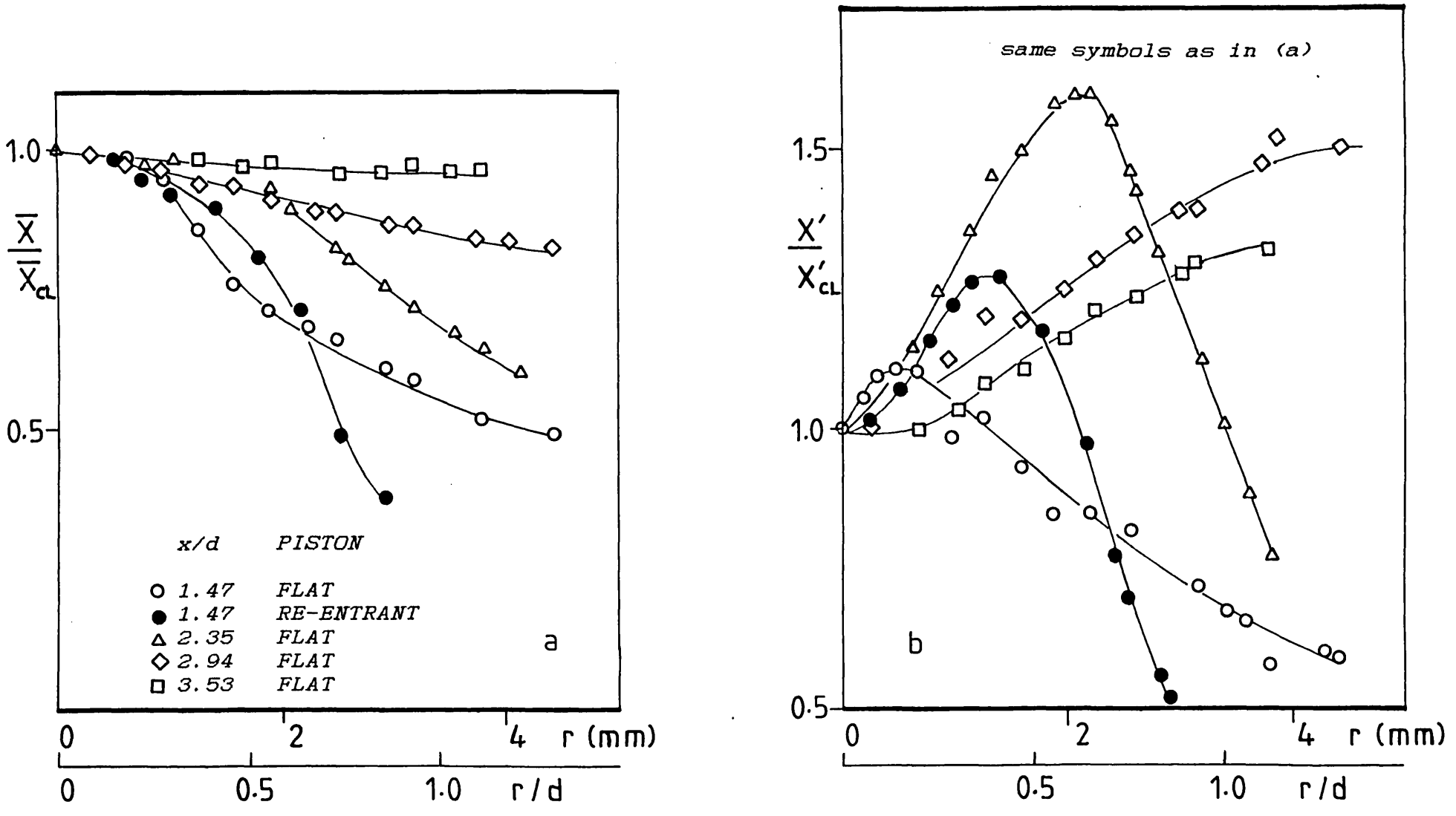


FIGURE 5.20 RADIAL DISTRIBUTIONS OF (a) MEAN and (b) RMS CONCENTRATION, AS INFLUENCED BY PISTON GEOMETRY FOR COMPRESSION RATIO 6.7 WITH NOZZLE A AND SF_6 (absence of swirl)

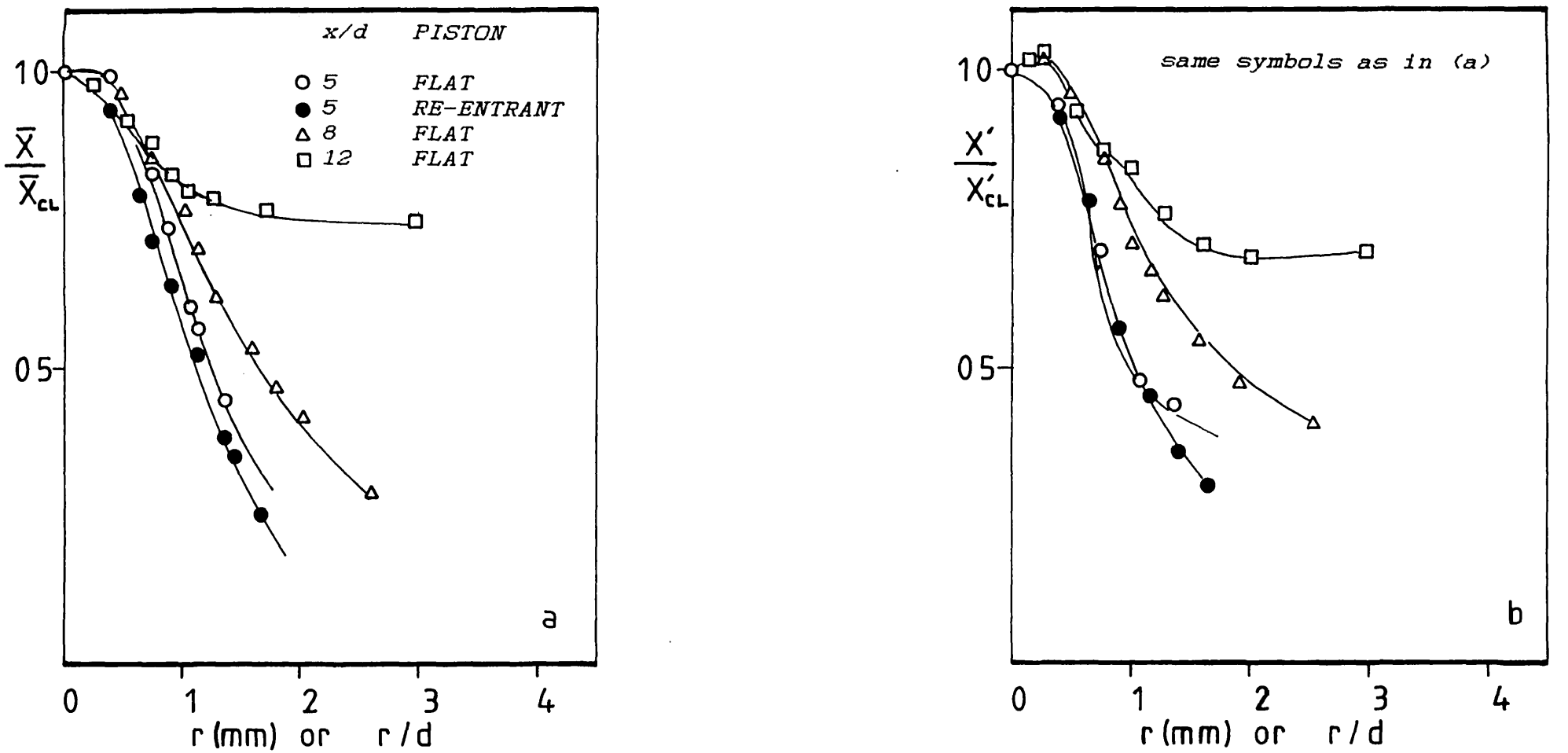


FIGURE 5.21 RADIAL DISTRIBUTIONS OF (a) MEAN and (b) RMS CONCENTRATION, AS INFLUENCED BY PISTON GEOMETRY FOR COMPRESSION RATIO 6.7 WITH NOZZLE C AND SF_6 (absence of swirl)

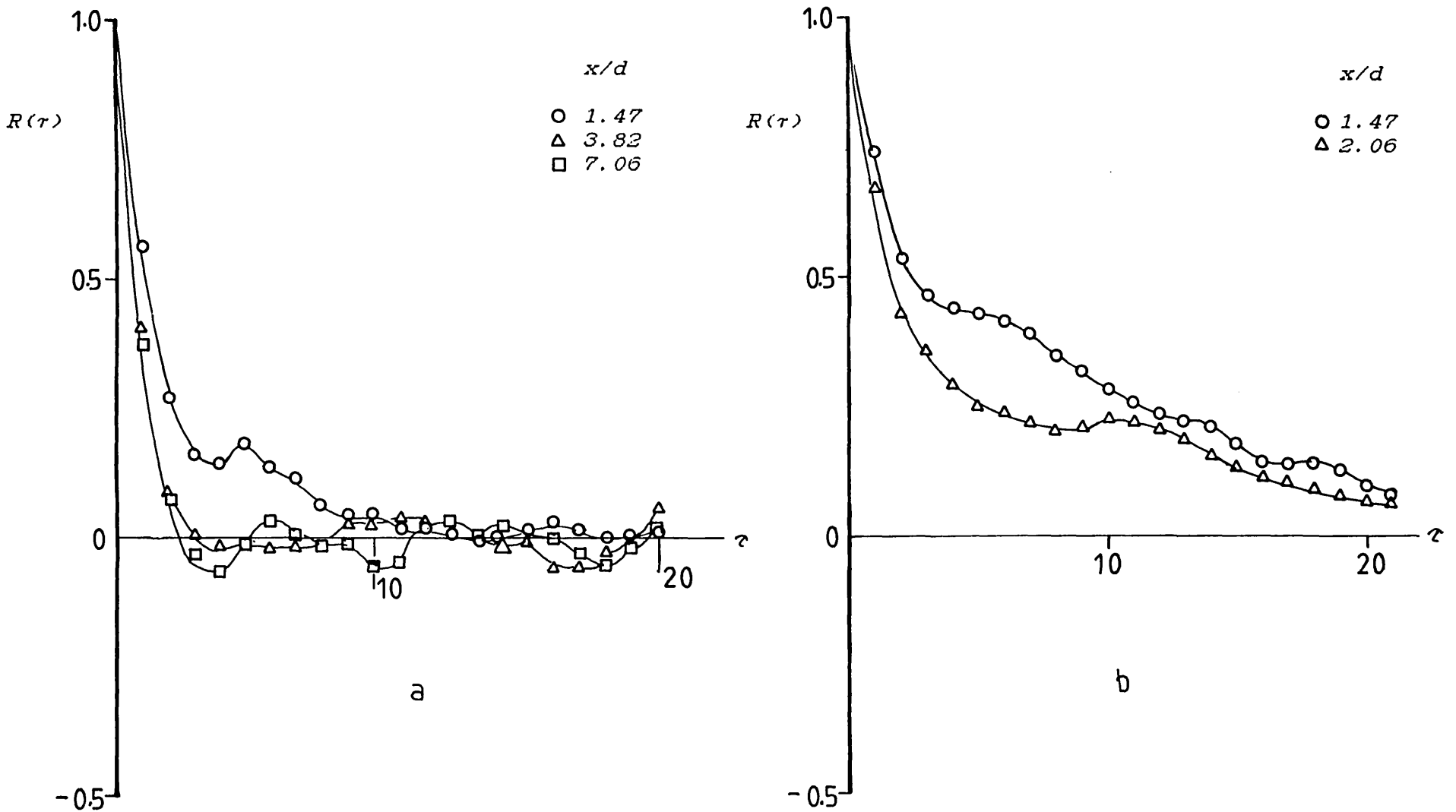
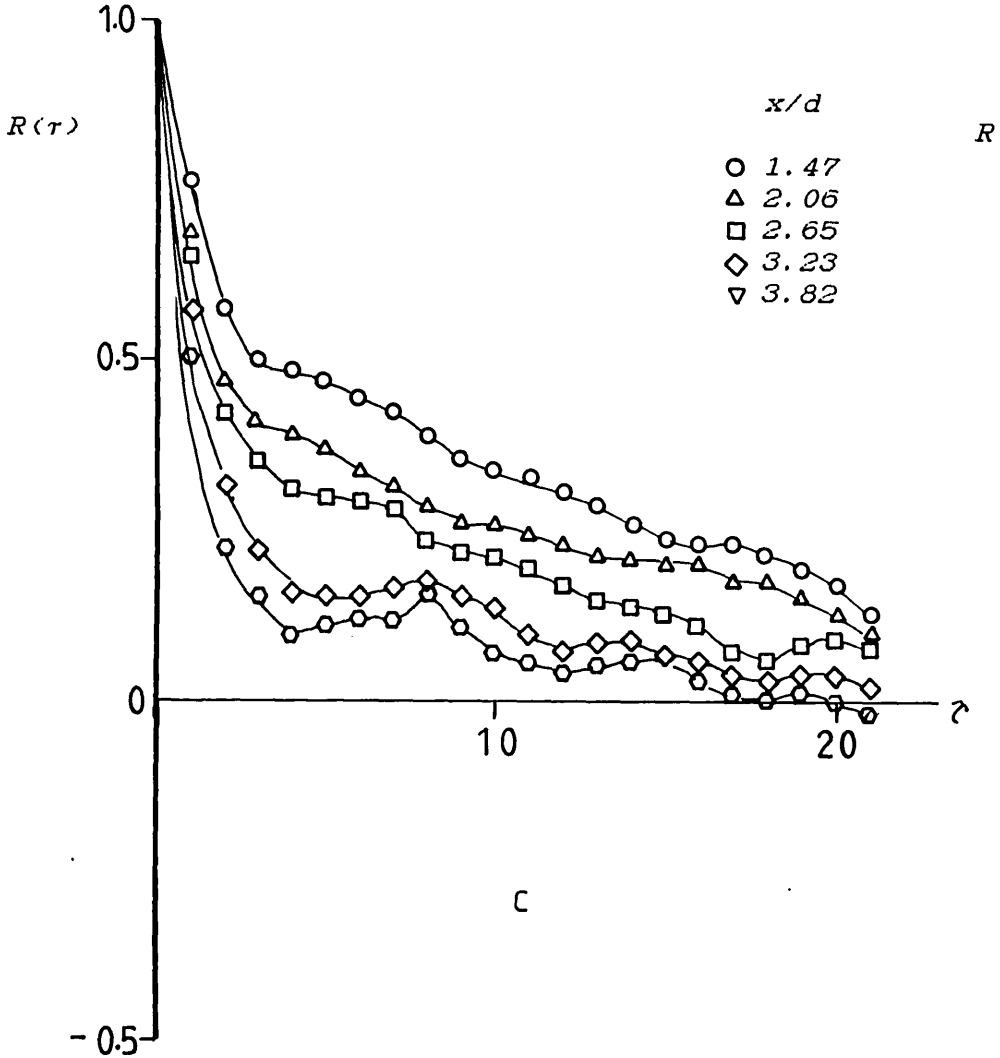
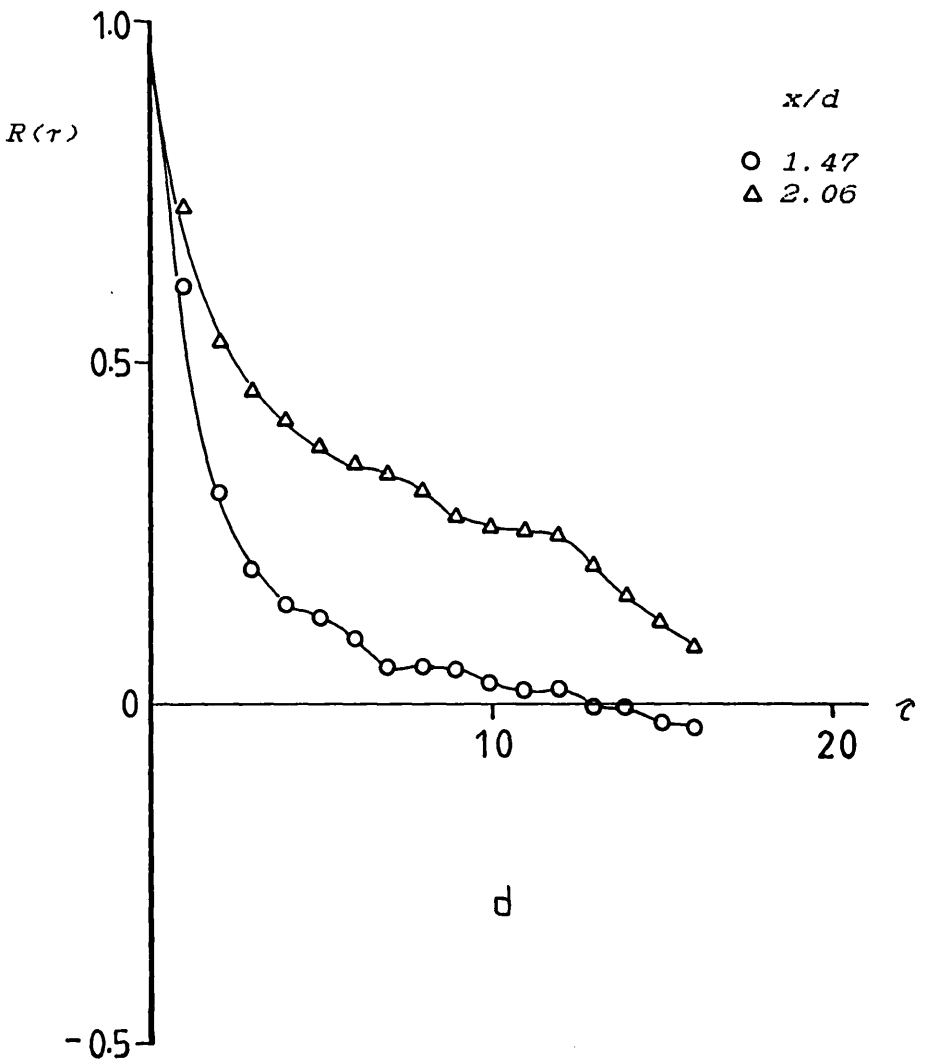


FIGURE 5.22 ENSEMBLE AUTOCORRELATION FUNCTIONS (based on 100 engine cycles) FOR SF_6 gas: NOZZLE A (a) RE-ENTRANT PISTON, 3.5 CR (b) RE-ENTRANT PISTON, 6.7 CR (c) FLAT PISTON, 6.7 CR (d) RE-ENTRANT PISTON, 6.7 CR (ensembled along $\Delta\theta$, FIGURE 5.4)


1.0
0.5
0
-0.5
R(τ)
x/d
1.47
2.06
2.65
3.23
3.82
10
20
τ
c


1.0
0.5
0
-0.5
R(τ)
x/d
1.47
2.06
10
20
τ
d

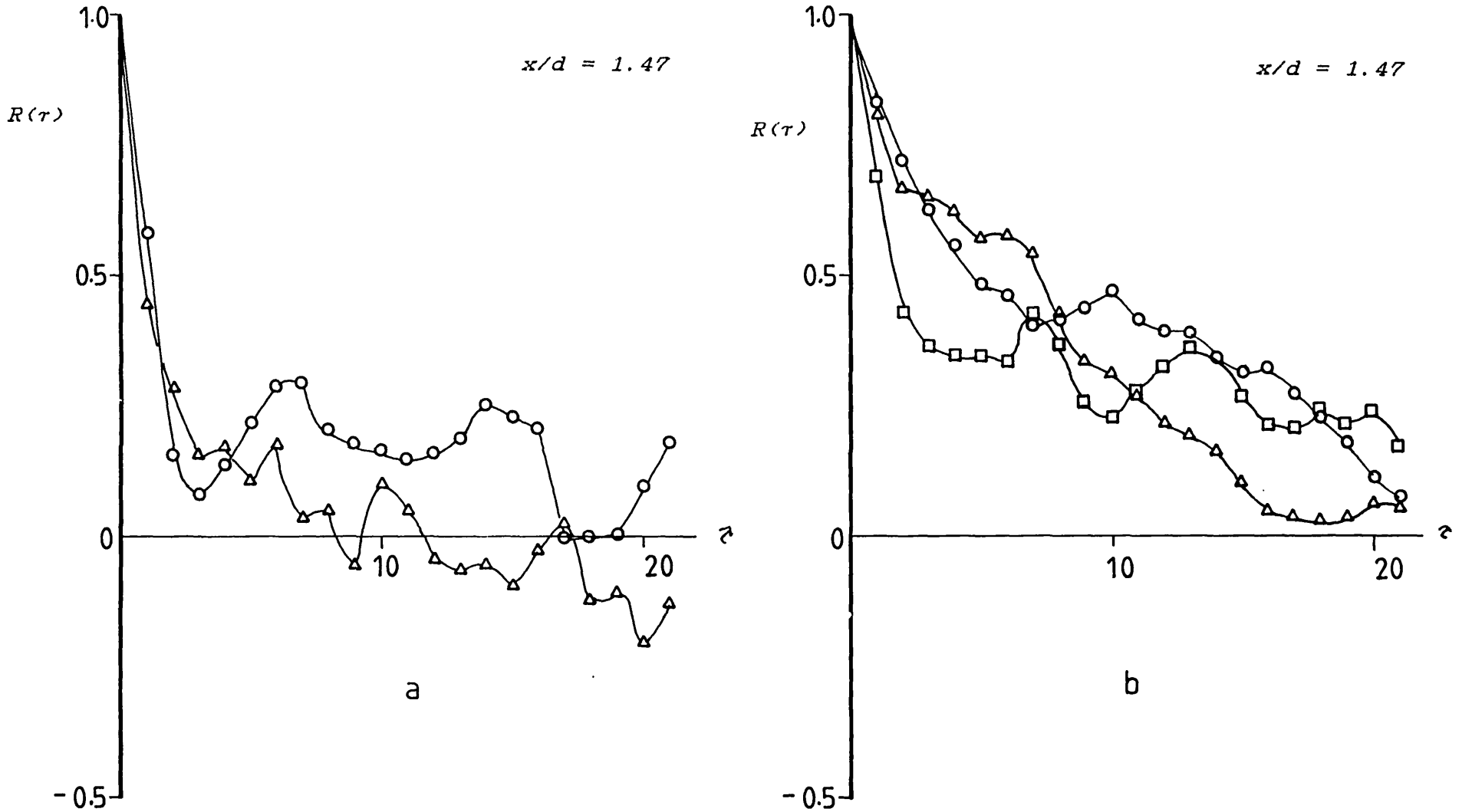
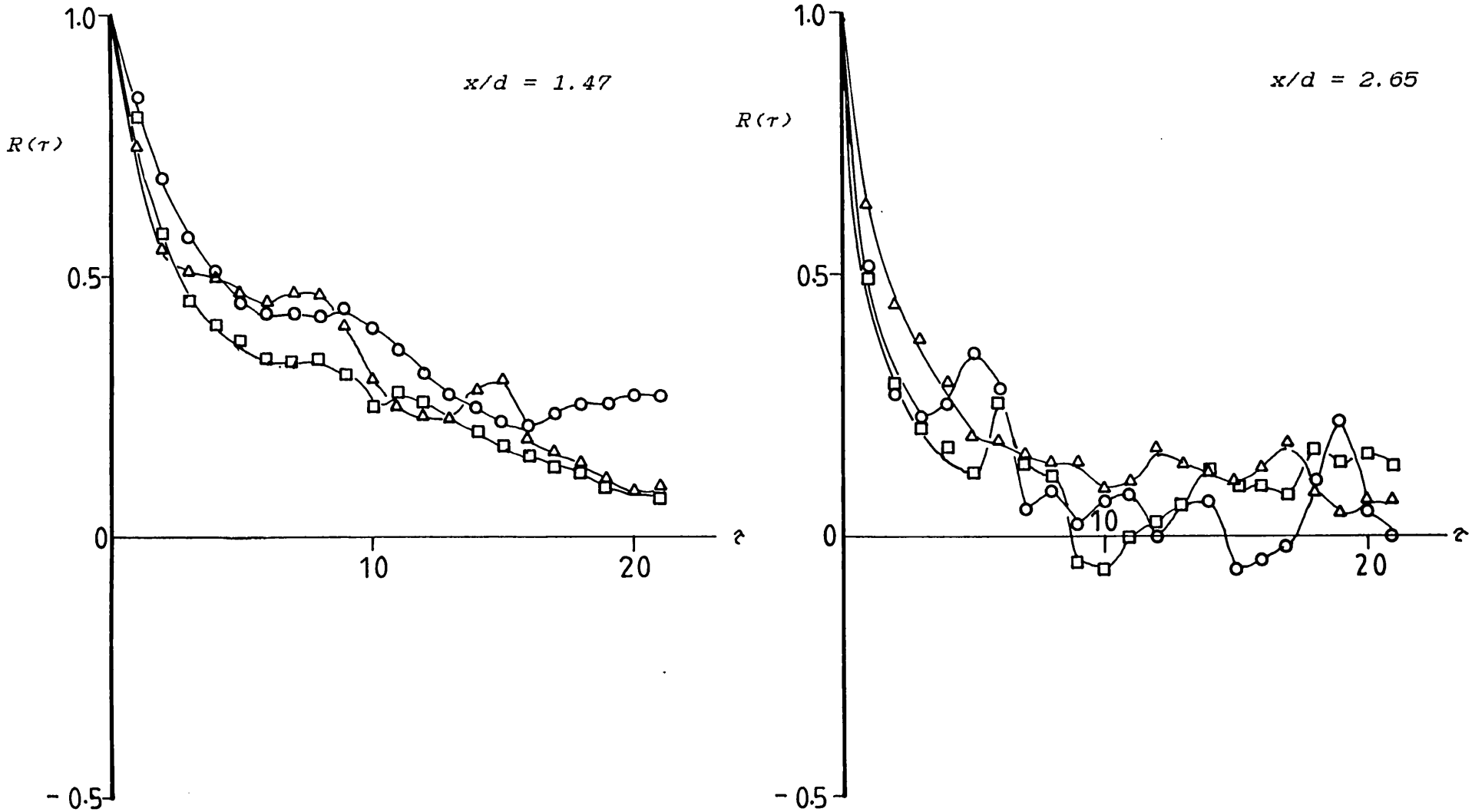


FIGURE 5.23 SINGLE-CYCLE AUTOCORRELATION FUNCTIONS FOR SF_6 gas: NOZZLE A (a) RE-ENTRANT PISTON, 3.5 CR (b) RE-ENTRANT PISTON, 6.7 CR (c) FLAT PISTON, 6.7 CR



(c)

CHAPTER 6 CHARACTERISTICS OF TRANSIENT JETS

6.1 INTRODUCTION

The present chapter presents results for the tip penetration of transient gas jets of Freon-12 and SF_6 issuing into quiescent air. They were obtained with a combination of laser Rayleigh scattering, high speed photography and photodiode arrays and are relevant to fuel sprays issuing from nozzles and, more specifically, to the simulations of engine configurations where high density gas jets are used to simulate liquid fuel sprays. The scaling of the transient, turbulent jets is considered and comparisons made with the known penetration characteristics of transient jets issuing into a medium of the same density. The results presented provide information of the tip penetration as a function of nozzle geometry, jet fluid density and initial velocity. Similar studies of tip penetration have been reported for air-into-air jets by Witze (1980) and with Diesel fuel sprays by Yule et al (1985).

The flow configuration and experimental system are described in the following section and presentation and discussion of results in a third section. The more important conclusions are summarized in a fourth section.

6.2 EXPERIMENTAL SYSTEM

6.2.1 Flow configuration

The transient jets made use of the nozzles A, B and C described in the last chapter (see Figure 5.1) and a line diagram of the flow system is shown in Figure 6.1. The transient jets were controlled in the same manner as discussed in Chapters 4 and 5 using an Angar Model 008 solenoid valve with

a firing frequency of 3Hz. Freon-12 or SF_6 gas was supplied to the inlet of the solenoid from pressurized gas bottles. The pressures used to operate the solenoid valve were 0.239, 0.377 and 0.584MPa; the highest pressure corresponds to the vapour pressure limit of the Freon-12. Since there are line losses through the flow circuit, particularly through the rotameter and solenoid, the backpressures indicated upstream of these components are greater than that across the nozzles, $\Delta P = P_u - P_{atm}$, where P_u is the exit nozzle pressure and P_{atm} that of the ambient surroundings. By measuring the exit plane velocities, using the gated LDA system of Chapter 4, ΔP was estimated from Bernoulli's law and used to find P_u. The estimate of P_u was then used to check that the pressure ratio $P^* = P_{atm}/P_u > P_{cr}$ where P_{cr} is the critical pressure ratio of the jet. For all the cases investigated, since it was determined that $P^* > P_{cr}$, the transient jets were not choked.

A summary of the experimental conditions is provided in Table 6.1 which shows the Reynolds numbers, exit momentum, mass flow rates, nozzle area ratios A*, jet to ambient density ratios ρ_j/ρ_a, and the jet time constants (as defined in Chapter 4) where $\tau_j = r_e/U_o$ and $r_e = r_o(\rho_j/\rho_a)^{\frac{1}{2}}$ is the effective nozzle radius. Differences in the viscosity of the Freon-12 and SF_6 are small and are expected to introduce a ngeligible effect; see, for example, Hopkins and Robertson (1967) and Reitz and Bracco (1979). The mass flow rate as shown by Table 6.1 is not a constant for the experiments but the total time the solenoid was operated allowed for a jet time Δt_{on} = 18ms. This value of Δt_{on} is about 1.3ms greater than used in the investigations of Chapters 4 and 5.

6.2.2 Optical and signal processing systems

The transient jet tip penetration rates were measured using three different experimental techniques: high speed photography, a linear photodiode array (PDA) technique and LRS. The LRS system is the same as that described in Chapter 2 with the argon-ion laser operated at 1.0W and 488nm and the instrumentation for the photography is the same as that described by Dyer (1979) with a HYCAM Model 41-0004 high speed camera operated at 5000 frames per second. Schlieren and shadowgraph techniques were used to image the transient jets for both the photography results and PDA measurements. The flow imaging assisted the development of the PDA instrumentation and a detailed discussion of the principles of the technique is given by Hopwood (1980). In the present application, the PDA provided a signal which was related to the refractive index of the image field and this was interpreted in terms of the jet tip which interfered with the detection of light as the array scanned the field of view. The PDA was similar to that described by Witze (1985) and a line diagram of the instrumentation and optical arrangements, as used for the measurements here, is shown in Figure 6.2. The PDA element is the principal component of the solid-state video camera (E.G. and G. Reticon Model LC110) and with the field of view imaged onto a line of 512 photodiodes having a centre-to-centre, C_c, spacing of 13μm. The optical characteristics are summarized in Table 6.2. The controlling electronics for the PDA provided a video scan rate for the field of view of 2.38KHz. Uncertainty in the location of the jet tip and arrival time using the PDA were 1.5% and 2%, respectively.

The LRS system was used to define the time of arrival of the jet tip by detecting the rapid rise of the mole fraction of injected gas. As the typical signal trace shows (see Figure 5.6) this rise can be identified within 25μs. A rise of 3% mole fraction of jet fluid was identified as the time

of arrival of the jet tip at a given measurement location and the time of arrival was defined as $t = t_m - \langle t_r \rangle$ where t_m is the time measured by the computer clock from the instant the command is issued to the solenoid to open (Appendix C) and $\langle t_r \rangle$ the average time of response for the solenoid to become fully opened.

6.3 RESULTS AND DISCUSSIONS

6.3.1 Jet characteristics

Figures 6.3 and 6.4 present Schlieren photographs for two firings of a transient jet of Freon-12 issuing from nozzle A and with an exit velocity of 37.7m/s. The structure and evolution of the jet is seen to consist of an initial head vortex which grows downstream followed by the steadying jet behaviour behind the head vortex. It can be seen that the initial jet development is similar from one jet firing to another in terms of a leading vortex, but that different characteristics result with respect to the structure of the jet boundary and shape of the head vortex. It is also evident that the developing jet width is greater than the steadying width and this is made clear by the long-time exposure of the steadying jet shown in Figure 6.3. Figures 6.3 and 6.4 show that several length and time scales are associated with the transient and steadying jet behaviour. Figure 6.5 shows traced details of the evolving jet from nozzle A with an initial velocity of 37.7m/s and Figures 6.6 and 6.7 show similar details for jets from nozzle B with initial velocities of 19.2m/s and 30.9m/s. One observation which can be made is that at higher initial velocity (corresponding to higher Reynolds numbers) the jet structure is comprised of smaller length scales (finer and more grainy) than the larger and more coarse length scales which result for the jets with lower initial

velocity, Figures 6.5 and 6.6. Pitts (1986) shows similar trends between Reynolds number and length scales in his shadowgraph studies of variable density steady jets. Figure 6.8 shows the penetration and radial growth characteristics which result for a jet from nozzle C with an exit velocity of 60m/s and the differences for the jet characteristics from nozzle B are made clear by comparison of Figures 6.6 and 6.8, which show the faster jet development and penetration rate resulting with nozzle C over that of nozzle B and with differences in characteristics of radial growth. From photographic results such as those of Figure 6.3 and 6.4 it is clear that the tip of the jet is not consistently located at the centreline and that variations in the tip location away from the centreline increase with increasing downstream distance. The results of this behaviour is to affect the interpretation of tip penetration when different measurements techniques are used. The PDA and LRS techniques require that the detection point is positioned at the axial centreline, and should provide smaller values of tip location than those determined from photographs where the tip location is defined as that of maximum penetration.

The photographic results (Figure 6.4) also show the end time of the jet where a diluted jet begins to form and a trailing patch of fluid is observed to convect towards the final stages of the jet. The patch referred to starts as a vortex at the nozzle but is highly mixed and dispersed by the time it reaches a distance of about $6r_o$. Figure 6.9 shows an instantaneous trace of the jet fluid concentration detected with LRS along the centrelin at x/d = 1.5 and shows the rise in concentration of the tail vortex of the jet (as expected from the photographic results). Witze (1986) has conjectured that the trailing vortex may not be a general result but that it may exist in some or many instances. Yule et al (1985) have reported similar diluting characteristics for the end time for Diesel fuel sprays resulting from the atomization of Diesel oil.

6.3.2 Comparison of technique results

The penetration distance and time data obtained with the techniques reported are power law correlated by $x(t) = at^n$ with a standard deviation of around 0.003 and Table 6.3 summarizes the values of a and n for the Freon jet results. Tip penetration data for SF_6 jets were determined with the LRS system only. The LRS system was also used for the case of Freon jets to allow comparison of the results with those obtained from the PDA technique and the high speed film.

Figures 6.10 and 6.11 show experimental data obtained with nozzles A and B for the jet tip penetration, x(t), versus time, t. By comparison, the LRS and PDA measurements tend to underpredict the tip position in a consistent manner relative to the values that were determined from analysis of the high speed film and the differences increase with distance from the nozzle; the data represent phase averaged results over 100 jet firings for each case. Yule et al (1985) have observed similar differences in results obtained with a PDA and high speed film, for the tip penetration studies of their Diesel fuel sprays. In contrast, however, Witze (1985) has observed that his PDA technique led to overprediction, when compared to results obtained with a stationary probe, of a propagating flame front position. The PDA in Witze's case was oriented to see the image of the plane of the flame front so that the flame front arrival detected by the PDA would be expected to see the flame front sooner than the probe, particularly when any part of the flame front arrives at locations away from the expected symmetry plane.

6.3.3 Tip penetration

Figures 6.12, 6.13 and 6.14 present results of the transient jet tip penetration for conditions of different nozzles, and exit velocities and with different jet fluids. The non-dimensional coordinates are $x^* = x/r_e$ for the penetration

distance and $t^* = t(U_o/r_e)$ for the time. Since the jet time constant τ_j is defined by r_e/U_o, the non-dimensional time becomes t/τ_j. As results from the Figures 6.12 - 6.14 show the scaling x^* and t^* results in collapse of the data for a given nozzle geometry. Comparison of results shown in physical coordinates (Figures 6.10 and 6.11) indicates that the penetration rate increases with initial velocity and that the penetration rate is dependent upon the nozzle geometry. When the data are collapsed for each nozzle in terms of x^* and t^* differences in results for the penetration rate between the nozzles remain but the effect of initial velocity for a given nozzle is accounted for in t/τ_j. Dependence on density ratio between the jet fluid and ambient is shown by the results of Figure 6.14 which shows that a faster penetration rate is predicted as the density ratio (ρ_j/ρ_a) increases. The comparisons here are made with the Freon-12 jets from nozzle C and those of air-into-air reported by Witze (1980)*.

The ratio of penetration distance $x(t)$ to $t^{\frac{1}{2}}$ tends to a constant, α, which is independent of nozzle geometry, density ratio (ρ_j/ρ_a), velocity U_o, and definition of jet tip arrival time. The constancy of α is an asymptotic value which varies with velocity and geometry and the time t_c after which the value of α becomes constant appears to also be influenced by initial conditions. From the present results, and those of Witze (1980)(and Kuo et al (1982, 1986) for transient laminar jets), analysis shows that

$$\alpha = x/\sqrt{t} = \text{const.}_{r_o, U_o, \rho}; \qquad t > t_c \qquad (6.1)$$

* It is noted that the arrival time of the jet tip is defined differently in Witze's case but even accounting for the difference in time of arrival, the penetration rate for the heavier density jets compared is greater

is an invariant for each transient jet for $t > t_c$ where t_c is interpreted as the time after which the effects of initial conditions are forgotten by the flow. From dimensional analysis, a collapse of all the variable density data onto the air jet results (Witze (1980)) for long enough times t* can be made using a time coordinate

$$t^{**} = k(\rho_j/\rho_a)^{\frac{1}{2}} \sqrt{\frac{t}{\tau_j}} = k(\rho_j/\rho_a)^{\frac{1}{2}} \sqrt{t^*} \qquad (6.2)$$

where the value of $k \sim 9.86$. The result (6.2) can be verified with the data of Figure 6.14 and it is interesting to note that $k \simeq \pi^2$. A good correlation for the penetration parameter α is obtained with $\alpha = (k\, r_e U_o)^{\frac{1}{2}}$ when $r_o > 1$ and, for $r_o < 1$, with $\alpha = r_o^{1/3}(k\rho_j/\rho_a U_o)^{\frac{1}{2}}$. The result of analysis using these correlations for the Freon, SF_6 and air jets is shown in Table 6.4. As the results there indicate, the nozzle radius r_o, exit velocity U_o and jet fluid density ρ_j are almost sufficient to describe the penetration characteristics. It is also seen from Tables 6.1 and 6.4 that when unequal density jets issuing from the same nozzle have the same exit momentum the penetration parameter α is also equal. Consistently, the penetration parameter α increases as U_o increases and with the increase in α proportional to $(U_o)^{\frac{1}{2}}$.

6.4 CONCLUSIONS

The investigation of tip penetration for transient jets of variable density discharging into still air revealed the following:

1. After the initial penetration of the jet, the penet-

ration distance is directly proportional to the square root of time and the ratio of $x(t)/\sqrt{t}$ obtains an asymptotic value which is different for different initial conditions of nozzle geometry, jet fluid density and exit velocity. The ratio $x(t)/\sqrt{t}$ was used to define a penetration parameter α which, for laminar and turbulent transient jets, was found to be an invariant of the flow.

2. For transient jets of different density, equal exit momentum and discharging from the same nozzle, there is a single value of the penetration parameter α.

3. As the initial velocity increases, α increases proportionally to the square root of velocity independent of other effects. Thus, the penetration rate of a transient jet is dependent on $(U_o)^{\frac{1}{2}}$ for a given family of geometries.

4. The time coordinate defined by equation (6.2) for the variable density transient jets has been shown to collapse the penetration distance x/r_e onto a single curve after the time t/τ_j becomes large. Verification of the constant k requires further studies.

5. The use of PDA technique to obtain measurements of the tip penetration of transient jets must be made with care and the interpretation of results requires an understanding of the flow characteristics which can be assisted by flow visualization. A technique such as LRS can also be used to obtain tip penetration information and with results which are similar to those obtained with the PDA technique.

TABLE 6.1 Summary of experimental conditions

NOZZLE	GAS	ρ_j/ρ_a	Solenoid Operating Pressure (MPa)	r (mm)	r_e (mm)	U_o (m/s)	R_e	M_o (kg.m/s^2) x 10^2	$\dot{m}$ (kg/s) x 10^3	$A^* = (\frac{dp}{d})^2$	τ_j (μs)
A	CCL_2F_2	4.18	.239	1.7	3.47	24.2	33,782	2.69	1.11	.886	143
		"	.337	"	"	30.7	42,855	4.32	1.41	"	113
		"	.584	"	"	37.7	52,627	6.52	1.73	"	92
	SF_6	5.11	.239	1.7	3.84	21.7	36,770	2.62	1.21	"	177
		"	.377	"	"	28.0	47,445	4.36	1.56	"	137
B	CCL_2F_2	4.18	.239	1.9	3.88	19.2	29,955	2.11	1.10	.709	202
		"	.377	"	"	25.8	40,252	3.81	1.48	"	151
		"	.584	"	"	30.9	48,209	5.47	1.77	"	126
	SF_6	5.11	.239	1.9	4.29	17.0	32,195	2.01	1.18	"	252
		"	.377	"	"	22.3	42,232	3.46	1.55	"	192
C	CCL_2F_2	4.18	.239	0.5	1.02	44.6	18,311	.789	.177	10.24	22
		"	.377	"	"	53.0	21,760	1.11	.210	"	18
		"	.584	"	"	60.0	24,634	1.73	.288	"	17
	SF_6	5.11	.239	0.5	1.13	39.3	19,586	.744	.189	"	28
		"	.377	"	"	48.0	24,420	1.16	.236	"	23

N.B.: For the conditions of the experiments the values of dynamic viscosity for the Freon-12 and SF_6 gas are (as specified by the supplier) $\mu_{SF_6} = 1.49 \times 10^{-5}$ (kg/ms) and $\mu_{CCL_2F_2} = 1.23 \times 10^{-5}$ (kg/ms)

TABLE 6.2 PDA optical parameters

Field of view, FOV (ℓ)	85.0mm
Array optical length, AOL (AOL = C_c x NE, C_c = 13 m, NE = 512) (NE = number of elements imaged)	6.656mm
Magnification, M = ℓ/AOL	11.3
Static spatial resolution of imaged field*, M x C_c	.146mm/array element

* N.B.: The best accuracy is estimated to be about 2M x C_c (see Hopwood, 1980)

TABLE 6.3 Values for a and n for the correlation of penetration distance and time (Freon-12 jets)

		PDA RESULTS			CINE-FILM RESULTS		
Solenoid operating pressure (MPa)		.239	.377	.584	.239	.377	.584
NOZZLE A	a	18.17	20.86	24.90	18.88	21.64	25.37
	n	.7559	.7919	.7745	.7613	.7800	.8134
NOZZLE B	a	15.80	18.40	21.46	17.30	19.36	24.11
	n	.8281	.8322	.8380	.7690	.8160	.7968
NOZZLE C	a	-	-	-	26.06	-	32.93
	n	-	-	-	.6987	-	.6962

TABLE 6.4 Penetration parameter (α) experimental correlation

GAS	r_o(mm)	U_o(m/s)	$(\alpha = \frac{x}{\sqrt{t}})_{exp}$	$(kr_eU_o)^{\frac{1}{2}}$	$r_o^{1/3} \times (k(\rho_j/\rho_a)U_o)^{\frac{1}{2}}$
Air	0.6	53	19.5		19.29
Air	0.6	103.5	27.3		26.89
Air	1.2	22	16.2	16.14	
Air	1.2	54.4	25.1	24.69	
Freon-12	1.7	24.2	29.1	29.08	
Freon-12	1.7	30.7	32.5	32.49	
Freon-12	1.7	37.7	37.3	36.00	
SF_6	1.7	21.7	27.7	28.6	
SF_6	1.7	28.0	31.9	32.5	
Freon-12	1.9	19.2	27.3	27.16	
Freon-12	1.9	25.8	31.3	31.48	
Freon-12	1.9	30.9	34.5	34.4	
SF_6	1.9	17.0	28.0	26.8	
SF_6	1.9	22.3	31.2	30.7	
Freon-12	0.5	44.6	34.2		34.3
Freon-12	0.5	60.0	39.5		39.0
SF_6	0.5	39.3	34.4		35.3
SF_6	0.5	48.0	38.7		39.0

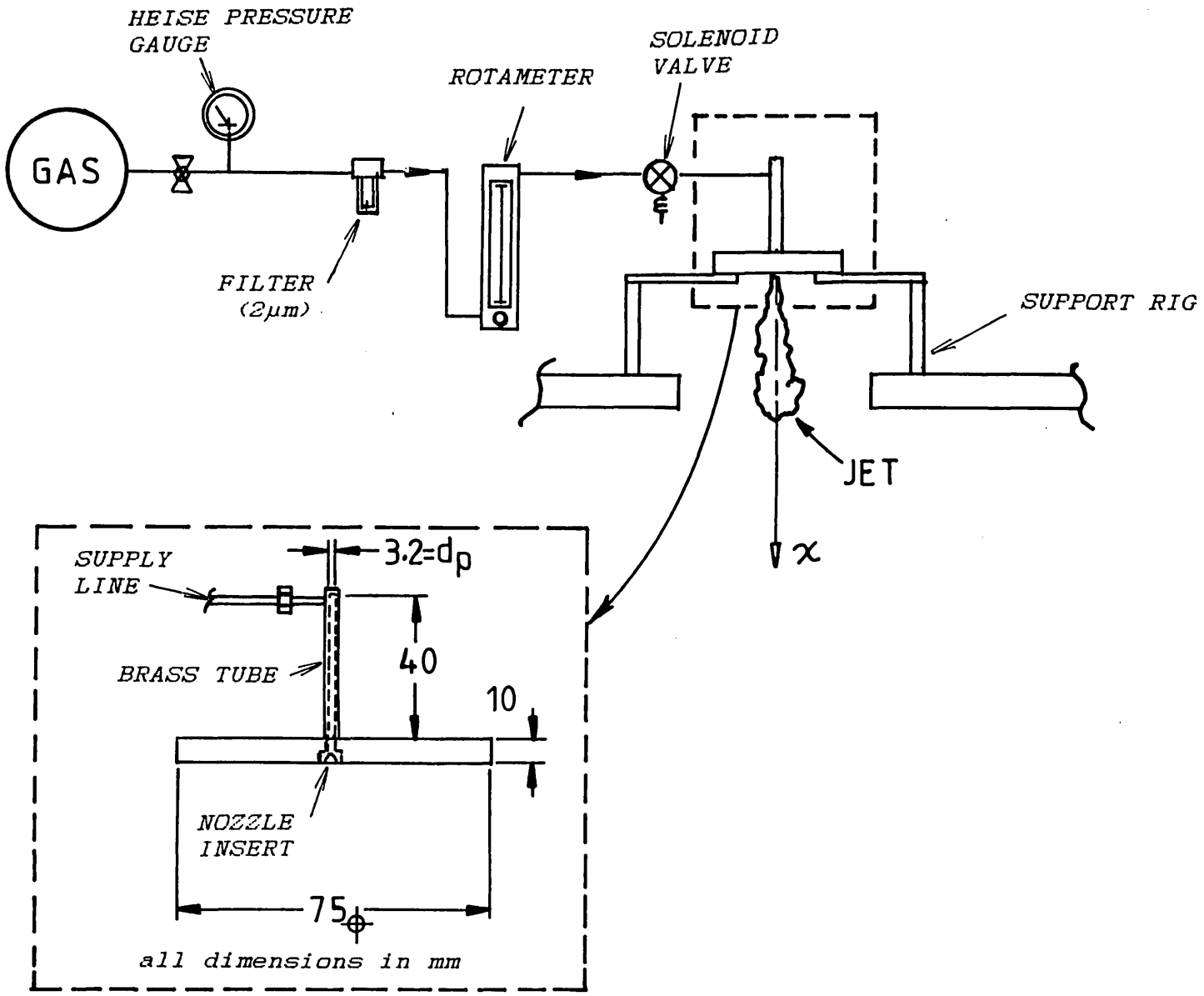


FIGURE 6.1 LINE DIAGRAM OF FLOW SYSTEM

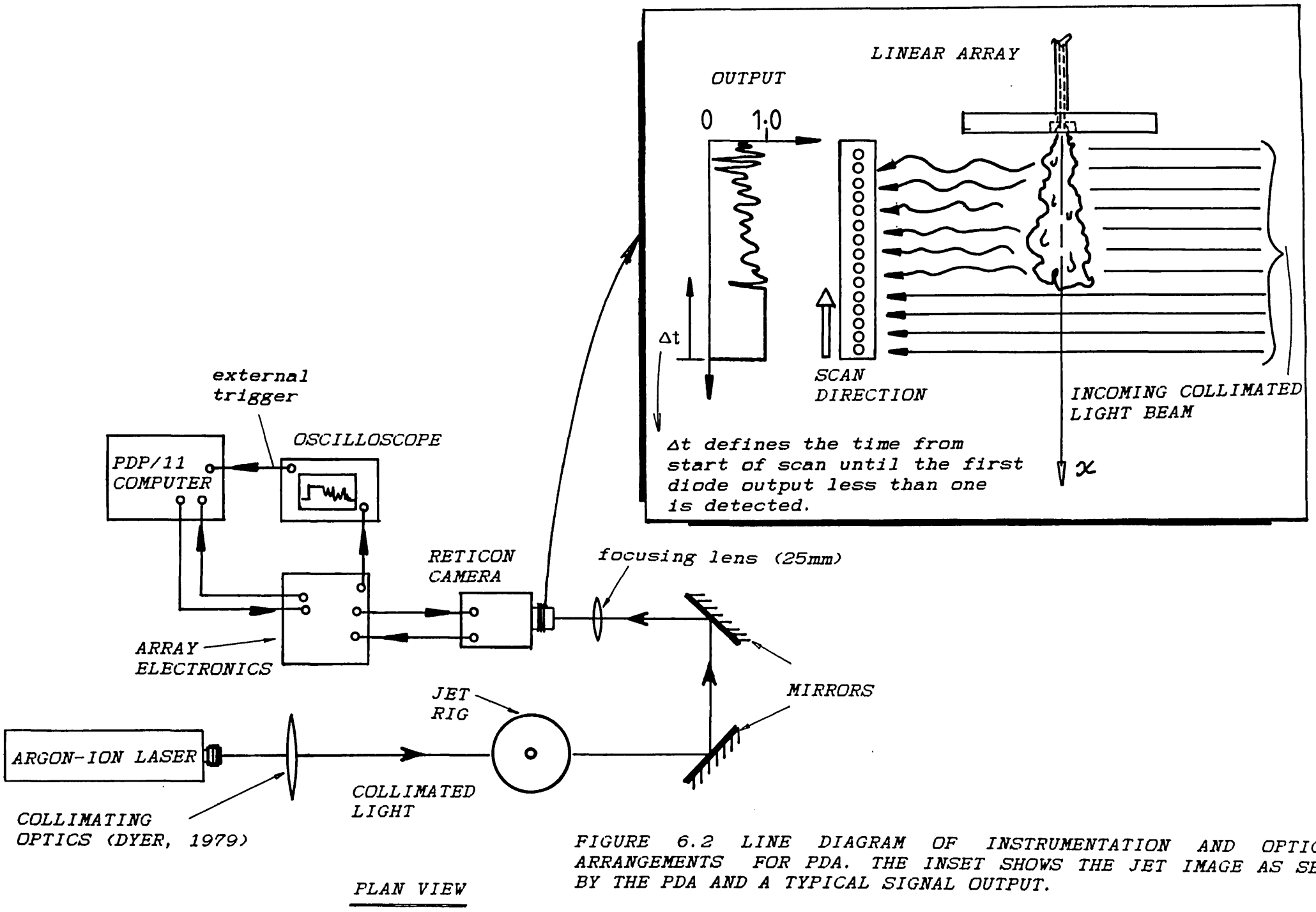


FIGURE 6.2 LINE DIAGRAM OF INSTRUMENTATION AND OPTICAL ARRANGEMENTS FOR PDA. THE INSET SHOWS THE JET IMAGE AS SEEN BY THE PDA AND A TYPICAL SIGNAL OUTPUT.

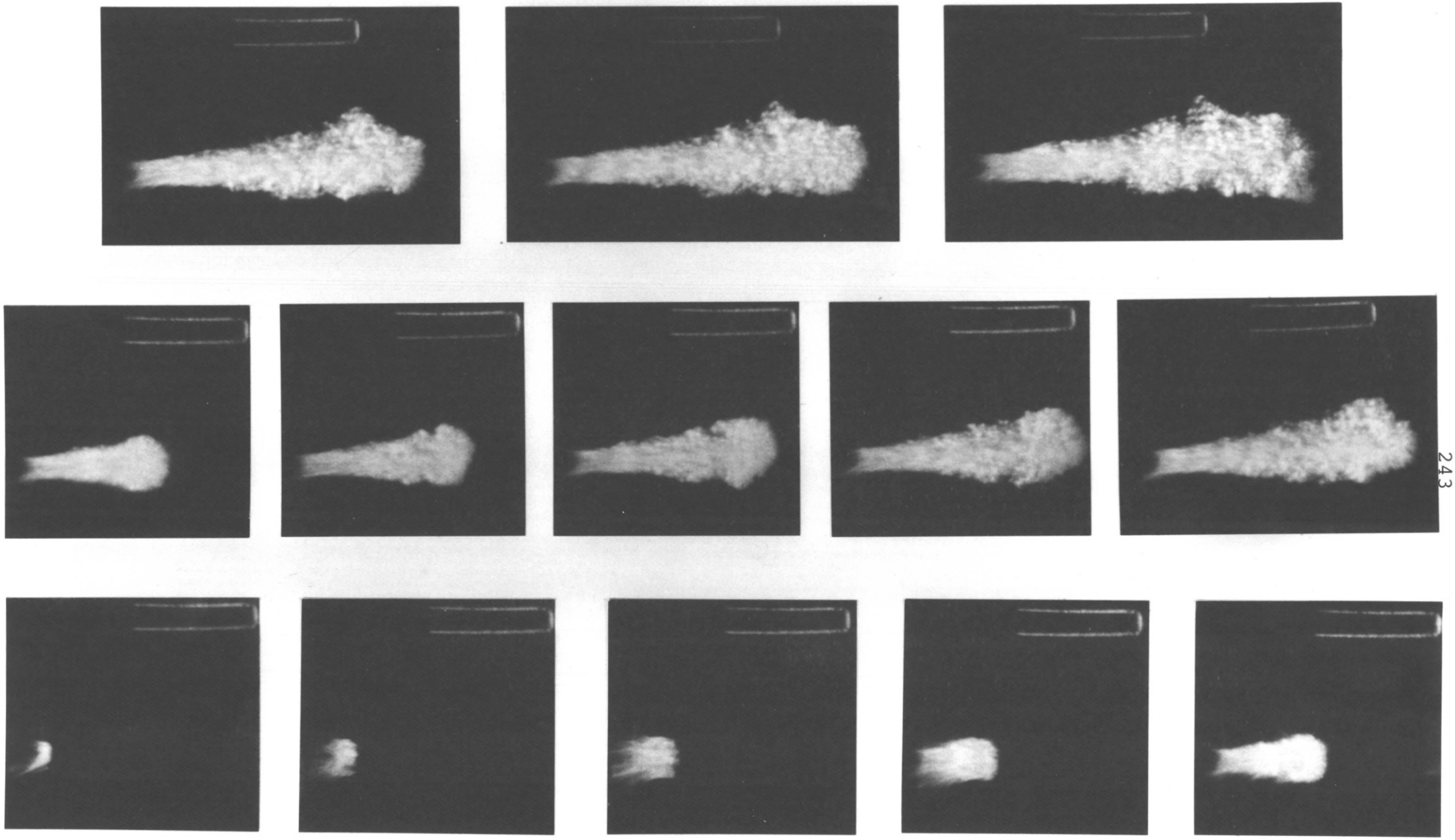
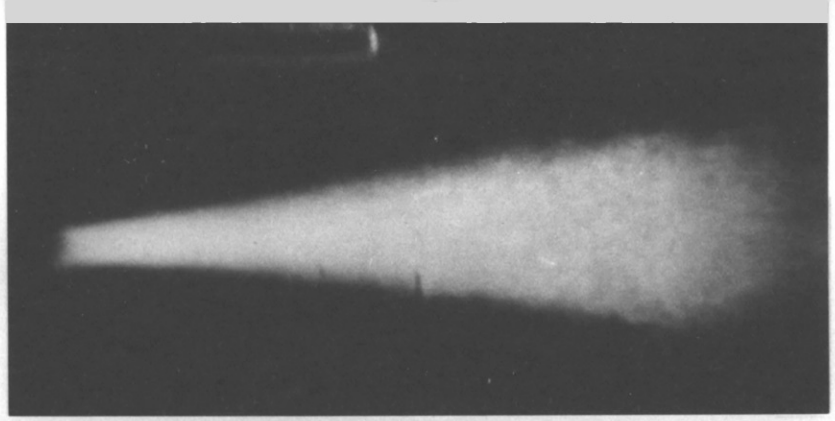


Figure 6.3 Schlieren photographs of a transient jet of Freon-12 from Nozzle A with U_o = 37.7m/s. The time in between exposures is 0.2ms and with the last frame showing the steadying jet boundary obtained from long time exposure



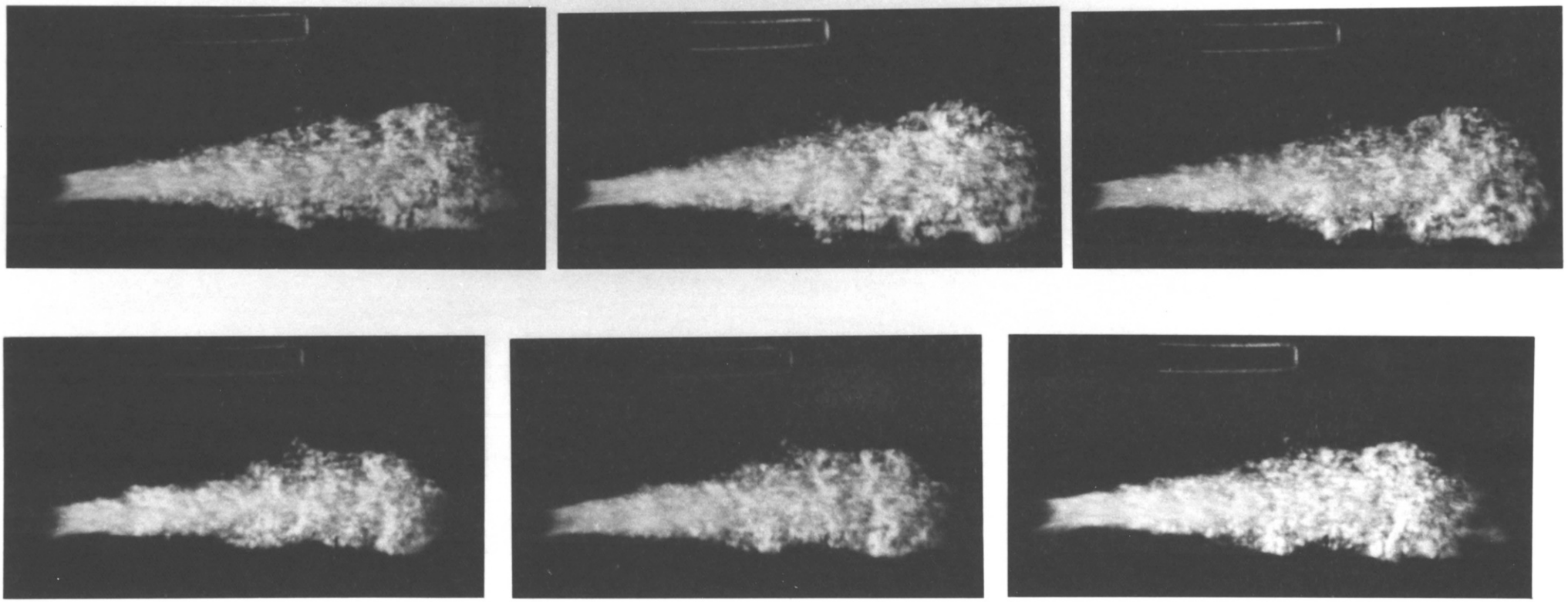


Figure 6.3 cont'd...

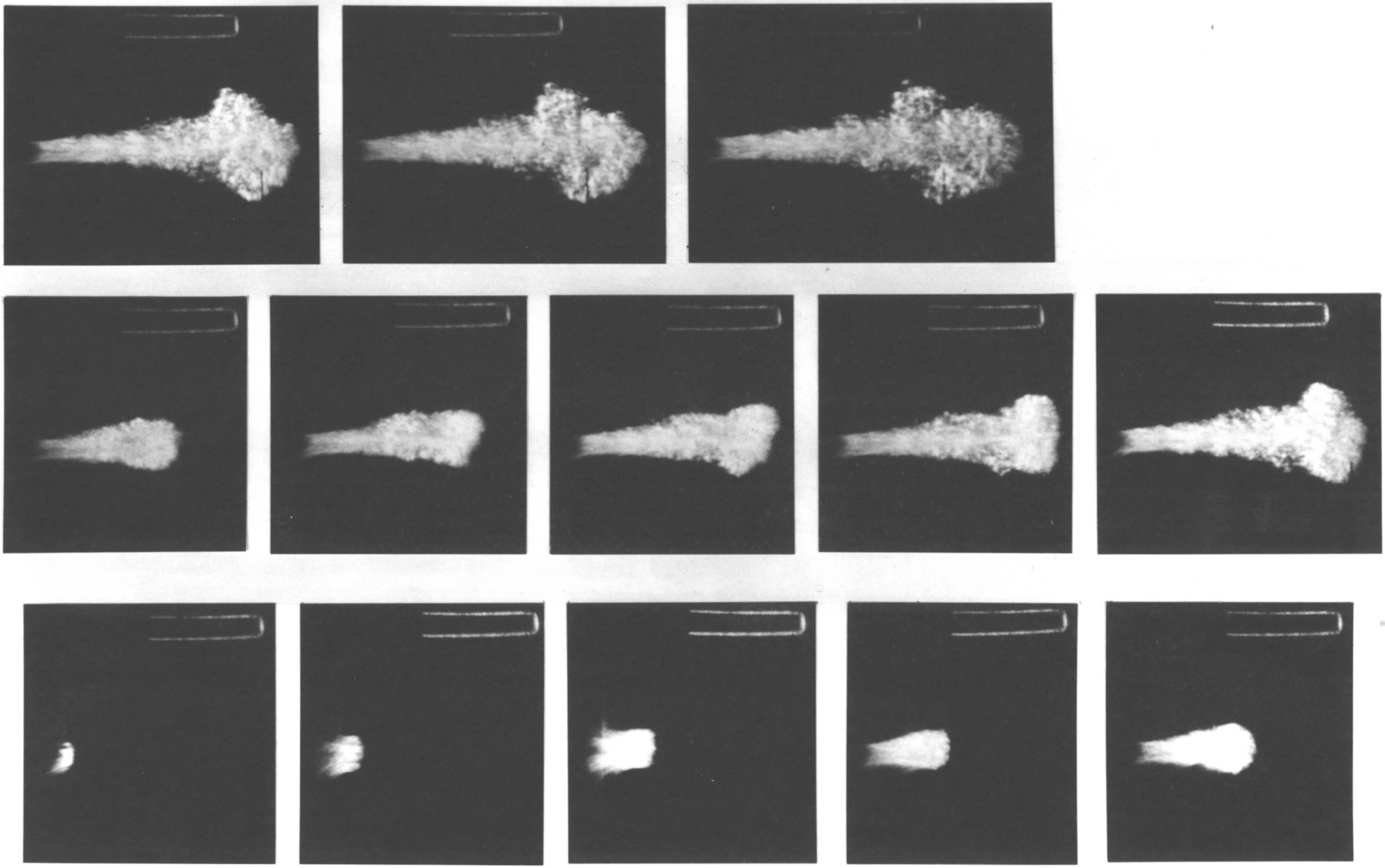
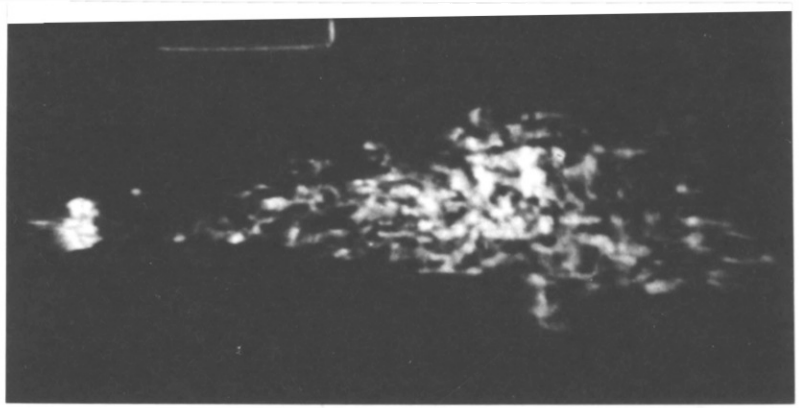
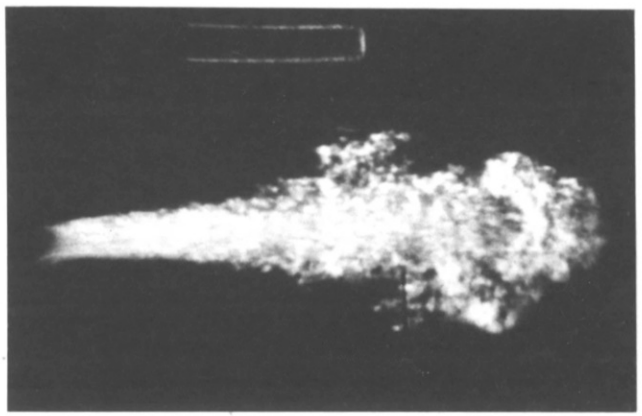
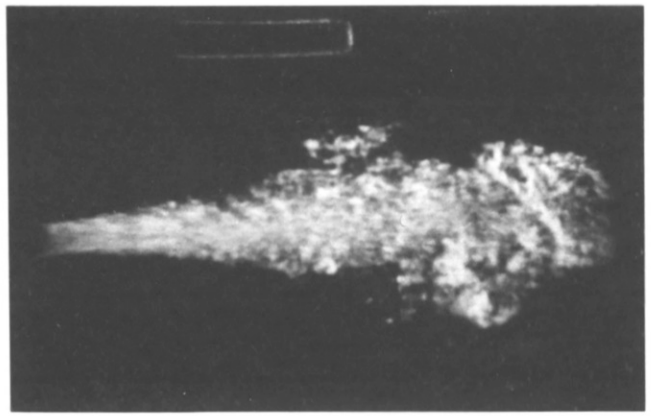
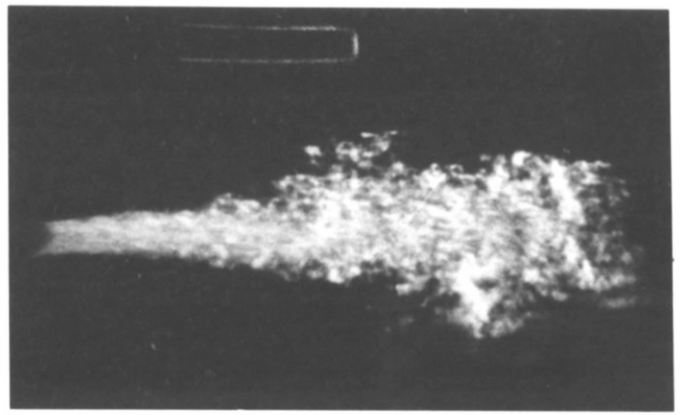


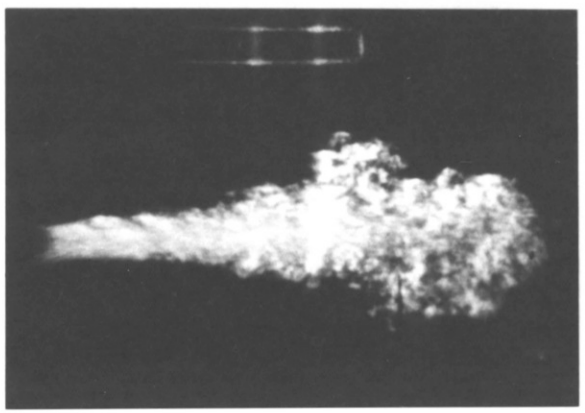
Figure 6.4 Second firing of a similar jet as in Figure 6.3. The last frame in this sequence is representative of the end time conditions as the jet approaches its "off" state

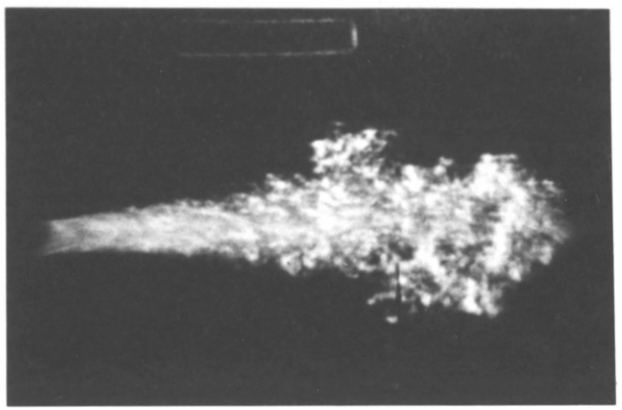












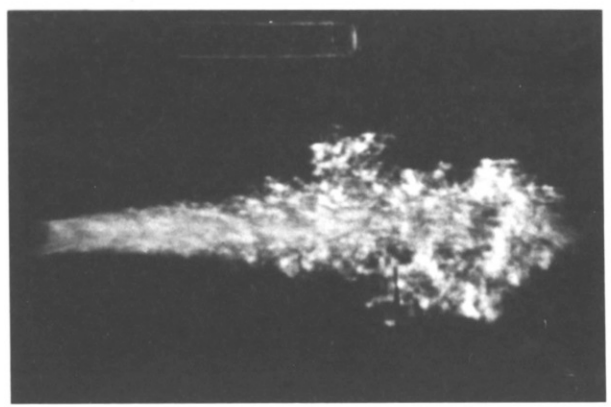
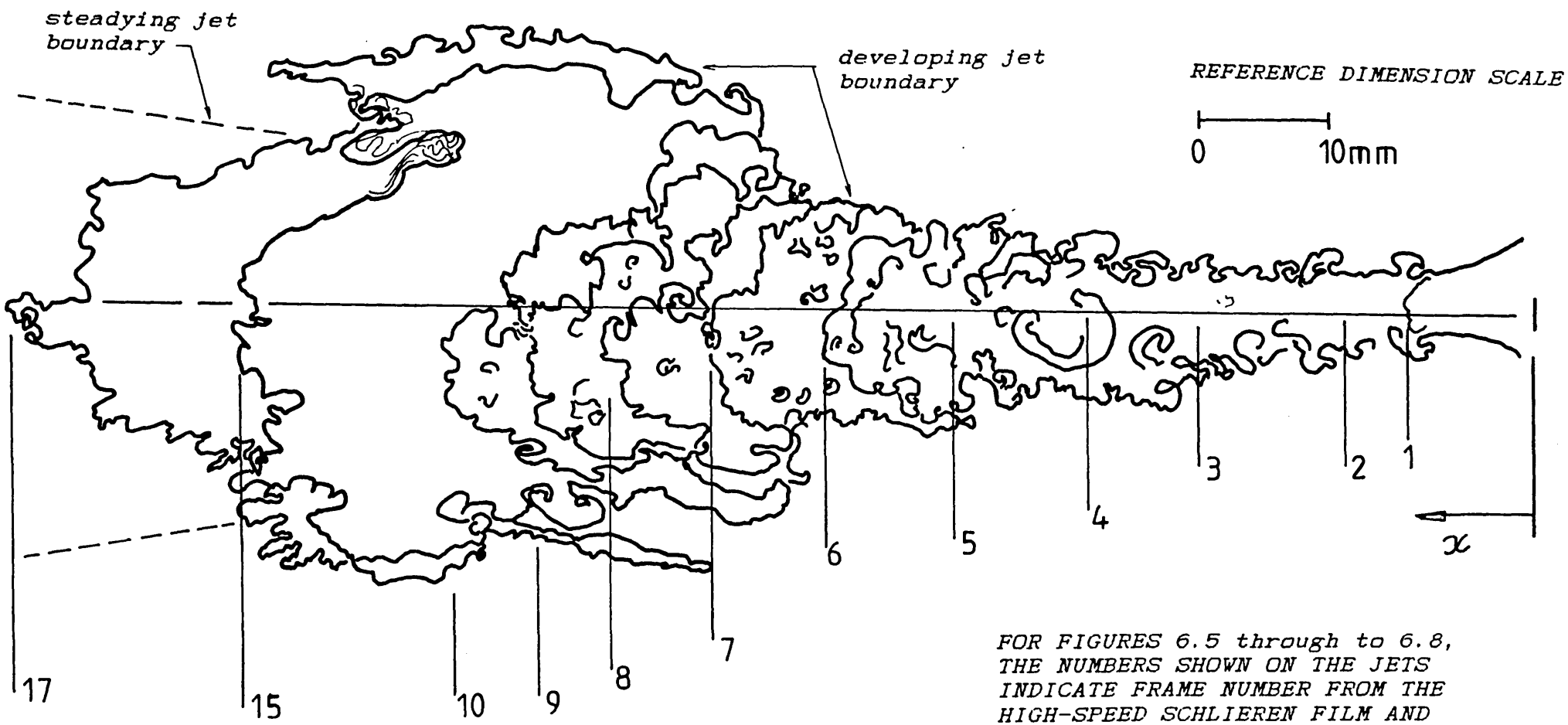


Figure 6.4 cont'd...



FOR FIGURES 6.5 through to 6.8, THE NUMBERS SHOWN ON THE JETS INDICATE FRAME NUMBER FROM THE HIGH-SPEED SCHLIEREN FILM AND ARE ALINGNED WITH THE SPATIAL POSITION OF MAXIMUM TIP PENETRATION.

FIGURE 6.5 FREON-12 JET FROM NOZZLE A, Uo=37.7 m/s

AT LOWER VALUES OF Uo, A MORE ORGANIZED STRUCTURE OF THE JET FRONT (AND LATERAL BOUNDARIES) RESULTS AND PARTICULARLY THE SYMMETRY OF THE HEAD VORTEX

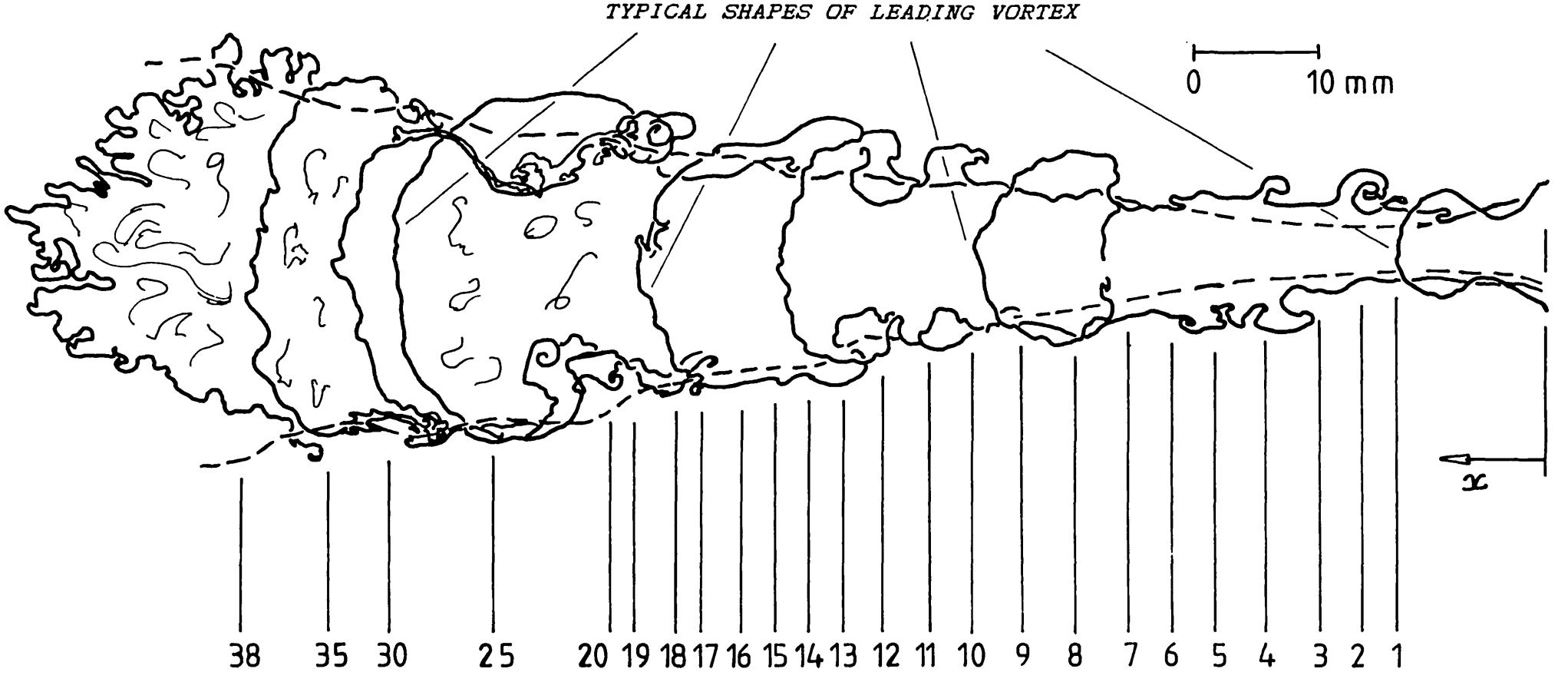


FIGURE 6.6(a) FREON-12 JET FROM NOZZLE B, Uo=19.2 m/s

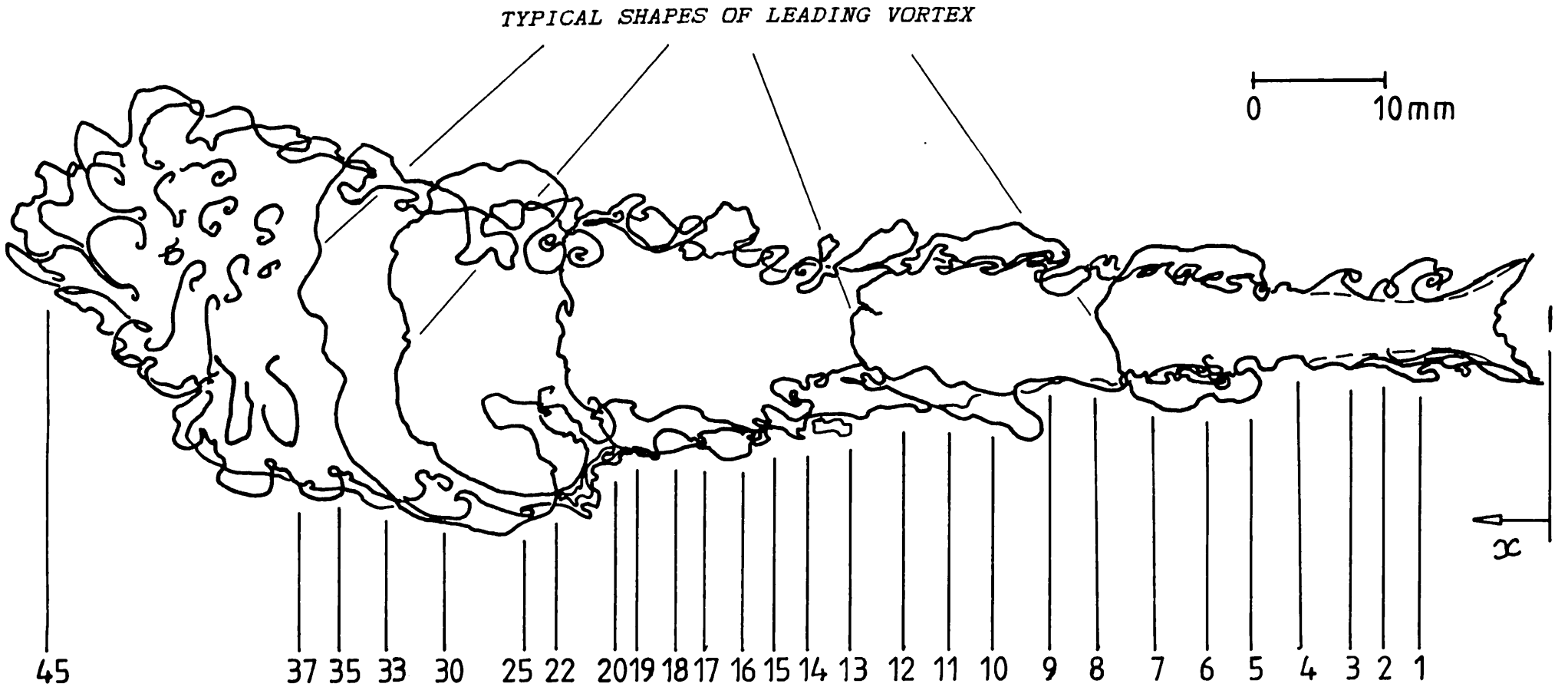


FIGURE 6.6(b) FREON-12 JET FROM NOZZLE B (second firing), Uo=19.2 m/s

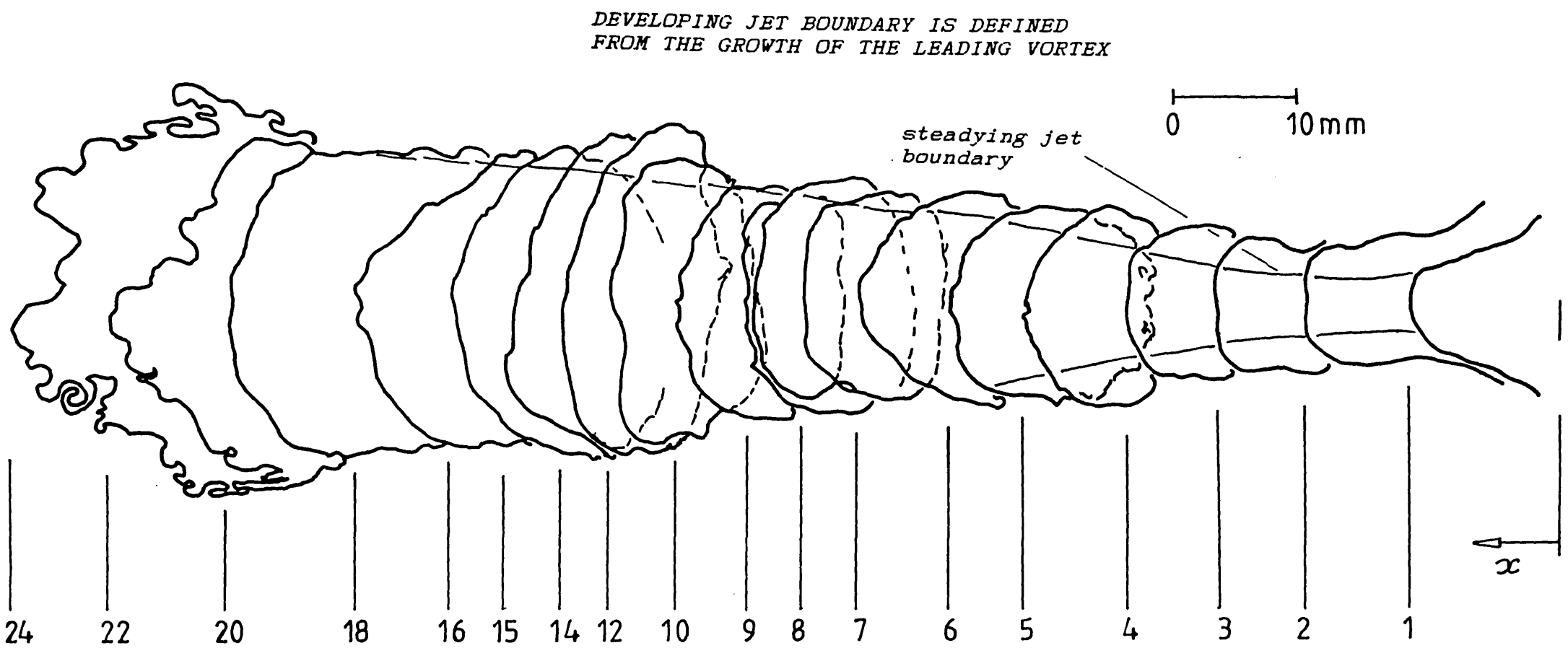


FIGURE 6.7(a) FREON-12 JET FROM NOZZLE B, Uo=30.9 m/s. THE FIGURE EMPHASIZES THE BOUNDARY AND GROWTH OF THE LEADING VORTEX AT DIFFERENT TIME INTERVALS OF 0.2 ms

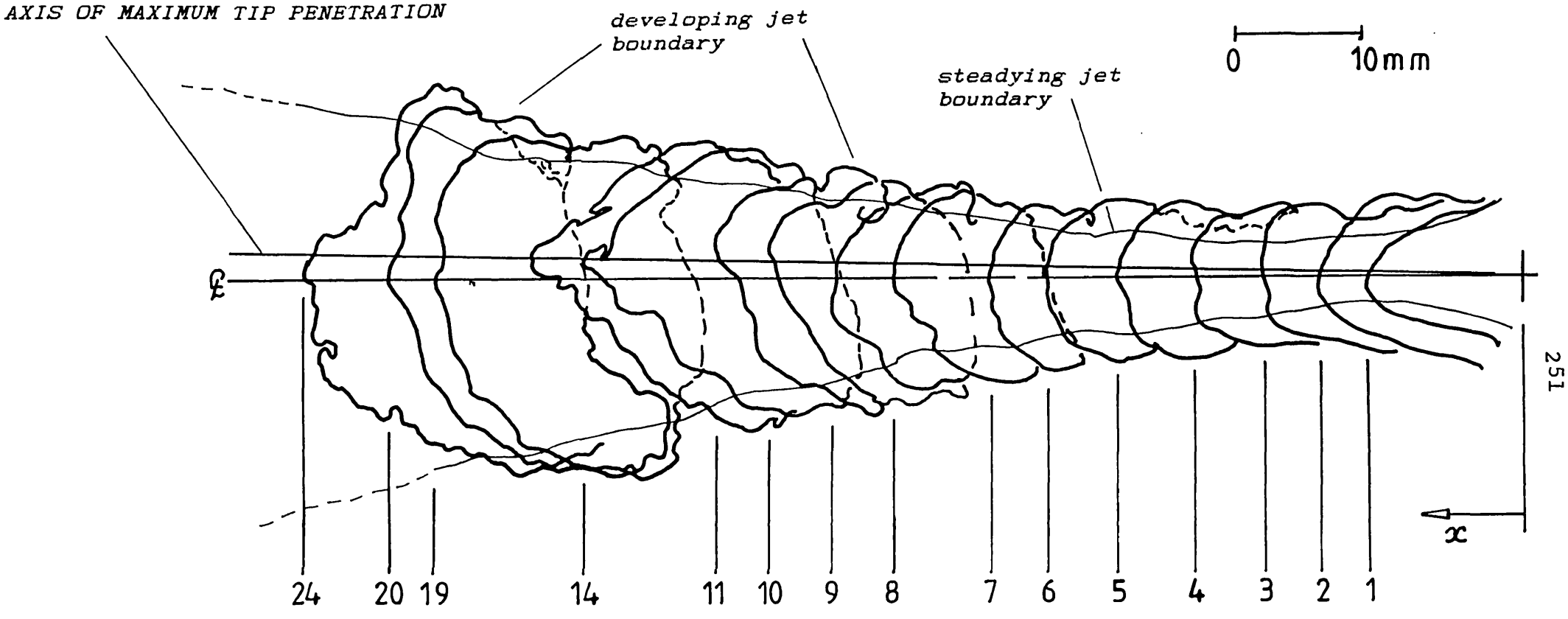


FIGURE 6.7(b) SIMILAR JET AS IN (a) , second firing

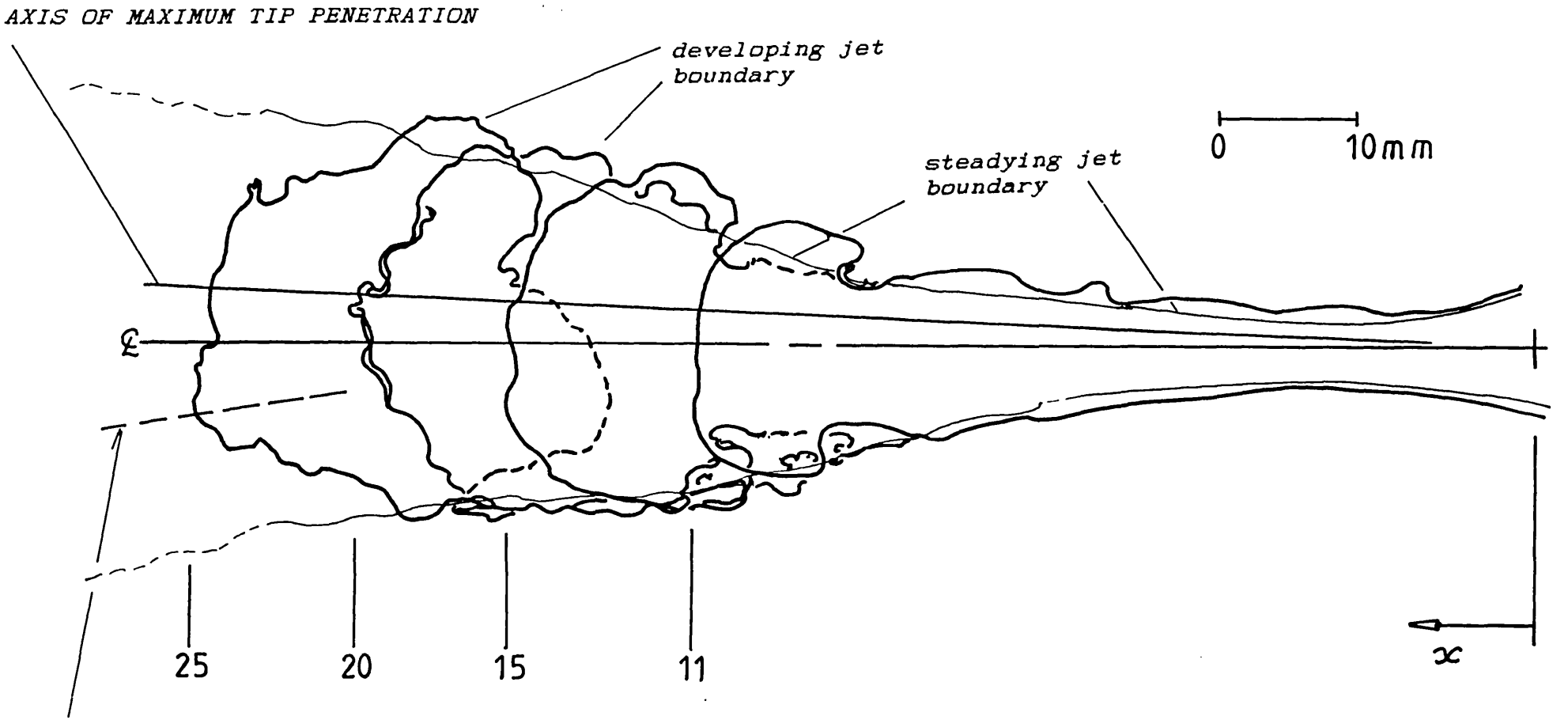


FIGURE 6.7(c) SIMILAR JET AS IN (a) and (b) (third firing) SHOWING VARIATION BETWEEN AXIS OF MAXIMUM PENETRATION AND THAT OF THE GEOMETRICAL CENTRELINE.

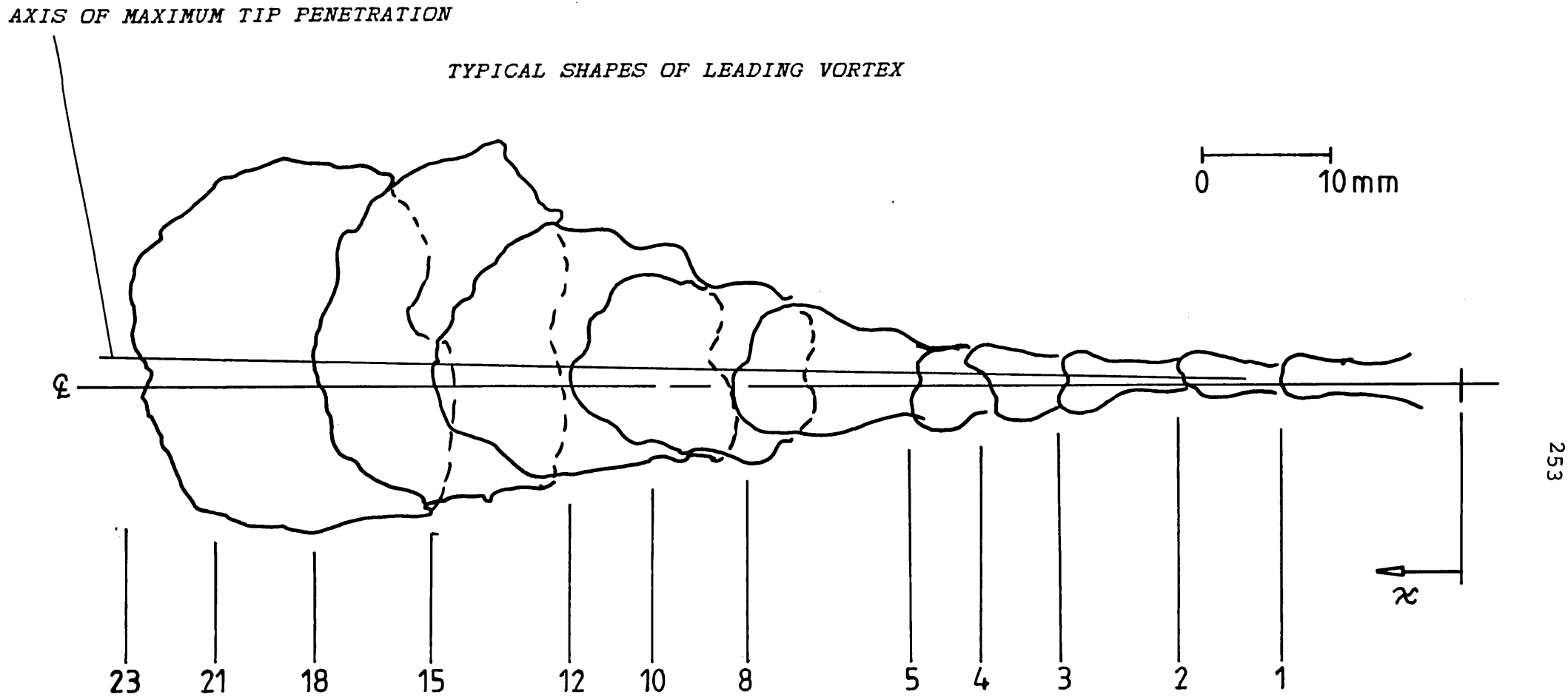


FIGURE 6.8 FREON-12 JET FROM NOZZLE C, Uo=60 m/s. TYPICAL LEADING VORTEX BOUNDARIES ARE SHOWN AND CAN BE COMPARED WITH RESULTS OF FIGURE 6.7

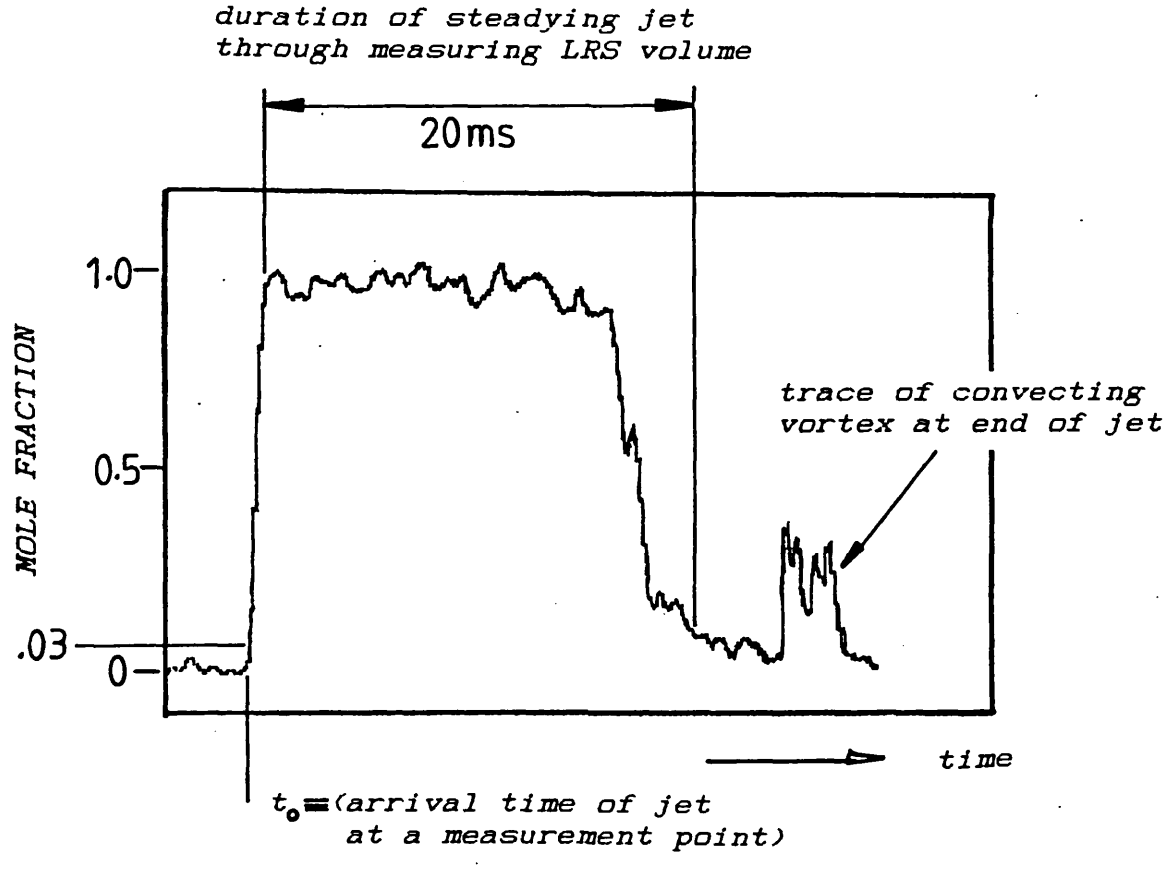


FIGURE 6.9 INSTANTANEOUS TRACE OF JET FLUID CONCENTRATION AT A MEASUREMENT POINT (x/d=1.5, r/d=0) USING LRS

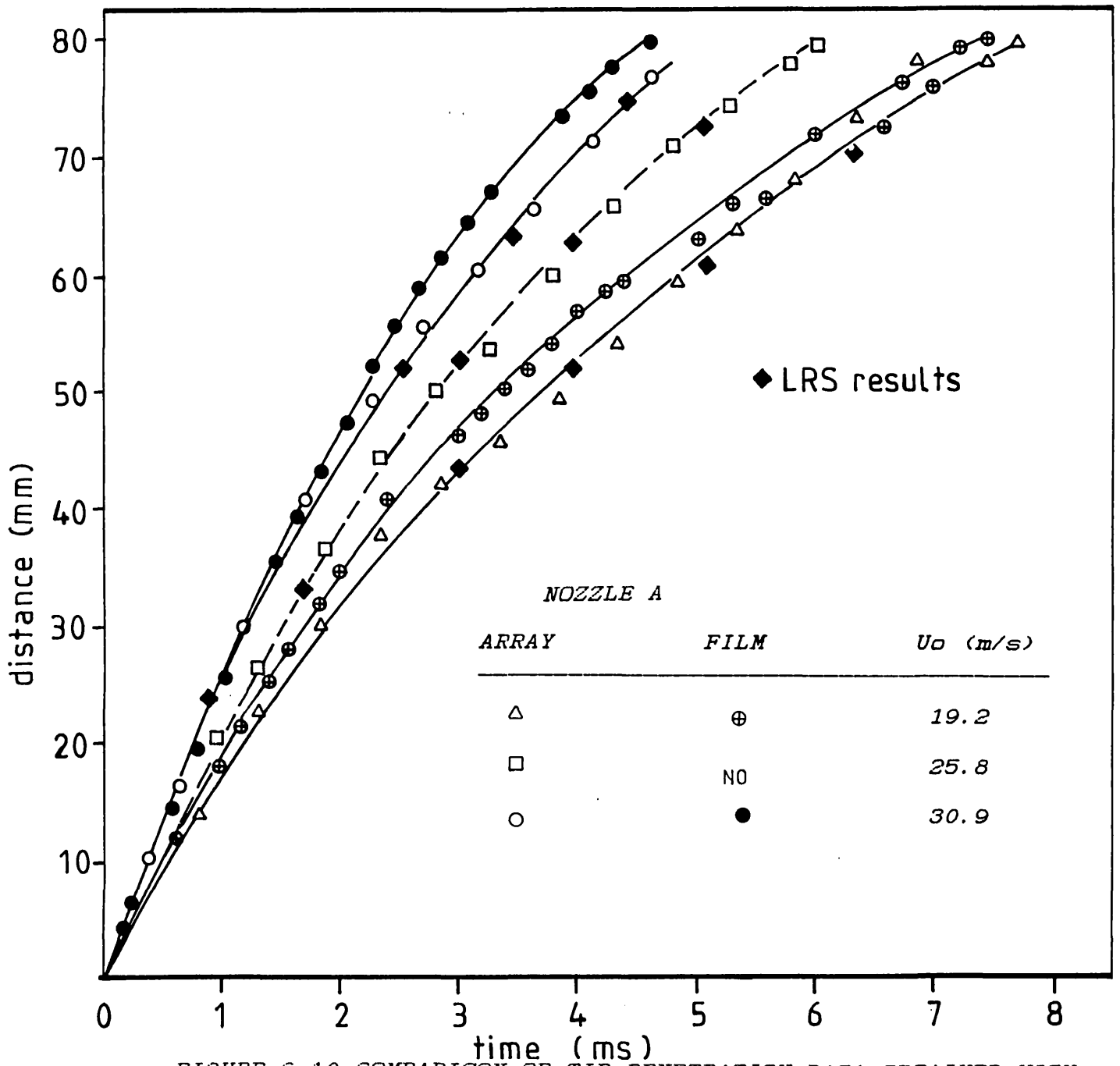


FIGURE 6.10 COMPARISON OF TIP PENETRATION DATA OBTAINED WITH THE PDA TECHNIQUE AND THOSE FROM THE LRS AND HIGH SPEED FILM (NOZZLE A, FREON-12)

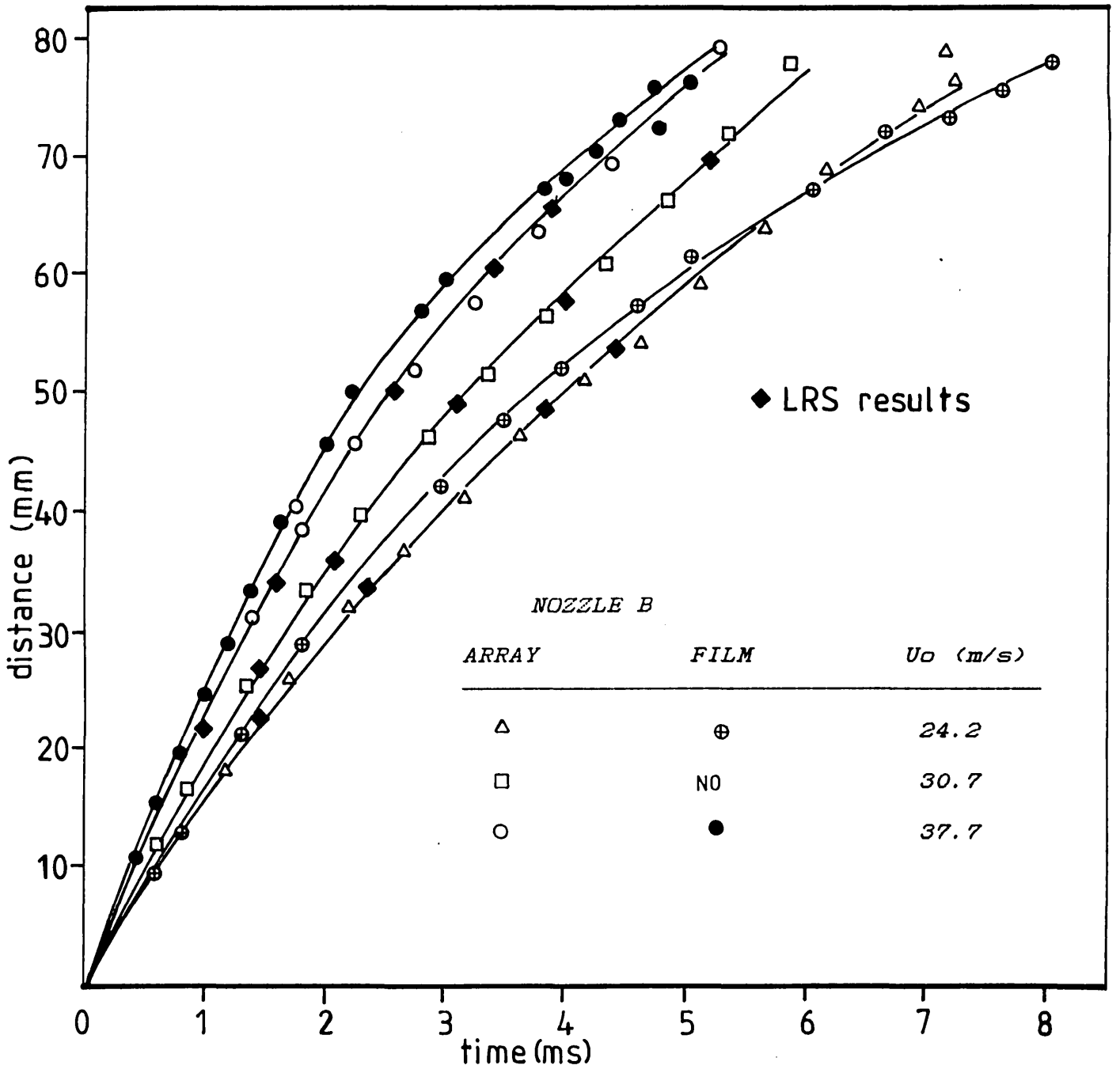


FIGURE 6.11 COMPARISON OF TIP PENETRATION DATA OBTAINED WITH THE FDA TECHNIQUE AND THOSE FROM THE LRS AND HIGH SPEED FILM (NOZZLE B, FREON-12)

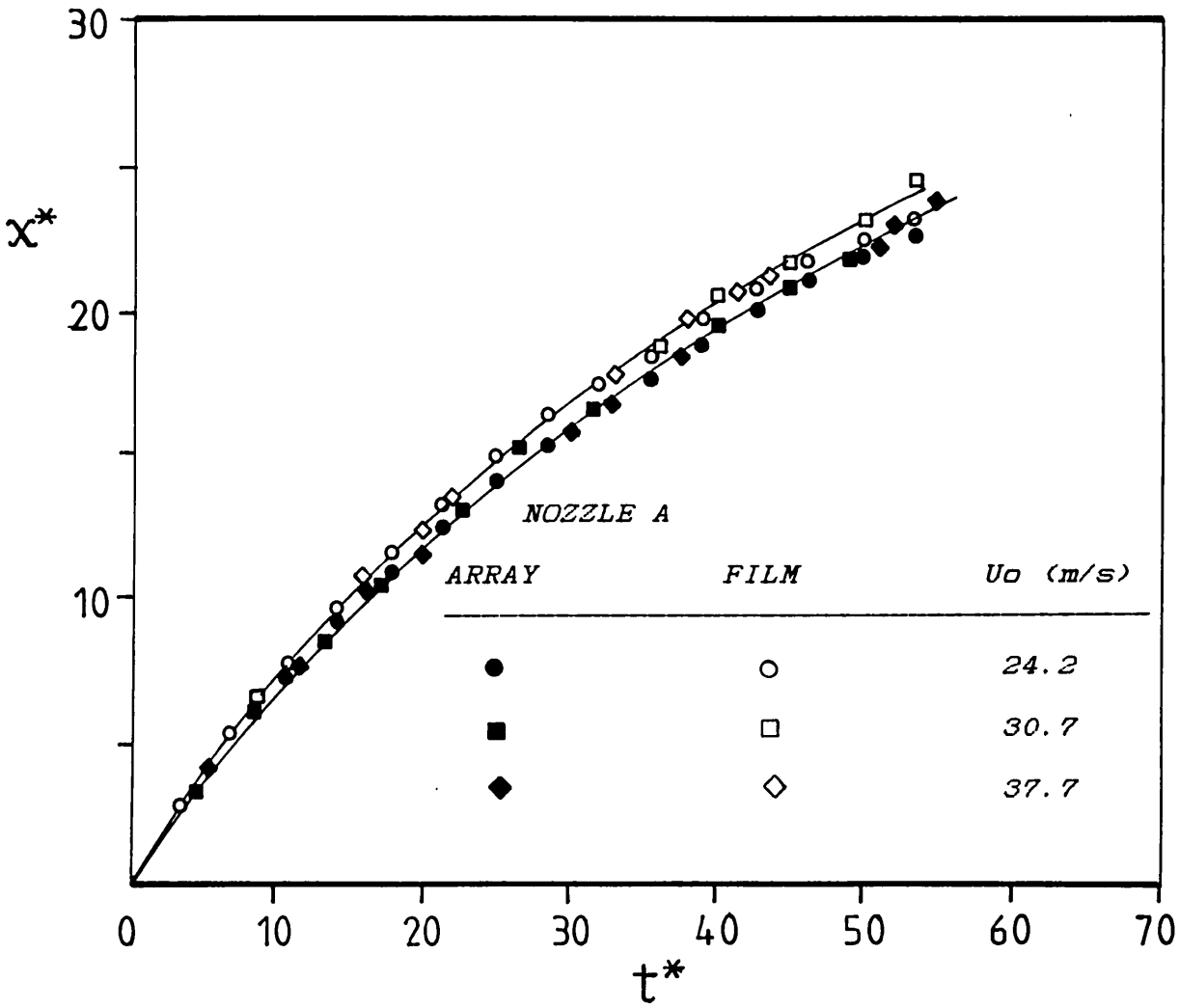


FIGURE 6.12 NORMALIZED PENETRATION DATA FOR JETS FROM NOZZLE A, FREON-12

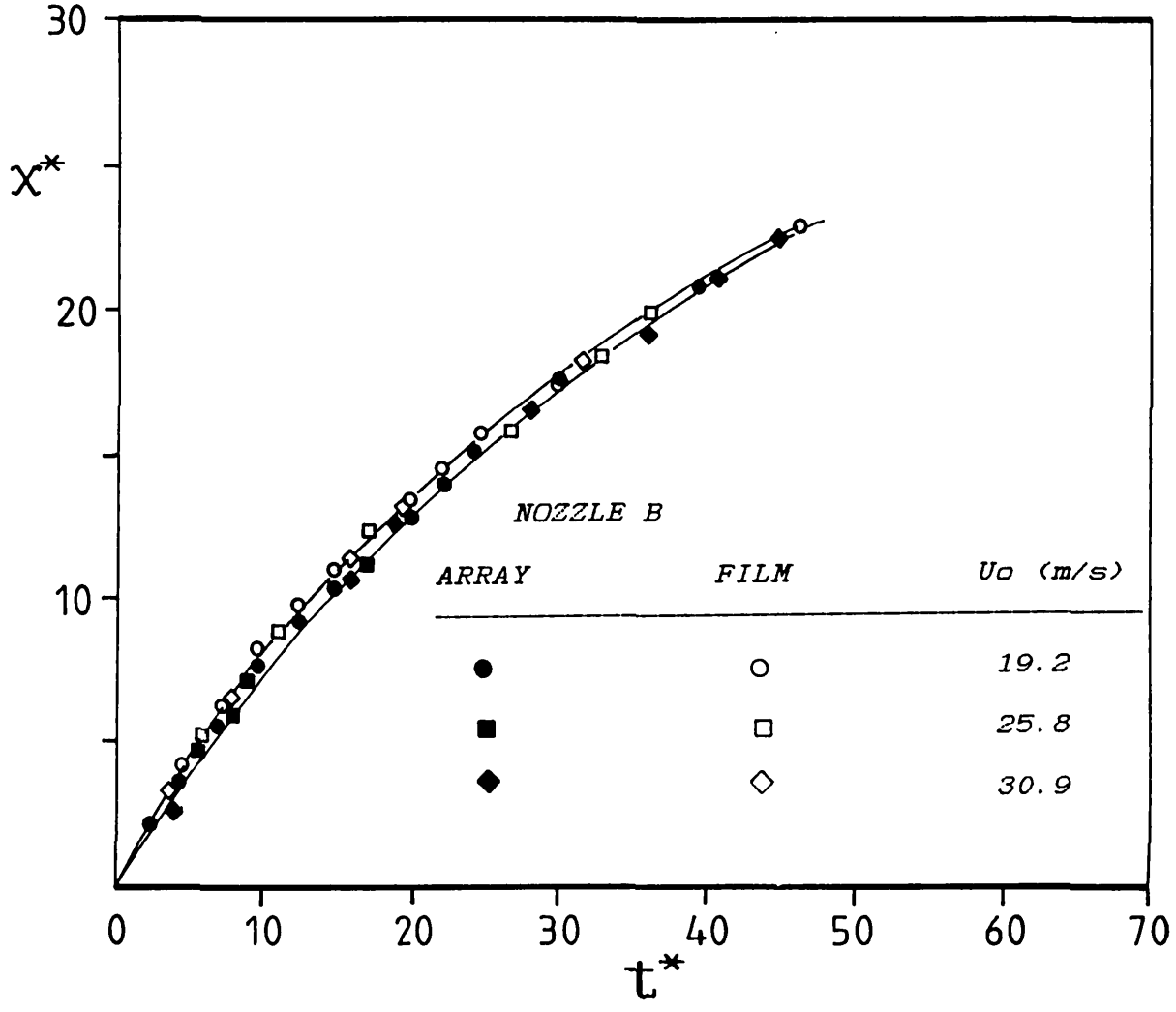


FIGURE 6.13 NORMALIZED PENETRATION DATA FOR JETS FROM NOZZLE B, FREON-12

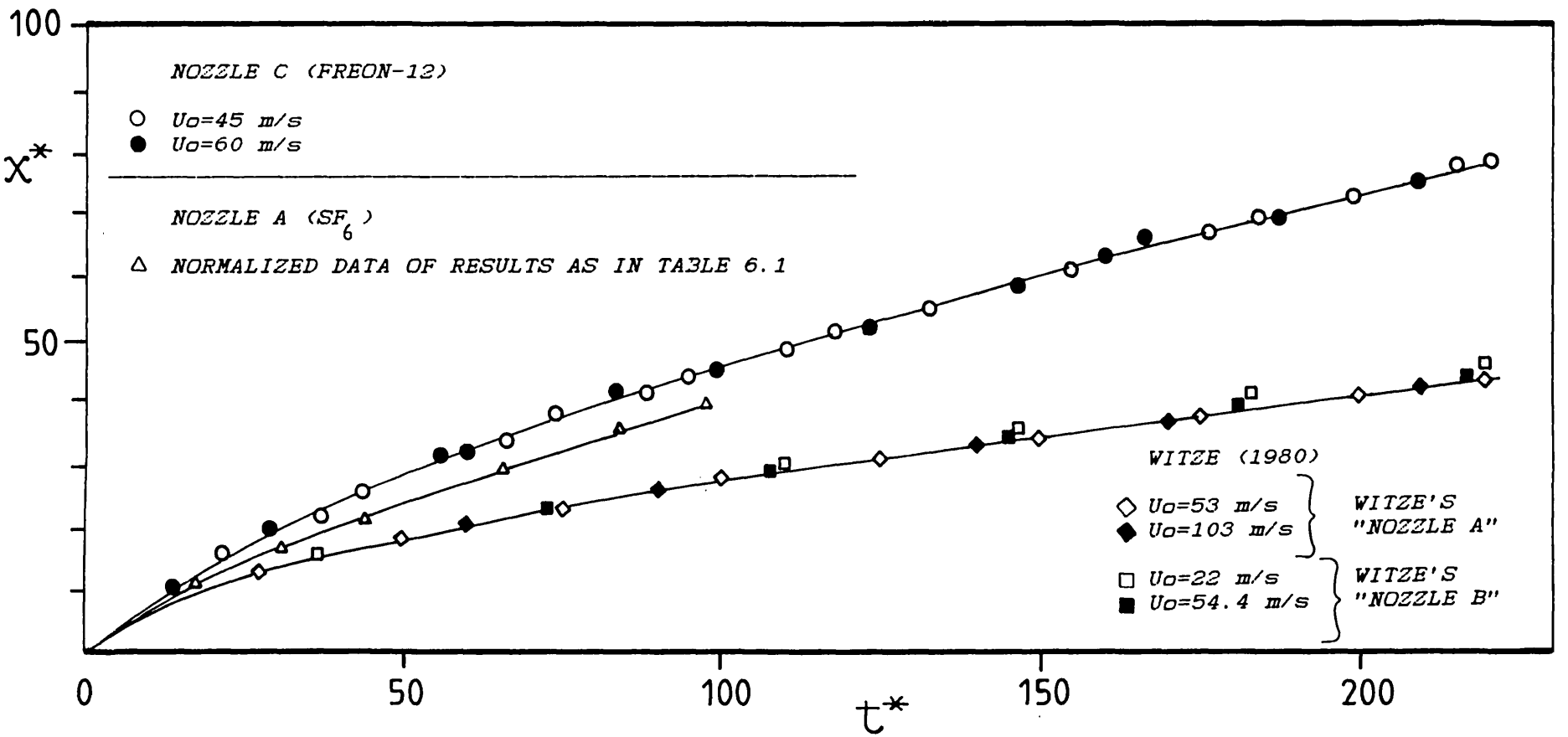


FIGURE 6.14 NORMALIZED PENETRATION DATA FOR JETS FROM NOZZLE C WITH FREON-12, NOZZLE A WITH SF_6 AND WITZE'S (1980) AIR JETS

CHAPTER 7 CLOSURE

7.1 FINDINGS AND CONCLUSIONS

The principal findings and conclusions which can be drawn from the work reported in this thesis are summarized by the following paragraphs:

1. Laser-induced Rayleigh light scattering has been developed for the study of free turbulent flows. The results show that measurements of mean concentration can be obtained with uncertainty of less than 2%. The measurement of time-dependent values of concentration can be obtained with similar accuracy and with frequency resolution of around 10KHz.

2. The results obtained in the steady jets of uniform and non-uniform density confirm the expected differences in the spread of mass and momentum and, in particular, show that the half-width of the scalar grows at a rate of 1.07 times that of velocity. The velocity and concentration fluctuations in the near field have the same dominant frequency with a corresponding Strouhal number which scale with the inverse of jet momentum.

3. The investigations of transient jets, used to simulate a fuel spray in direct-injection engines, show that:

(i) The scalar field spreads and decays more rapidly than momentum; this result is in agreement with that reported for steady jets

(ii) The spread and decay rates for the scalar and momentum have a marked dependence on nozzle geometry so that increase in the initial angle of the nozzle leads to greater spread and decay

rates. The design of the nozzle also affects the mass flow rates for a fixed injection time duration and backpressure. For nozzles of equal upstream diameter, the flow rates are affected by the square of the ratio of the upstream to exit diameter.

(iii) Impingement of the unsteady jet on a flat piston leads to faster mixing and more uniform mixtures than was obtained with a re-entrant or cylindrical bowl geometry where impingement of the jet is delayed due to the increased penetration distance.

(iv) The influence of pressure on the jet characteristics was determined. The compression process leads to increase in the in-cylinder air density and thus to increased rate of decay of jet momentum, equivalent to a reduction in density ratio between the jet and ambient, and consequently to more rapid spread, decay and mixing of the fuel jet. The findings suggest that compression ratio has a bigger effect on the mixing of air and fuel than nozzle or piston geometry.

(v) Swirl is important with all nozzles, piston geometries and jet densities investigated and, for example, the combination of swirl and a flat piston geometry resulted in the fastest mixing rates.

4. The investigation of transient-jet penetration revealed that the ratio of the penetration distance of the jet tip to the square root of time achieves an asymptotic value. This penetration parameter was found to be the same for laminar and turbulent transient jets but varies with nozzle geometry, jet fluid density and

exit velocity. It is constant for jets of different density but equal momentum flux.

5. The time constant parameter proposed by Witze (1980), defined as the ratio of nozzle radius to exit velocity, must involve the effective nozzle radius $r_e = r_o(\rho_j/\rho_a)^{\frac{1}{2}}$ to represent non-uniform transient jets.

7.2 SUGGESTIONS FOR FURTHER WORK

Suggestions for further work are made below and follow from the findings discussed above.

1. The instrumentation used to measure the concentration characteristics of a passive scalar can be combined with hot-wire or laser Doppler anemometers to provide measurements of correlations between velocity and the scalar. In the case of the hot-wire, the calibrations will be required to involve concentration and, with the laser anemometer the need for particles will provide a severe test of the software filter described in Chapter 2. The required development and testing is likely to be worth while since there are few measurements of the vector-scalar correlation and they are needed to help improve understanding of heat and mass transfer processes.

2. The measurements obtained in steady jets are confined to the near field so that it is desirable that they should be extended to the far field. The ability to measure vector-scalar correlations, proposed above, would allow the investigation of the influence of density throughout the jet to provide knowledge of the scalar flux and joint probability functions which, in turn, would benefit and allow better appraisal of assumptions currently made in calculation methods.

3. The techniques of this thesis, and the extension suggested in paragraph 1, should be used to investigate a wider range of unsteady jets. The present work has been confined to axisymmetric flows, with a limited range of injection characteristics. This range needs to be extended and the configurations expanded to include multiple jet flows and impinging arrangements as result with fuel sprays in direct-injection engines and impinging fuel and oxidizer jets.

APPENDIX A

A.1 Interpretation of LRS Signals

LRS detects the time-average of concentration fluctuations in the measurement volume as opposed to the density weighted average. Thus, for an instantaneous scalar property ϕ the volumetric time-average $\langle\phi\rangle$ is obtained which is different from the density-weighted (i.e. Favre-average) quantity $\langle\rho\phi\rangle$ and the result $\langle\rho\phi\rangle/\langle\rho\rangle$ is not equal to $\langle\phi\rangle$. The differences between time-averaged and density-weighted (Favre-average) results have been reported on by Libby (1976), Pope (1978), Bilger (1975) and Whitelaw (1984).

The relationship between the detected scattered light intensity I_s, absolute pressure P and temperature T of a multicomponent gas mixture is given by

$$I_s = \frac{KP}{T} \Sigma X_i \sigma_i \qquad , i = 1, \ldots m \qquad (A.1)$$

where X_i is the mole fraction (percent by volume) of the i^{th} species and σ_i the respective angular scattering cross-sections. The conservation of mass requires $\Sigma X_i = 1$. The constant K is empirically determined to account for optical efficiences and P/T is a measure of the total number density per unit volume, $N = \Sigma N_i$. The three cases which are of interest in connection with equation (A.1) are:

(i) isothermal, isobaric flow of variable composition

(ii) isothermal, non-isobaric flow of variable composition

(iii) non-isothermal, non-isobaric flow of variable composition

These three cases will be treated separately below in section A.3 with reference to the measurements which are

reported in the text of the thesis. In the remainder of this section and A.2, the general parameters of equation (A.1) are discussed.

Assuming isotropic molecules for a single gas of number density N, the scattering cross-section (i.e, angular cross-section) σ_A is given by (for scattered light observed at 90^o)

$$\sigma_A = \frac{4\pi^2(n-1)^2}{N^2\lambda^4} \tag{A.2}$$

where λ is the incident light wavelength and n the refractive index of the gas. Thus, assuming 100% optical efficiency and isotropic molecules a single component gas (with $N \equiv P/T$, the number density of scatterers), the scattered light intensity is

$$I_s = \sigma_A N I_o \tag{A.3}$$

where I_o is the incident light intensity (i.e. irradiance at the measurement control volume). Intensity as used here refers to the magnitude of the Poynting vector (i.e. the flux vector of electromagnetic energy) and has units of Power/Area; W/m^2 or, if referring to limited angular collection of light, W/sr. When the scatterers under consideration are anisotropic a correction to (A.2) is usually made in the form of

$$(\sigma_A)_a = \sigma_A\left(\frac{3}{3-4\rho^*}\right) \tag{A.4}$$

where ρ^* is the depolarization ratio and is small for most molecules but can be as large as 0.15. Cabannes (1921) was the first to account for the problem of depolarization (even for scattering from pure and clean gases) and proposed an anisotropy correction to Rayleigh's result. The determination of the depolarization factor $3(3-4\rho^*)^{-1}$ is very difficult to make and is considered in detail with respect

to measurements of Rayleigh scattering by George et al (1965), Rudder and Bach (1968), Fabelinskii (1968), Penney (1969) and Vriens and Adriaansz (1974). In Chapter 1 (sections 1 and 4) of Fabelinskii (1968) and in the article by Young (1981) a detailed account of the effects of anisotropy in Rayleigh scattering is given. In general, the correction factor in (A.4) can differ from unity and with few exceptions can be neglected; Muller-Dethlefsard and Weinberg (1979) report values.

That Rayleigh's result (A.3) is valid for N number density throughout a volume of space V follows from the assumption of independence. This assumption states that the light scattered by a large number of randomly distributed molecules in V sums to give the total scattered intensity I_s per unit incident intensity; the light scattered by the molecules is expected to be completely incoherent. The basis for this assumption and its justification are reported in Kerker (1969) and van de Hulst (1981). Lavan (1978) considers the further problem of the secondary scattering effects from N scatterer for arbitrarily shaped and small scattering volumes.

The assumption of independence is central (and essential) in order to account for the total scatter intensity I_s to be the sum of the scatter intensity of all the scatterer (molecules and particles) present in the probe control volume. The requirement for satisfying independence is that the scatterer be located at great distances from one another. We thus consider that each particle or molecule present in the scattering volume causes real scattering independent of all the others that are present. In a gas, statistical fluctuations of the molecular arrangements cause real scattering (see for example Barron (1982)). The assumption of independence thus implies that no coherent scattering results. The assumption further implies that for a volume containing N molecules, the intensity (and not the amplitude) of the total scattered light is the sum of the contribution from each of the molecules present in the observation volume.

As suggested by van de Hulst (1981) a distance of around 3 radii can be accepted as a sufficient condition for independence; see also Kerker (1968). For Rayleigh scattering, the expression for the scattered flux intensity (not considering anisotropic effects) is (Kerker (1968)),

$$I = I_o \frac{16\pi^4 a^6}{r^2\lambda^4} \left(\frac{n^2-1}{n^2+2}\right)^2 \tag{A.5}$$

and is the definition for the case of an incident beam perpendicularly polarized with respect to the scattering plane. For N scatterer contained in a probe control volume V under the assumption of independence,

$$I = \frac{NI_o 9\pi^2 V^2}{r^2\lambda^4} \left(\frac{n^2-1}{n^2+2}\right)^2 \tag{A.6}$$

where n is the relative refractive index, λ the wavelength of the incident beam, r the distance to the light scatter detector and I_o the incident beam intensity. Clearly the larger the scatterer the more intense is the scattering as I is proportional to the sixth power of the scatterer characteristic size (i.e. from V^2).

The number density N is that of the whole gas given by $N = \Sigma N_i$, where N_i is the number density of the i^{th} species. Considering only a single species from the relationship between mass m, volume V and density ρ (ρ = m/V) the number density is thus $N = \rho/m$; m is the mass per molecule. From the equation of state for an ideal gas PV = RT, where T is the absolute temperature and R the universal gas constant defined by $R=k(MW)/m$ where MW is the molecular weight and k a constant, the number density can thus be found from

$$N = \rho/m = \frac{P}{Tk} \qquad (A.6)$$

The molecular mass m is related to the molecular weight by $MW = 16m/m_o$ where m_o is the mass of an atom of oxygen ($m_o = 2.657 \times 10^{-23}$g) and $16/m_o$ is known as Loschmidt's number N_L (= 6.023×10^{23}). Noting that $N_L \times V = N_o$ (note, when $V=1cm^3$ for STP conditions N_o is also referred to as Avogadro's number) then making the appropriate substitutions, one obtains from equations (A.1) and (A.3)

$$I_s = I_o(N_o P/RT).K'\Sigma X_i \sigma_i \qquad (A.7)$$

with K' defining the optical efficiency and, as suggested by Pitts and Kashiwagi (1984), K' can be estimated from

$$K' = n_L n_c \varepsilon l \Omega \qquad (A.8)$$

where,

n_L = optical transmission coefficient between the laser and observation volume

n_c = optical transmission coefficient between the observation volume and the detector (photomultiplier)

ε = quantum efficiency of photomultiplier

Ω = solid angle (steradians) over which scattered light is collected, $\Omega = \Delta S/r^2$, ΔS is taken as the collecting lens area and r as its focal length

l = length of the observed volume

We note that it is often reported that the value of Loschmidt's number is that associated with computing Avogadro's number and in fact the value $6.023 \times 10^{23} cm^{-1}$ is also referred

to as Avagadro's number which is only true, clearly, when the number of molecules being considered are those in one cubic centimeter of gas at STP, thus from V = RT/P (for standard T and P) one finds $6.023 \times 10^{23}/(RT/P) = 2.687 \times 10^{19} cm^{-1}$ and it is this value which, conversely, is referred to in the literature as Loschmidt's (or "a Loschmidt") number. Loschmidt's number is $N_L = 16/m_o = 6.023 \times 10^{23}$/mol and the number 2.687×10^{19} is the number density of molecules of gas (any gas) at STP conditions and it is incorrect therefore to refer to this latter value as Loschmidt's number.

If in equation (A.7) I_o is replaced with I_L (i.e. the laser output in photons/s), then the photon rate to be expected from LRS experiments can be estimated from

$$\dot{N}_p = n_L n_c \varepsilon l \Omega I_L N \Sigma X_i \sigma_i \quad \text{(photons/s)} \qquad \text{(A.9)}$$

with values for the parameters typical to our experimental conditions given by

$n_L = .71$
$n_c = .45$
$\varepsilon = .14$
$l = .10cm$
$\Omega = .071$ sr
$N = 2.546 \times 10^{19}/cm^3$ (P = 1 atm T = 15°C)

Considering the laser as an ideal source emitting photons, the number of photons over a time t are

$$(N_p)_L = \left(\frac{P\lambda}{hc}\right) t \qquad \text{(A.10)}$$

where λ is the laser operating wavelength, h is Planck's constant ($h = 6.626 \times 10^{-34}$ J-S), c the speed of light ($c = 2.997 \times 10^{8}$ m/s) and P the laser output power J/s ≡ Watts.

The photon rate (per second) at the wavelengths used in most of the experiments here is $I_L = (N_p)_L/t = P\lambda/hc$ or,

$$K'I_L = 7.804 \times 10^{14} \times P, \quad \lambda = 4880\text{Å}$$

and $$K'I_L = 8.229 \times 10^{14} \times P, \quad \lambda = 5145\text{Å}$$

A.2 Evaluation of Angular Scattering Cross-sections

We note that different definitions arise at times in connection with scattering cross-sections (i.e. Rayleigh scattering cross-section, differential scattering cross-section and angular cross-section). The definition of these different scattering cross-sections are given below.

Rayleigh (volume) scattering cross-section

$$R = \frac{32\pi^3}{3N\lambda^3}(n-1)^2 \tag{A.11}$$

Differential scattering cross-ection

$$\frac{d\sigma}{d\Omega} = \sigma_o \frac{1}{2}(1 + \cos^2\theta) \tag{A.12}$$

Angular cross-section

$$\sigma_o = \frac{4\pi^2}{N^2\lambda^4}(n-1)^2 \tag{A.13}$$

where N is number density, n the refractive index of the gas and λ the incident light wavelength. For the differential scattering cross-section, $d\sigma$ represents the scattered energy per unit solid angle and $d\Omega$ the incident energy per unit area, $d\sigma/d\Omega$ is their ratio. Consistent use of any of (A.11), (A.12),

or (A.13), however, can allow for the ratio obtained between two gases to be conveniently used to define the intensity ratio

$$\frac{I_A}{I_B} = \left(\frac{n_A - 1}{n_B - 1}\right)^2 = \frac{\sigma_A}{\sigma_B} \qquad \text{(A.14)}$$

where I_A and I_B are the detected scattered light intensities as result in an experiment; subscripts A and B denote two different gases. The predicted ratio A.14 can be used to ensure against systematic errors being introduced into measurements by checking that the detected scattering light intensity ratio does not deviate by more than a small amount from the value expected (A.14); accuracy in agreement will depend on purity of the gas and values used for n.

For an assumed composition for air of 79% N_2 and 21% O_2, the value for σ_o can be found using

$$(\sigma_o)_{air} = 0.79(\sigma_o)_{N_2} + 0.21(\sigma_o)_{O_2}$$

and results in the same value for (σ_o) air as for when a value of $n_{air} = 1.000292$ is used; this approach to estimating σ_o is useful when considering gas mixtures, in particular, where the refractive index may not be known. The value of several refractive indices are provided in Table A.1 and a summary of calculation results for σ_o given in Table A.2. Results of measurement and prediction for Rayleigh scattering experiments of scattering cross-sections and gas refractive indices for conditions of variable pressure, temperature and composition have been summarized, for example, in the work of Theimer (1964), Horvath (1967), Shardanand and Rao (1977), Bilger and Dibble (1982) and Namer and Schefer (1985).

TABLE A.1

Summary of some useful refractive indices

O_2	-	1.000271
N_2	-	1.000296
A_r	-	1.000280
H_e	-	1.000036
CH_4	-	1.000444
CCl_2F_2	-	1.00133
Air	-	1.000292

TABLE A.2

Summary of calculations for σ_o

$$\sigma_o = \frac{4\pi^2}{N^2}\left(\frac{n-1}{\lambda^4}\right)^2, \quad N = 2.687 \times 10^{19}\,cm^{-3}$$

gas	$(n-1)^2$	λ (Å)	$\sigma_o(\lambda)$ $(\frac{cm}{sr})$	$\sigma_o/(\sigma_o)_{air}$
He	1.2960×10^{-4}	4880	1.2495×10^{-24}	0.015
		5145	1.0113×10^{-29}	
Air	8.5264×10^{-8}	4880	8.2207×10^{-28}	1.00
		5145	6.6535×10^{-28}	
CH_4	1.9714×10^{-7}	4880	1.9007×10^{-27}	2.31
		5145	1.5384×10^{-27}	
Freon-12	1.7689×10^{-6}	4880	1.7055×10^{-26}	20.74
		5145	1.3803×10^{-26}	
N_2	8.7616×10^{-8}	4880	8.4475×10^{-28}	1.0276
		5145	6.8370×10^{-28}	
O_2	7.3441×10^{-8}	4880	7.0808×10^{-28}	0.8613
		5145	5.7309×10^{-28}	
Air (N_2+O_2)		4880	8.1605×10^{-28}	1.01
		5145	6.6047×10^{-28}	

Note: For $\lambda = 4880$ Å

$$\sigma_o(\lambda) = 9.6415113 \times 10^{-21}\,(n-1)^2$$

For $\lambda = 5145$ Å

$$\sigma_o(\lambda) = 7.8033823 \times 10^{-21}\,(n-1)^2$$

A.3 Experiments Using LRS

(i) isothermal, isobaric flow of variable composition (measurements reported in Chapters 2, 3, 4 and 6)

For constant pressure and constant temperature flow of variable composition, the LRS signal varies directly (and is linearly proportional) to the species mole fraction. Because Rayleigh scattering is non species specific, experiments aiming to detect and quantify turbulent mixing (via measurements of concentration) can only be accomplished with binary gas mixtures and not with mixtures having more components. For a two species system consisting of the components A and B (for which the scattering cross-sections are different), determination of the Rayleigh scattered intensity (I_R) for one of the pure species allows the instantaneous mole fraction X_A for that species to be determined from the linear result,

$$X_A = \frac{I_g}{I_A} \tag{A.15}$$

where the ratio I_g / I_A defines X_A; the mole fraction of the species A. I_A is the detected scatter intensity of a pure sample of gas A and I_g the scattered instantaneous intensity of the mixture consisting of unknown quantities of A and B; I_A should be the intensity for the gas having the largest scattering cross-section and it is assumed in (A.15) that the scatter intensity for component B in a pure state is referenced with respect to a zero output level (see below A.4.2).

(ii) isothermal, non-isobaric flow of variable composition (measurements reported in Chapter 5)

Based on the theory for Rayleigh scattering, the scattered light intensity should linearly increase with increase in pressure. Thus for scattering from a fixed composition gas at atmospheric pressure, say, the scattered

intensity at any other absolute pressure (for isothermal conditions) becomes

$$I_A(P) = P.I_A \tag{A.16}$$

For a mixture with components A and B (with $\sigma_A > \sigma_B$) the instantaneous mole fraction at any pressure can be related to the equivalent mole fraction at some fixed reference pressure from equations (A.15) and (A.16) by

$$X_A = \frac{I_g(P)/|P \pm P_o|}{I_A(P_o)} \tag{A.17}$$

where $I_g(P)$ is the instantaneous scatter intensity of the gas mixture at any arbitrary (absolute) pressure P and $I_A(P_o)$ the scatter intensity at a fixed reference pressure P_o. Taking P_o as the atmospheric pressure,

$$X_A = \frac{I_g(P)/P}{I_A(P_o)} \tag{A.18}$$

The result (A.18) indicates that if the LRS intensity is measured simultaneously with the total absolute pressure of the flow field, then LRS can be used to determine species mole fraction concentration by detecting the intensity $I_g(P)$ and correcting it for the effect of pressure by dividing through by P. That this result is valid can be confirmed by calibrations made at constant temperature using a pressure vessel having optical access and gases of known mixture concentrations (air and Freon-12 in the present case). The results of such calibrations are shown in Figure A.1; similar calibrations are reported for numerous gases by Shardanand and Rao (1977) and for propane by Dyer (1979). Clearly, for a fixed gas composition, it is possible, conversely, to determine total mixture pressure using LRS as indicated by the result (A.16)

(iii) non-isothermal, non-isobaric flow of variable composition (measurements reported in Chapter 5)

For the case of a non-isothermal, non-isobaric flow of variable composition the application of LRS can be limited. In summary, the simultaneous measurement of the instantaneous absolute pressure and temperature of the flow at the probe volume would have to be made along with the detected scatter light intensity. In terms of the effects of temperature, the scattered light intensity is hyperbolic in the temperature (Equation (A.7)). When pressure, temperature and concentration simultaneously differ, the mixture number density N will differ simultaneously along with variations in the refractive index. The problem of the simultaneous effects of pressure and temperature on the scattering cross-section (via the influence of number density and refractive index) has been considered in detail by Penndorf (1957) and a general analysis is given in Chapter 4 of Fabelinskii (1968). Namer and Schefer (1985) have reported on the effect of temperature on LRS signal interpretation noting, in particular, the simultaneous influence exerted on the scattered light intensity by the scattering cross-section dependence on temperature for refractive index variation and number density; pressure as a constant.

The measurements reported in Chapter 5 of this thesis (in the model engine with a compression ratio of 6.7) are influenced by temperature, pressure and mixture composition. For a fixed composition at any instant of time, the scatter intensity ratio relative to some reference state (o) (and at the same composition) is, under the assumption of ideal gas behaviour,

$$\frac{I(t)}{I_o} = \left(\frac{P(t)}{P_o}\right)\left(\frac{T_o}{T(t)}\right)\left(\frac{\sigma(t)}{\sigma_o}\right) \qquad (A.19)$$

The scattering cross-section ratio is simply,

$$\frac{\sigma(t)}{\sigma_o} = \left(\frac{n(t)-1}{n_o-1}\right)^2 = \left\{\left(\frac{1+\alpha T_o}{1+\alpha T}\right)\frac{P}{P_o}\right\}^2 \qquad (A.20)$$

where n(t) is the instantaneous refractive index of the gas, T the absolute temperature, P the absolute pressure and α is a constant. In the case of the compressing engine, the total pressure is determined by direct measurement with a transducer mounted on the engine cylinder and the temperature is determined from the assumption of a polytropic process for which

$$\frac{T(t)}{T_o} = \left(\frac{P_o}{P(t)}\right)^{\frac{1-m}{m}} \tag{A.21}$$

where m is the polytropic exponent, determined from calibration measurements of P(t) in the engine with the intake gas to the engine controlled to be at fixed concentrations (for the case of the measurements in Chapter 5 , using: SF_6, Freon, and air). From equations (A.19), (A.20) and (A.21) the following sequence is followed for calibration:

(a) The scattered light intensity for a known mixture concentration is measured, $I_g(t)$

(b) The measured values $I_g(t)$ are normalized by I_o, the scattered light intensity of the gas with the largest angular scattering cross-section, σ.

(c) The temperature T(t) is determined from (A.21) from measurements of P(t), and, P(t) and T(t) then used in computing $\sigma(t)/\sigma_o$, equation (A.20).

(d) The result of (c) provides the theoretical prediction of the right hand side of equation (A.19). The results were comapred to those actually measured ((a) and (b)) and excellent agreement is obtained (Figure A.2) between measured ratios of intensity and those predicted by (A.19).

The results outlined in (a) - (d) provide a direct method by which to correct the measured scattered intensities (as result from unknown mixture concentrations in the engine flow) in order to determine the mole fraction concentrations without having to directly measure T(t); clearly, the accuracy of

the quantified mole fraction X_i will be less than if the actual temperature were known; the modelling of the temperature by (A.21), however, showed in the present work to be adequate as the results of Figure A.2 suggest, in particular, along the time interval typical for the in-cycle measurements (an estiate of the errors are given in Chapter 5). Smith (1978) and Rambach, Dibble and Hollenbach (1979) have similarly considered measurements with LRS involving change in temperature and species concentration.

A.4 Uncertainty, Sources of Noise and Data Analysis

A.4.1 Uncertainty and Noise

The uncertainties which can arise in measurements with LRS are due to fluctuations in laser output, noise introduced into the signal by the use of a photomultiplier, optical interference due to the presence of walls if the flow is enclosed and overall noise from the instrumentation used for signal processing. The problem of noise from photomultipliers and the subsequent uncertainty introduced into measurements of light intensity have been accounted for in detail by Robben (1971, 1976), Becker (1976), Shaughnessy and Morton (1977), Wright (1982a, b), Barton (1982), Oliver (1982) and Ruck and Durst (1982). Pitts and Kashiwagi (1984) have considered the specific problems in connection with LRS. From analysis as indicated by these authors, the largest uncertainty in LRS measurements results from electronic shot noise; assuming that there is no particle scatter interference in the detected signal. Under the assumption of Poisson statistics, the measure of relative uncertainty in LRS experiments can be estimated from

$$\frac{\mathrm{var}(\eta)^{\frac{1}{2}}}{\eta} = 1/(\dot{N}_p \Delta t)^{\frac{1}{2}} \qquad \text{(A.22)}$$

where η is the number of detected photons during a time period Δt and $\dot{N}_p$ is taken as an estimate of η as given by equation A.9. The term Δt is taken to be the effective time period

related in turn to the cut-off frequency Δf_{co} by $(\Delta t)_{eff} = 1/2\Delta f_{co}$, thus the relative uncertainty (r.v.) can be found from

$$r.v. = (2\Delta f_{co}/\dot{N}_p)^{\frac{1}{2}} \qquad (A.23)$$

and the signal-to-noise ratio (SNR) is equal to $1/r.v. = (\dot{N}_p/2\Delta f_{co})^{\frac{1}{2}}$. Using the results of equation (A.9) and (A.10) and those of Table A.2, a summary of the relative uncertainty for LRS from pure air, SF_6 and Freon-12 gas (and the corresponding SNR's) is provided in Table A.3 for conditions representative of those of the experiments reported in this thesis.

TABLE A.3

Estimates of Uncertainties for Typical LRS Instrumentation Conditions

		SNR		r.v.%	
F_{co}	KHz	4880	5145	4880	5145
Air					
	2	64	59	1.56	1.69
	5	40	37	2.50	2.70
SF_6					
	2	167	154	0.60	0.65
	5	106	97	0.94	1.03
Freon-12					
	2	291	268	0.34	0.37
	5	184	170	0.54	0.59

NB: values shown are for a laser power of 1W and for atmospheric conditions of pressure and temperature. When scattering results for conditions at other than atmospheric, the SNR changes by $(P/T)^{\frac{1}{2}}$; similarly for different laser power levels P_L, the change in SNR can be accounted for by a factor $(P_L)^{\frac{1}{2}}$. The value of refractive index used in determining σ_o must take account of any change in pressure and temperature (see equation (A.13) and section A.3 (iii).

The values of relative uncertainty r.v. indicated in Table A.3, in particular, for the scattering from SF_6 gas and Freon-12, are on average about 1% lower than when compared to estimates made empirically by detecting scatter intensities (averaged over long times) from the potential core of a jet where, theoretically, fluctuations in the gas concentration should be zero. There, the ratio of signal rms to signal mean indicated values of about 1.8% for Freon-12 and about 2.12% for scattering from SF_6 for the case when Δf_{co} = 5KHz and λ = 5145Å. The uncertainties introduced into LRS measurements by optical sources are considered in detail in Appendix B, where it is shown that the optical noise to LRS needs to be determined for individual applications and, at present, the optical noise effects (and methods of deconvolution) cannot be generalized.

A.4.2 Data Analysis

Mean Concentration

The mean mole fraction concentration $\bar{X}$ is determined directly from the ratio of mean scattered intensities $\bar{I}$ from

$$\bar{X}_A = \frac{\bar{I}_g - \bar{I}_B}{\bar{I}_A - \bar{I}_B} \tag{A.24}$$

where $\bar{X}_A$ is the mean mole fraction (i.e. percent by volume) of species A, $\bar{I}_A$ is the mean Rayleigh scattering intensity from a pure sample of species A and $\bar{I}_B$ that from species B. The term $\bar{I}_g$ is the measured mean intensity of the flow at the particular measurement location. The mean intensities are found from the ensemble

$$\bar{I} = \frac{1}{n} \sum_{i=1}^{n} I_i \tag{A.25}$$

Similarly, the instantaneous mole fraction can be found from

$$X_A = \frac{I_g - \bar{I}_B}{\bar{I}_A - \bar{I}_B} \qquad (A.26)$$

where now I_g is an instantaneous (discrete) signal value. The values of X_A given by equation A.26 are used to compute the probability density distributions of X_A. If the output of the instrumentation is arranged to set $\bar{I}_B = 0$, clearly

$$\bar{X}_A = \bar{I}_g/\bar{I}_A, \text{ or } X_A = I_g/\bar{I}_A \qquad (A.27)$$

The difficulty in setting an accurate zero level for I_B, however, makes the use of (A.24) and (A.26) more reliable although computations using (A.27) are faster.

Higher Moments of Concentration

The shot noise associated with measurements of the Rayleigh scattered light intensities can lead to large errors in the calculated values of higher moments of the concentration field (i.e. the variance, skewness and kurtosis) when the noise levels are comparable to intensity changes in the Rayleigh scattered light due to concentration fluctuations. Birch et al (1978) have reported on the use of a method proposed by Pike (1969) to statistically compensate for the effects of shot noise allowing for separation of the actual moments of the concentration field from the noise. Birch et al (1978) applied Pike's method to results obtained with Raman spectroscopy and Pitts and Kashiwagi (1984) have adopted it to measurements using LRS; Haumann and Leipertz (1984) have also used this method for measurements using

Rayleigh scattering with a photon correlator.

Briefly, the results of Pike (1969) state that the moments of the photon number distribution are identical to the factorial moments of the detected photon distribution. Letting N_p be the photoncount collected during the time Δt, the r^{th} factorial moment $\mu'(r)$ for N_p is

$$(\mu'_{(r)})_{pc} = \frac{1}{n} \sum_{i=1}^{n} (N_p)_i^{(r)} \tag{A.28}$$

where the subscript pc refers to the photoncount distribution and $N_p^{(r)} = N_p!/(N_p-r)!$. Denoting $(\mu')_{pf}$ as the photonfield moments, the higher moments are found by converting these to central moments through

$$(\mu_r)_{pf} = \sum_{j=1}^{r} (-1)^j \binom{r}{j} (\mu'_{r-j})_{pf} (\mu'_1)^j_{pf} \tag{A.29}$$

Having obtained the central moments (A.29), the higher moments are found by normalizing (A.29) by

$$(\mu_r)_A = \frac{(\mu_r)_{pf}}{(\bar{I}_A - \bar{I}_B)} \tag{A.30}$$

and this is to include only contributions from the scattering in the measurement volume. Defining rms, skewness and kurtosis, as is usual, these are

$$X'_A = \frac{\sqrt{(\mu_2)_A}}{\bar{I}_A - \bar{I}_B} \qquad \text{(rms)} \tag{A.31}$$

$$S_A = \frac{(\mu_3)_A}{(\mu_2)_A^{3/2}} \qquad \text{(skewness)} \tag{A.32}$$

$$K_A = \frac{(\mu_4)_A}{(\mu_2)_A^2} \qquad \text{(kurtosis)} \qquad \text{(A.33)}$$

A perfect Gaussian distribution is defined when S = 0 and K = 3.

To apply the above results, the values of N_p (equation A.28) are determined by finding a conversion factor to multiply the Rayleigh scattered intensities detected in an experment; a specific example is provided below.

For the assumption that the detection of photons by the photomultiplier is a Poisson process,

$$\frac{\sigma}{\bar{I}_R} = \frac{\sqrt{N_P}}{N_P} \qquad \text{(A.34)}$$

where $\bar{I}_R$ is the mean Rayleigh scattered signal intensity and σ the signal variance. Consider two gases A and B and with the scattering cross-section of the gas A greater than that of gas B. The Rayleigh scatter contribution of gas A is,

$$\bar{I}_R = \bar{I}_A - \bar{I}_B \qquad \text{(A.35)}$$

and the requirement now is to find a conversion factor, C_f, such that $C_f \times \bar{I}_R = N_p$; from equation (A.34) N_p is clearly $(\sigma/\bar{I})^{-2}$.

Using typical values from an experiment as given by

$$\bar{I}_A = 409.6 \quad , \quad \bar{I}_B = 2.42 \quad , \quad \sigma_A = 8.2$$

The mean Rayleigh scatter intensity of gas A is (A.35)

$$\bar{I}_R = 409.6 - 2.42$$

$$= 407.18$$

thus,

$$\left(\frac{\sigma}{\bar{I}_R}\right)_A = \frac{8.2}{407.18} = 0.020$$

and the predicted count from (A.34) is,

$$N_p = \frac{1}{(.02)^2} = 2465.7$$

The conversion factor required for multiplying the detected signal intensities is therefore

$$C_f = \frac{2465.7}{407.18} = 6.05$$

Thus for an experiment where I_R, the instantaneous Rayleigh scatter intensity is determined, the values N_p are defined from $N_p \equiv (\bar{I}_R/\sigma^2) I_R$.

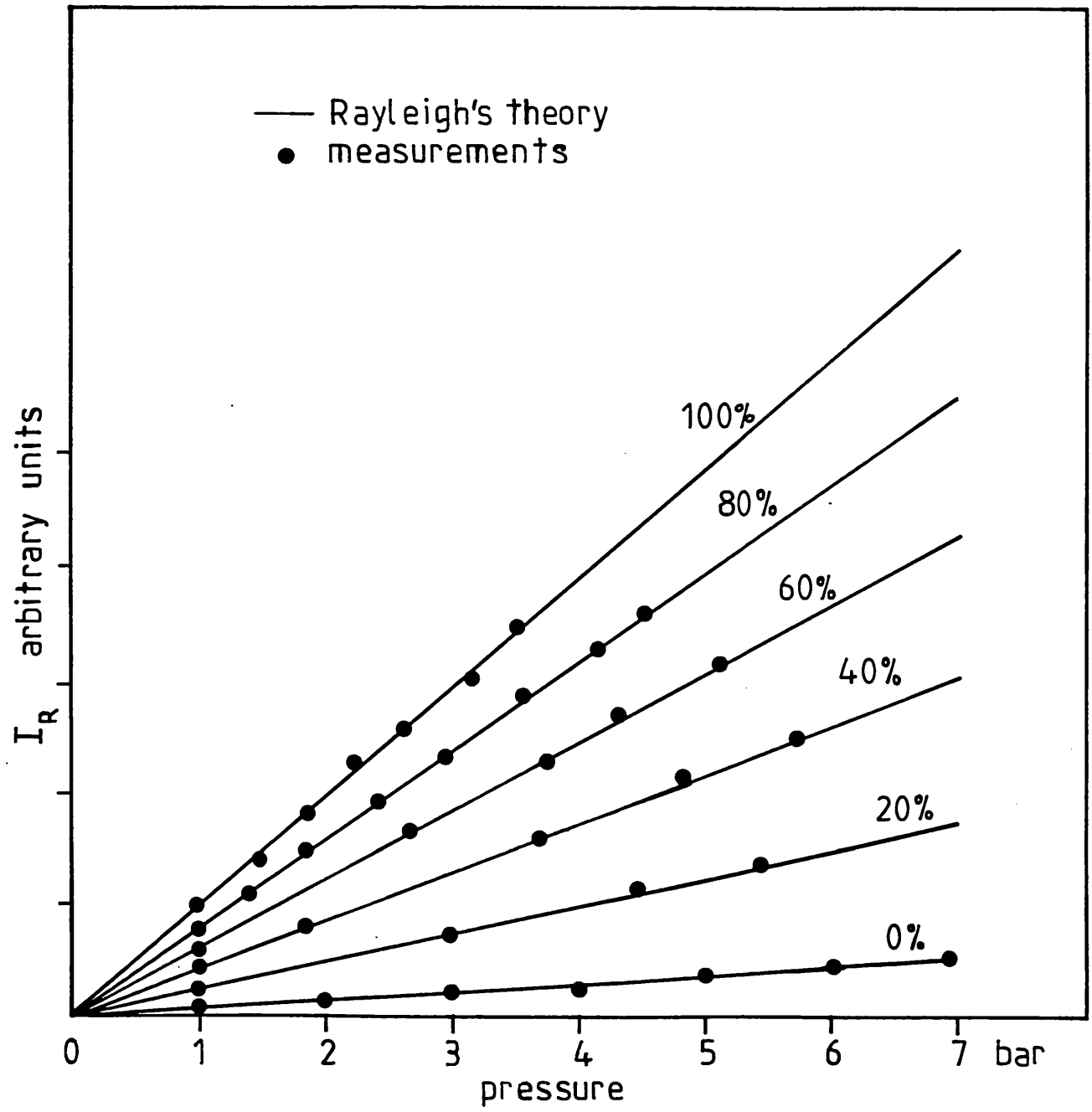


FIGURE A.1 RAYLEIGH SCATTERED LIGHT INTENSITY AS INFLUENCED BY PRESSURE FOR DIFFERENT FREON-12 CONCENTRATION (%) IN AIR (isothermal conditions)

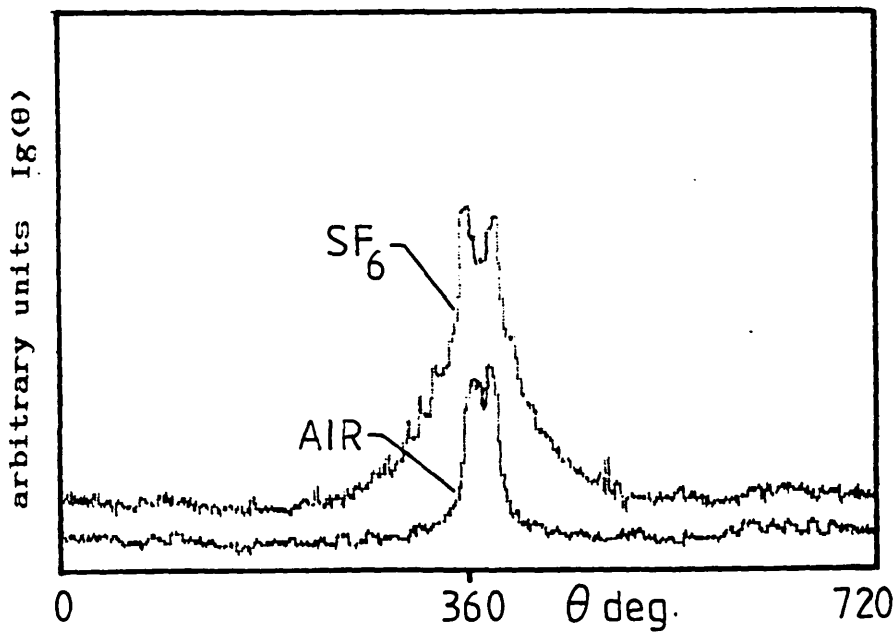


FIGURE A.2(a) RAYLEIGH SCATTERED LIGHT INTENSITIES DURING AN ENGINE CYCLE (6.7 CR ENGINE) OBTAINED WITH INTAKE OF PURE SF AND PURE AIR

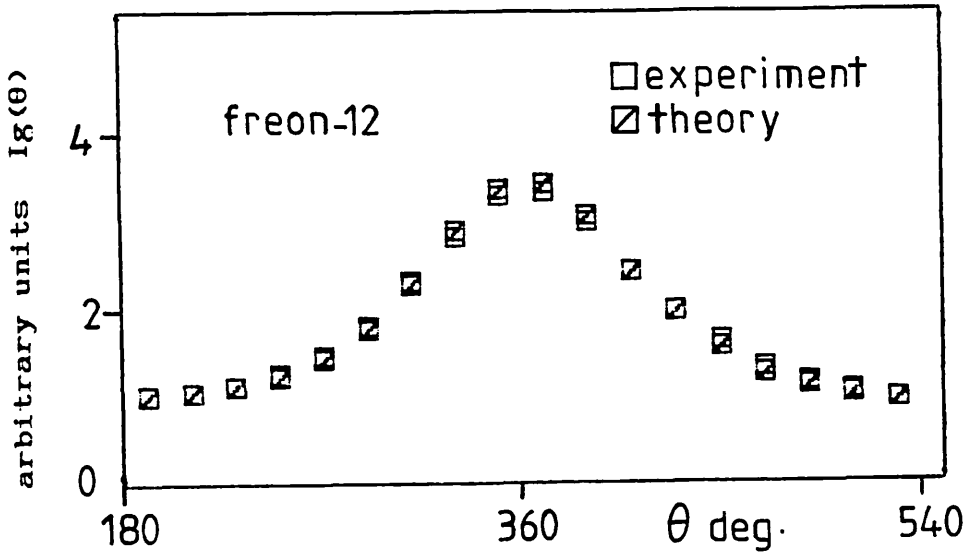


FIGURE A.2(b) COMPARISON OF EXPERIMENT AND RAYLEIGHS THEORY FOR THE SCATTERED LIGHT INTENSITY DURING AN ENGINE CYCLE INTERVAL (3.5 CR ENGINE AND WITH FREON-12 AS INTAKE GAS). THE THEORETICAL RESULT WAS OBTAINED WITH EQUATION A.19 AND WITH THE ASSUMPTION THAT $\sigma(t)/\sigma=1$; ie, negligible temperature and pressure influence on refractive index

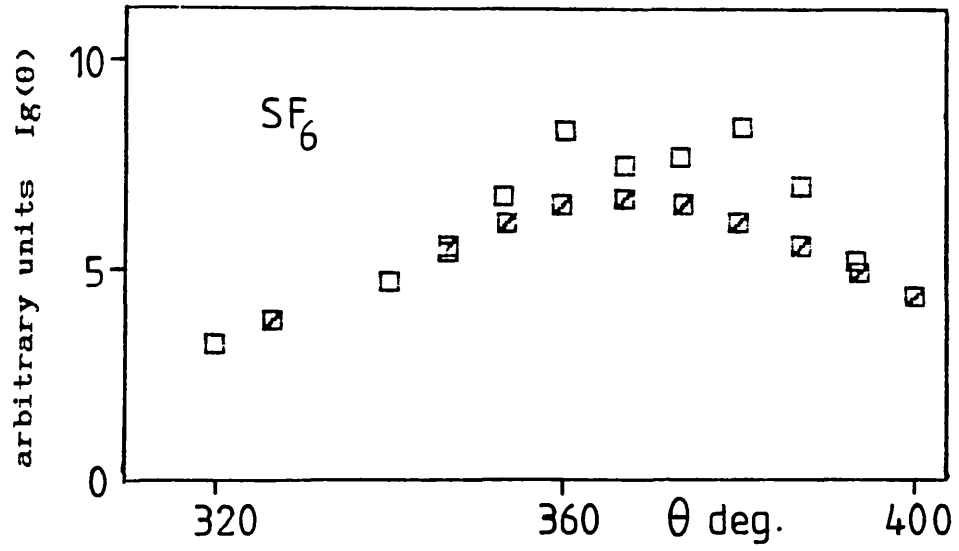


FIGURE A.2(c) COMPARISON OF EXPERIMENT AND RAYLEIGHS THEORY FOR THE SCATTERED LIGHT INTENSITY DURING AN ENGINE CYCLE INTERVAL (6.7 CR ENGINE AND WITH SF AS INTAKE GAS). THE THEORETICAL RESULT WAS DETERMINED AS NOTED IN FIGURE A.2(b)

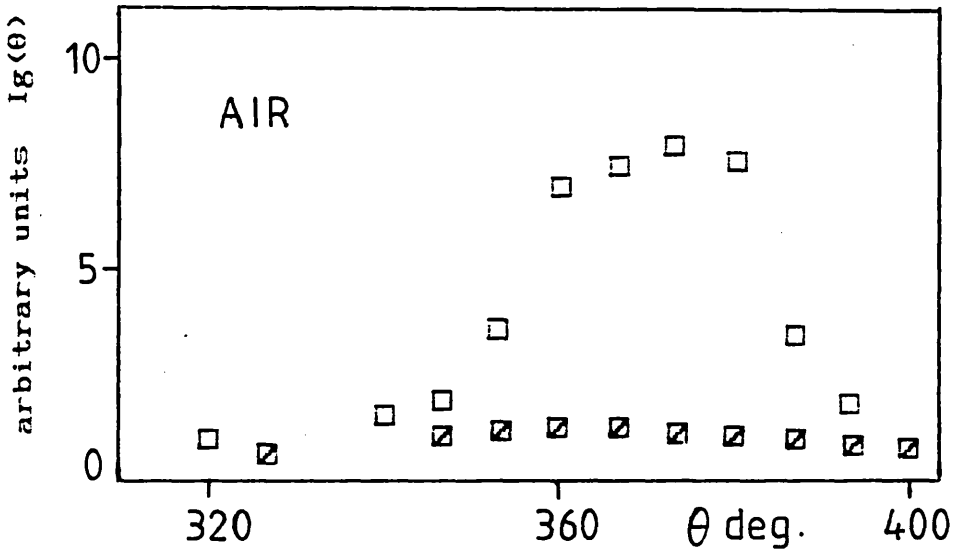


FIGURE A.2(d) SIMILAR RESULTS AS IN FIGURE A.2(c) BUT OBATINED WITH AIR AS THE INTAKE GAS; THE LARGER DISCREPENCY INDICATED HERE BETWEEN EXPERIMENT AND THEORY (ASSUMING NEGLIGIBLE INFLUENCE OF TEMPERATURE ON THE REFRACTIVE INDEX VARIATION) IS DUE TO THE LOWER HEAT CAPACITY OF AIR

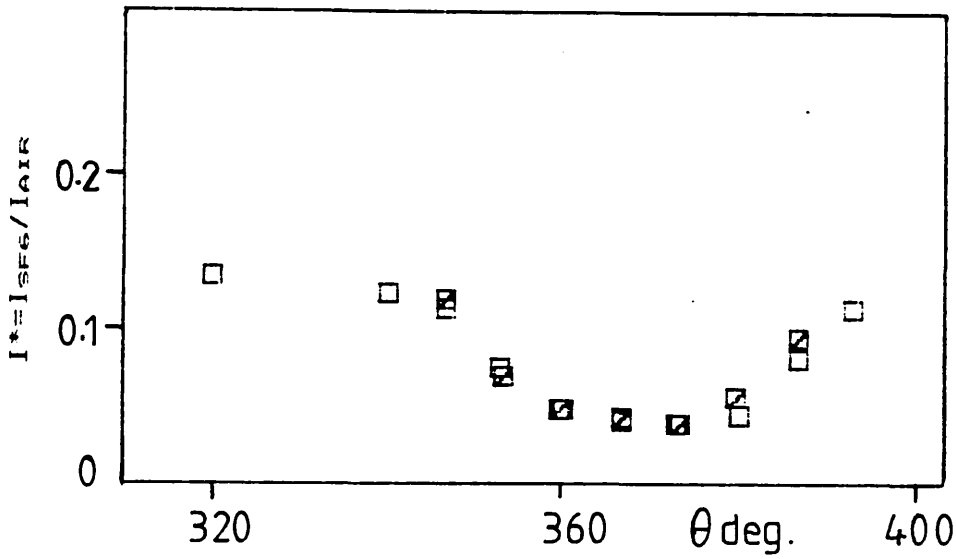


FIGURE A.2(e) THE SAME RESULTS AS IN FIGURE A.2 (c) and (d) BUT WITH ACCOUNT OF TEMPERATURE AND PRESSURE INFLUENCE FOR BOTH THE NUMBER DENSITY AND REFRACTIVE INDEX VARIATIONS; THE RESULTS SHOWN WERE OBTAINED WITH EVALUATING THE CORRESPONDING POLYTROPIC EXPONENTS FROM THE IN-CYCLE MEASURED PRESSURE RESULTING WITH THE USE OF THE DIFFERENT GASES (the values were 1.08 for SF and 1.31 for AIR in the crank angle interval of interest, ie 330 to 360 degrees of crank angle)

APPENDIX B

B.1 Optical Considerations of LRS in Confined Flows

In confined flows the intensity of the incident and scattered laser light can be affected significantly as light passes through flat or cylindrical walls of various materials. Since the scalar quantities of interest are deduced from the measurement of the scattered light intensity, any attenuation or enhancement of the incident or scattered light due to wall and surface imperfections or stray light from the surroundings will give erroneous results unless proper corrections are applied to the detected signal. In this Appendix, the effect that optical quality materials of practical importance such as quartz, pyrex glass and plexiglass (perspex) have on the incident and Rayleigh scattered light from a confined Freon-12 jet are examined and a calibration procedure is presented for correcting the photomultiplier output from contributions unrelated to the Rayleigh signal.

A circular Freon-12 free jet as used in Chapter 3 has also been employed in the present study. The jet exit velocity of Freon-12 was 4.1m/s corresponding to a Reynolds number of 1.7×10^4 based on nozzle diameter and Freon-12 density at atmospheric pressure. The jet was confined by a cylindrical wall of 75mm ID. Three cylinder materials of similar thickness (3-7mm) have been investigated which are widely used in studies requiring optical access to internal flows; quartz (fused silica), pyrex glass and plexiglass (perspex). The effect of the cylindrical wall on the time-averaged Rayeligh signal has been examined by comparing mean concentration results in the initial region of the jet to those obtained with a sampling probe. The transmittance of the incident and scattered light through flat walls has also been investigated since in many applications small flat windows are employed when full optical access is not required or when it is difficult to do otherwise.

B.2 Experimental System

The Rayleigh light scattering system is the same as described in Chapter 2; in the present case the laser was operated at 0.6W and 5145Å. A low pass filter was set at 5KHz while the data sampling frequency was 10KHz. The Rayleigh system was tested first in the initial region of the Freon-12 free jet in the absence of wall confinement and interference from dust particles; the mean Freon concentration was found to be within 1.5% from the sampling probe results in both the axial (Figure B.1) and radial (Figure B.2) directions. The linearity of the Rayleigh signal as a function of the incident laser light was tested for three different gases at ambient conditions and found to be very satisfactory (Figure B.3). The amount of incident laser light was monitored by a Spectra-Physics power meter.

In the present investigation only time-averaged mean concentration has been estimated and therefore shot noise effects were directly deconvoluted by the averaging procedure. Background light from solid surfaces needs to be estimated and subtracted from the total signal since in many cases it overshadows the Rayleigh scattered light. There are various methods of estimating it: for example in reacting flows, the laser can be switched off during the background measurement time or the light can be mechanically chopped at fixed intervals. Alternatively and with the laser on, the background light can be estimated by moving the collection optics a small distance to either side of the scattering volume in order to allow the slits to block the direct light from it. Assuming a linear light distribution between the two points, the average background light can then be calculated at each measurement location and subtracted from the total scattered light. This method works well in unconfined flows but in confined flows the background light scattered from the walls may vary significantly between the two adjoining points and the measured average may therefore not be representative of

the background light at the flow measurement location. A preferred solution in confined flows is to either use flat windows which do not distort the signal the way that cylindrical walls do or to cut slots, if a cylinder is used, to provide access to the entering and exiting laser beam or even to the scattered light at 90^{o} to the plane of polarization of the incident light. However, opening holes or slots may influence the flow field locally and introduce beam steering due to refractive index variations along the beam path when small pressure variations exist between the internal and ambient flows. The effect of beam steering on the Rayleigh signal can be alleviated by imaging the laser beam orthogonal to the photomultiplier slits thus providing a finite depth of field to the collection optics. When the use of a window is unavoidable it has to be of optical quality, flat and antireflection coated or uncoated but in such a case it would need to be placed at Brewster's angle to the incident beam. Since in certain applications (eg. internal combustion engines) it is not convenient to have more than one window but rather a completely transparent cylinder of adequate thickness to withstand high pressures, the investigation carried out here uses different materials to examine the effect of flat and cylindrical walls on the output signal from the Rayleigh system and its correct interpretation as mean concentration in a confined steady Freon-12 jet. It should be mentioned that in all cases the part of the wall opposite the collecting optics should be painted black internally or covered externally by a black absorbing surface since it was observed that the photomultiplier output was extremely sensitive to stray light behind the scattering volume.

B.3 Light Transmission Through Flat Walls

The experimental set-up for measuring attenuation losses of the laser light through flat walls is shown in Figure B.4.

The simple case is when the incident laser light passes through a flat wall (a) before it is focused at a point in the potential core of the Freon-12 jet and there are no other walls around to interfere with the beam. The effect of the presence of additional walls in the forward or 90^{o} scattering direction will be examined later by introducing successively walls of equal thickness at locations (c) and (b). In each case the reading of the laser power meter measuring the transmission of light through the wall(s) is compared with the light intensity variation observed by the Rayleigh scattering system at a point in the potential core of the jet.

Theoretically, when a beam of laser light in air passes through a flat wall at nearly normal incidence and independent of its state of polarization* a small part of the incident light is reflected off the surface and the rest is transmitted through the wall. The amount of reflected light R depends on the refractive indices of the wall material n_w and surrounding medium n_m, and for $n = n_w/n_m$ is given by (see Bohren and Huffman (1983))

$$R = \left(\frac{n-1}{n+1}\right)^2 \qquad (B.1)$$

The total transmission D through the wall depends mainly on surface reflection but also on wall absorption according to the following expression

$$D = (1-R)^2 e^{-kx} \qquad (B.2)$$

where k is the absorption coefficient of the wall material and x is the wall optical thickness; both k and n are functions of the incident light wavelength. In Table B.1, the surface reflectance and total transmission for the three optical materials investigated are given assuming zero absorption; for materials free from internal impurities and a thickness of

* for oblique incident on a flat boundary the polarization state of the laser light becomes important, Bohren and Huffman (1983)

10mm, the estimated absorption is in all cases less than 5%. The values listed in Table B.1 are only valid for uncoated, optically smooth flat surfaces since surface irregularities, dust deposition or even fingerprints can cause diffused reflection of the incident light over a distribution of angles with a subsequent reduction in the total light transmitted through the wall. For polarized laser light, material inhomogoneities may be detrimental due to birefringence effects which can cause arbitrary changes in the polarization orientation of the scattered light (Dainty (1985)). In Rayleigh scattering applications this is totally undesirable because of the strong dependence of the scattered light intensity on polarization orientation of the incident.

TABLE B.1

Wall Material	Refraction Index (514.5nm)	Surface Reflectance (%)	Total Transmission
Heralux * fused silica (quartz)	1.46181	3.5	93
Pyrex glass	1.52049	4.3	91.6
Perspex**	1.49	3.9	92.2

* Heraeus trade mark

** Imperial Chemical Industries Ltd. trade mark

Although the theoretically calculated transmission losses were in all cases less than 9%, the measured losses by the light power meter and the Rayleigh system were higher (Table B.2). When the flat perspex wall was introduced in location (a)

vertically to the laser beam, the laser power at the transmission end was attenuated by 13% according to the power meter and by 16% according to the Rayleigh scattered intensity from the Freon molecules. Theoretically the two attenuation losses should have been equal since the scattered light is linearly proportional to the incident on the scattering volume laser light. The higher attenuation losses measured by the two methods compared to the theoretical value of ∿9% are attributed to surface irregularities which increase the amount of reflected/scattered light from the perspex wall. The difference between the two methods is more likely due to the reduced resolution of the power meter. When the thickness of the perspex wall was doubled, very small differences were observed in the amount of transmitted light which confirmed the insignificant effect of wall absorption on the incident on the scattering volume laser light. However, when two separate perspex pieces of the same thickness as in (a) were attached to one another thus introducing two additional surfaces in the beam's path, the transmission losses increased to 26% and 30% as measured by the power meter and the Rayleigh system respectively. Almost identical attenuation loss has been observed by the power meter when the two walls were placed at positions (a) and (c) as shown in Figure B.4; although in this case the Rayleigh system was not influenced by the presence of the wall at (c) and resulted in a similar loss to the single wall case. This was expected since the incident beam on the scattering volume was only affected by the presence of the wall at (a).

TABLE B.2

Measurement Method	Attenuation losses (%)			
	a	a+a	a+c	a+b+c
Power Meter	13	26	26	26
LRS	16	30	16	27

The effect of wall confinement in the scattering direction on the Rayleigh signal has been investigated by placing an identical to (a) and (c) flat surface at position (b). This configuration, with the three flat walls fully enclosing the Freon jet, resulted in an overall attenuation loss of 27% which is slightly less than the 30% measured with the two attached walls in position (a). This indicates that the wall in the scattering direction (b) plays a similar role to the incident wall (a) in attenuating the Rayleigh signal and reducing the overall sensitivity of the system.

B.4 Light Transmission Through Cylindrical Walls

When laser light passes through transparent curved walls, the beam orientation with respect to the surface becomes very important since any significant deviations from the normal incidence increase the transmission losses due to internal reflections which tunnel the light around the curved material. The cylindrical wall, which is one of the most widely used practical configurations, represents an extreme case of a curved surface and requires special attention when optical techniques based on light intensity are employed.

The effect of the wall on the Rayleigh signal obtained from a Freon jet confined axisymmetrically by cylindrical walls of various optical materials, has been investigated in terms of axial and radial profiles of Freon concentration (mole fraction) and compared with the results obtained by the sampling probe. As Figure B.5 shows, the direct interpretation of scattered light as mole fraction of Freon-12 underestimates the true Freon concentration by a maximum of 10% at $x/d = 8$; this is true for perspex, quartz and pyrex glass walls. The Freon mole fraction in the radial direction was also underestimated (Figure B.6) by $\sim$5% which clearly indicates that the effect of the optical wall independent of material type can be significant in confined flows. The

reasons for the observed discrepancy will be made clear in the following paragraphs.

Figure B.7 provides a relative measure of the levels of scattered light from Freon and air in the presence and absence of the cylindrical wall. Without any wall confinement, the intensities of scattered light from Freon and air, respectively, are I_F and I_A while in the presence of the cylindrical wall the corresponding signals from the same point in the jet become $I_{F,W}$ and $I_{A,W}$. It is interesting to note that wall scattering increased the air signal ($I_{A,W}>I_A$) although the amount of laser light incident on the scattering volume was less and as a result the intensity of the scattered light from air was expected to be reduced relative to the unconfined case. When Freon was injected inside the cylinder however, the signal level instead of increasing relative to the free jet due to the observed previously scattering of light from the cylindrical wall, was significantly reduced. This is more likely due to absorption of the scattered light inside the cylinder by both the Freon molecules and internal reflections from the cylindrical wall rather than to attenuation of the incident laser beam between the wall and the scattering volume; with the flat wall this was found to be insignificant.

The use of Freon-12 as a scattering medium may have implications on the obtained results due to its efficiency for absorption of the scattered light directed towards the photomultiplier. Considering the general case of an absorbing and scattering medium, the radiative transfer is given by (Becker (1976))

$$\frac{\partial I_{\lambda,d\Omega}}{\partial r} + K_\lambda I_{\lambda,d\Omega} = K_\lambda J_{\lambda,d\Omega} \qquad (B.3)$$

where $I_{\lambda,d\Omega}$ is the intensity of scattered light at the laser wavelength λ in a point r into a solid angle $d\Omega$, $\partial I_{\lambda,d\Omega}/\partial r$ is the rate of change of $I_{\lambda,d\Omega}$ in the direction of d_Ω, K_λ is

the extinction coefficient and $J_{\lambda,d\Omega}$ is the source function which represents the rate of increase of $I_{\lambda,d\Omega}$ with distance from r along the direction of $d\Omega$ due to secondary scattering of light coming from other directions into d_{Ω} by Freon and air molecules along the same path. The term $K_{\lambda}J_{\lambda,d\Omega}$ can be further written as

$$K_{\lambda}J_{\lambda,d\Omega} = (K_{\lambda a} + K_{\lambda s})\ J_{\lambda,d\Omega} \qquad (B.4)$$

where $K_{\lambda a}$ is the absorption coefficient which is related to the concentration of absorbing particles in the same way as $K_{\lambda s}$ is related to the concentration of scattering particles; the absorbing or scattering particles may or may not be the same. In the case of an air jet confined by a cylindrical wall, the scattered light by the air molecules is partly absorbed by air molecules along the optical path while the stray light from the wall opposite the collecting optics is much stronger and results to higher intensities as indicated by $I_{A,W}$ in Figure B.7. The net effect of the wall in the air jet case is to increase the total signal intensity by I_W. By placing the laser power meter opposite to the laser (Figure B.4) and applying the results of the last wall investigation, whereby the attenuation effect of wall (b) on the Rayleigh signal was found to be similar to that of (c), the transmission loss of the laser beam through the cylinder can be measured and used to estimate the absorption of the scattered light by the gas molecules. If I_L is the intensity of incident laser light in the absence of the cylindrical wall and I_A the intensity of scattered light from pure air, then the effect of the wall will be to reduce I_L and at the same time reduce even more the amount of scattered light, i.e.

$$I_A = KI_L \qquad (B.5)$$

and similarly,

$$I'_{A,W} = K'I'_L \tag{B.6}$$

where K and K' are the calibration constants for the unconfined and confined case, respectively. If the reading of the power meter in the presence of the wall is I'_L then $I'_{A,W} = (I_L'/I_L)I_A < I_A$ since there is no difference in molecular absorption for the two cases and the wall always attenuates the incident and scattered light. If the measured intensity $I_{A,W}$ is higher than $I'_{A,W}$, the difference is attributed to wall scattering in the direction of the collecting optics, i.e.

$$I_{A,W} - I'_{A,W} = I_W \tag{B.7}$$

In the case of the Freon jet the same procedure applies; again the reading of the power meter will indicate the transmission losses through the wall but in this case absorption may be significant and an additional correction is required. If the signal from Freon is I_F, then

$$(I'_{F,W} - I'_{A,W}) = (I_L'/I_L)\ (I_F - I_A) \tag{B.8}$$

$$(I'_{F,W} - I_{A,W}) = (I_{F,W} - I_{A,W}) + C_{a,W} \tag{B.9}$$

where $C_{a,W}$ represents at each measurement location the difference between the measured signal in the presence of the wall $(I_{F,W} - I_{A,W})$ and that estimated from the transmission loss indicated by the power meter and the signal from the free jet $(I_F - I_A)$. This correction factor, when added to the measured signal by the Rayleigh system, accounts for the absorption losses by the Freon molecules inside the cylinder and furthermore for the underestimation of the Freon concentration in Figures B.5 and B.6. When this correction procedure was applied to the results of Figure B.5 for the three different cylinder materials, the Freon mean concen-

tration was found to be within a maximum of 5% from the sampling probe results which are considered to be accurate. This degree of accuracy is considered to be very satisfactory on the basis of the assumptions involved in the analysis and the resolution of the laser power meter.

The variation of background light from the walls along the radius has been examined and as shown in Figure B.8 increases towards the wall for both quartz and perspex walls. This is true for air and Freon although the ratio of their respective signals does not remain constant with increasing radius. The observed difference in slope of the background light intensity between the two gases partly explains the underestimation of the true Freon concentration in the radial profile of Figure B.6. For Rayleigh measurements at larger radii, the cone of scattered light gets out of focus for the fixed collecting system and thus requires refocusing which can only be achieved by rotating the light collecting system around the cylinder. As can be seen in Figure B.8, the background light from the wall increases with radius and eventually overshadows the Rayleigh signal due to the defocusing of the collecting optics. Measurements away from the central part of the cylinder require careful calibration and are expected to be less accurate than those along the cylinder axis due to background effects and distortion of the scattering volume image.

Variation of the background light along the cylinder axis has been observed in the three optical materials investigated and found to be significant. As shown in Figure B.9 the signal from air within the cylinder fluctuates around a mean value along the axis as a result of surface irregularities and wall inhomogenities which are more prominent with the perspex wall and less with quartz. This can introduce significant errors to the centreline Freon concentration when it is deduced directly from the measured signal intensity. Figure B.10 shows the centreline distribution of the scattered light when the cylinder used by Arcoumanis et al (1984) is

filled with pure Freon and pure air and when Freon is injected in a transient manner through an injector nozzle. From these three signals, the Freon mean concentration has been calculated by two methods.

1. Using the procedure described by Arcoumanis et al (1984) and estimating the uncorrected Freon-air signal assuming uniform wall scattering, i.e.

$$\frac{\bar{X}}{\bar{X}_o} = \frac{(I-I_A)}{(I_F-I_A)} \qquad \text{(B.10)}$$

where I_A is the average background intensity estimated by offsetting the collecting lens symmetrically to either side of the scattering volume.

2. Employing a new procedure whereby the signal from pure 100% Freon is used as a correction factor to account for wall and surface inhomogenities along the cylinder axis. By considering at each measurement location the difference between the local signal with 100% Freon and the average 100% Freon signal, the Freon mean concentration can be obtained as

$$\frac{\bar{X}}{\bar{X}_o} = \frac{(I-I_A)_i \pm C_i(I_F-\bar{I}_F)_i}{(I_F-I_A)_o} \qquad \text{(B.11)}$$

where C_i is a correction factor ($0<C_i<1$) based on the local Freon jet concentration and accounting for all spatial intensity contributions, i.e.

$$C_i = \frac{1}{I_o(r)} \int_{-\infty}^{\infty} I(r)\, dr$$ which is approximated in terms of local effects by

$$C_i = \frac{(I-I_A)_{i-1} + (I-I_A)_{i+1}}{2(I_F-I_A)_o} \qquad \text{(B.12)}$$

where the subscript i represents the measurement location and o the reference condition (potential core of the jet). The corrected signal shown in Figure B.10 does not exhibit the fluctuations of the uncorrected signal and, as expected, the corrected mean Freon concentration decays gradually along the axis. Since the results of Figure B.10 have been obtained in a perspex cylinder which according to Figure B.9 is more susceptible to variations of the scattered light from the walls, a similar correction procedure can be employed with any optical material. In addition, since the centreline concentration results in the model engine reported by Arcoumanis et al (1984) have been obtained with the same perspex cylinder but without having been corrected for wall inhomogeneities they are in error especially around a distance from the nozzle of about 4 diameters (i.e. 12mm). Results in the same engine (see Chapter 4) did not exhibit any significant variations of mean concentration along the cylinder axis because these measurements have been intentionally obtained at a selected axial plane where background scattering from the wall was nearly uniform. The effect of wall inhomogeneities in the temporal intensity distribution was also considered and found to be insignificant in terms of the computed higher moments due to the relative, rather than absolute, effect of the wall on the instantaneous signal. Designating two arbitrary orientations of the cylinder by α and β and the conditions at the nozzle exit by (o), if the effects on rms, for instance, were absolute then

$$\frac{\sqrt{C'^2_\alpha}}{\bar{C}_o} = \frac{\sqrt{C'^2_\beta}}{\bar{C}_o} = \text{const.} \qquad \text{(B.13)}$$

where C' is the ensemble variance and $\bar{C}_o$ the mean concentration. The result (B.13), however, does not hold in the presence of optical inhomogeneities. The correct result found is given by

$$\left(\frac{\sqrt{C'^2}}{\bar{C}}\right)_\alpha = \left(\frac{\sqrt{C'^2}}{\bar{C}}\right)_\beta = \text{const.} \tag{B.14}$$

similarly, it is found that another constant results if the values (C'^2) and $\bar{C}_j$ are referenced to an absolute maximum result, $(C'^2)_m$ and $(\bar{C})_m$ in the form of differences

$$\frac{(C'^2_m - C'^2_\alpha)^{\frac{1}{2}}}{\bar{C}_m - \bar{C}_\alpha} = \frac{(C'^2_m - C'^2_\beta)^{\frac{1}{2}}}{\bar{C}_m - C_\beta} = \text{const.} \tag{B.15}$$

The result (B.15) can be verified from Figure B.11 where the mean and variance of scattered light intensity detected from the potential core of the jet are shown as a function of displacing the collecting lens over increments δ_i. The quantities shown are all normalized with respect to their respective values at $\delta_i = 0$ (i.e. collecting lens focused).

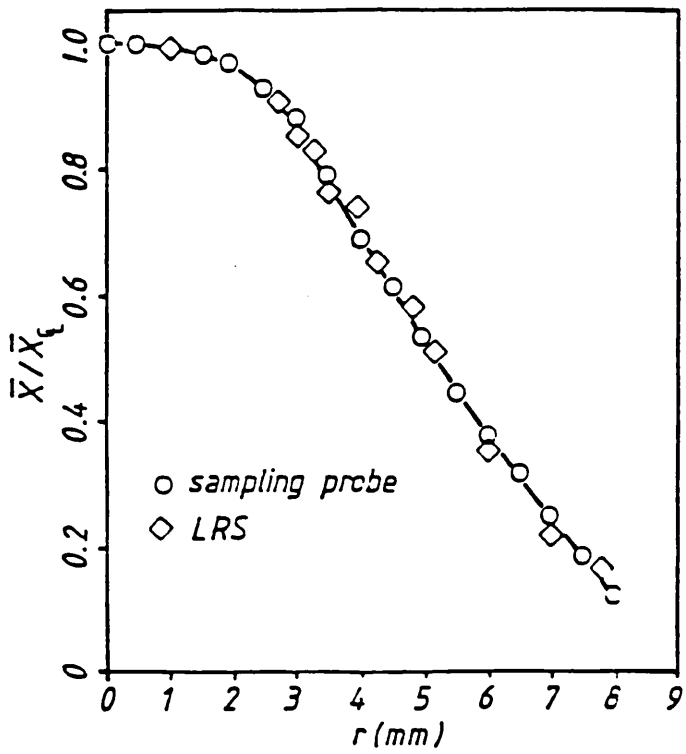


FIGURE B.1 CENTRELINE FREON-12 CONCENTRATION (FREE JET)

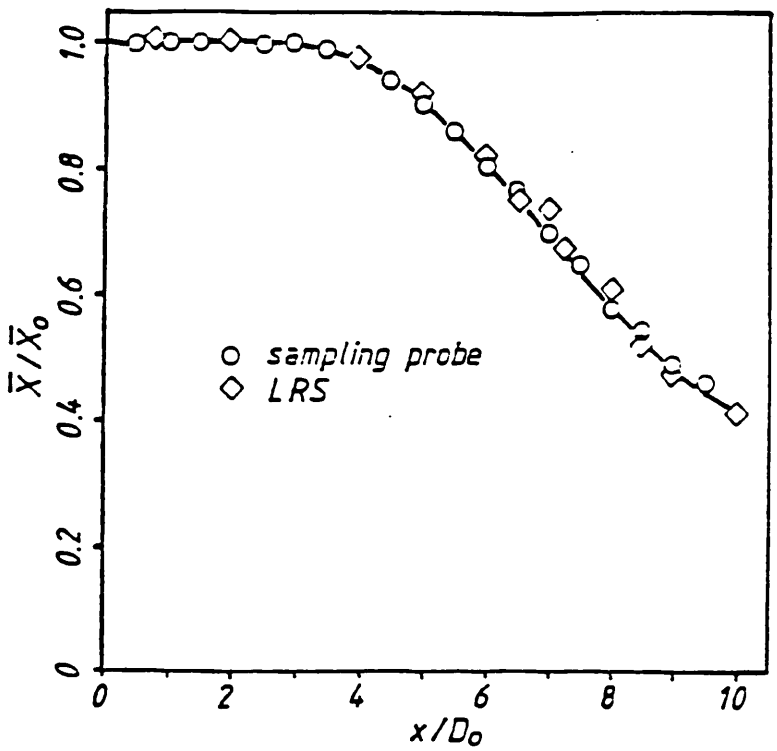


FIGURE B.2 RADIAL FREON-12 CONCENTRATION AT x/d=3 (FREE JET)

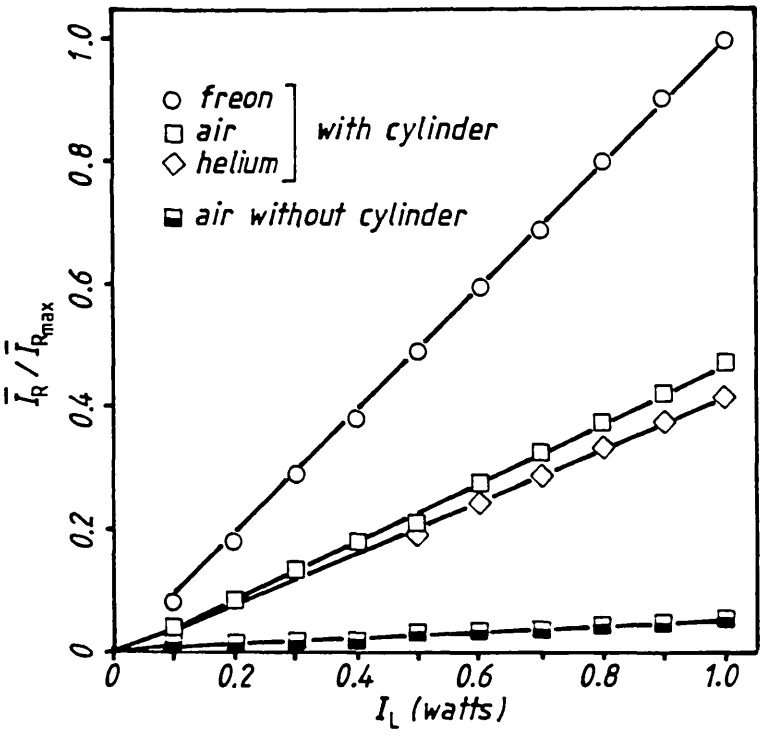


FIGURE B.3 RAYLEIGH SIGNAL AS A FUNCTION OF INCIDENT LASER LIGHT

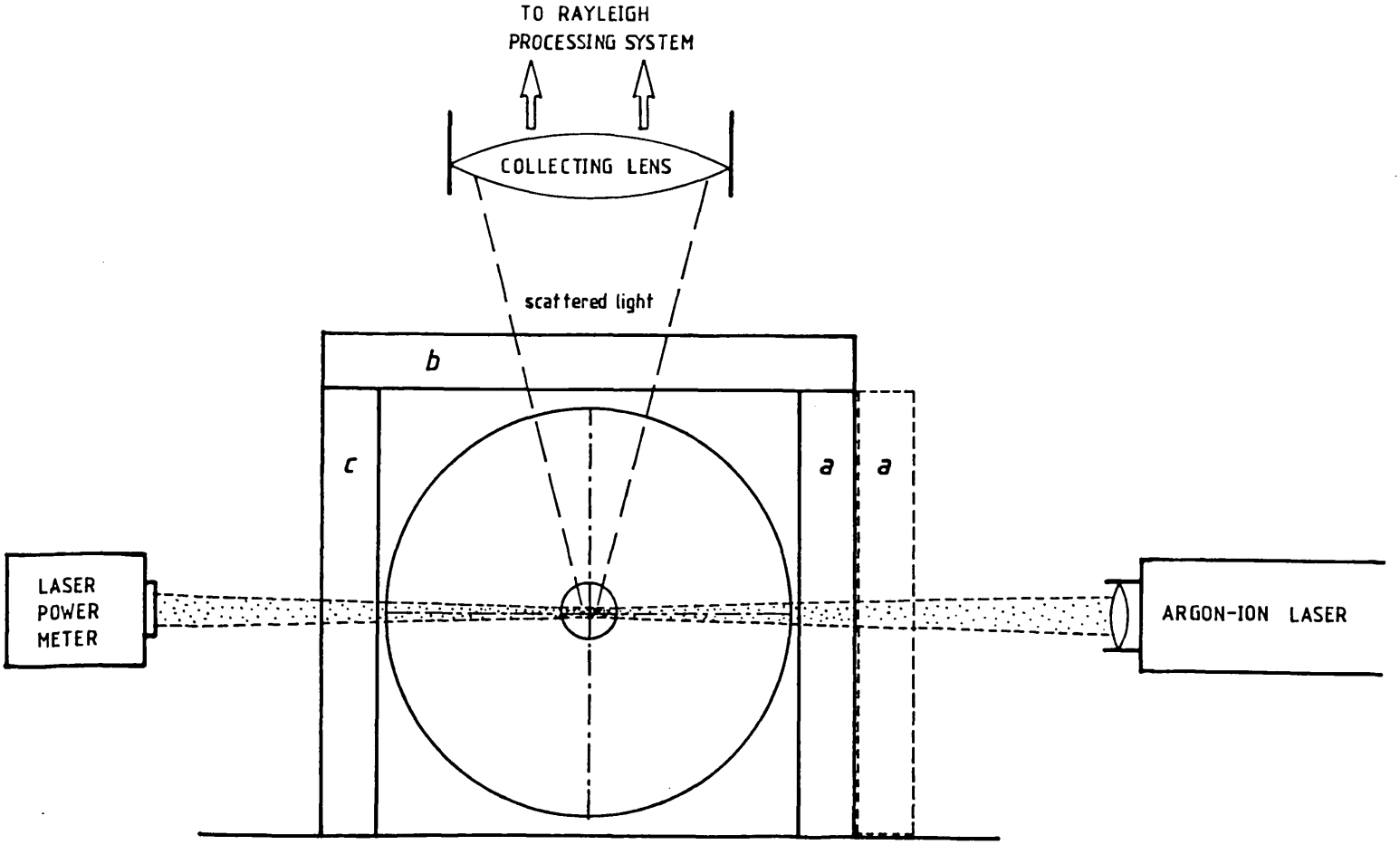


FIGURE B.4 EXPERIMENTAL SYSTEM FOR INVESTIGATING THE EFFECT OF FLAT AND CYLINDRICAL WALLS ON THE RAYLEIGH SIGNAL FROM A FREON-12 JET

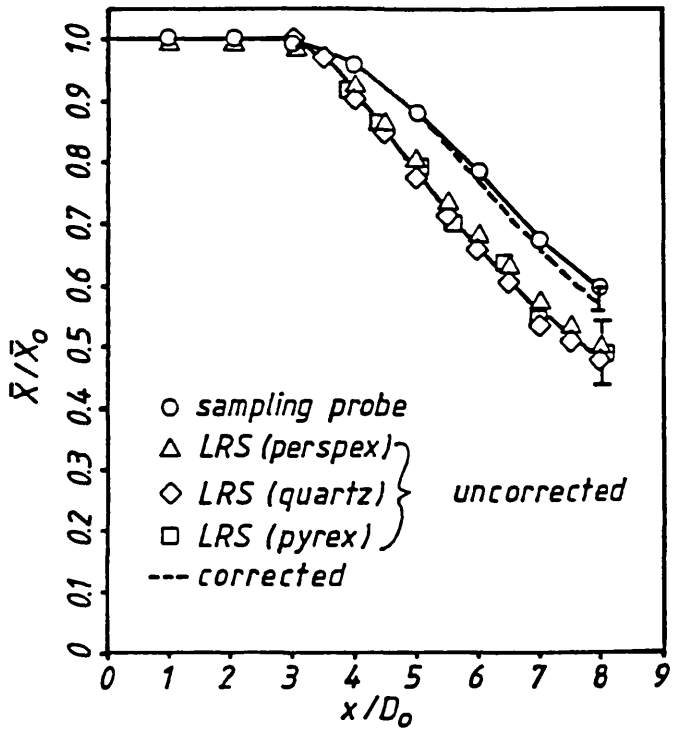


FIGURE B.5 CENTRELINE FREON-12 CONCENTRATION (CONFINED JET): the bars denote maximum uncertainy

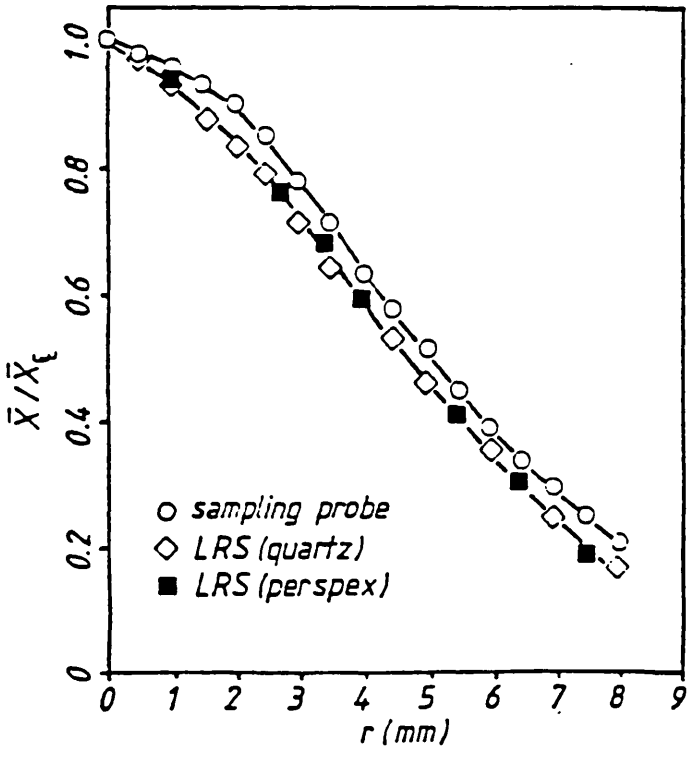


FIGURE B.6 RADIAL CONCENTRATION AT x/d=5 (CONFINED JET)

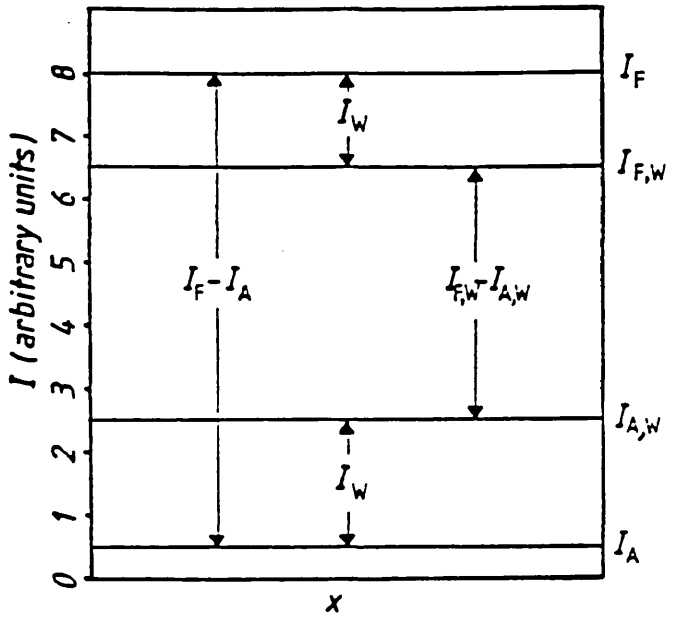


FIGURE B.7 SCATTERED LIGHT DISTRIBUTION IN THE PRESENCE OR ABSENCE OF CYLINDRICAL WALLS

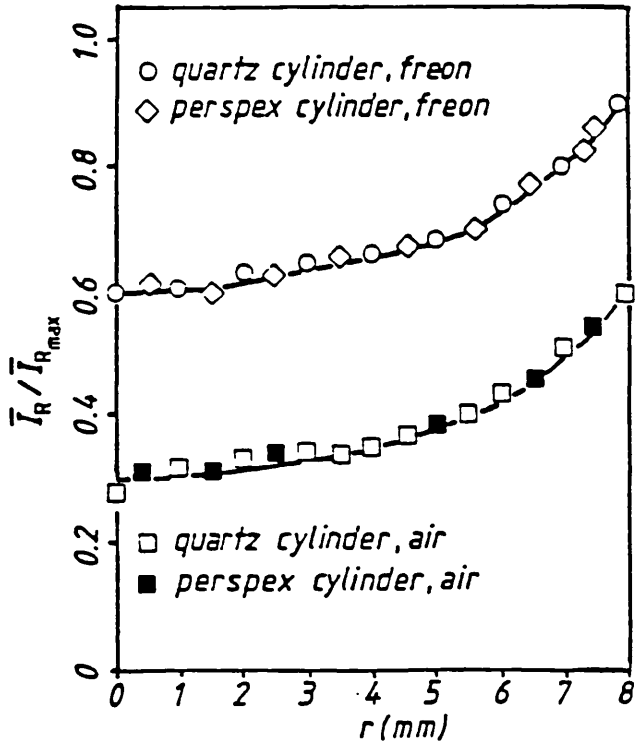


FIGURE B.8 RADIAL DISTRIBUTION OF SCATTERED LIGHT (SCATTERING FROM PURE GASES AS INDICATED IN CYLINDERS OF DIFFERENT OPTICAL MATERIALS)

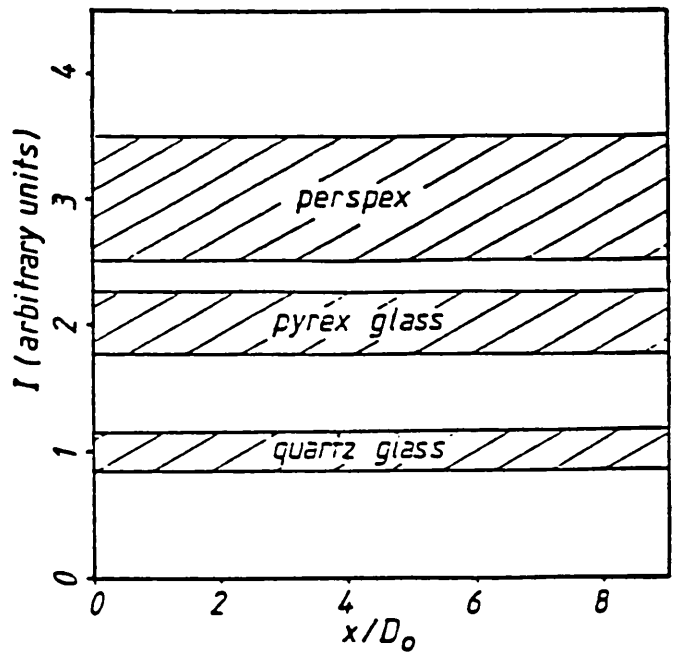


FIGURE B.9 AXIAL DISTRIBUTION OF SCATTERED LIGHT (maximum variations indicated at different axial planes)

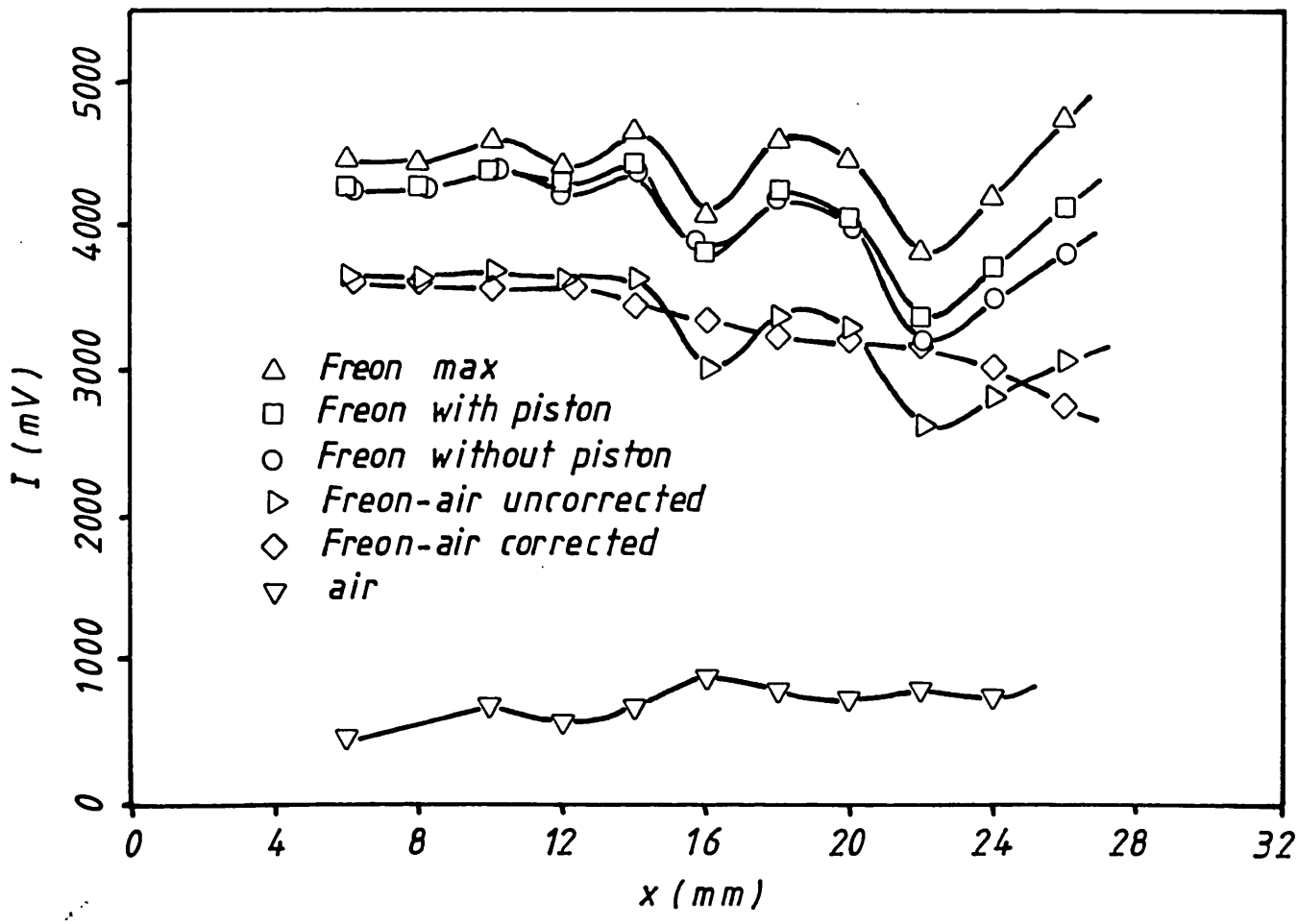


FIGURE B.10 AXIAL DISTRIBUTION OF SCATTERED LIGHT (CONFINED TRANSIENT FREON-12 JET)

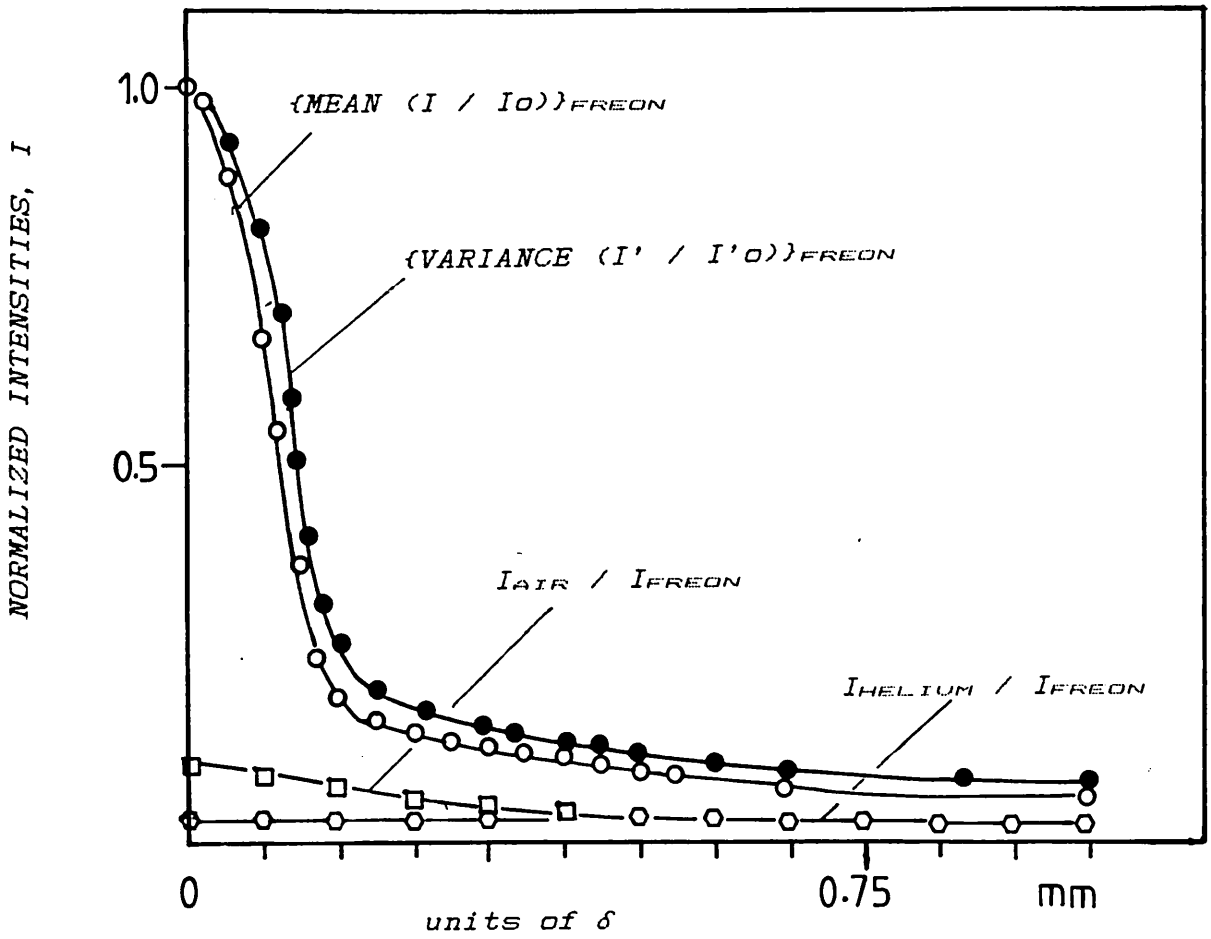


FIGURE B.11 DETECTION OF RAYLEIGH SCATTERED LIGHT ALONG THE FIELD OF VIEW OF COLLECTING LENS (see FIGURE 2.1) OBTAINED BY DISPLACING THE LENS IN INCREMENTS OF δ=.0375 mm AWAY FROM THE FOCUSED BEAM CENTRE. THE MEAN AND VARIANCE VALUES SHOWN ARE NORMALIZED BY THEIR RESPECTIVE VALUES OBTAINED WITH THE LENS FOCUSED ONTO THE LASER BEAM CENTRE. THE MEAN VALUES FOR AIR AND HELIUM ARE NORMALIZED BY THE MEAN VALUE OF FREON TO INDICATE THEIR RELATIVE INTENSITY TO FREON. NOTE THAT AT A SUFFICIENT DISTANCE AWAY FROM THE FOCUSED BEAM CENTRE, (0), THE SCATTERING LEVEL FROM AIR REPRESENTS THE EQUIVALENT INTENSITY LEVEL AS HELIUM (ie, the optical background level) AT THE FOCUSED LENS CENTRE.

APPENDIX C

C.1 Microcomputer Software for Transient Flow Measurements

Nomenclature:

f_m	maximum frequency measured
f_s	sampling frequency
N_c	number of engine cycles
N_p	number of encoder pulses per cycle
N_s	number of data samples
T_i	fuel injection time
T_μ	total measurement time
TM	measurement start flag (TM = 1)
TM_2	measurement stop flag (TM_2 = 1)
X(t)	instantaneous fuel concentration (mole fraction)
$\bar{X}$	mean concentration (mole fraction
$\bar{X}_o$	mean concentration at nozzle exit
x	axial coordinate
$\Delta\theta$	crank angle window
θ	crank angle

This Appendix describes in detail the software developments for a measurement system which is microcomputer based and used to study the turbulent fuel/air mixing process in a non-compressing and compressing model Diesel engine employed and described in Chapters 4 and 5. The software developments have been motivated by the need to carry out extensive

measurements requiring high accuracy, minimal time and to be able to provide a general system for use in other transient flow environments. In summary, this involved the data sampling and analysis, developing special purpose graphics and the interface of the microcomputer to analogue devices. The software developed serves to (i) conditionally sample the injection process (ii) control the injection process during each engine cycle and (iii) fully automate the data acquisition, storage and analysis. Data analysis includes the calculation of statistics, autocorrelation and frequency spectrum of the concentration fluctuations. The experimental system and presentation of typical results are reported in the subsequent sections.

C.2 Signal Processing

A laser Rayleigh scattering system as described in Chapter 2 is used. The output of the photomultiplier is displayed on an oscilloscope and input to a software controlled data acquisition system. The data acquisition hardware consists of a four-channel 12-bit A.D. convertor digitising the input voltage at 30KHz. The system uses Analogic MP6812 data acquisition modules to manage multiplexing, samplehold and A/D conversion. The microcomputer is a 48 K RAM APPLE-II which is built around the MOS 6502 microprocessor. Collected data can be stored on either floppy or hard disk. A gating system with input from an optical shaft encoder connected to the crank shaft of the engine is used to control both the measurement and injection times. The shaft encoder provides 1000 pulses per revolution and has a marker pulse synchronised with the top-dead-centre (TDC) position of the engine. The pulses from the shaft encoder are used to activate the gating system based on pre-programmed sequences issued as commands from the microcomputer. When measurements are made in the compressing engine the output from the pressure transducer

is simultaneously read with the photomultiplier output; a line diagram of the signal processing system is shown in Figure C.1.

C.3 Software Developments

Data Sampling

The sampling of data in the engine flow to accurately represent the mean and fluctuating concentrations of injected fuel is complicated since the transient and periodic flow can vary from cycle to cycle. Therefore, an on-line conditional sampling scheme was developed to measure events in each cycle which represent similar conditions from cycle to cycle. The procedure involved monitoring the time of arrival of a specified crank angle degree (CAD) and monitoring the rpm before and after a set of data are collected during a cycle. Formulation of the software is based on the user being able to specify the sampling frequency, number of cycles, measurement time in the cycle and window (in terms of crank angle degrees) over which data are to be collected; the limitations on these parameters being defined by the execution time of the software as defined by the hardware response. When pressure measurements were made specification could also be made of pressure deviations from cycle to cycle, in particular, for peak cycle pressure and pressure at the start and stop of fuel injection.

The CAD's relative to TDC may be determined from

$$\hat{\theta} = \frac{\Delta\theta_{max}/\text{rev}}{1000 \text{ pulses/rev}} \times N_p \qquad \text{(C.1)}$$

where θ_{max} is the number of CAD's in a complete engine cycle and N_p is the number of pulses counted after the marker pulse. The time which elapses over a given measurement window of, say, $\Delta\theta$ is

$$T_\mu = \frac{\Delta\theta}{RPM} \times \frac{60}{\theta_{max}} \text{ (sec)} \qquad \text{(C.2)}$$

where $\Delta\theta = \Delta N_p \times \theta_{max}/1000$ and ΔN_p is the relative pulse count monitored from the shaft encoder. For a constant sampling frequency, f_s, the total samples which can be obtained during the time T_μ are

$$N_s = T_\mu f_s + 1 \qquad \text{(C.3)}$$

From equations (C.2) and (C.3) the result for N_s can then be expressed as

$$N_s = \frac{\Delta\theta}{RPM} \left(\frac{60}{\theta_{MAX}}\right) f_s + 1 \qquad \text{(C.4)}$$

and the theoretical maximum frequency measured is $f_m = f_s/a$ where a should be chosen to be greater than or, as a minimum, equal to 2 (i.e. the Nyguist Criterion).

The measurement software follows the flow chart of Figure C.2 and was programmed in APPLESOFT BASIC with the data sampling routine, QUIK, in assembly language for the 6502. The transition diagram for QUIK is shown in Figure C.3 and two versions were developed. One version has a fixed sampling frequency of 26KHz while the second has a variable sampling frequency ranging from 900Hz to 18KHz. The constraint on the number of data collected per engine cycle, apart from the definition in equation (C.4), depends on the memory allocation scheme used for measured data. For the present application it was adequate to allocate as a maximum 768 RAM bytes of the micro for data storage per cycle per measured signal. However, since a 12-bit word (2-bytes) was

used to represent each output voltage value, this address count permits a maximum of 384 actual data pairs per cycle to be measured and stored. If the value for N_s found for a choice of parameters in equation (C.4) is less than the maximum, the memory bytes allocated for each cycle is then adjusted accordingly by the software. The limits on the sampling frequency range arise from the A/D and Apple synchronization requirements and the cpu clock which governs the execution time for the machine programmed operations. For the variable frequency program the upper and lower limits on N_s are defined by

$$\frac{1}{f_{s_{MAX}}}(N_{s_{MIN}} - 1) \leqslant \frac{\Delta\theta}{6RPM} \leqslant \frac{1}{f_{s_{MIN}}}(N_{s_{MAX}} - 1) \qquad (C.5)$$

The program QUIK also carried out real-time control of the injection process and checks against systematic errors in the measurements. For example, the time associated with a measurement window as given by equation (C.2) defines what the expected data count (C.4) should be. Rounded off to the lowest integer value, this number of samples should appear in the computers memory for each cycle. If this is not the case the engine cycle data is considered corrupted and not kept.

To provide enough data for computing statistical quantities, such as the ensemble-averaged mean and rms of the concentration fluctuations, a minimum of 4096 data were collected over a number of engine cycles, N_c. This number, for an arbitrary number of samples, say N, is found from

$$N_c = \left(\frac{N}{k + RPM}\right)RPM \qquad (C.6)$$

where $k \propto \Delta\theta x f_s$.

Gating System Control

Control of the gating system is carried out by commands issued from the microcomputer. Two gates are addressed independently by software to control commencement and duration of both the fuel-injection and measurement times. The shaft encoder pulse train is input to the gating system and monitored by software to decide what events should be carried out.

Typical measurements of interest correspond to fuel injection initiated at 40 degrees before TDC and terminated at 20 degrees before TDC. For the engine speed of 200 rpm the time of arrival of the pulse indicating start of injection is about 267ms. If the pulse arrives $\pm$0.3ms away from this time data are not collected for the cycle. When the pulse arrival time is acceptable, the rpm immediately prior to sampling and after sampling is recorded and compared subsequently to a preset value. If a drift greater than $\pm$0.5% in rpm is detected data collected for the cycle is then rejected. The time for issuing a pulse from the gating system to close the solenoid valve is counted in real-time by a software clock and ensures that the same times elapse in between start and stop of each injection to within $\pm$0.1ms.

Data Analysis

Mean flow quantities are computed by ensemble averaging data collected for the total number of engine cycles measured at a particular location. For ensemble averaging purposes data are collected over a finite crank angle window, typically 5 CAD's during the time when the fuel injection process behaves quasi-steady. This measurement window is centred at 28.5 degrees before TDC and is represented in Figure 4.4. The implications of this averaging technique in engine flows have been discussed by several authors, see for instance Witze et al (1984). The algorithms for computation of mean concentration, rms and higher moments, such as skewness and

kurtosis, are executed with machine coded instructions addressing a floating point arithmetic processor (California Computer Systems - Model 7811) for fast arithmetic execution. The equations used follow from discrete signal statistics and account for the photon statistics associated with the LRS signal. These are presented and discussed in Appendix A.

The determination of spectral information and autocorrelations for the transient data are made with the direct transform method of Gaster and Roberts (1975, 1977); see also Bendat and Piersol (1971) for the discussions on computation of the autocorrelation function for transient and non-stationary signals.

Data processing can be carried out on-line to provide checks on the results being measured and perform system calibration. The bulk processing of all measured data, however, was performed automatically and involved reading a data file, computing required quantities and appending the data file with the final results. Once the results were available, additional software could access these and create a specific data base for interactive analysis.

Graphics

Graphics were developed to provide on- and off-line visualization of both raw data and analysed results using the high resolution graphic features of the APPLE. The key aspect of the graphics package was its access to any number of data files to search for specific results (i.e. arbitrary cycle results) and combine presentation on the VDU or perform specific plots of temporal injection distributions, autocorrelation functions and log-log plots of the frequency spectrum. The results could then be hard copied or continuously updated if graphics were used on-line.

C.4 Software Integration

The features of the software described above were combined and organised to provide rapid access and execution under the general name MONA. The software system was menu driven and the general structure as shown in Figure C.4 was arrived at to permit ease of software use in the current application and make modification of the individual modules, or addition of new modules, independent of the measurement environment. The executive program, MONA.Ø, was used to initialise the measurement system, provide access to the hard disk utilities, update a measurement log and prompt the user to proceed. The program MONA.1 was then called and used as a controlling program to access all system software. The programs MONA.RUNX were configured on-line as shown in Figure C.5. A brief description of the programs is given below:

MONA.RUN1	User defines all parameters as listed in Table C.1 and specifies program flow
MONA.RUN2*	Automatic version for commencing injection and measurement at set Θ's with sampling at 10KHz. Measurements are made over 5 degree window, ensemble-averaged on-line and results are stored and displayed.
MONA.RUN3*	Automatic version to measure instantaneous injection trace for a 40 degree window. Data are sampled at 5 or 10 KHz.

* Only require initial input for the total number of measurements and respective coordinates

MONA.ECAL	Data analysis program
MONA.GRPH	Graphics program
MONA.PC	A program containing the rpm monitoring and gating system software for use with other instrumentation requiring timing information

TABLE C.1 Input parameters for MONA.RUNX

Engine Parameters:

. Engine speed (rpm)

. θ to start injection (deg)

. θ to stop injection (deg)

. θ to start measurement (deg)

. θ to stop measurement (deg)

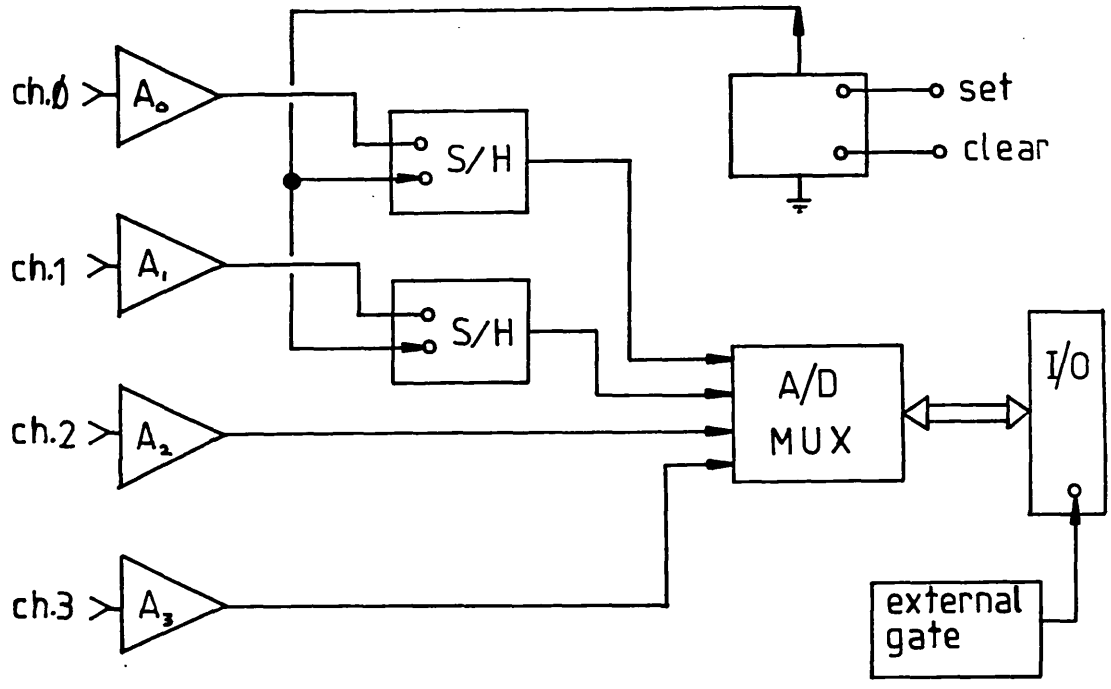
Measurement Parameters:

. Axial position (mm)

. Radial position (mm)

. Highest frequency to sample (KHz)

. Number of engine cycles



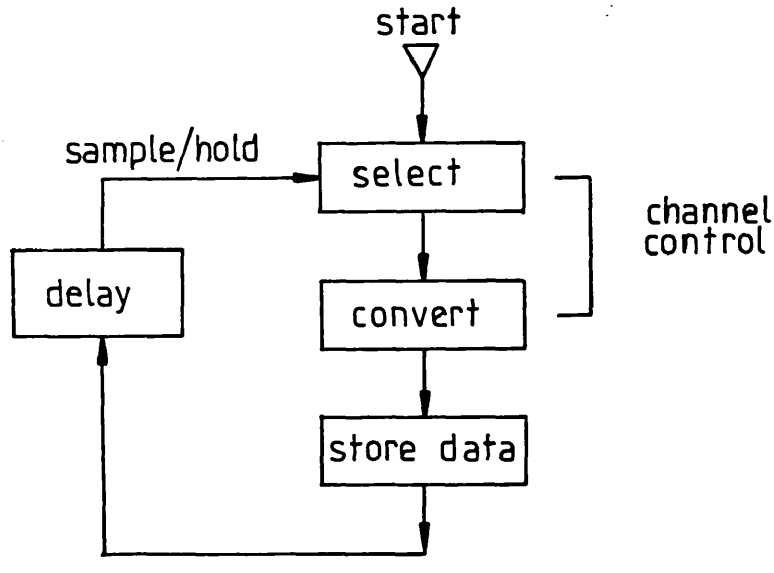


FIGURE C.1 (a) LINE DIAGRAM OF SIGNAL AQUISITION ELECTRONICS (b) FLOW CHART OF DATA CHANNEL SELECT AND SAMPLE

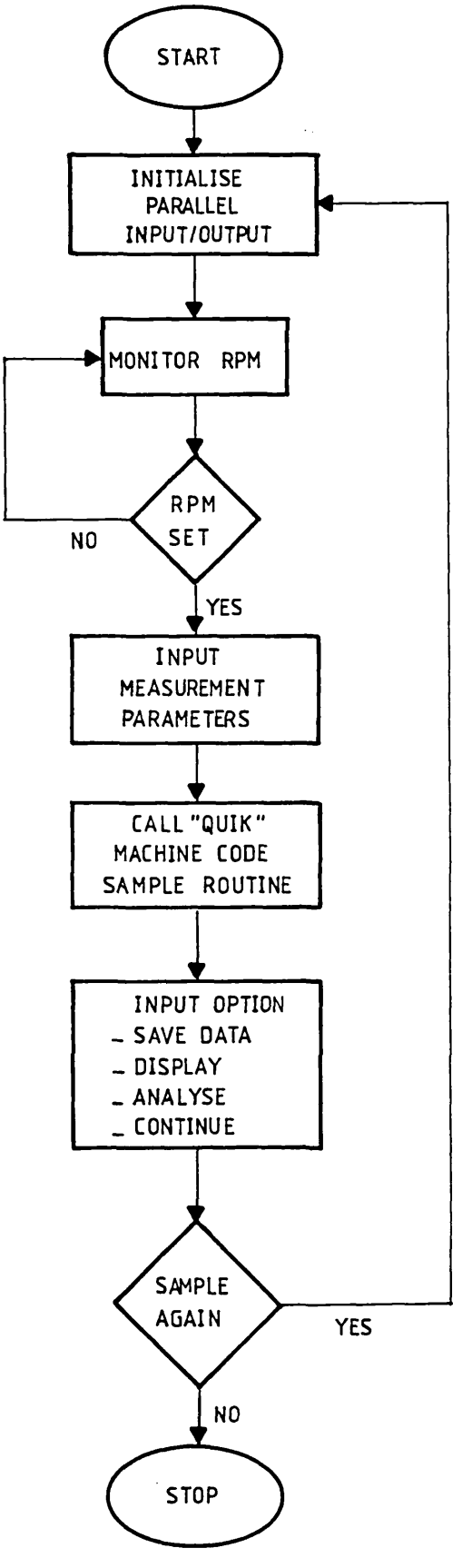


FIGURE C.2 FLOW CHART OF MEASUREMENT SOFTWARE

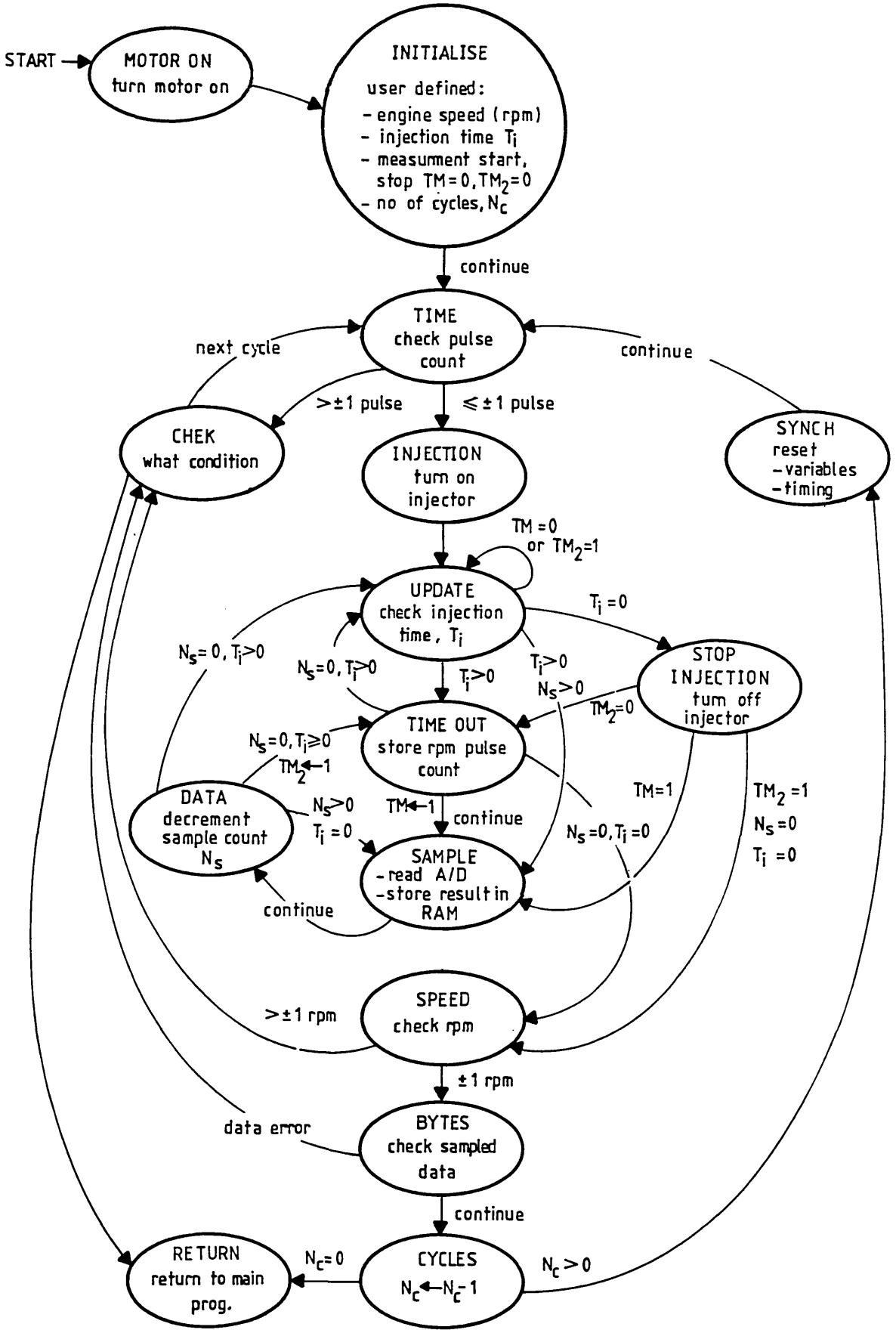


FIGURE C.3 TRANSITION DIAGRAM OF SAMPLING ROUTINE "QUIK"

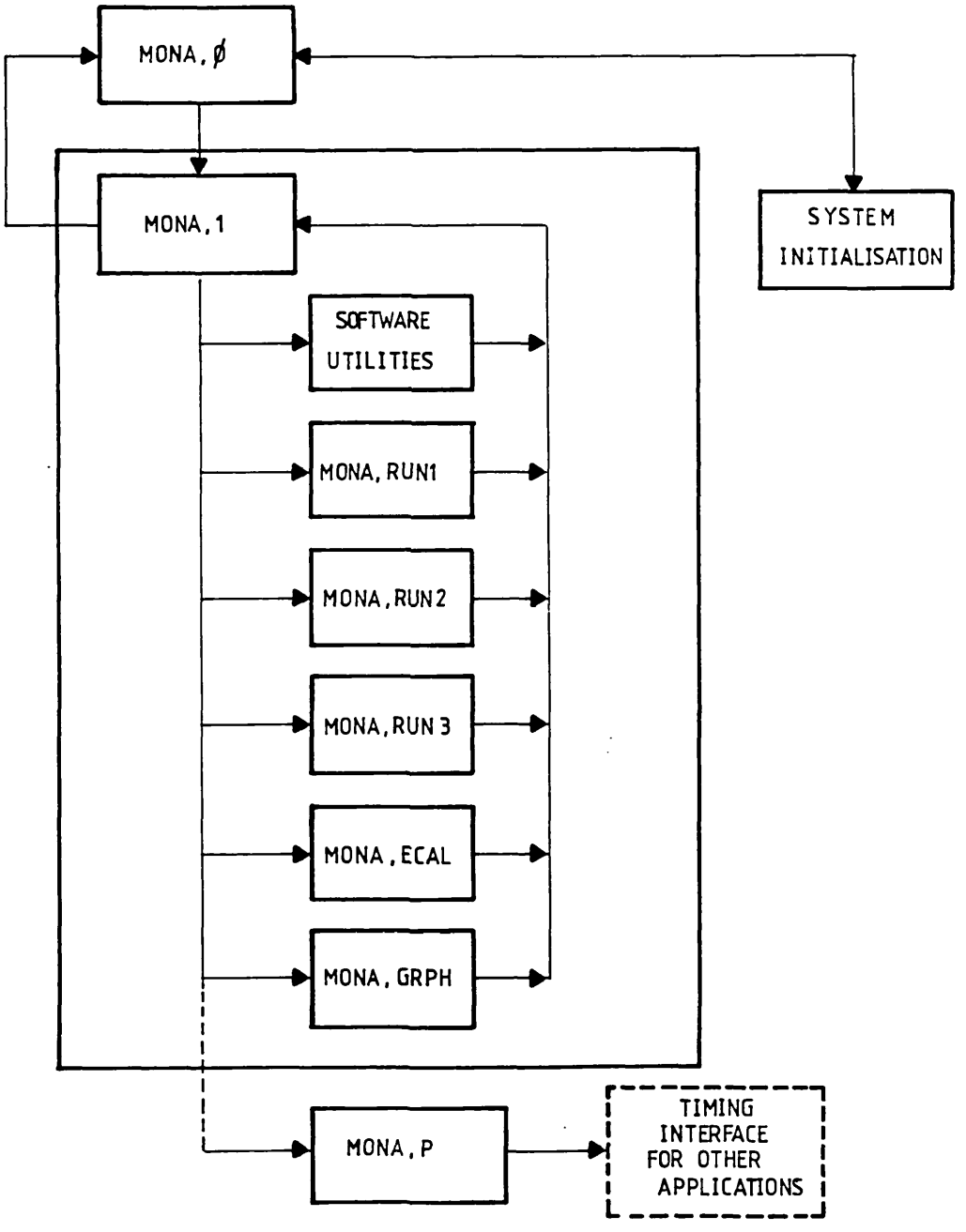


FIGURE C.4 DIAGRAM OF INTEGRATED SOFTWARE SYSTEM "MONA"

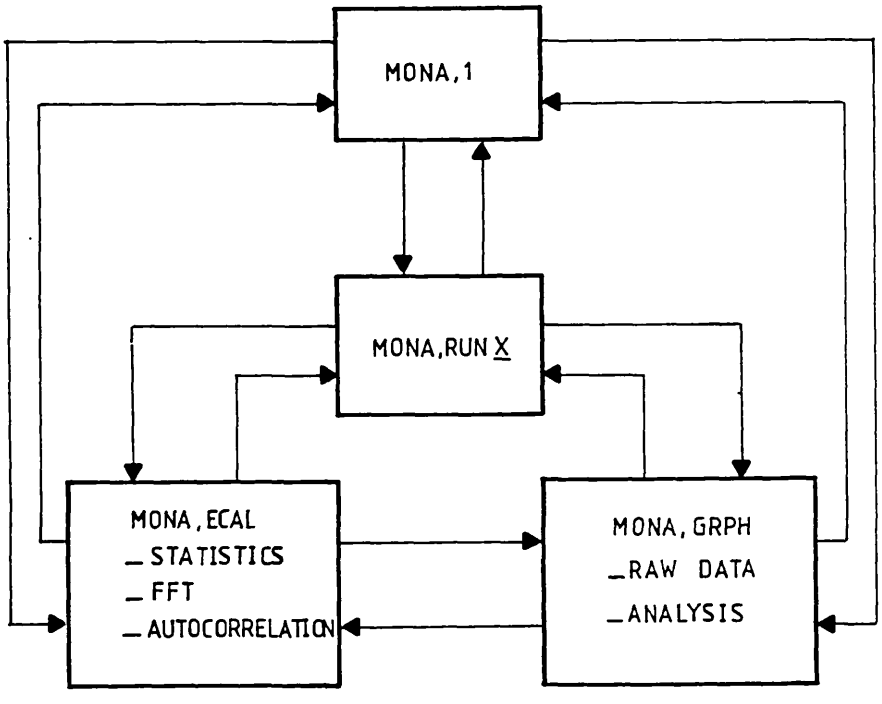


FIGURE C.5 ON-LINE MEASUREMENT MODULE CONFIGURATION

REFERENCES

Abraham J, Bracco F V and Reitz R D (1985) "Comparison of computed and measured premixed charge engine combustion", Comb. and Flame, vol. 60, 309

Abramovich G N (1963) : The Theory of Turbulent Jets, MIT Press

Abramovich G N, Yakovlevsky O V, Smirnova I P, Secundov A N, and Krasheninnikov S, (1969) "An investigation of the turbulent jets of deifferent gases in a general stream", Ast. Acta, vol. 14, 229

Abramovich S and Solan A (1973) "The initial development of a submerged laminar round jet", Journ fluid Mech., vol. 59, 791

Abramovich S and Solan A (1973) "Turn-on and turn-off times for a laminar jet", Journ. Dyn. Sys. and Ctrl., vol. 95, 155

Amano R S and Brandt H (1984) "Numerical study of turbulent axisymmetric jets impinging on a flat plate and flowing into an axisymmetric cavity", Journ. Fluids Engineering, vol. 106, 410

Anderson J S and Williams T J (1968) "Base pressure and noise produced by the abrupt expansion of air in a cylindrical duct", Journ. Mech. Engr. Sci., vol., 10, 262

Anderson R and Bejan A (1985) "The instability of a round jet surrounded by an annular shear layer", Journ. Fluids Engr., vol. 107, 258

Antonia R A, Prabhu A, and Stephenson S E (1975) "Conditionally sampled measurements in a heated turbulent jet", Journ. Fluid Mech., vol. 72, 455

Antonia R A and Rajagopalan S (1984) "Comparison of temperature and velocity spectra in a slightly heated jet", AIAA Journ., vol. 22, 311

Arcoumanis C, Green H G and Whitelaw J H (1984) "The application of laser Rayleigh scattering to a reciprocating model engine", SAE Paper 840376

Aref H (1983) "Integrable, chaotic and turbulent vortex motion in two-dimensional flows", Ann. Rev. Fluid Mech., vol. 15, 345

Barron L D (1982) "Molecular light scattering and optical activity", Cambridge University Press

Barton J C (1982) "Basic Physics and statistics of photomultipliers", Thorn EMI Report R/P 063

Bashir J and Uberoi M S (1975) "Experiments on turbulent structure and heat transfer in a two-dimensional jet", Phys. of Fluids, vol. 18, 405

Batchelor G K (1959) "Small-scale variation of convected quantities like temperature in turbulent fluid: Part 1, General discussions and the case of small conductivity", Journ.Fluid Mech., vol.5 , 113

Batchelor G K, Howells I D and Townsend A A (1959) "Small-scale variation of convected quantities like temperature in turbulent fluid: Part 2, The case of large conductivity", Journ. Fluid Mech., vol. 5, 134

Becker H A, Hottel H C and Williams G C (1963) "Mixing and flow in ducted turbulent jets", Ninth Symposium International, The Comb. Inst., 7

Becker H A, Hottel H C and Williams G C (1967) "On the light-scatter technique for the study of turbulence and mixing", Journ. Fluid Mech., vol. 30, 259

Becker H A, Hottel H C and Williams G C (1967) "The nozzle-fluid concentration field of the round, turbulent, free jet", Journ. Fluid Mech., vol. 30, 285

Becker H A, Hottel H C and Williams G C (1967) "Concentration fluctuations in ducted turbulent jets", Eleventh Symposium International, The Comb. Inst., 791

Becker H A and Massaro T A (1968) "Vortex evolution in a round jet", Journ Fluid Mech., vol. 31, 435

Becker H A and Brown A P G (1969) "Velocity fluctuations in turbulent jets and flames", Twelveth Symposium International, The Comb. Inst., 1059

Becker H A and Booth B D (1971) "Mixing in the interaction zone of two free jets", Rept. Dept. Chem. Engr., Queen's Univ., Ontario, Canada

Becker H A and Brown A P G (1974) "Response of Pitot probes in turbulent streams" Journ. Fluid Mech., vol. 62, 85

Becker H A (1976) "Mixing, concentration fluctuations and marker nephelometry", Studies in Convection, ed. B.E. Launder, vol. 2, Academic Press, 45

Bendat J S and Piersol A G (1971) Random data: analysis and measurement procedures, Wiley-Interscience

Bergwerk W (1959) "Flow pattern in diesel nozzle spray holes", Proc. Instn. Mech. Engrs., vol. 173, 665

Bernard P S (1981) "Computation of the turbulent flow in an internal combustion engine during compression", Journ. Fluids Engr., vol. 103, 75

Beretta F, Cavaliere A and D'Alessio A (1984) "Drop size and concentration in a spray by sideward laser light scattering measurements", Comb. Sci. and Tech., vol. 36, 19

Bertollini G P, Oberdier L M and Lee Y H (1985) "Image processing system to analyze droplet distributions in sprays", Optical Engr., vol. 24, 464

Bhardwaja P S, Charlson R J, Waggoner A P and Ahlquist N C (1973) "Rayleigh scattering coefficients of Freon-12, Freon-22 and CO2 relative to that of air", Appl.Optic, vol. 12, No. 1, 135

Bicen A F (1983) "Air flow charateristics of model internal-combustion engines", Ph.D Thesis, University of London

Bilger R W (1975) "A note on Favre averaging in variable density flows", Comb. Sci. and Tech., vol. 11, 215

Bilger R W, Antonia R A and Sreenivasan K R (1976) "Determination of intermittency from the probability density function of a passive scalar", Phys. of Fluids, vol. 19, 1471

Bilger R W and Dibble R W (1982) "Differential molecular diffusion effects in turbulent mixing", Comb. Sci. and Tech., vol. 28, 161

Bill Jr, R G, Namer I, Talbot L, Cheng R K and Robben F (1981) "Flame propagation in grid-induced turbulence", Comb. and Flame, vol. 43, 229

Bill Jr, R G, Namer I, Talbot L and Robben F (1982) "Density fluctuations of flame in grid-induced turbulence", Comb. and Flame, vol. 44, 277

Binder G and Favre-Marinet, M (1973) "Mixing improvement in pulsating turbulent jets", Proc. Symp. Fluid Mech. of Mixing, ASME, 167

Birch A D, Brown D R and Thomas J R (1975) "Photon correlation spectroscopy and its application to the measurement of turbulence parameters in fluid flow", Journ. Physics, D, vol. 8, 438

Birch A D, Brown D R, Dodson M G, and Thomas J R (1978) "The turbulent concentration field of a methane jet", Journ. Fluid Mech., vol. 88, 431

Birch A D, Brown D R, Dodson M G and Swaffield F (1984) "The structure and concentration decay of high pressure jets of natural gas", Comb. Sci. and Tech., vol. 36, 249

Black P C and Chang R K (1978) "Laser-Raman optical multichannel analyzer for transient gas concentration profile and temperature determination", AIAA Journ., vol. 16, 295

Boguslawski L and Popiel Cz.O (1979) "Flow structure of the free round turbulent jet", Journ. Fluid Mech., vol. 90, 531

Bohren C F and Huffman D R (1983) ; Absorption and scattering of light by small particles, Wiley Interscience

Bonczyk P A and Sangiovanni J J (1984) "Optical and probe measurements of soot in a burning fuel droplet stream", Comb. Sci. and Tech., vol. 36, 135

Bopp S and Whitelaw J H (1985) "In-cylinder flow field of a production disk-type engine and the influences of swirl and rotational speed", Rept. Mech. Engr. Dept., FS/85/40, Imperial College of Science and Technology, London

Born M, and Wolf E (1959) Principles of Optics, Pergamon Press, New York

Box G E P and Jenkins G M (1971) Time Series Analysis (forecasting and control), Holden-Day

Bracco F V (1985) "Modelling of engine sprays", SAE paper 850394

Bradbury L J S (1965) "The structure of a self-preserving turbulent plane jet", Journ. Fluid Mech., vol. 22, 161

Bradbury L J S and Riley J (1967) "The spread of a turbulent plane jet issuing into a parallel moving stream", Journ. Fluid Mech., vol. 27, 381

Bradshaw P, Ferriss D H and Johnston R F (1964) "Turbulence in the noise-producing region of a circular jet", Journ. Fluid Mech., vol. 88, 133

Bradshaw P (1983) : Turbulent shear flows; course notes, Aeronautics Dept., Imperial College of Science and Technology, London

Bremhorst K and Harch W H (1974) "On the correlation of the acoustic pressure and velocity fields of an unheated pulsating air jet", Proceed. Noise, Shock and Vib. Conf., Monash Univ., Melbourne, 247

Bremhorst K and Harch W H (1978) "The mechanism of jet entrainment", AIAA Journ., vol. 16, 1104

Bremhorst K and Harch W H (1979) "Near field velocity measurements in a fully pulsed subsonic air jet", Proc. First Symp. Turbulent Shear Flows, London

Bremhorst K and Watson R D (1981) "Velocity field and entrainment of a pulsed core jet", Journ Fluids Engr., vol. 103, 605

Browand F K and Trout T R (1985) "The turbulent mixing layer: geometry of large vortices", Journ. Fluid Mech., vol. 158, 489

Brown G L and Roshko A (1974) "On density effects and large structure in turbulent mixing layers", Journ. Fluid Mech., vol. 64, 775

Bywater R J (1981) "Velocity space description of certain turbulent free shear flow characteristics", AIAA Journ., vol. 19, 969

Cabannes J (1915) C. R. Acad. Sci., vol. 160, 62

Cabannes J (1921) Ann. Pysique (9) 15, 5

Cantwell B J (1981) "Organized motion in turbulent flow", Ann. Rev. Fluid Mech., vol. 13, 457

Carlomagno G M (1985) "The initial region in a plane two-dimensional jet", Heat and Tech., vol. 3, 123

Carr A E, Cuthbert L G and Oliver A D (1981) "Digital signal processing for target detection in FMCW Radar", IEE Proc., vol. 128, 331

Chatfield C (1984) The analysis of time series: an introduction, Chapman and Hall

Chen C J and Rodi W (1980) Vertical Turbulent Buoyant Jets: A Review of Experimantal Data, Pergamon Press

Cheng R K, Bill J R and Robben F (1981) "Experimental study of combustion in a turbulent boundary layer", Eighteenth Symposium International, The Comb. Inst., 1021

Chevray R and Tutu N K (1978) "Intermittency and preferential transport of heat in a round jet", Journ. Fluid Mech., vol. 88, 133

Chew H, Kerker M and Cooke D D (1977 (a)) "Electromagnetic scattering by a dielectric sphere in a diverging radiation field", Phys. Rev. A, vol. 16, 320

Chew H , Kerker M and Cooke D D (1977 (b)) "Light scattering in converging beams", Optics Let., vol. 1, 138

Chiger N A and Yule A J (1979) "The structure of eddies in turbulent flames", Rept. Dept. Chem. Engr., Univ. Sheffield, Sheffield (also Technical Report, Project Squid)

Cho S H and Becker H A (1985) "Response of static pressure probes in turbulent streams", Exp. in Fluids, vol. 3, 93

Clark J A and Kit L (1980) "Shear layer transition and the sharp-edged orifice", Journ. Fluids Engr., vol. 102, 219

Cole J B and Swords M D (1980) "Measurement of concentration fluctuations in an internal combustion engine", Journ. Phys. D, vol.13, 733

Coles D (1981) "Prospects for useful research on coherent structure in turbulent shear flow", Proc. Indian Acad. Sci. (Eng. Sci), vol. 4, 111

Constantinides A G (1985) private communication

Corke T C and Guezennec Y G (1986) "Discrimination of coherent features in turbulent boundary layers by the entropy method", AIAA Journ., vol. 24, 377

Corrsin S and Uberoi M S (1950) "Further experiments on the flow and heat transfer in a heated turbulent jet", NACA Report 998

Crabb D and Whitelaw J H (1979) "The influence of geometric asymmetry on the flow downstream of a row of jets discharging normally into a free stream", Journ. Heat Trans., vol. 101, 183 (see also, Matthews L and Whitelaw J H (1971), Rept. Mech. Engr. Dept. EHT/TN/A/34, Imperial College, London)

Crabb D, Durao D F G and Whitelaw J H (1981) "A round jet normal to a crossflow", J. Fluids Engr., vol. 103, 142

Csanady G T (1963) "On the energy balance of a turbulent mixing layer", Journ. Fluid Mech., vol. 15, 545

Csanady G T (1967) "Concentration fluctuations in turbulent diffusion", Journ. Atmospheric Sci., vol. 24, 21

Cummings A (1984) "Acoustic non-linearities and power losses at orifices", AIAA Journ., vol. 22, 786

Dainty J C (1984) Private communication

Dash R (1980) "Strouhal number influences on flight effects on jet noise radiated from convecting quadrupoles", AIAA Journ., vol. 18, 337

Dash S M and Wolf D E (1984) "Interactive phenomena in supersonic jet mixing problems, Parts 1 and 2", AIAA Journ., vol. 22, 905-913 and 1395-1404

Davies P O A L, Fisher M J and Barratt M J (1962) "The characteristics of the turbulence in the mixing region of a round jet", Journ. Fluid Mech., vol. 15, 337

Davis M R (1971) "Measurements in a subsonic turbulent jet using a quantitative Schlieren technique", Journ. Fluid Mech., vol. 46, 631

Davis M R and Davies P O A L (1979) "Shear fluctuations in a turbulent jet shear layer", Journ. Fluid Mech., vol. 93, 281

Davis M R (1975) "Intensity, scale and convection of turbulent density fluctuations", Journ. Fluid Mech., vol. 70, 463

Deiwert G S (1984) "Supersonic axisymmetric flow over boattails containing a centered propulsive jet", AIAA Journ., vol. 22, 1358

Dent J C (1971) "A basis for the comparison of various experimental methods for studying spray penetration", SAE Paper 710571

Dibble R W, Hollenbach R E and Rambach G D (1980) "Temperature measurements in turbulent flames via Rayleigh scattering", Laser Probes for Combustion Chemistry, ed: D R Crosley, Amer. Chem. Society

Dibble R W and Hollenbach R E (1981) "Laser Rayleigh thermometry in turbulent flames", Eighteenth Symposium (Intl) on Comb., The Comb. Inst., 1489

Dibble R W, Rambach R E, Hollenbach R E, and Ringland J T (1981) "Simultaneous measurement of velocity and temperature in flames using LDV and CW laser Rayleigh thermometry", Symposium on Turbulence, Dept. of Chem. Engr., Univ. of Missouri, Rolla, USA, 64

Dibble R W, Kollmann W and Schefer R W (1984) "Conserved scalar fluxes measured in a turbulent nonpremixed flame by combined laser Doppler velocimetry and laser Raman scattering", Comb. and Flame, vol. 55, 307 (see also, SAND84-8860)

Dopazo C (1975) "Probability density function approach for a turbulent axisymmetric heated jet centreline evolution", Phys. of Fluids, vol. 18, 397

Dopazo C and O'Brien E E (1976) "Statistical treatment of non-isothermal chemical reactions in turbulence", Comb. Sci. and Tech., vol. 13, 99

Drake M C, Lapp M, Penney C M, Warshaw S and Gerhold (1981) "Measurements of temperature and concentration fluctuations in turbulent diffusion flames using pulsed Raman spectroscopy", Eighteenth Symposium International, The Comb. Inst., 1521

Durao D F G (1971) "Experimental investigations of co-axial jets", Rept. Mech. Engr. Dept., DTA RC/5, Instituto Superior Tecnico, Lisboa, Portugal

Durao D F G and Whitelaw J H (1972) "Turbulent mixing in the developing region of co-axial jets", Rept. Mech. Engr. Dept., ET/TN/A/19, Imperial College of Science and Technology, London

Durao D F G and Whitelaw J H (1974) "Performance characteristics of two frequency-tracking demodulators and a counting system measurements in an air jet", Proc. 2nd Int. Laser Vel., Purdue, No. 1, 170

Durao D F G and Whitelaw J H (1979) "Relationship between velocity and signal quality in laser Doppler anemometry", Journ. Phys., E, vol. 12, 47

Durao D F G and Pita G (1984) "Coherent structures in the near field of round jets", Exp. in Fluids, 2

Durbin P A (1983) "High frequency Green functions for aerodynamic noise in moving media, Part I and Part II", Journ. Sound and Vib., vol. 91, 519

Durst F, Melling A, and Whitelaw J H (1976) Principles and practice of laser Doppler anemometry, Academic Press

Durst F (1982) "Review - Combined measurements of particle velocities, size distributions, and concentrations", Journ. Fluids Engr., vol. 104, 285

Dyer T M (1979) "Characterization of one- and two-dimensional homogeneous combustion phenomena in a constant volume bomb", SAE Trans., vol. 88, Paper 790353, 1196

Dyer T M (1979) "rayleigh scattering measurements of time-resolved concentration in a turbulent propane jet", AIAA Journ., vol. 17, 912

Dyer T M (1985) "New experimental techniques for in-cylinder engine studies", SAE Paper 850396, also SAND84-8901

Dziomba B and Fiedler H E (1985) "Effect of initial conditions on two-dimensional free shear layers", Journ. Fluid Mech., vol. 152, 419

Eickhoff H (1982) "Instability of coherent structures in jet flames. Recent contributions to fluid mechanics", Springer - Verlag, 50

Eickhoff H and Winandy A (1985) "Visualization of vortex formation in jet diffusion flames", Comb. and Flame, vol. 60, 99

Elghobashi S E, Samuelson G S, Wuerer J E and LaRue J C (1981) "Prediction and measurement of mass, heat and momentum transport in a nonreacting turbulent flow of a jet in an opposing stream", Journ. Fluids Engr., vol. 103, 127

Escoda M C and Long M B (1983) "Rayleigh scattering measurements of the gas concentration field in turbulent jets", AIAA Journ., vol. 21, 81

Fabelinskii I L (1968) ; Molecular Scattering of Light, New York, Plenum Press

Fansler T D (1985) "Laser velocimetry measurements of swirl and squish flows in an engine with a cylindrical piston bowl", SAE paper 850124

Favre A (1969) "Statistical equations of turbulent gases", Prob. in Hydrodynamics and Continuum Mechanics,pp.231-266 SIAM, Philadelphia, PA., USA

Favre-Marinet M, Binder G and Hac T V (1981) "Generation of oscillating jets", Journ. Fluids Engr., vol. 103, 609

Forstall W and Shapiro A H (1950) "Momentum and mass transfer in coaxial gas jets", Trans. ASME Journ. Appl. Mech., 399

Fujii S, Nishiwaki H and Takeda K (1981) "Suppression of jet noise peak by velocity profile reshaping", AIAA Journ., vol. 19, 872

Gargett A E (1985) "Evolution of scalar spectra with the decay of turbulence in a stratified fluid", Journ. Fluid Mech., vol. 159, 379

Gaster M and Roberts J B (1975) "Spectral analysis of randomly sampled signals", Journ. Inst. Math. Applics., vol. 15, 1975

Gaster M and Roberts J B (1977) "The spectral analysis of randomly sampled records by a direct transform", Proc. Royal Society of London, Series A, vol. 354, 27

Gebhart B (1979) Buoyancy induced fluid motions characteristic of applications in technology", Journ. Fluids Engr., vol. 101, 5

George T V, Goldstein L, Slama L and Yokoyama M (1965) "Molecular scattering of ruby-laser light", Physical Rev., vol. 137, A369

George W K and Lumley J L (1973) "The laser-Doppler velocimeter and its application to the measurement of turbulence", Journ. Fluid Mech., vol. 60, 321

Gibson M M (1963) "Spectra of turbulence in a round jet", Journ. Fluid Mech., vol. 15, 161

Gibson M M and Younis B A (1986) "Calculation of swirling jets with a Reynolds stress closure", Physics of Fluids, vol. 29, 38

Gibson C H and Schwarz W H (1963) "The universal equilibrium spectra of turbulent velocity and scalar fields", Journ. Fluid mech., vol 16, 365

Ginzburg I P and Ugryumov Ye A (1975) "Interaction between a baffle and transient gas jets emanating from two- and four-nozzle setups", Fluid Mech., Soviet Research, vol. 4, 89

Givi P, Sirignano W A and Pope S B (1984) "Probability calculations for turbulent jet flows with mixing and reaction of NO and O_3", Comb. Sci. and Tech., vol. 37, 59

Gouldin F C and Dandekar K V (1984) "Time-resolved density measurements in premixed turbulent flames", AIAA Journ., vol. 22, 655

Graham S C, Grant A J and Jones J M (1974) "Transient molecular concentration measurements in turbulent flows using Rayleigh light scattering", AIAA Journ., vol. 12, 1140

Graham S C (1979) Comments to Muller-Dethlefs and Weinberg, Seventeenth Symposium International, The Comb. Inst., 992

Gulati A and Driscoll J F (1986) "Velocity-density correlations and Favre averages measured in a premixed flame", Comb. Sci. and Tech., vol. 48, 285

Gutmark E, Wolfshtein M and Wygnanski I (1978) "The plane turbulent impinging jet," Journ. Fluid Mech., vol. 88, 737

Gutmark E and Ho, C M (1983) "Preferred modes and the spreading rates of jets", Physics of Fluids, vol. 26, 2932

Habib M A and Whitelaw J H (1979) "Velocity characteristics of a confined coaxial jet", Journ. Fluids Engr., vol. 101, 521

Halthore R N and Gouldin F C (1984) "Laser scattering measurements for density in a swirling flow combustor", AIAA Paper 84-0199, pressented at the AIAA 22nd Aerospace Sciences Meeting, Reno Nevada

Hanson R J and Thomas A (1984) "Flame development in swirling flows in closed vessels", Comb. and Flame, vol. 55, 255

Hasan M A Z and Hussain A K M F (1982) "The self-excited axisymmetric jet", Journ. Fluid Mech., vol. 115, 59

Hasan M A Z and Hussain A K M F (1984) "Jet noise modification by the 'Whistler nozzle' ", AIAA Journ., vol. 22, 340

Haumann J and Leipertz A (1984) "Flame-temperature measurements using the Rayleigh scattering photon-correlation techinque", Optics. Let., vol. 9, 487

Haumann J and Leipertz A (1985) "Time-resolved concentration measurements using Rayleigh scattering correlation technique", Meas. Tech. in Heat and Mass Trans., ed: R I Soloukhin and N H Afgan, Hemisphere Publ. Corp., 111-122

Hay N and Jones P L (1972) "Comparison of the various correlations for spray penetration", SAE Paper 720776

Hay J A and Rose E G (1970) "In-flight schock cell noise", Journ. Sound and Vib., vol. 11, 411

Hetsroni G and Sokolov M (1971) "Distribution of mass, velocity and intensity of turbulence in a two-phase turbulent jet", Trans. ASME Journ. Appl. Mech., 315

Hill R J (1978) "Models of the scalar spectrum for turbulent advection", Journ. Fluid Mech., vol. 88, 541

Hill Jr. W G and Greene P R (1977) "Increased turbulent jet mixing rates obtained by self-excited acoustic oscillations", Journ. Fluids Engr., vol. 99, 520

Hinze J O and Van Der Hegge Zijnen B G (1948) "Transfer of heat and matter in the turbulent mixing zone of an axially symmetrical jet", Appl. Sci. Res., vol. A1, 453

Hinze J O (1975) : Turbulence, McGraw-Hill, New York

Hisashi M (1980) "Free jet expansion in a rapidly rotating gas", AIAA Journ., vol. 18, 471

Hoffman M A, Takahashi R K and Monson R D (1980) "Annular liquid jet experiments", Journ. Fluids Engr., vol. 102, 344

Hoggarth M L and Jones D A (1973) " Design and performance of a variety of injector systems", Journ. Mech. Engr. Sci., vol. 15, 422

Hooker R J and Rumble R H (1981) "Noise characteristics of a pulsed jet", Noise Control Engr., vol. 17, 113

Hopkins D F and Robertson J M (1967) "Two-dimensional incompressible fluid jet penetration", Journ. Fluid Mech., vol. 29, 273

Hopwood R K (1980) "Design considerations for a solid-state image sensing system", Proc. Soc. Photo-Optical Inst. Engr., vol. 230, 72, Washington D C , USA

Horvath H (1967) "The refractive index of Freon-12", Applied Optics, vol. 6, 1140

Hottel H C (1953) "Burning in laminar and turbulent fuel jets", Fourth Symposium International, The Comb. Inst., 97

Hsia Y, Baganoff D, Krothapalli and Karamcheti K (1984) "An enhanced flow visualization technique for planar free shear layers", AIAA Journ, vol. 22, 439

Hussain A K M F and Husain Z D (1980) "Turbulence structure in the axisymmetric free mixing layer," AIAA Journ. vol. 18, 1462

Hussain A K M F and Zaman K B M Q (1981) "The 'prefered mode' of the axisymmetric jet", Joun. Fluid Mech., vol. 110, 39

Hussain A K M F (1983) "Coherent structures-reality and myth", Phys. of Fluids, vol. 26, 2816

Hussain A K M F and Zaman K B M Q (1985) "An experimental study of organized motions in the turbulent plane mixing layer", Journ. Fluid Mech., vol. 159, 85

Hussain A K M F and Hasan M A Z (1985) "Turbulence suppression in free turbulent shear flows under controlled excitation: Part 2. Jet-noise reduction", Journ. Fluid Mech., vol. 150, 159

Islam S M N and Tucker H J (1980) "Flow in the initial region of axisymmetric turbulent jets", Journ. Fluids Engr., vol. 102, 85

Jenkins G M and Watts D B (1969) : Spectral analysis and its application, Holden-Day

Kalghatgi G T (1985) "Early flame development in a spark-ignition engine", Comb. and flame, vol. 60, 299

Kalghatgi G T (1980) "Study of coherent structures in axisymmetric jets using an optical technique", AIAA Journ., vol. 18, 225

Kamimoto T, Aoyagi Y, Matsui Y and Matsuoka S (1980) "The effects of some engine variables on measured rates of air entrainment and heat release in a DI diesel engine", SAE Paper 800253

Kerker M (1969) : The scattering of light and other electromagnetic radiation, Academic Press

Kibens V (1980) "Discrete noise spectrum generated by an acoustically excited jet", AIAA Journ., vol. 18, 434

Ko N W M and Chan W T (1979) "The inner regions of annular jets", Journ Fluid Mech., vol. 93, 549

Ko N W M and Au H (1981) "Initial region of subsonic coaxial jets of high mean velocity ratio", Journ. Fluids Engr., vol. 103, 335

Kollmann W (1979) "Closure of the transport equation for the probability density function of turbulent scalar fields", Journ. Non-equilibr. Therm., vol. 4, 47

Kollmann W (1984) "Prediction of the intermittency factor for turbulent shear flows" AIAA Journ., vol. 22, 486

Kolmogorov A N (1962) "A refinement of previous hypotheses concerning the local structure of turbulence in a viscous incompressible fluid at high Reynolds number", Journ. Fluid Mech., vol. 13, 82

Komori S and Ueda H (1985) "The large-scale coherent structure in the intermittent region of the self-preserving round free jet", Journ. Fluid Mech., vol. 152, 337

Kraichnan R H (1974) "On Kolmogorov's inertial-range theories", Journ. Fluid Mech., vol. 62, 305

Kuo T W (1982) "On the scaling of transient laminar, turbulent and spray jets", PhD Thesis , Princenton University

Kuo T W and Bracco F V (1982) "On the scaling of transient laminar, turbulent, and spray jets", SAE Paper 820038

Kuo T W and Bracco F V (1982) "On the scaling of impulsively started incompressible turbulent round jets", Journ. Fluids Engr., vol. 104, 191

Kuo T W and Yu R C (1984) "Modeling of transient evaporating spray mixing processes - Effect of injection characteristics", SAE Paper 840226

Kuo T W, Syed S A and Bracco F V (1986) "Scaling of impulsively started, incompressible, laminar round jets and pipe flows", AIAA Journ., vol. 24, 424

Lafrance P (1977) "The breakup length of turbulent liquid jets", Trans. ASME (June 1977), Journ. Fluids Engr., 414

Lau J C, Morris P J and Fisher M J (1979) "Measurements in subsonic and supersonic free jets using a laser velocimeter", Journ. Fluid Mech., vol. 93, 1

Lau J C (1980) "Mach number and temperature effets on jets", AIAA Journ., vol. 18, 609

Laufer J, Kaplan R E and Chu W T (1974) "On the generation of jet noise", AGARD Conf. Proc. no. 131, Paper 21

Lavan M J (1978) "Approximate formula for second-order Rayleigh scattering from N particles", Optics Comm., vol. 26, 357

Leconte J (1858) Phil. Mag., vol. 15, 235

Leipertz A and Fiebig M (1979) "Experimental investigation of small single and multiple free jets by laser Raman spectroscopy", Optical Engr., vol. 18, 409

Leipertz A (1982) "Rayleigh measurements in a CO2 jet", Applied Optics, vol. 21, 2872

Leipertz A, Haumann J and Wu G (1985) "Space resolved probing of gas concentration and temperature strcutures", IUTAM Symposium Liblice, Czechoslovakia, 1984, ed: M. Pichal, Springer-verlag ,1985, Berlin

Lepicovsky J (1986) "Laser velocimeter measurements of large-scale structures in a tone excited jet", AIAA Journ., vol. 24, 27

Lessen M (1978) "On the power laws for turbulent jets, wakes and shearing layers and their relationship to the principle of marginal instability", Journ. Fluid Mech., vol. 88, 535

Libby P A (1976) "Studies in variable-density and reacting turbulent shear flows" in Studies in Convection, vol. 2, 1, ed: B E Launder, Academic press

Libby P A, Sivasegaram S and Whitelaw J H (1984) "Premixed combustion", Rept. Mech. Engr. Dept. FS/84/17, Imperial College of Science and Technology, London

Libby P A (1984,1986) Private communication

Liepmann H W, Laufer J and Liepmann K (1951) "On the spectrum of isotropic turbulence", NACA Technical note 2473

List E J (1982) "Turbulent jets and plumes", Ann. Rev. Fluid Mechs., vol. 14, 189

Liu J T C (1974) "Developing large-scale wavelike eddies and the near jet noise field", Journ. Fluid Mech., vol. 62, 437

Lockwood F C and Moneib H A (1980) "Fluctuating temperature measurements in a heated round free jet", Comb. Sci. and Tech., vol. 22, 63

Lohmann R P, Markowski S J and Brookman E T (1979) "Swirling flow through annular diffusers with conical walls", Journ. Fluids Engr., vol. 101, 225

Long M B, Chu B T and Chang R K (1981) "Instantaneous two-dimensional gas concentration measurements by light scattering", AIAA Journ., vol. 19, 1151

Long M B and Chu B T (1981) "Mixing mechanism and structure of an axisymmetric turbulent mixing layer", AIAA Journ., vol. 19, 1158

Long M B, Levin P S and Fourguette D C (1985) "Simultaneous two-dimensional mapping of species concentration and temperature in turbulent flames", Optics Letters, vol. 10, 267

Long D F and Arndt R E A (1984) "Jet noise at low Reynolds number", AIAA Journ., vol. 22, 187

Maczynski J F J (1962) "A round jet in an ambient co-axial stream", Journ. Fluid Mech., vol. 12, 507

Maestrello L and Fung Y T (1979) "Quasi-periodic structure of a turbulent jet", Journ. of Sound and Vib., vol. 64, 107

Manela J and Seginer A (1986) "Jet penetration height in transonic flow", AIAA Journ., vol. 24, 67

Marrero T R and Mason E A (1972) : Gaseous Difussion Coefficients, J Phys. Chem. Ref. Data, vol. 1, no.1

Martinelli L, Reitz R D and Bracco F V (1983) "Comparison of computed and measured dense spray jets", Ninth International Colloquium on Dynamics of Explosions and Reactive System, Poiters

McGowan R S and Larson R S (1984) "Relationship between static, flight and simulated flight jet noise measurements", AIAA Journ., vol. 22, 460

Melling A and Whitelaw J H (1975) "Optical and flow aspects of particles", Proc. LDA-Symposium Copenhagen, 382

Melton R B (1971) "Diesel fuel injection viewed as a jet phenomena", SAE Paper 710132

Melton L A and Verdieck J F (1985) "Vapor/liquid visualization for fuel sprays", Comb. Sci. and Tech., vol. 42, 217

Michalke A and Fuchs H V (1975) "On turbulence and noise of an axisymmetric shear flow", Journ. Fluid Mech., vol. 70, 179

Middleton D (1970) "Theoretical and experimental investigations into the acoustic output from ejector flows", Journ. Sound and Viv., vol. 11, 447

Morris C J and Dent J C (1976) "The simulation of air fuel mixing in high swirl open chamber diesel engines", Proc. Inst. Mech. Engrs., vol. 190, 503

Morrison G L and Mclaughlin D K (1980) "Instability process in low Reynolds number supersonic jets", AIAA Journ., vol. 18, 793

Morse A P (1980) ; Axisymmetric Turbulent Shear Flows With and Without Swirl, PhD Thesis, University of London

Muller-Dethlefs K and Weinberg F J (1979) "Burning velocity measurement based on laser Rayleigh scattering", Seventeenth Symposium (International) on Combustion, The Combustion Institute, 985

Mugal M G, Dimotakis P E and Broadwell J E (1984) "Turbulent mixing and combustion in a reacting shear layer", AIAA Journ., vol. 22, 797

Musinski D L, Steinman D A, Pattinson T R and Jacobs R B (1982) "Gas jet IF targets", Journ. Vac. Sci. Tech., vol. 20, 1366

Naboko I M, Golub V V, Eremin A V, Kochnev V A and Kulikovsky A A (1977) "Wave structure and density distribution in a nonstationary gas jet"
Archives of Mech., vol. 29, 69

Namer I, Bill Jr. R G, Talbot L and Robben F (1984) "Density fluctuations in a flame in a Karman vortex street", AIAA Journ., vol. 22, 647

Narain J P (1976) "Momentum flux development from three-dimensional free jets", Trans ASME Journ. Fluids Engr., 257

Nelson P A, Halliwell N A and Doak P E (1981) "Fluid dynamics of a flow excited resonance: part I", Journ. Sound and Vib., vol. 78, 15

Nelson P A, Halliwell N A and Doak P E (1983) "Fluid dynamics of a flow excited resonance: part II", Journ. Sound and Vib., vol. 91, 375

Newman J A and Brzustowksi T A (1971) "Behavior of a liquid jet near the thermodynamic critical region", AIAA Journ., vol. 9, 1595

Nir A and Pismen L M (1978) "The effect of a steady drift on the dispersion of a particle in turbulent fluid", Journ. Fluid Mech., vol. 94, 369

Nye J O and Brodkey R S (1967) "The scalar spectrum in the viscous-convective subrange", Journ. Fluid Mech., vol. 29, 151

Oliver C J (1982) "A comparison of current-measurements with photon-counting in the use of photomultiplier tubes", EMI Report R/P 066

Otis D R (1976) "Choking and mixing of two compressible fluid streams", Trans ASME Journ. Fluids Engr., June 1976, 311

Otnes R K and Enochson L (1978) : Applied time series analysis, John Wiley and Sons

Parikh P G and Moffat R J (1982) "Resonant entrainment of a confined pulsed jet", Journ. Fluids Engr., vol. 104, 482

Parker T E, Forsha M D, Stewart H E, Hom h, Sawyer R F and Oppenheim A K (1985) "Induction period for ignition of fuel sprays at high temperatures and pressures", SAE Paper 850087

Penndorf R (1957) "Tables of the refractive index for standard air and Rayleigh scattering coefficient for the spectral region between 0.2 and 20.0μ and their application to atmospheric optics", Journ. Opt. Soc. Amer., vol. 47, 176

Penney C M (1969) "Light scattering in terms of oscillator strengths and refractive indicies", Journ. Opt. Soc. Amer., vol. 59, 34

Penney C M, Warshaw S, Lapp M and Drake M "Observations of fast turbulent mixing in gases using a continuous-wave laser", Laser Probes for Combustion Chemistry, ed: D R Crosley, Amer. Chem. Society

Perry A E and Lim T T (1978) "Coherent structures in coflowing jets and wakes", Journ. Fluid Mech., vol. 88, 451

Petersen R A (1978) "Influence of wave dispersion on vortex pairing in a jet", Journ. Fluid Mech., vol. 89, 469

Phillips H (1972) "Ignition in a transient turbulent jet of hot inert gas", Comb. and Flame, vol. 19, 187

Phillips W F (1981) "The effect of Froude number on entrainment in two-dimensional line plumes", Journ. Fluids Engr., vol. 103, 471

Pike E R (1969) "Photon statistics", Riv. Nuovo Cim - 1 (Numero Speciale), 227

Pimbley W T and Rickenbach D H (1979) "Fillet size in a liquid jet", Journ. Fluids Engr., vol. 101, 105

Pirouz-Panah V and Williams T J (1977) "The influence of droplets on the properties of liquid fuel jets", Inst. Mech. Engrs., vol. 191, 299

Pitts W M and Kashiwagi T (1984) "The application of laser-induced Rayleigh light scattering to the study of turbulent mixing", Journ. Fluid Mech., vol. 141, 391

Pitts W M (1986) "Effects of global density and Reynolds number variations on mixing in turbulent, axisymmetric jets", NBSIR 86-3340, submitted to Journ. Fluid Mech.

Pitz R W, Cattolica R, Robben F, and Talbot L, (1976) "Temperature and density in a hydrogen-air flame from Rayleigh scattering", Comb. and Flame, vol. 27, 313

Plaschko P (1979) "Helical instabilities of slowly diverging jets", Journ. Fluid Mech., vol. 92, 209

Platzer M J, Simmons J M and Bremhorst K (1978) "Entrainment characteristics of unsteady subsonic jets", AIAA Journ., vol. 16, 282

Pope S B (1976) "The probability approach to the modelling of turbulent reacting flows", Comb. and Flame, vol. 27, 299

Pope S B (1979) "The statistical theory of turbulent flames", Phil. Trans., Soc. of London, vol. 291, 529

Pope S B (1984) "Calculations of a plane turbulent jet", AIAA Journ., vol. 22, 896

Pope S B (1984) "Monte Carlo Calculations of turbulent diffusion flames", Comb. Sci. and Tech., vol. 42, 13

Radcliffe A (1953) "The performance of a type of swirl atomizer", Inst. Mech. Engrs., 93

Rahimi A, and Mote C D (1983) "Identification of the frequency spectrum through signal modeling", ASME paper 83-WA/DSC-36

Rajan S, Smith J R and Rambach G D (1984) "Internal structure of a premixed turbulent flame using Rayleigh scattering", Comb. and Flame, vol. 57, 95

Rajaratnam N (1976) ; Turbulent Jets, Elsevier Scientific Publishing Company, Amsterdam-Oxford-New York

Rambach G D, Dibble R W and Hollenbach R E (1979) "Velocity and temperature measurements in turbulent diffusion flames", Sandia National Laboratories, Report SAND 79-8775

Rankin G W and Sridhar K (1978) "Developing region of laminar jets with uniform exit velocity profiles", Journ. Fluids Engr., vol. 100, 55

Rankin G W and Sridhar K (1981) "Developing region of laminar jets with parabolic exit velocity profiles", Journ. Fluids Engr., vol. 103, 322

Rayleigh (Lord) (1871) Phil. Mag., (4) 41, 107

Rayleigh (Lord) (1881) Phil. Mag., (5) 12, 81

Rayleigh (Lord) (1899) Phil. Mag., (5) 47, 375

Rayleigh (Lord) (1896) The Theory of Sound, Vol. 1, Dover Edition 1945

Reitz R D and Bracco F B (1979) "On the dependence of spray angle and other spray parameters on nozzle design and operating conditions", SAE Paper 790494

Reitz R D and Bracco (1979) "Ultra-high-speed filming of atomizing jets", Physics of Fluids, vol. 22, 1054

Reitz R D and Bracco F B (1982) "Mechanism of atomization of a liquid jet", Phys. of Fluids, vol. 25 1730

Ribeiro M M and Whitelaw J H (1975), "Statistical characteristics of a turbulent jet", Journ. Fluid Mech., vol. 70, 1

Ribeiro M M and Whitelaw J H (1976) "Turbulent mixing of coaxial jets with particular reference to the near exit region", Journ. Fluids Engr., vol. 98, 284

Ribeiro M M and Whitelaw J H (1980) "The structure of turbulent jets", Proc. Royal Society London A 370, 281

Ribeiro M M and Whitelaw J H (1980) "Coaxial jets with and without swirl", Journ. Fluid Mech., vol. 96, 769

Ribner H S (1981) "Perspectives of jet noise", AIAA Journ., vol. 19, 1513

Ricou F P and Spalding D B (1961) "Measurements of entrainment by axisymmetrical turbulent jets", Journ. Fluid Mech., vol. 11, 21

Robben F (1971) "Noise in the measurement of light with photomultipliers", Appl. Optics, vol. 10, 776

Robben F (1976) "Comparison of density and temperature measurement using Raman scattering and Rayleigh scattering", Comb. Measurement, ed. by R Goulard, New York, Academic Press, 180

Rockwell D and Schachenmann A (1982) "The organized shear layer due to oscillations of a turbulent jet through an axisymmetric cavity", Journ. Sound and Vib., vol. 85, 371

Rodi W (1975) "A review of experimental data of uniform density free turbulent boundary layers", pp 79-165, Studies in Convection, Part 1, ed: B E Launder, Academic Press

Rodi W (1982) : Turbulent Buoyant Jets and Plumes (Rodi, editor)

Rosenweig R E, Hottel H C and Williams G C (1961) "Smoke-scattered light measurement of turbulent concentration fluctuations", Chem. Engr. Sci., vol. 15, 111

Ruck B and Durst F (1982) "Influence of signal detection and signal processing electronics on mean property measurements of LDA-frequencies", LDA Symposium (International), Lisboa, Portugal

Rudder R R and Bach D R (1968) "Rayleigh scattering of ruby laser light by neutral gases", Journ. Opt. Soc. Am., vol. 58, No. 9, 1260

Saffman P G (1962) "On the stability of laminar flow of a dusty gas", Journ Fluid Mech., vol. 13, 120

Sami S, Carmody T and Rouse H (1967) "Jet diffusion in the region of flow establishment", Journ. Fluid Mech., vol. 27, 231

Sarohia V and Massier P F (1980) "Effect of density on noise radiation from subsonic inverted velocity profile jets", AIAA Journ., vol. 18, 630

Savas O and Coles D (1985) "Coherence measurements in synthetic turbulent boundary layers", Journ. Fluid Mech., vol. 160, 421

Schaffar M (1979) "Direct measurements of the correlation between axial in-jet velocity fluctuations and far field noise near the axis of a cold jet", Journ. Sound and Vib., vol. 64, 73

Schefer R W and Dibble R W (1985) "Simultaneous measurements of velocity and density in a turbulent nonpremixed flame", AIAA Journ., vol. 23, 1070

Scott C J and Rask D R (1977) "Free turbulent shear layers on plug nozzles", Trans. ASME, Journ. Fluids Engr., 301

Seiner J M and Yu J C (1984) "Acoustic near-field properties associated with broadband shock noise", AIAA Journ., vol. 22, 1207

Sforza P M and Mons R F (1978) "Mass, momentum and energy transport in turbulent free jets", Int. Journ. Heat and Mass Trans., vol. 21, 371

Shardanand and Prasad Rao A D (1977) "Absolute Rayleigh scattering cross sections of gases and freons of stratospheric interest in the visible and ultraviolet regions", NASA Technical Note TN D-8442

Shaughnessy E J and Morton J B (1977) "Laser-light scattering measurements of particle concentration in a turbulent jet", Journ. Fluid Mech., 129

Siebers (1985) private communication

Siebers (1985) "Ignition delay characteristics of alternative Diesel fuels: Implications on Cetane number", SAE Paper 852102

Sinnamon J F, Lancaster D R and Steiner J C (1980) "An experimental and analytical study of engine fuel spray trajectories", SAE Paper 800135

Skibenko E I, Maslov A I and Yuferov V B (1976) "Space-time characteristics of pulsed supersonic gas jet", Soviet Phys. Tech. Phys., vol. 21, 951

Smith J R (1978) "Rayleigh temperature profiles in a hydrogen diffusion flame", Proc. Soc. Photo-Optical Instrumentation Engineers, vol. 158, (Laser Spectroscopy), 84

Smith J R (1980) "Temperature and density measurements in an engine by pulsed Raman spectroscopy", SAE paper 800137

Smith J R (1982) "The influence of turbulence on flame structure in an engine", Proc. Symposium on Flows in Internal Combustion Engines, ASME Winter Annual Meeting, Phoenix

Smith J R (1982) "Turbulent flame structure in a homogeneous-charge engine", SAE Trans., vol. 89, Paper 820043

Snyder W H and Lumley J L (1971) "Some measurements of particle velocity autocorrelation functions in a turbulent flow", Journ. Fluid Mech., vol. 48, 41

Spalding D B (1971) "Concentration fluctuations in a round turbulent jet", Chem. Engr. Sci., vol. 26, 95

Sreenivasan K R, Antonia A and Britz D (1979) "Local isotropy and large structures in a heated turbulent jet", Journ. Fluid Mech., vol. 94, 745

Stanford R A and Libby P A (1974) "Further applications of hot-wire anemometry to turbulence measurements in helium-air mixtures", Physics of Fluids, vol. 17, 1353

Starner S H (1983) "Joint measurements of radial velocity and scalars in a turbulent diffusion flame", Comb. Sci. and Tech., vol. 30, 145

Starner S H (1985) "Conditional sampling in a turbulent diffusion flame", Comb. Sci. and Tech., vol. 42, 283

Starner S H (1986) "Some triple correlation measurements of velocity and scalars in a turbulent diffusion flame", Comb. Sci. and Tech. , vol. 48, 99

Stewart R W (1956) "Irrotational motion associated with free turbulent flows", Journ. Fluid Mech., vol. 2, 593

Subramanian V and Ganesh (1984) "A technique to enhance entrainment by a particle laden double concentric jet", Comb. Sci. and Tech., vol. 36, 39

Sullivan J P, Windall S E and Ezekiel S (1973) "Study of vortex rings using a laser Doppler velocimeter", AIAA Journ., vol. 11, 1384

Sunavala P O, Hulse C and Thring M W (1953) "Mixing and combustion in free and enclosed turbulent diffusion flames", Comb. and Flame, vol. 1,179

Sunyach M and Mathieu J (1969) "Zone de melange d'un jet plan fluctuations induites dans le cone a potentiel-intermittence", Int. J. Heat and Mass Transfer, vol. 12, 1679

Takagi T, Okamoto T and Ohtani A (1982) "Simultaneous measurement of velocity and concentration in two-componenet gas flows by LDV and laser Rayleigh scattering", Faculty of Engr., Osaka Univ., Osaka, Japan

Takeuchi K, Senda J and Shikuya M (1983) "Transient characteristics of fuel atomization and droplet size in Diesel fuel spray", SAE Paper 830449

Tanabe H, Ohnishi M, Fujimoto H and Sato G T (1982) "Experimental study of the transient hydrogen jet using a fast response probe", Int. J. Hydrogen, vol. 7, 967

Tanaka Y "On the structure of pulse jet", Bul. JSME, vol. 27, 1667

Thring M W and Newby M P (1953) "Combustion length of enclosed turbulent jet flames", 4th Symp. (Intl) on Comb., 789

Tishkoff J M, Pinchak A C and Ostrach S (1979) "Turbulent co-current gas-liquid flow in a tube with and without swirl", Journ. Fluids Engr., vol. 101, 61

Tishkoff J M, Hammond Jr. D C, and Chraplyvy A R (1982) "Diagnostic measurements of fuel spray dispersion", Journ. Fluids Engr., vol. 104, 313

Topham D R, Clements R M and Smy P R (1984) "Turbulent mixing in a pulsed plasma-jet exhaust", Journ. Fluid Mech., vol. 148, 207

Torrest R S and Ranz W E (1970) "Concentration fluctuations and chemical conversion associated with mixing in some turbulent flows", AIChE Journal, vol. 16, 930

Townsend A A (1976) : The Structure of Turbulent Shear Flow, second edition, Cambridge University Press

Tso J, Kovasznay L S G and Hussain A K M F (1981) "Search for large-scale coherent structures in the nearly self-preserving region of a turbulent axisymmetric jet", Journ. Fluids Engr., vol. 103, 503

Turner J S (1962) "The starting plume in neutral surroundings", Journ. Fluid Mech., vol. 13, 356

Turner J S (1963) "The flow into an expanding spherical vortex", Journ. Fluid Mech., vol. 18, 195

Vafidis C (1984) "Influence of induction swirl and piston configuration on air flow in a four-stroke model engine", Proc. Inst. Mech. Engrs., Part C, vol 198, 71, see also PhD Thesis (1986), University of London

van de Hulst, H C (1981) : Light scattering by small particles, Dover Publication, New York

Venkataramani K S, Tutu N K and Chevray R (1975) "Probability distributions in a round heated jet", Phys. of Fluids, vol. 18, 1413

Vriens L and Adriaansz M (1974) "Light scattering from Ne, Ar, and Xe arcs", Journ. Appl. Physics, vol. 45, 4422

Wakuri Y, Fujii M, Amitani T and Tsuneya R (1960) "Studies on the penetration of fuel spray in a diesel engine", Bul. JSME, vol. 3, 123

Warshaw S, Lapp M, Penney C M and Drake M C (1980) "Temperature-velocity correlation measurements for turbulent diffusion flames from vibrational Raman- scattering data", Laser Probes For Combustion Chemistry, ed: D R Crosley, Amer. Chem. Soc.

Watson R D and Clark M K (1965) "Rayleigh scattering of 6943A laser radiation in a nitrogen atmosphere", Phys. Rev. Let., vol. 14, 1057

Way J and Libby P A (1971) "Application of hot-wire anemometry and digital techniques to measurements in a turbulent helium jet", AIAA Journ., vol. 9, 1567

Weinstein H and Todd C A (1963) "A numerical solution of the problem of mixing of laminar coaxial streams of greatly different densities - isothermal case", NASA TN D-1534

Whiffen M C and Ahuja K K (1983) "An improved schlierem system and some new results on acoustically excited jets", Journ. of Sound and Vib., vol. 86, 99

Whitaker K W and Morrison G L (1984) "Acoustic measurements in high-speed subsonic jets", AIAA Journ., vol. 22, 756

Whitelaw J H (1984) "Measurement techniques for combusting flows", Rept. Mech. Engr. Dept. FS/84/11, Imperial College of Science and Technology, London

Williams G C, Hottel H C and Gurnitz R N (1969) "A study of premixed turbulent flames by scattered light", 1081, Twelfth Symposium International, The Comb. Inst.

Wilson R A M and Danckwets P V (1964) "Studies in turbulent mixing", Chem. Engr.Sci., vol. 19, 885

Wilson L N and Damkevala R J (1970) "Statistical properties of turbulent density fluctuations", Journ. Fluid Mech., vol. 43, 291

Witze P O and Dwyer H A (1976) "The turbulent radial jet", Journ. Fluid Mech.,vol. 75, 401

Witze P O and Dwyer H A (1976) "Influence of laminar wall boundary layers on turbulent jet behavior", Journ. Fluids Engr., vol. 98, 773

Witze P O (1980) "Influence of air motion variation on the performance of a direct-injection stratified-charge engine", I. Mech. E. Paper C394/80

Witze P O (1980) "The impulsively started incompressible turbulent jet", Sandia National Laboratories, Report SAND80-8617

Witze P O and Vilchis F R (1981) "Stroboscopic laser shadowgraph study of the effect of swirl on homogeneous combustion in a spark-ignition engine", SAE Paper 810226

Witze P O (1983) "Hot-film anemometer measurements in a starting turbulent jet", AIAA Journ., vol. 21, 308

Witze P O, Martin J K and Borgnakke C (1983) "Measurements and predictions of the precombustion fluid motion and combustion rates in a spark ignition engine", SAE Paper 831697, see also SAND83-8652

Witze P O, Martin J K and Borgnakke C (1984) "Fluid motion during flame propagation in a spark ignition engine", SAE Paper 840377

Witze P O (1985) "An optical imaging technique for measuring time-resolved flame position", Exp. in Fluids, vol. 3, 174

Witze P O and Dyer T M (1986) "Laser measurement techniques applied to turbulent combustion in piston engines", Experiments in Fluids, vol. 4, 81

Witze P O (1986) private communication

Wright A G (1982) "Design of photomultiplier output circuits for optimum amplitude or time response", EMI Report R/P065

Wu K-J, Coghe A, Santavicca D A and Bracco F V (1983) "LDV measurements of drop velocity in diesel-type sprays", AIAA Journ., vol. 22, 1263

Yavuzkurt S (1984) "A guide to uncertainty analysis of hot-wire data", Journ. Fluids Engr., vol. 106, 181

Young A T (1981) "Rayleigh scattering", Appl. Optics, vol. 20, 533

Young A T (1982) "Rayleigh scattering", Physics Today, January 1982, Amer. Soc. of Physics

Yu J C and Dixon N R (1980) "Experimental study of sound radiation from a subsonic jet in simulated flight noise", AIAA Journ., vol. 18, 427

Yule A J (1978) "Large-scale structure in the mixing layer of a round jet", Journ. Fluid Mech., vol. 89, 413

Yule A J and Chiger N A (1979) "Coherent structures in turbulent flames", Rept. Dept. Chem. Engr. and Fuel Technology, University of Sheffield, Sheffield, England

Yule A J, Mo S L, Tham S Y and Aval S M (1985) "Diesel spray structure", Proc. ICLASS-85, IIB/2/1, London,

Zaman K B M Q and Hussain A K M F (1984) "Natural large-scale structures in the axisymmetric mixing layer", Journ. Fluid Mech., vol. 138, 325

Zaman K B M Q (1985) "Far-field noise of a subsonic jet under controlled excitation", Journ. Fluid Mech., vol. 152, 83